KTH ROYAL INSTITUTE
OF TECHNOLOGY

# Development of Photovoltaic System Simulator:
# PV Remote Lab

Jesus Querol Puchal

**KTH ROYAL INSTITUTE OF TECHNOLOGY**

DEPARTMENT OF ENERGY TECHNOLOGY

**Author**

Jesus Querol Puchal <jesusqp@kth.se>

MSc Sustainable Energy Engineering, DM -KTH & Universitat Politècnica de València – TSUEM

KTH Royal Institute of Technology

**Place for Project**

Stockholm, Sweden

**Supervisor**

Taras Koturbash

Stockholm

KTH Royal Institute of Technology

**Examiner**

Jeevan Jayasuriya

Stockholm

KTH Royal Institute of Technology

**TRITA**

TRITA-ITM-EX 2024:30

# Abstract

Currently, a sustainable energy transition is underway to reduce $CO_2$ emissions. To meet the targets outlined in international agreements like the Kyoto Protocol, a rapid expansion of renewable energy sources, particularly photovoltaic (PV) systems, is underway. Due to photovoltaic technology's rapid development and integration, reliable testing and evaluation methods are essential.

This master's thesis is dedicated to developing a PV system simulator to study the PV systems. PV simulators serve as precious tools due to their capacity to control and replicate the environmental conditions experienced by PV panels. Consequently, these simulators facilitate thorough research, design refinement, and PV system performance assessment.

The developed PV system simulator is essentially a PV remote lab, offering the capability to monitor, gather data, and evaluate the performance of the PV system remotely. The proposed system's flexibility and scalability enable its application to study various types of PV installation. The PV remote lab is expected to be a training centre for students and industry professionals.

A comprehensive literature review on photovoltaic technology has been undertaken. Following the literature review, the different components that form a PV system have been defined and selected. The system will have a communication block to achieve a flexible and scalable PV remote lab. In this way, different configurations of the PV panels and different system outputs can be implemented. This commutation block can be remotely controlled using an Arduino, and an interface can be designed where the desired PV panel configurations and system outputs can be selected. In this interface, visualising the tests' results will also be possible.

**Keywords**

# Sammanfattning

För närvarande pågår en hållbar energiomställning för att minska koldioxidutsläppen. För att uppfylla de mål som fastställts i internationella avtal som Kyotoprotokollet pågår en snabb utbyggnad av förnybara energikällor, särskilt solcellssystem (PV). På grund av solcellsteknikens snabba utveckling och integration är tillförlitliga test- och utvärderingsmetoder av avgörande betydelse.

Denna masteruppsats handlar om att utveckla en solcellssimulator för att studera solcellssystem. PV-simulatorer är värdefulla verktyg eftersom de kan kontrollera och återskapa de miljöförhållanden som PV-panelerna utsätts för. Följaktligen underlättar dessa simulatorer grundlig forskning, designförbättring och bedömning av PV-systemets prestanda.

Den utvecklade PV-systemsimulatorn är i grunden ett fjärrstyrt PV-labb som gör det möjligt att övervaka, samla in data och utvärdera PV-systemets prestanda på distans. Det föreslagna systemets flexibilitet och skalbarhet gör att det kan användas för att studera olika typer av solcellsinstallationer. PV-fjärrlabbet förväntas bli ett utbildningscenter för studenter och yrkesverksamma inom branschen.

En omfattande litteraturgenomgång om solcellsteknik har genomförts. Efter litteraturgenomgången har de olika komponenterna som bildar ett solcellssystem definierats och valts ut. Systemet kommer att ha ett kommunikationsblock för att uppnå ett flexibelt och skalbart PV-fjärrlabb. På så sätt kan olika konfigurationer av solcellspanelerna och olika systemutgångar implementeras. Detta kommutationsblock kan fjärrstyras med en Arduino och ett gränssnitt kan utformas där de önskade konfigurationerna av solcellspaneler och systemutgångar kan väljas. I detta gränssnitt kommer det också att vara möjligt att visualisera testresultaten.

### Nyckelord

PV-paneler, PV-solsimulator, karakteriseringsmetoder, kommuteringsblock, konfigurationer

# Acknowledgements

To my family,

to my tutors,

to my classmates,

thank you for accompanying me during this journey.

# Acknowledgements

# Table of Contents

# 8. Conclusion

# 9. Next Steps

# <u>Appendix</u>

# Table of Figures

# Table of Tables

# List of Abbreviations

| | |
|---|---|
| PV | Photovoltaic |
| IEA | International Energy Agency |
| NZE | Net-Zero Emission |
| BESS | Battery Energy Storage System |
| IPCC | Intergovernmental Panel on Climate Change |
| EL | Electroluminescence |
| UCI | User Control Interface |
| LCOE | Levelized Cost of Energy |
| STC | Standard Test Conditions |
| NOTC | Nominal Operating Cell Temperature |
| I-V | Current-Voltage |
| P-V | Power-Voltage |
| $P_{MPP}$ | Power at the maximum power point |
| $V_{MPP}$ | Voltage at the maximum power point |
| $I_{MPP}$ | Current at the maximum power point |
| $V_{OC}$ | Open Circuit Voltage |
| $I_{SC}$ | Short Circuit Current |
| EVA | Encapsulant Sheet |
| PWM | Pulse Width Modulation |
| MPPT | Maximum Power Point Tracking |
| RTD | Resistance Temperature Detector |
| IEC | International Electrotechnical Commission |
| JB | Junction Box |
| CBS | Commutation Block Scheme |
| RCP | Reference Constant Parameter |
| DC | Direct Current |
| AC | Alternating Current |
| PSC | Partial Shading Conditions |
| RPL | Relative Power Loss |

# 1. Introduction

## 1.1. Background

Nowadays, the world is in front of a green energy transition to fight climate change, one of the most critical challenges that has never been faced. The Kyoto Protocol was the first step proposed by the governments to confront climate change, followed by the Paris Agreement in which most countries took part (1) (2). Both agreements have been decisive in contemplating suggestions and defining procedures to reduce greenhouse gas emissions in the world, with the goal of not reaching a world average temperature increment of more than 1.5ºC and thus preventing dangerous anthropogenic interference with the climate system (2).

A global energy transition was initiated to reduce greenhouse gas emissions. The main key pillar of global energy transition, as defined by the International Energy Agency (IEA) , are the energy efficiency, the behavioural changes, and the technological revolution that replaces fossil fuel technologies with renewable technologies, hydrogen-based fuels, and infrastructure electrification (3).

Energy efficiency is a cornerstone of achieving global sustainable development. Total final consumption in 2021 amounted to around 410 EJ in 2020, while in the Net-Zero Emission (NZE) Pathway by 2050, the global energy demand should decrease by 8% compared with todays status. The main difference between todays situation and NZE's (2050) pathway is that in the forecast defined by the IEA, the population is increased by 2 billion people with an economy of more than twice as big (4). The four drivers to reach the goals of the NZE Scenario related to energy efficiency are the efficiency benefits with the appropriate use of biomass, sustainable equipment usage and building envelopes, efficiency benefits of electrification and improved energy habits (5). Renewable energy systems, such as PV energy and wind energy, have been defined as the two most important technologies to decarbonise the energy sector. In 2025, the total installed power capacity by wind and PV will be doubled, and electricity generation will increase. This renewable electricity generation increase is expected to meet 99% of the global electricity demand increase during 2020 – 2025 (6).

All these renewable energy systems rely on ambient conditions such as solar irradiation, wind speed, or rain, considered intermittent technologies.  For this reason, the battery energy storage system (BESS) will be essential as a backup technology with energy surplus storage. Hydrogen is another technology that can help renewables to form a reliable energy mix with different purposes (7).

To sum up, there are many key pillars to combat climate change. In the following years, policymakers should listen to scientists considering all the necessary measures to reach all the objectives proposed. Engineers in the sector should be prepared with an appropriate background and knowledge to implement those measures correctly and efficiently, in order to contribute towards the sustainable energy generation.

## 1.2. Objectives

The main goal of this thesis is to develop, test and commission the Photovoltaic System Simulator: PV Remote Lab. The PV remote lab will be used at the Department of Energy Technogy (KTH) as a PV training and testing facility for students' and professionals' education. The test rig would allow conducting various experiments with the components of a PV system components relevant to studying to understanding the typical PV system.

During the MSc thesis project, the working principles of PV technology will be explained and the main components of a PV system will be described. Once the introduction to the field is achieved, PV panel characterisation methods will be defined in order to be used to assess the state of the PV panels. There is also a description of the main defects that can appear in PV panels, explaining their causes and how to identify them.

Apart from getting practical exposure to design system configuration, there will be a knowledge acquisition related to laboratory skills such as good usage of electronic equipment, interface development, or teamwork with laboratory technicians to implement the experimental

## 1.3. Motivation and Justification

Renewable energy is presented as one cornerstone to reach the green energy transition. For this reason, in recent years, the implementation of PV installations and other renewable technologies has grown massively worldwide.

PV installations are designed to achieve maximum power generation possible for the given location. However, in some cases, PV panels are installed without a monitoring system to track the performance of the PV installation. The result is that if the problems occur in the PV installation, they might go unnoticed, thus reducing energy generation capacity. The use of PV system simulators make it possible to detect defects so that they can be repaired. Therefore, PV system simulators should continuously monitor PV installation performance, detect possible defects, and maximise the power generation of PV installation.

The PV remote lab will be offered to KTH students. The hands-on experience that students would gain from the simulator would play a crucial role in understanding the underlying physical phenomena of photovoltaics. The PV system simulator can be used as a training centre/laboratory to train the professionals and improve their knowledge in the design, analysis, and monitoring of the behaviour of PV systems. With such hands-on approach, students and industry representatives should acquire a broader understanding of PV technology.

## 1.4. Methodology

The methodology for this thesis is illustrated in Figure 1 and described below:

1. Introduction.

   ❖ Provide an overview of the energy transition and the important role of PV technology.
   ❖ Define the main objectives and applications of the Master Thesis.

2. Literature Reviewed of PV Technology

   ❖ Conduct a historical review of the evolution of PV technology.
   ❖ Definition of the principle of operation of photovoltaic cells and description of the layers that conform it. In addition, the most relevant the electrical parameters of a photovoltaic cell are defined and the two types of configurations that can be realized between photovoltaic cells are presented.
   ❖ Definition of a PV system and description of its main components.
   ❖ Literature review of the PV characterisation methods: I-V curve, dark I-V curve and electroluminescence method.
   ❖ Description of the causes and effects of the most common degradation modes in PV panels.

3. PV System Simulator

   ❖ Selection and description of the PV panels that make up the PV system.
   ❖ Movable trolley design according to LASS requirements.
   ❖ Design of the commutation block scheme and presentation of the scenarios that can be implemented in the "Double PV String Commutation Block".
   ❖ Application diagram of the system through Arduino.
   ❖ Selection of the main components that will make up the PV system simulator.

4. PV Remote Lab Assembly

   ❖ Installation of the PV panels in the movable trolley according to the design
   ❖ Assembly of the commutation block components in the DIN rail supports.
   ❖ Mounting of the commutation block on the trolley trolley.

5. Methods for PV Panels Characterisation

   ❖ Installation of the PV panels in the movable trolley according to the design
   ❖ Assembly of the commutation block components in the DIN rail supports.

6. Tests and Results

   ❖ Definition of the procedures to develop characterization methods
   ❖ Experimental validation of the procedures

7. User Control Interface

   ❖ Design of the different interfaces in order to be able to remotely control the solar PV simulator.

The flowchart of the working path followed during this MSc project is presented in Figure 1.
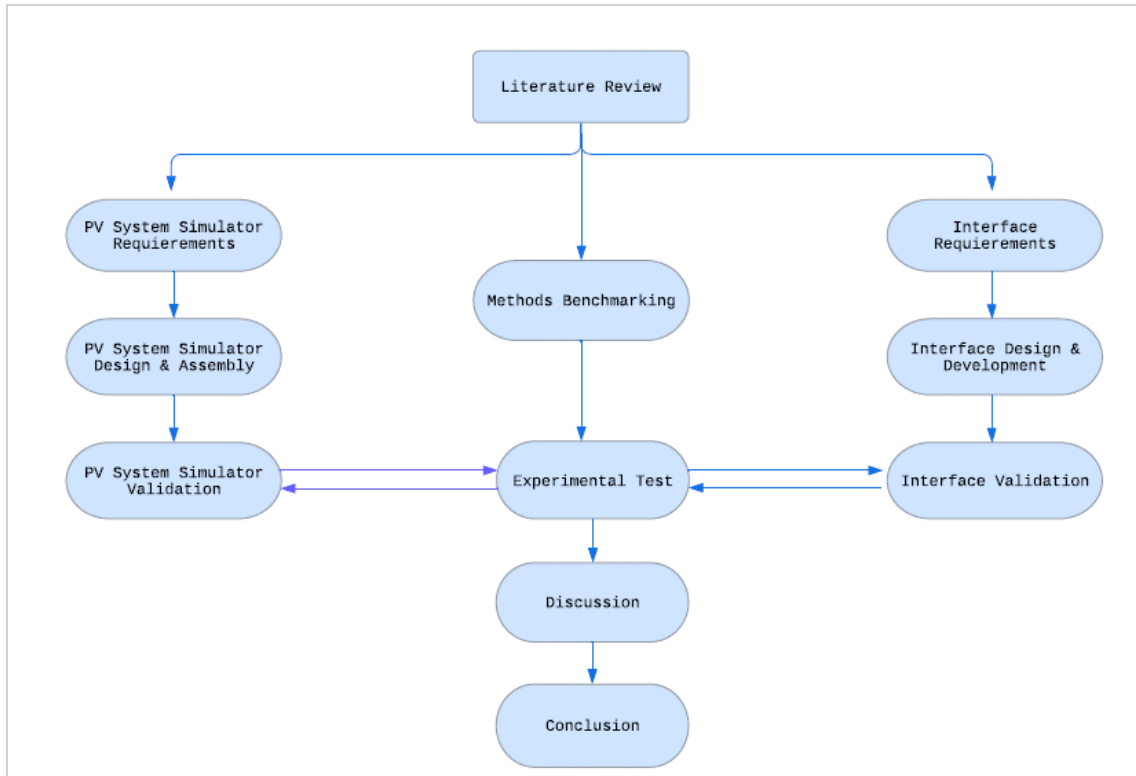


*Figure 1. Flowchart of the working path.*

# 2. Literature Review of Photovoltaic Technology

## 2.1. Historical Overview

In the middle of 20th century, Russel Ohl discovered that silicon had a higher photo potential than the materials used until then: copper oxide or selenium. The 0.5 V photo potential barrier was overcome. This breakthrough was followed by discovering the p-n (positive-negative) junction, hence, doping phenomena (8). During the following years, there was intense research activity with the primary goal of achieving higher efficiency. In 1952, 1% solar cell efficiency was reached by implementing the Ohl method. The technology multiplied in the next three years, with the introduction of lithium wraparound, led and boron diffusion reaching 11% efficiency in 1955. Finally, in 1959, the contacting metallic grids were introduced in the technology, achieving an efficiency of around 14 %.

All these achievements were accomplished under the pressure of the different governments involved in the space conquest. The lack of sufficient stored energy in aerospace vehicles was the main drawback of conquering space. In 1961, a USA satellite powered by photovoltaic technology was launched.

In 1970, the term "violet cell", the antireflection process, was found. More discoveries were made during the following decades to obtain a profitable cost to put the technology on the market.

Figure 2 shows the price evolution of PV panels from 1975 to the present. PV panel commercial price during the 70s was around 110 $/W. However, the price plummeted during the following decades until it reached a PV panel watt cost of 0.27 $ in 2020 (9). The main drives causing this plummeting cost are the government policy helping the growing markets and incentivising the technology with subsidies, research and development, achieving higher efficiencies, improving production processes and the scale economies (10).
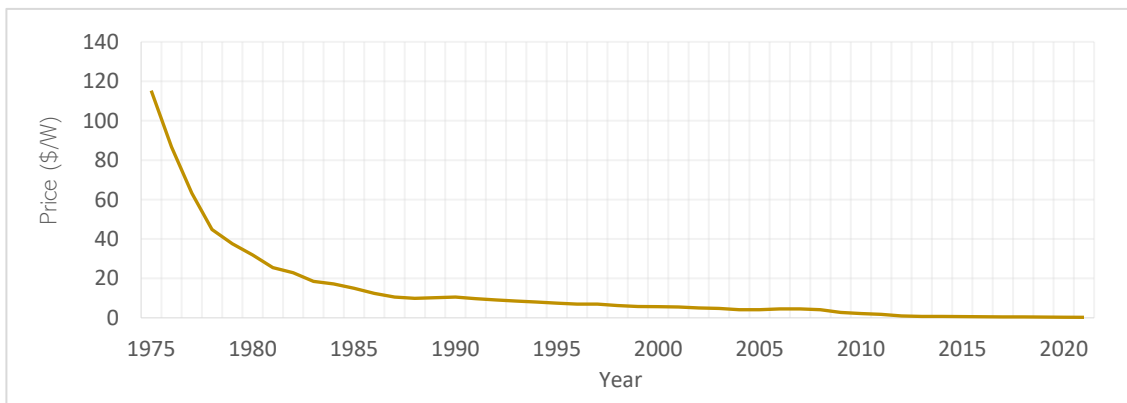


*Figure 2. PV panel Cost Evolution (9).*

Figure 3 shows the LCOE evolution during the last years of different renewable technologies. The price of solar photovoltaic technology has fallen during the previous few years, and combined with higher performance, the LCOE has dropped to values near onshore wind technology. Two-thirds of the newly installed renewable power in 2021 had lower costs than the cheapest fossil fuel-fired option in the G20 (11).
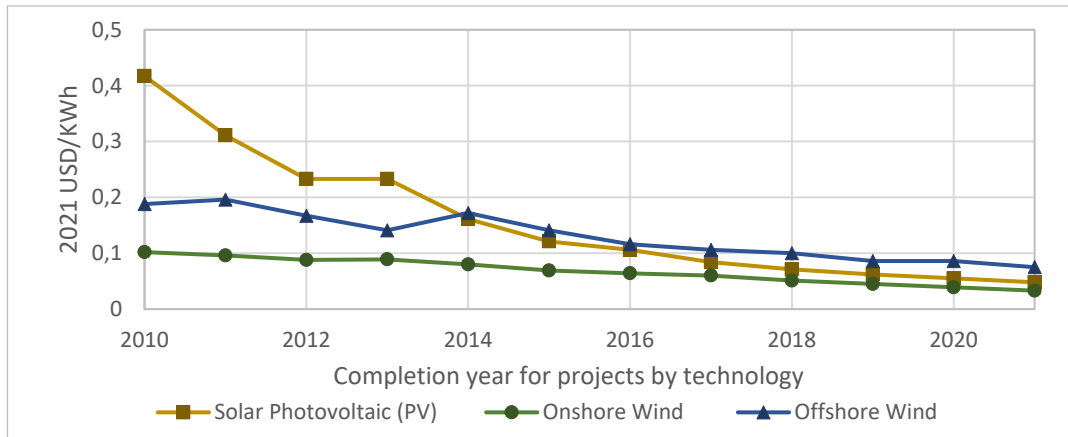
*Figure 3. LCOE Evolution of Renewable Technologies (11).*

Recent reports define the solar power generation in 2030 Net Zero Scenario will be 7 413.9 TWh with a power capacity installed of 5 041.9 GW. In context, in 2021, the solar power generation was around 1,000 TWh with a solar capacity of about 900 GW (12). These numbers show the importance of the photovoltaic field, focusing on utility-scale plants but pairing with an increasing installation amount in the residential, commercial and industrial segments.

## 2.2. Photovoltaic Cell

In the following subsections, the photovoltaic cell working principle will be explained, and the main photovoltaic cell parameters will be defined to understand the parameters shown in a PV panel datasheet and how they affect PV panel operation.

### 2.2.1. Working Principle

A PV panel is an element composed of photovoltaic cells connected in series and parallel, depending on the target application. Typically, a PV panel has 60-72 solar cells connected in series. Every cell works independently and can convert the photons from the sunlight that arrives at the cell surface into electrical energy. The solar cell comprises a silicon semiconductor doped with phosphorus and boron, resulting in a p-n junction device, as shown in Figure 4 (13).
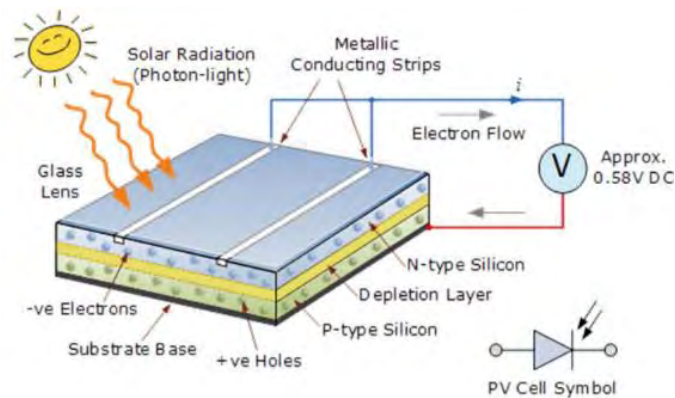


*Figure 4. Construction Diagram of a PV Cell (13).*

When the solar irradiance (photon light) reaches the PV cell, the photon absorption in the p-n junction electronic semiconductor to separate the electrodes of the valence band. When the photon absorption has higher energy than the gap energy of the doped semiconductor material, the electron will be excited, sending it from the valence band to the conduction band and leaving a hole at the valence level, which another electron can fill. When the energy level of an electron-hole pair in a semiconductor exceeds a certain threshold, the excess energy is dissipated as heat. The p-n junction creates an electric field separating the electrons extracted during electricity generation. This electric field causes the holes to move away through the p-region, effectively leaving the junction. In contrast, electrons flow out across the n-region. This electron flow forms an electric current. Once the electrons have passed through the load, they recombine with the holes (14).

### 2.2.2. Photovoltaic Cells Layers

A photovoltaic cell comprises several layers with different functions to ensure correct cell operation. As shown in Figure 5, a photovoltaic cell is a multi-layered unit consisting of the following parts (15):

- The cover glass is a transparent glass layer that protects internal components from the outdoor conditions. For example, dust and water a can cause damage to the PV cell and panel.

- The transparent adhesive layer firmly attaches the cover glass to the rest of the solar cell.

- The anti-reflective coating is a layer that incorporates a material intended to minimise light reflection reaching the cell, thereby enhancing the cell's ability to absorb the maximum amount of energy.

- The front contact is the layer where the electric current is transmitted.

- The positive-negative junction comprises a n-type semiconductor layer and a p-type semiconductor layer. Both are thin-layer silicon. The n-type is mixed with phosphorus, while the p-type is mixed with boron to provide better-conducting conditions.

- The back contact is used to transmit the electric current.
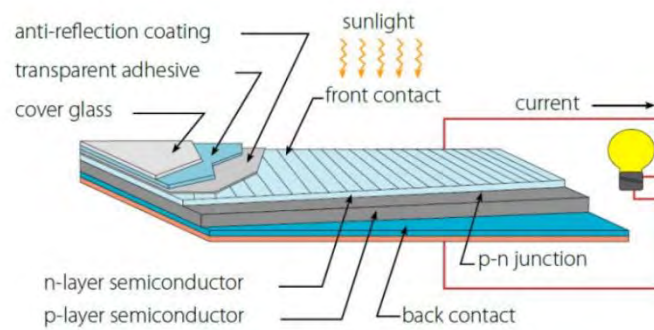


*Figure 5. Components of a Photovoltaic Cell (15).*

### 2.2.3. Photovoltaic Cell Parameters

The main parameters of PV panels are always shown in the PV panel's datasheets and are essential to understanding their behaviour and limitations. According to IEC 60891, most of the parameters shown in a datasheet are measured in the Standard Test Conditions (STC):

- Irradiation: 1 000 W/m²
- Cell temperature: 25 ºC
- Air mass: 1.5 global spectrum

Some parameters of PV panels are reported for Nominal Operating Cell Temperature (NOCT):

- Irradiation: 800 W/m²
- Air temperature: 20 ºC
- Air mass: 1.5 global spectrum
- Wind speed: 1 m/s

The I-V curve of a photovoltaic cell is shown in Figure 6. This I-V curve illustrates all the operational points at which the photovoltaic cell can function under STC (16). As can be seen from the figure, the curve goes from the $I_{SC}$ point to the $V_{OC}$ point, passing through the maximum power point. The power-voltage (P-V) curve allows identification of the maximum power point of the PV panel. For maximum power point ($P_{MPP}$), there will be corresponding voltage $V_{MPP}$ and current $I_{MPP}$. The P-V curve provides complementary information to the I-V curve.
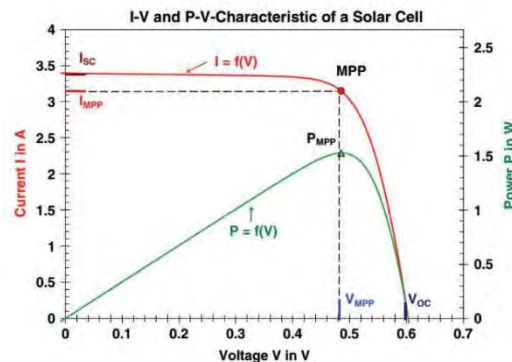


*Figure 6. I-V and P-V Curves of a Photovoltaic Cell (16).*

The three more important points of the I-V curve at STC are:

- Maximum voltage (0, $V_{OC}$)
- Maximum current ($I_{SC}$,0)
- Maximum power ($I_{MPP}$, $V_{MPP}$).

The parameters that describe the I-V curve at STC are:

→ **Open Circuit Voltage, $V_{OC}$**

It is the maximum voltage that a cell can deliver, at which no current flows in the external circuit (no load is connected). The $V_{OC}$ corresponds to the forward bias voltage, while the reverse saturation current compensates for the photocurrent.

→ **Short Circuit Current, $I_{SC}$**

It occurs when the current across the photovoltaic cell is the maximum current that the cell can deliver. The $I_{SC}$ depends on the area of a solar cell and the photon flux density

incident. Therefore, it depends on the spectrum of the incident light to the photovoltaic cell surface.

→ **Maximum Power Point, P$_{MPP}$**

It is the maximum output power the photovoltaic cell can provide. The maximum power voltage (V$_{MPP}$) and the maximum power current (I$_{MPP}$) should be given to find the maximum power point.

→ **Fill Factor, FF**

The fill factor measures the squareness of the current-voltage (I−V) curve and indicates how the total internal electrical resistances affect the output current. A square-shaped curve, meaning a fill factor close to 1, shows high efficiency and maximum power output.

$$FF = \frac{P_{MPP}}{V_{OC} \; I_{SC}}$$

Other critical parameters that are provided in the PV panel's datasheet by the manufacturer are the following ones:

→ **Cell Efficiency**

→ It is the portion of irradiation that arrives in the cell from the sunlight and can be converted by the solar cell to electricity through photovoltaic phenomena.

→ **Operating Module Temperature**

→ It is the range where the module can work without damage and failure.

→ **Maximum System Voltage**

It is a vital parameter to know how many PV panels can be connected to a PV facility.

→ **Temperature Coefficients**

These parameters describe the temperature influence in the voltage, current and power to correct this value if the working conditions differ from the STC.

The I-V curve depends on the irradiance and temperature, as shown in Figure 8 and Figure 7 ([1]). The solar irradiation variation is directly proportional to the photons that can be absorbed by the photovoltaic cell. Hence, the less irradiation, the lower the current on the photovoltaic cell is. Regarding the temperature, the photovoltaic cell experiences an increase in voltage as the temperature decreases. The temperature has a minor effect on the current. Although, it is important to define that with a higher the cell temperature, a higher I$_{SC}$ is achieved.
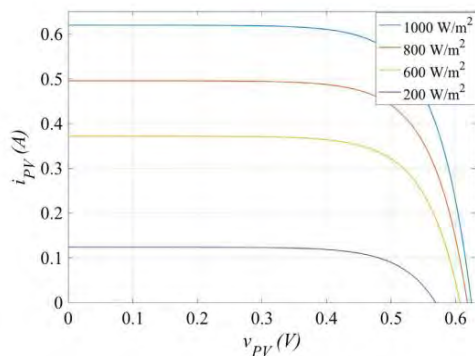


Figure 8. Behaviour of the I-V Curve depending on the Irradiation at STC (17).
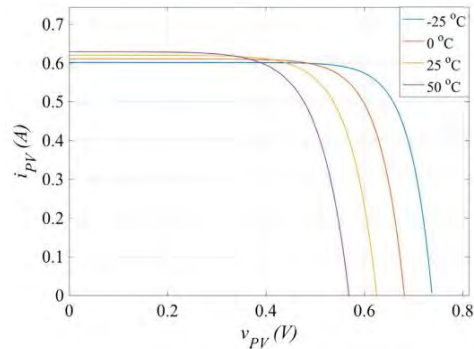
Figure 7. Behaviour of the I-V Curve depending on the Temperature at STC (23).

If PV parameter where not measured at STC, an adjustment to STC is required according to ASTM (1985) and ABNT (1991) (18) (19). The following equations allow the correction of the short-circuit current and open-circuit voltage points to the STC:

$$I_{SC(STD)} = \frac{G_{STD}}{G} I_{SC_{(measured)}} + \alpha (T_{STD} - T_{cell})$$

where:

- $I_{SC(STD)}$ is the short-circuit current of the module at STC.
- $G_{STD}$ is the standard irradiance.
- G is the solar irradiance on the surface of the module.
- $I_{SC(measured)}$ is the measured short-circuit current of the module.
- $T_{STD}$ is the standard cell temperature.
- $T_{CELL}$ is the measured cell temperature.
- $\alpha$ is the temperature coefficient of the $I_{SC}$ of a PV cell.

$$V_{OC(STD)} = V_{OC_{(measured)}} + N \beta (T_{STD} - T_{cell}) + N \frac{nKT_{cell}}{e} \ln\left(\frac{G_{STD}}{G}\right)$$

where:

- $V_{OC(STD)}$ is the module's open circuit voltage at STC.
- $V_{OC(measured)}$ is the measured open-circuit voltage of the module.
- $\beta$ is the temperature coefficient of the $V_{OC}$ of a PV cell.
- K is the Boltzmann constant.
- N is the number of cells associated in series.
- e is the electron charge.
- n is the diode ideality factor.

And for the rest of the points, the following equations should be used to correctly calculate the STC adjustment:

$$I_{(STD)} = I_{(measured)} + I_{SC_{(measured)}}\left(\frac{G_{STD}}{G} - 1\right) + \alpha (T_{STD} - T_{cell})$$

where

- $I_{(STD)}$ is the current of the module at STC
- $I_{(measured)}$ is the measure module current

And

$$V_{(STD)} = V_{(measured)} + \beta (T_{STD} - T_{cell}) - F_{CC} I_{(STD)}(T_{STD} - T_{cell}) - R_S(I_{STD} - I_{(measured)})$$

where

- $V_{(STD)}$ is the voltage of the module at STC.
- $V_{(measured)}$ is the measured module voltage.
- $F_{cc}$ is the curve correction factor.
- $R_S$ is the series resistance of the module.

### 2.2.4. Cells Technology

Photovoltaic cells are often classified based on their design and manufacturing technology. The most common commercial pv panels in the market are the following ones (20):

→ **Monocrystalline technology**

This technology comprises thinly pure silicon crystal bars or another semiconductor material. Photovoltaic cells should be identical, with high efficiencies of around 25%. This high-efficiency technology is associated with a higher cost than other technologies.



*Figure 9. Monocrystalline PV Panel (22).*

→ **Polycrystalline technology**

This technology is made of several silicon crystals or other semiconductor materials, which are melted and poured into a square mol. The resulting silicon crystal is less pure than in the monocrystalline PV cell technology. The efficiency is around 20%. The manufacturing process is more straightforward than the monocrystalline procedure, resulting in a lower price.



*Figure 10. Polycrystalline PV Panel (22).*

In 2022, the most common commercial PV panels used are the p-type monocrystalline PERC technology, with almost 60% market share (21). However, n-type will become mainstream for concepts such as passivated contacts, achieving 50% of the market in the next decade. Otherwise, bifacial technology will significantly grow during the next decade, accounting for almost 80% of the production by 2031 (22).

Multijunction solar cells have higher efficiencies due to a doped layer taking advantage of a specific wavelength, which can cover a broader spectrum of solar energy (23). The thin-film technologies and perovskite cells have made a considerable development. Despite recent discoveries, these cell types do not have a competitive cost. The solar cell with the highest recorded efficiency is a four-junction solar cell featuring a new antireflection coating. This remarkable achievement was made by the Fraunhofer Institute for Solar Energy Systems ISE, with an impressive efficiency rating of 47.6% (24).

### 2.2.5. Cell Configuration

#### 2.2.5.1 Series Configuration

The photovoltaic cells could be connected in series as a string. The starting point in the combination in cell series is the negative terminal, while the ending is the positive terminal. The negative terminal is connected to the positive terminal of the next cell, allowing a smooth flow of electrons and so on for all the rest cells.

The resulting resistance is calculated with the following equation:

$$R_T = R_1 + R_2 + R_3 + \cdots + R_n,$$

where n is the number of cells in the system.

The resultant voltage is the sum of the different cell voltages generated while the current carried throughout the circuit remains the same (25). In Figure 11, the cell in series configuration is presented.
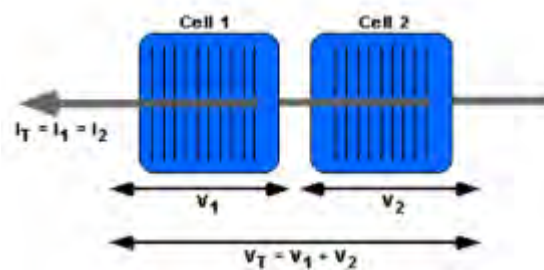


*Figure 11. Schematic Diagram of Series Connected Cells (25).*

#### 2.2.5.2 Parallel Configuration

The photovoltaic cells could be connected in parallel, creating different ways where the current can go. In this case, all the positive terminals are connected to the same point, and the same happens with the negative terminals.

The resulting resistance is calculated with the following equation:

$$\frac{1}{R_T} = \frac{1}{R_1} + \frac{1}{R_2} + \frac{1}{R_3} + \cdots + \frac{1}{R_n},$$

where n is the number of cells in the system.

The voltage is the same across every component in a combination of cells, while the total current is the sum of the current of all the cells in the system (25). In Figure 12, the cell in parallel configuration is presented.
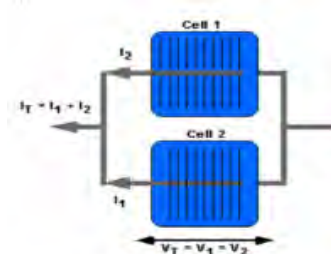


*Figure 12. Schematic Diagram of Parallel Connected Cells (25).*

Typically 60 to 72 photovoltaic cells are connected in series in a PV panel. In most PV installations, the PV panels are connected in series to reduce the wire cost. However, the parallel configuration has a clear advantage: a failure of a cell does not affect the whole system. The current can flow through other photovoltaic cells/panels.

### 2.2.6. Diodes

The diode is an electric component composed of two terminals that only allow the electrical current in one direction. They are made of semiconductor material, typically silicon. The unidirectional current allowed by the diode happens due to the resistance in one of the terminals. If the current flows, the anode is connected to the positive terminal (with a low, ideally zero, resistance value). In contrast, the cathode is connected to the negative terminal (with a high, ideally infinite resistance value). In the inverse case, the current is not allowed to pass.

PV panels use diodes with different goals, such as blocking or bypassing the current.

Blocking diodes allow current flow from a solar panel to the grid, but prevent/block the current flow from the grid to the solar panel. In the case of using batteries, it prevents the battery from discharging (26).

The bypass diode is connected antiparallel between the positive and negative output terminals of a small group of the series cell. Most used solar panels have around 60 - 72 solar cells, divided into groups of 20 - 24 to improve the performance. In the case of solar cell failure in one of these strings, the diode bypasses the faulty series cell by providing current in an alternative flow path, thereby maintaining the continuity of power production (27). However, when the bypass diode lets the current flow, it consumes some of its energy.

Bypass diodes are installed in the junction box on the backside of PV panels, as shown in Figure 13. When PV panel is in the partial shading conditions , the bypass diode will activate, rerouting the current around these shaded  cells (28).



*Figure 13. PV Panel Junction Box (28).*

## 2.3. PV System

Apart from PV panels and inverters, which are major components of a PV system, there are other essential elements, such as solar charge controllers or measurement equipment. The different components that comprise a PV system will be introduced and described in this subsection.

In Figure 14, the components that make up a grid-connected PV installation with energy storage are shown. This type of PV system is the most comprehensive as it harnesses all the energy generated by the PV installation through the accumulation of energy in batteries in case the energy generated is not consumed at the time.
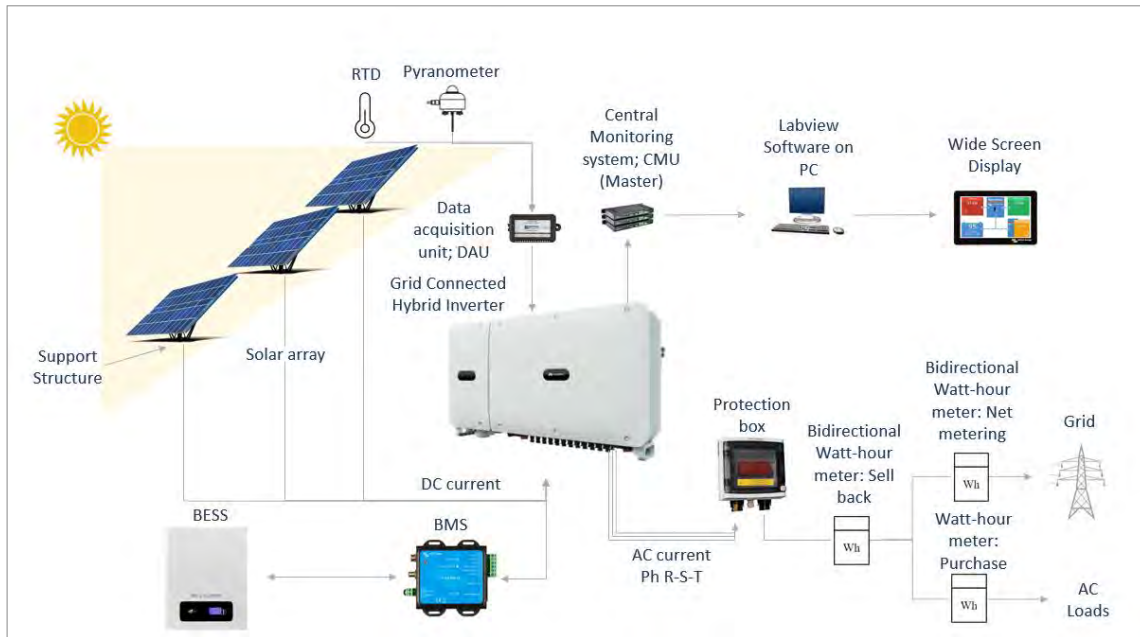


*Figure 14. Grid-Connected PV System.*

The PV system is mainly composed of the following components:

❖ PV panels: a component that converts incident irradiation into electric current. PV panels should be installed on a support structure that ensures optimal tilt to maximize energy generation.

❖ Temperature and irradiation sensor: sensors used to measure the temperature and irradiation of a PV installation in order to adjust the electrical parameters to STC and have the ability to check the performance of the installation. It is necessary to install a data acquisition unit for monitoring.

❖ Battery energy storage system: components that store the energy generated by the installation when there is no consumption greater than the generated energy. They should be accompanied by a battery management system to manage and control the battery's charge and discharge properly.

❖ Inverter: a component that transforms the energy from direct current to alternating current. In most cases, inverters have integrated solar chargers to maximize energy generation.

❖ Central Monitoring System: a system component that centralizes all information for subsequent visualization through the use of a graphical programming environment such as LabVIEW.

❖ Protection Box: When connecting the PV system to the grid and to the power point, it is essential to install a protection box according to regulations to protect both, the installation and the energy-consuming elements.

Depending on the end user's energy requirement and the electric production ability, there are different PV systems (29): Off-grid PV systems, Grid-connected PV systems, Hybrid system.

The off-grid solar power systems are independent and are used where the grid connection is unavailable. A BESS is incorporated to store surplus energy generated during sunny hours, serving as a backup technology to create a reliable energy system. The main disadvantage of this off-grid configuration is the system's reliability due to the dependence on climate conditions.

The grid-connected PV systems are connected to the grid and are more reliable. The energy surplus can be sold to the grid, while the energy can be purchased on the grid during hours without sufficient PV production. Most of the time, these systems can help their national grid with a demand reduction. A protection box is required in a grid-connected PV system and should comprise under-voltage relays or circuit breakers, among others.

Hybrid systems are needed in large-scale systems such as the national grid to meet the national demand. In most countries, renewable energy technologies such as PV systems and wind turbines are combined with fossil fuels or nuclear power plants to cover the energy demand required. In small-scale poly-generation systems, different energy sources, such as wind and solar, can be hybridised to get the energy output needed for the end user.

### 2.3.1. PV Panel

The PV panel is the main component of a PV system. PV panel is composed of photovoltaic cells in series. To reach the desired power, the PV panels can be connected in series or parallel and would determine the output power (30). Figure 15 shows the progressive connection of the photovoltaic cells, panels and arrays to reach the required power.
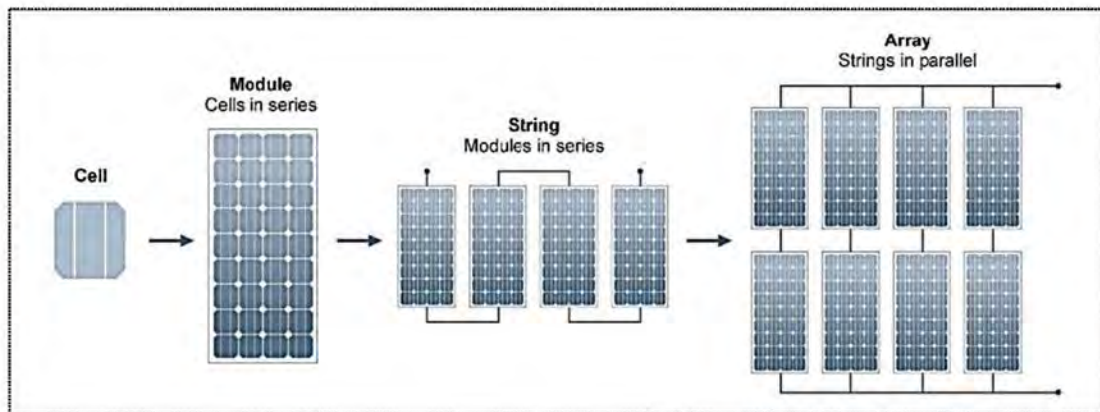


*Figure 15. Photovoltaic Cell, Module and Array Configuration (30).*

A standard PV panel, Figure 16, comprises different components and layers to ensure the correct operation mode. The front glass, encapsulation sheet, back sheet and the second encapsulant sheet are the layers of a PV panel, while the junction box, the aluminium frame and the edge seal are components that form the PV panel (31).
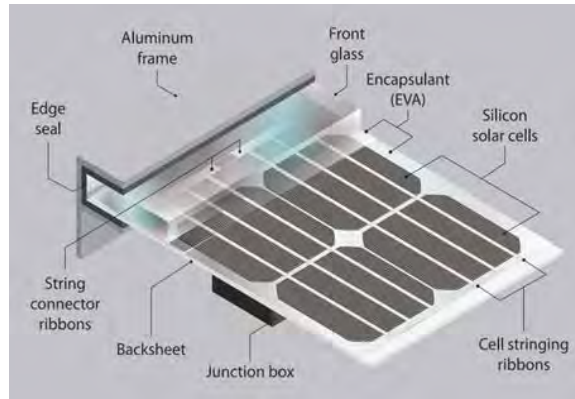
*Figure 16. PV Panel Components and Layers (31).*

The front glass and the back sheet are two layers in charge of isolating and protecting the silicon solar cells from outdoor phenomena. The encapsulant sheet (EVA) is a transparent polymer material laminated onto glass. It has different purposes: hold silicon solar cells in place, provide electrical insulation, and protect components from mechanical stress, corrosion and electrical shock (32). The encapsulant sheet (EVA) is fixed above and below the silicon photovoltaic cells, the cell stringing ribbons and the string connector ribbons where the silicon photovoltaic cells are connected in series. The edge seal and the aluminium frame surround the PV panel, protecting the string connector ribbons and isolating the different layers from the outdoor environment. The junction box is installed in the back skin of the module with adhesive, which contains the various electrical connections which provide current paths to the outside wiring of the PV panel (33).

It is important to emphasise that module efficiency has a lower value than cell efficiency due to the separation between photovoltaic cells and the bus bar of the PV panel.

## 2.3.2. Solar Charge Controller

Solar charge controllers regulate the amount of energy from the PV panels that flow into the utility grid, battery, or end-point consumption. Solar controllers have several functions (34):

- Control and regulate the voltage from the PV panels.
- Prevent battery discharge and overcharge.
- Allow different DC load usage and supply them with an appropriate voltage.
- Monitor and display the load power and energy.
- Protect from abnormal conditions.

Nowadays, there are two main types of solar charge controllers: Pulse Width Modulation (PWM) and Maximum Power Point Tracking (MPPT). PWM controllers have been the most widely used. However, during the last few years MPPT controllers have started to be more and more used due to their better performance.

### 2.3.2.1 PWM

The PWM controller is based on an oscillating circuit where pulse width depends on the current battery voltage. Placed between the PV panel and battery voltage, the PWM controller decides how to control the load and charge the battery. The charging current depends on the difference between the battery voltage and the charge set point value. With a higher battery voltage, the pulse width of the PWM reduces, and with a lower battery storage voltage, the pulse width will rise (35). The battery voltage increases with a higher state of charge of the battery (36).

The battery has a prolonged life using PWM because the charge and discharge stages have been carried out with less stress (37).

### 2.3.2.2 MPPT

Maximum power point tracking is based on adjusting the electrical load on the PV panels by changing their voltage to find the maximum power point (38). The three factors that should be considered to extract the maximum power are the irradiance, which changes the current operating point; the temperature, which varies the voltage operating point; and the load, a reference for the current and voltage (38).

MPPT controllers offer an efficiency increase of up to 30% compared to PWM controllers. Despite their higher initial cost, their well-suited design for large PV systems results in a faster return on investment (37).

PWM and MPPT charge controllers exhibit different behaviours when connected to a battery with an operational voltage of 13 V, as shown in Figure 17. The blue line is the I-V curve, while the red line is the P-V curve. For PWM, the voltage of the PV panel and the battery is practically the same without considering wire losses, which means that the maximum power achieved following the P-V curve is 81 W (39). PWM can not change voltage value to increase the power generation. In this case, MPPT adapts voltage and current values with the help of a DC-DC transformer to achieve the maximum power point, 100 W. In this case, the power generated difference is about 19 %.
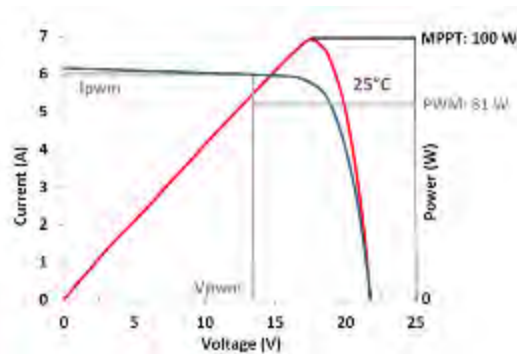


*Figure 17. I-V & P-V Curves Traced with PWM and MPPT (39).*

### 2.3.3. Inverter

In PV systems, the inverter transforms direct current (DC) from the PV to alternating current (AC) used in the electrical grid. The overall efficiency of an inverter is between 93% - 95%.

Different inverters ensure the correct system behaviour depending on the system design and requirements. The full H-bridge topology scheme circuit, the most widely used in grid-connected photovoltaic inverters, comprises four transistors and unipolar PWM modulation (40).

The regulated source, voltage or current, is an essential parameter in the inverter's classification. The voltage source inverters (VSI) control the output voltage with a minimal impedance, while on the current source inverter (CSI), the output current is controlled with a high impedance. Depending on the design requirements, both types of inverters can be applied in three-phase or single-phase applications (29).

Depending on how the PV modules relate to the power conditioning unit, there are four different inverter uses: centralised inverter topology, string inverter topology, multi-string topology and modular topology.

The centralised inverter topology is used in photovoltaic systems of several MW when a considerable number of PV modules, which comprise arrays, are connected and controlled by the inverter. The string inverter topology is when every string of PV panels is connected to an individual inverter. This topology is used for power installation of around 2-3 kW. Multi-string topology is used when multiple strings are connected to the same inverter, but with a DC-DC converter for maximum power point tracking per string. A modular topology, a microinverter, converts DC to AC in a single module.

Grid-connected inverters can also be categorised depending on the number of processing stages: decoupling capacitors, isolation between AC and DC side and synchronisation with the power grid. The three types of processing stages are:

- First stage. When the inverter can provide the MPPT, grid current control and voltage amplification.
- Second stage. It is based on an additional DC-DC converter for MPPT.
- Third stage. The inverter can control grid current and the module array is connected independently to its own DC/DC converter and then to the inverter itself.

Decoupling capacitors are relevant to define the life of the inverter (29).

Nowadays, the solar inverters used are the 3rd generation launched in 2007. A standard 3rd generation inverter is shown in Figure 18 (29). Most of these inverters have a solar charge controller built into them.
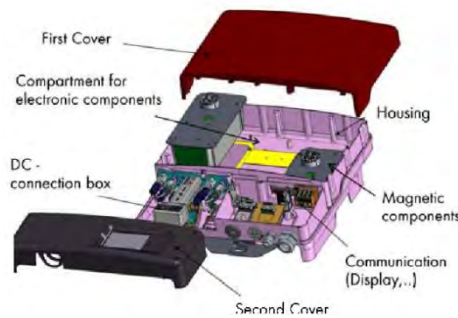


*Figure 18. Standard 3rd Generation Inverter (29).*

### 2.3.3.1 Microinverter

A microinverter is a small device that only operates in a low power range. Different control applications exist for microinverters: grid-connected, island mode, reactive power consumption, PV system with BESS and multiple operation modes.

The main advantages of this type of inverter are flexibility, a proper way to detect defaults, the ability to be installed in complex structures and the possibility of having PV panels installed with different orientations (41). With the implementation of microinverters, the PV mismatching and partial shading effects can be removed, increasing the energy performance of the PV installation. This positions microinverters as a promising solution for residential installations (42). However, nowadays, there is a low market share, less than 10%, due to the low reliability and low operating power range.

### 2.3.4. Measurement Equipment

In a PV installation is important to have measurement equipment in order to collect the necessary data to analyze the performance of the installation. The main essential parameters that should be considered are the energy generation, irradiation and temperature.

#### 2.3.4.1 Energy Measurement

The inverter typically has a metering device that measures the DC energy converted to AC. In the case of a battery energy storage system installed, hybrid converters as multi-output converters can provide simultaneous DC and AC outputs (43). Hybrid converters can manage the energy generated by the PV system, in order to optimize the battery charging and discharging procedure. In case of full battery charge, the energy can be used to feed the load or supplied to the grid.

To control the energy consumed by the grid and the energy delivered to the grid, a bi-directional energy metering device should be installed at the border point of the installation (44).

#### 2.3.4.2 Irradiation Measurement

To evaluate the performance of a PV installation, it is essential to have irradiation measurement equipment to calculate the performance ratio of the PV installation.

There are several solutions in the market depending on the type of installation and the requirements needed. The most common irradiation measurement equipment are:
- Pyranometer                    **PV reference cell sensor**

**Pyranometer**

The pyranometer is a thermopile-based sensor designed to measure the broadband density of the solar flux (45). The irradiation absorbed on the surface is calculated with the differential measurement between a white-sector temperature not exposed to the sun and a black-sector temperature exposed to the sun. Irradiation is measured indirectly by measuring the temperature difference between the two surfaces (45). The main component is a thermocouple with a sensitivity range of 300 to 2 800 nm. This equipment is expensive but more accurate than a photodiode or photovoltaic pyranometer (45).

The pyranometer's physical behaviour differs from that of a PV module. A pyranometer measures the whole spectral range of the sun, not only the spectral part which can be converted to electricity. The reflection of the pyranometer is lower than a photovoltaic cell. The response time is up to 30 seconds, and it is an expensive PV monitoring system device (46). A pyranometer is shown in Figure 19.



*Figure 19. Irradiation Measurement: Pyranometer (46).*

**PV Reference Cell Sensor**

The reference cell sensor is based on converting the solar irradiation that comes to the cell surface into a proportional current by the solar cell. A shunt resistor and a thermo-resistive device can determine the measured voltage with a temperature correction. The voltage will be converted to irradiation with the multiplication of a sensitivity value provided by the manufacturer (47).

The reference cell measures the spectral part the photovoltaic cell can convert to electricity. Hence, the measurement is very accurate with a reflection with more similarities to a photovoltaic cell. The response time is milliseconds, which matches the PV module response. This device has a lower cost than pyranometer, being a robust and feasible solution (46). A PV reference cell sensor is shown in Figure 20.



*Figure 20. Irradiance Measurement: PV Reference Cell Sensor (46).*

### 2.3.4.3 Temperature Measurement

The commercial sensors for temperature measuring in PV systems are analogue Resistance Temperature Detector (RTD) such as PT100. The RTD working principle is the resistance variation due to temperature changes. This technology provides high accuracy in a wide range with excellent stability compared to thermocouples. A RDT installed in the backsheet is shown in Figure 21.



*Figure 21. Resistance Temperature Detector.*

The commercial sensors for temperature measuring in PV systems are analogue Resistance Temperature Detector (RTD) such as PT100. The RTD working principle is the resistance variation due to temperature changes. This technology provides high accuracy in a wide range with excellent stability compared to technicians.

## 2.4. Methods for PV Characterisation

The photovoltaic industry is experiencing rapid global development, with a focus on advancements in applications, efficiency, and reliability. Accurate and consistent performance assessment, good practices, monitoring systems and maintenance are primary keys to conserving PV installations' performance over the years. These actions yield benefits to all stakeholders involved in this industry.

This chapter describes several fast and accurate methods for characterising PV panels and identifying possible degradation modes. The methods described are the I-V curve, dark I-V curve and electroluminescence. In addition, the different degradation modes that can be detected using these methods will be defined.

### 2.4.1. Performance Characterisation Methods

#### 2.4.1.1 I-V Curve & P-V Curve Measurement

I-V curve tracing is the most popular method for analysing a PV installation. Different loads are applied, transitioning the PV panel state from open circuit to short-circuit conditions. This process requires multiple measurement points to create a complete I-V curve for analysis. The electric current generated and the operational voltage are the parameters that should be registered.

In this subsection, different I-V Curve tracing methods are discussed. The method implemented in the PV remote lab is selected in the final discussion.

**Variable Resistor**

The variable resistor method is the simplest I-V curve tracing method. Allows capturing the different points of the I-V curve from the short circuit to the open circuit through manual resistance adjustment.

Figure 22 shows the I-V curve tracing system with several resistors. The resistance values of the resistors should be preliminarily calculated to allow trancing of the entire I-V curve. The $I_{SC}$ is achieved when the resistor array with the lower resistance is closed. Then, the different resistor arrays will be gradually applied to measure the various points of the I-V curve until $V_{OC}$ is achieved when the maximum resistive load is applied (49).
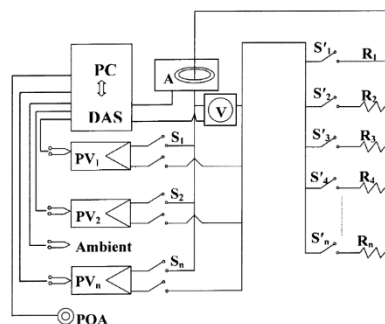


*Figure 22. Scheme of I–V Sequencer System with Variable Resistance (49).*

The variable resistor method offers distinct advantages, such as cost-effectiveness and a direct measurement the I-V curve. Nevertheless, the $I_{SC}$ cannot be precisely reached; it is a slow method vulnerable to weather-related fluctuations and has a limited number of measurement points (50).

**Capacitive Load**

The capacitive load method traces the entire I-V curve by employing a capacitor as a passive load. The capacitive load scheme is shown in Figure 23. The I-V curve measurement starts with the $I_{SC}$ condition, achieved by closing S3 and S2 to discharge the capacitor. Then, with S3 and S2 open and S1 closed, the current provided by the PV panel gradually decreases while the voltage increases until the capacitor is charged, achieving the $V_{OC}$ (51).
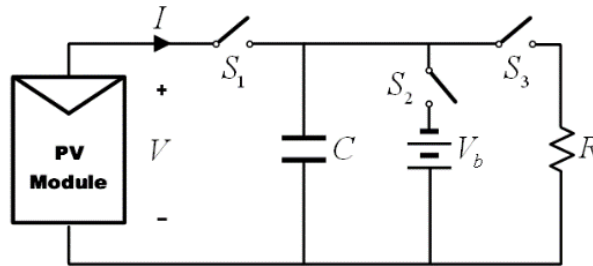


*Figure 23. Capacitive Load Scheme (49).*

The value of the capacitor is directly proportional to the $I_{SC}$ and inversely proportional to the $V_{OC}$ (50). The relationship between the capacitor value and the time of establishment ($t_s$) is as follows:

$$C = \frac{t_s}{2} \frac{I_{SC}}{V_{OC}}$$

This method offers several key advantages, including high accuracy, speed and a cost-effectiveness. However, it does require high-quality capacitors with low equivalent series resistance and minimal losses. It does not allow for partial reproductions; complete cycles are necessary to obtain the I-V curve data (50).

**Electronic Load**

In the electronic load method, a transistor, commonly a MOSFET, controls and varies the load applied to the PV panel. This is achieved by modulating the gate-source voltage of the transistor between its terminals, which facilitates the tracing of the I-V curve (50). Figure 24 shows the circuit design to obtain the I-V curve with the electronic load method.
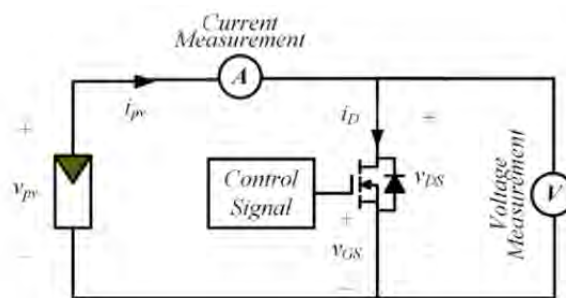


*Figure 24. Electronic Load Scheme using MOSFET(17).*

The three fundamental parameters that define the behaviour of the MOFSET are: $V_{GS}$, which represents the gate-source voltage; $V_{DS}$, which stands for the drain-source voltage; and $I_D$, which denotes the drain current of the MOSFET (17).

The electronic load method is an automated process that uses a MOSFET with a variable power supply to regulate the load applied to the PV panel. This method offers the advantage of being faster than the capacitor and resistor method and, in specific scenarios, more cost-effective than the capacitive load approach. However, it is primarily suitable for low to medium-power

applications due to the transistor's need to dissipate current, which can create additional electric resistance (50).

## Four-Quadrant Power Supply

A four-quadrant power supply method consists of a power source and four transistors. The transistor configuration is typically arranged in an H-bridge configuration, allowing energy consumption and delivery enabling bidirectional power flow.

Figure 25 shows the four-quadrant power supply scheme. There are three primary operating modes associated with this method (51):

- When V(t) exceeds the open-circuit voltage of the PV panel, and S1 and S2 are closed, the current is negative, and the voltage is positive, operating in the fourth quadrant.
- The I-V curve is traced in the first quadrant when V(t) is lower than the open-circuit voltage, and S1 and S4 are closed.
- In the second quadrant, a negative voltage is observed when S2 and S3 are closed, defining the photovoltaic operating point in this quadrant.
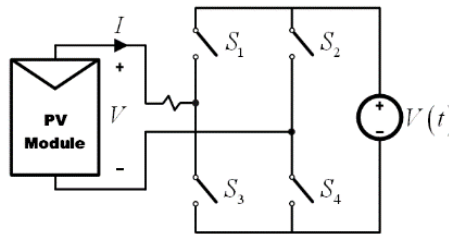


*Figure 25. Four-Quadrant Power Supply Scheme (51).*

The resultant I-V curve chart is shown in Figure 26.
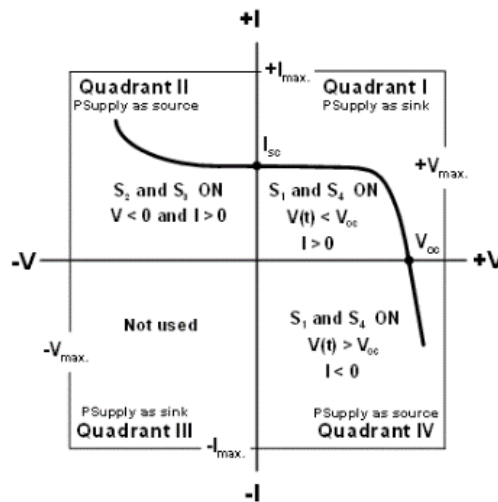


*Figure 26. I-V Curve Characteristic with Four-Quadrant Power Supply (51).*

With a computer control strategy implementation, the four-quadrant power supply becomes one of the most accurate and fastest methods for obtaining precise I-V curves from PV panels. Nevertheless, there is a limitation to utilising this method in laboratory experiments, mainly stemming from the high cost and the substantial space needed for the required components (17).

## DC-DC

The most comprehensive method for measuring characteristic curves involves using DC-DC converters. These power electronic circuits contain storage elements, filters, diodes, resistors, and switches. These circuits modulate the triggering signal of the associated switch to vary the voltage from the power source and thus trace the I-V curve. DC-DC converters can change polarity by adjusting the DC voltage, enabling a more versatile and accurate measurement process.

There are mainly three kinds of DC-DC converters: boost, buck and buck-boost converters. Boost converters are typically used to elevate the voltage of a power source. Still, they are limited in their ability to simulate more minor resistance than the load, making it challenging to approach values close to the $I_{SC}$. Buck converters are employed to reduce the voltage of a power source but cannot effectively emulate higher resistance than the load, thus not reaching values near $V_{OC}$. Buck-boost converters can trace the entire I-V curve from the $I_{SC}$ to the $V_{OC}$ (52).

The circuit design of the book, buck and buck-boost converters are shown in Figure 27, Figure 28 and Figure 29.
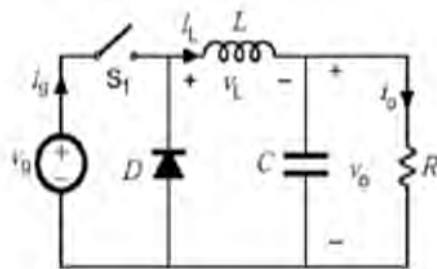


*Figure 29. DC-DC: Buck Converter Scheme (53).*
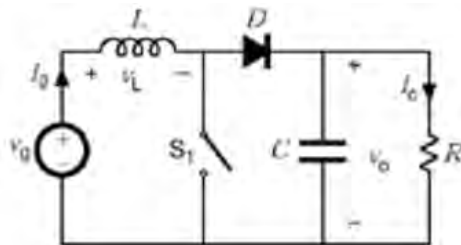


*Figure 28. DC-DC: Boost Converter Scheme (53).*
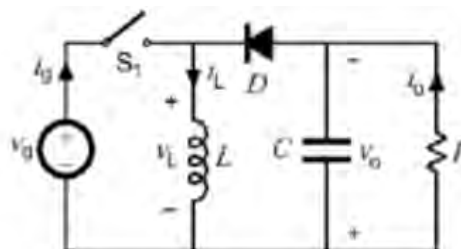


*Figure 27. DC-DC: Buck-Boost Converter Scheme (53).*

The main essential parameters which describe the DC-DC converter's behaviour are (53):

- The duty cycle (δ) is the relation between the commutation time (TC) and the conduction time (TO).
- The input resistance of the converter ($R_i$).
- The converter inductance (L).
- The load resistance ($R_L$).

DC-DC converters can configure the speed and direction of the sweep, having high flexibility. In terms of modularity, an expansion of the system is possible by connecting more converters in parallel. The DC-DC is the most reliable method despite working in a high-speed sweep. Due to the DC-DC converter's flexibility, modularity and reliability, the system is less expensive than other methods (51). The main disadvantage is the noise created during the measurement because of the commutation of the internal elements, such as the transistor or the inductor (50).

## Discussion

Table 1 summarizes the various methods for measuring the I-V curve focusing on the key characteristics to aid in selecting the optimal option (51).

*Table 1. Characteristics of the different methods(51).*

|  | Flexibility | Modularity | Fidelity | Fast Response | Direct Display | Cost |
|---|---|---|---|---|---|---|
| **Variable Resistor** | Medium | Medium | Medium | Low | No | Low |
| **Capacitive Load** | Low | Low | Medium | Low | No | High |
| **Electronic Load** | High | High | Medium | Medium | Yes | High |
| **4 - Quadrant Power Supply** | Low | Low | High | High | Yes | High |
| **DC-DC Converter** | High | High | High | High | Yes | Low |

Although the DC-DC converter method seems to offer the highest effectiveness, it frequently requires equipment that might not be readily available in a laboratory setting. Given the constraints of laboratory equipment, the electronic load method emerges as the top choice. It offers notable advantages regarding flexibility and modularity in the experimental process.

### 2.4.1.2 Dark I-V Curve Measurement

Dark I-V curve measurement is a standard method to evaluate PV panel performance (54). To implement the dark I-V curve measurement a power supply have to be connected to the two electrical terminals (+, -) of the PV panel in direct polarization. This configuration allows to perform a voltage sweep, where the voltage provided by the DC power supply is increased from zero to $V_{OC}$ with a simultaneous current and voltage measurement (54).

The dark I-V curve method should be implemented in a dark environment to eliminate the current generated by irradiation. For this purpose, the entire surface of the PV panel should be covered or the test should be performed in a dark environment. Moreover, regarding environmental conditions, the dark I-V curve measurements are performed at a temperature of 25ºC to be compared with the light I-V curve under STC (54).

The measured data points from tracing the dark I-V curve should be plotted on a graph to be compared with the I-V curve of the PV panel, as shown in Figure 31. Moreover, the current can be plotted in logarithmic scale, Figure 30, where the shunt resistance and the shunt resistance of the PV panel can be analysed (54).
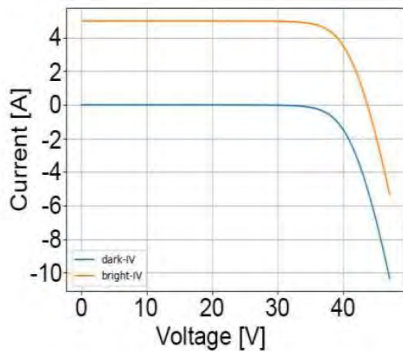


*Figure 31. Comparison between Dark I-V Curve and I-V Curve (54).*
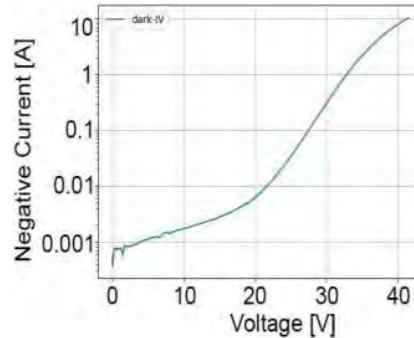
*Figure 30. Dark I-V Curve in logarithmic scale (54).*

The Dark I-V curve measurement can be used to determine the four key photovoltaic cell parameters: the saturation current, the series resistance, the ideality factor and the shunt conductance. These parameters are used to estimate the quality of the junction and the grid and contact resistances of the photovoltaic cell. There are three techniques that are used to calculate these key photovoltaic cell parameters: the modified Gromov method, the simple conductance method, and the derivative AC method (55).

During the test, the fast sweep times can provoke problems with highly capacitive cells. Moreover, the shading of cells during the testing can lead to heat dissipation in certain parts of the module. This may cause damage to the bypass diode within the module.

Table 2 illustrates the degradation modes that can be identified through dark I-V measurements in PV module and PV string levels.

*Table 2. Detection failure possibilities with dark I-V curve (54).*

| Type of Failure | PV Module Level Dark I-V | PV string level Dark I-V |
|---|---|---|
| Series Resistance | Easy | Easy |
| PID | Easy | Easy |
| Cracked Cells | Possible | Difficult |
| Shorted Byppas Diodes | Easy | Easy |
| Open Byppas Diodes | Possible, reverse voltage | Possible, reverse voltage |
| ISC Mismatch | Impossible | Impossible |

### 2.4.1.3 Electroluminescence

Electroluminescence imaging is a common technique used for analyzing defects in PV panels. In this method, a direct polarization electric current is applied to the photovoltaic cell, causing the cell to emit infrared light. This emitted light can then be captured by a CCD camera or a similar device for further analysis (56). As is reported in the 60904-13 standard by the IEC, EL imaging is commonly performed at module temperatures between 20 and 30ºC  (57).

The PV panel under study is typically supplied with a DC voltage able to achieve the $I_{sc}$ and $V_{oc}$ of the PV module in a dark environment (58). But there are also recent studies where outdoor testing in daylight conditions has been made with coherent results with the introduction of shrouds to cover the module or with cameras able to work in a nearly dark environment such as sunset (59).

This forward bias electric current supplied by the DC load is visualised with a camera sensitive to the emission spectra of the analysed material (58). The key specification for an EL camera for a crystalline silicon solar module is the emission spectra, which peak at 1150 nm (60). The charge-coupled device (CCD) is a camera which tends to be the most popular for this purpose due to its relatively low cost and high resolution (61). To improve the image resolution, two images are captured. The first image is when there is a forward bias current through the PV module, and the second is without a current supplied (62). The second image is subtracted from the first to eliminate the camera's dark signal and reduce external light dependence.  The camera should take the pictures perpendicularly and close to the PV module as shown in Figure 32.
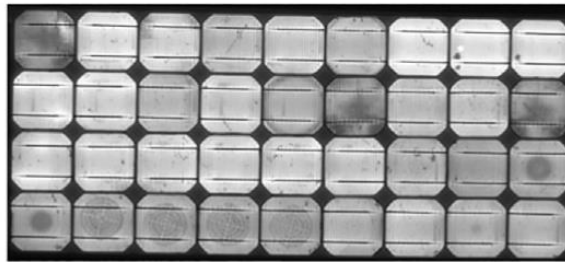


*Figure 32. Electroluminescence image of a PV panel with defects (62).*

Electroluminescence imaging is a valuable technique for qualitative analysis in the PV industry, as it enables the detection of various types of defects and irregularities within PV cells and panels. Electroluminescence implementation has successfully detected various issues within the metal grid of the PV cell, microcracks, potential-induced degradation (PID), shunts between the base and emitter, as well as disruptions in interconnection(63).

In addition to employing the electroluminescence method for detecting failures during the operation and maintenance stage, capturing images of the PV modules before installation would ensure they are delivered correctly.

### 2.4.2. Degradation modes of PV panels

The degradation of PV modules can be aggravated by the appearance of common defects, which can be defined as degradation modes. The module efficiency and the identification of degradation modes are crucial parameters that play a significant role in determining the lifespan and reliability of PV systems.

According to the National Renewable Energy Laboratory (NREL), Figure 33, the common degradation modes are hot spots, ribbon discolouration, glass breakage, encapsulant discolouration, cell breakage, and potential-induced degradation (PID) (64).
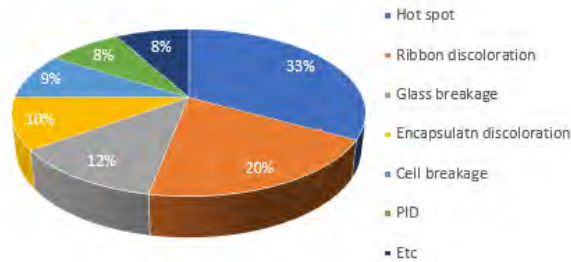


*Figure 33. Common degradation modes in PV modules during the last 10 years.*

The degradation modes can be categorised into three stages:

- Infant-failure
- Midlife-failure
- Wear-out failure

The graphical view of PV panel degradation modes is shown in Figure 34. The contact failure in the junction box, string interconnect failure, loose frame and glass breakage are infant-failures. These failures are provoked during the first months of the installation due to the transport process, installation process or default manufacturer design. In the midlife-failure, the most common failures are PID, diode failure, and cell interconnect breakage. The EVA discolouring, cracked cell isolation, and delamination are considered wear-out failures, starting the degradation in the infant-failure stage and increasing the degradation until the end of the module lifespan (65).
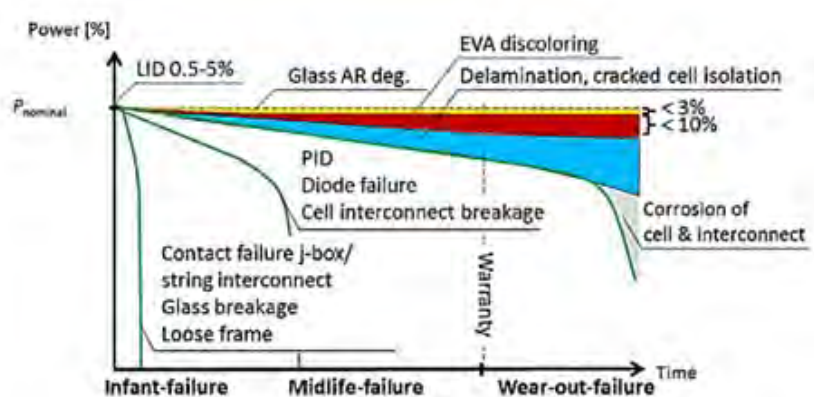


*Figure 34. Degradation Modes Effects during PV Panel Lifespan (64).*

The principal degradation causes are high humidity, extreme temperature, wind, ultraviolet radiation, high system voltage, hail, and corrosion or broken interconnects. The causes of degradation in PV panels differ based on the installation location (66).

In the following subsections, the causes and effects of the methods are explained in more detail, as well as which characterization method to implement to correctly detect the defect.

### 2.4.2.1 Hot Spot

A hot spot is one of the most common modes of degradation in PV panels. Partial shading, cell mismatches and diode failures cause this defect, in which a reverse bias is created and the affected cell dissipates energy, reaching high temperatures (67).

A hot spot is considered when a cell point reaches over 60°C. If the temperature surpasses 100°C, it exceeds the acceptable temperature limit for PV panels, potentially creating a hot spot that could ignite and cause a fire, as shown in Figure 35 (65). Bypass diodes are usually used to prevent hot spot phenomena (68).



*Figure 35. Hot spot in a PV Panel Surface (67).*

In large-scale PV systems, the preferred method for identifying hot spots involves the application of infrared thermography. This method can obtain thermal images of the PV panels under inspection. A wide range of colours represents different temperatures.

In Figure 36, an example of IR thermography is shown. IR thermography is an easy and non-destructive way to identify hot spots (69). The location, number of hot spots and temperature gradients can be determined with this method (70).
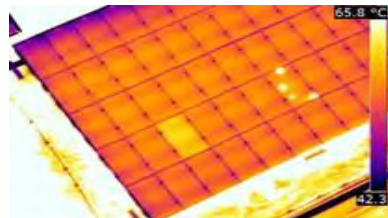


*Figure 36. IR Thermography on PV Panel to Identify Hot Spot (70).*

### 2.4.2.2 Partial Shading

PV facilities are expected to have partial shading (71). This phenomenon happens when one or more PV cells are shaded and less irradiated than others connected in the same array.

There are two types of partial shadows. The permanent partial shading condition (PSC) rises when the shadow remains extended, such as shadows caused by a tree or adjacent buildings. The most critical scenario occurs when shaded cells operate under reverse bias conditions, leading to the hot spot phenomenon. On the other hand, temporal PSC gives rise when the shading disappears quickly, such as the shadow caused by clouds or birds, where the effects are negligible.

A photovoltaic cell within a PV substring becomes a power consumer when there is a difference of approximately 20% in the incident light compared to the rest of the interconnected PV substring. When such a difference exists, the bypass diode of the substring is activated. However, the hot spot due to partial shading may still occur despite a bypass diode with a possible leakage current loop appearance (72).

An experimental test reported by the IET Renewable Power Generation in 2021 showed different shading situations and their results (73). Figure 37 shows the standard cell configuration in a PV module with the implementation of three bypass diodes. The black cell is shaded in different irradiance levels to know the effect of this on the whole system. The P-V curve resultant chart of
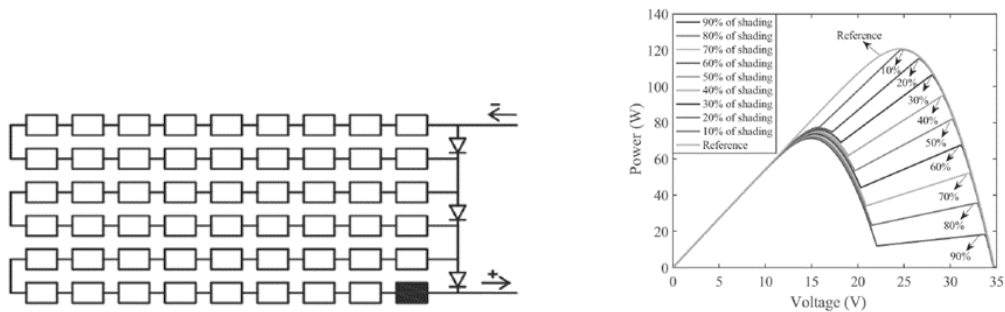



*Figure 37. PV Panel Configuration with a Cell Shaded (73).*   *Figure 38. P-V Curve with Different Shading Levels (73).*

a module with a cell shaded is shown in Figure 38.

The temperature is measured during the test performance to prevent hot spots. As we can see in Figure 39, the temperature is measured from 10% to 90% shading. With 10% shading, the cell temperature can remain at 40ºC for hours. However, with 80% of shading level, the cell temperature can reach 105ºC at 2 500 seconds (73).

### 2.4.2.3 Diode Failure

Failures in bypass diodes frequently cause substantial power losses in PV modules. Defective diodes have the highest risk priority among the degradation modes regarding safety and performance (74).

The bypass diode's primary function is to protect the PV module from current mismatch and significant reverse bias. The current mismatch can occur with nonuniform radiation between modules connected in the same string, partial shading or hotspots.

In recent studies, bypass diode degradation was defined as the highest single factor providing a
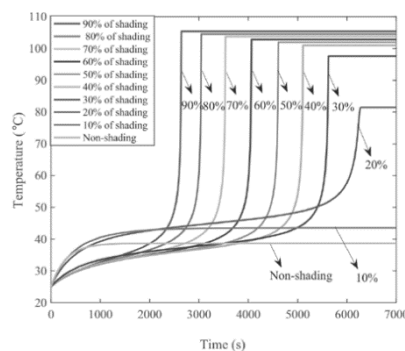


*Figure 39. Temperature Evolution with Different Shading Levels (73).*

higher power loss per year, 11% in hot and dry climates and 25% in moderate temperatures (75). The bypass diode failure can have a power loss influence in different ways (76):

- Short circuit the cells of the substring in the module that should protect with a loss of one-third of the module power.
- Diode bypass failure in an open circuit forces reverse bias flowing through the cells and modules in series connection when shaded.

- Hot spot, module breakage and possible fire.

The different reported external causes of diode bypass failure involved externally applied stress, thermal runaway, lighting strikes, or long-term overstress in forward bias. Furthermore, impurities and crystalline defects may lead to losses.

The effect of the diodes in shading conditions is essential to have a higher PV performance. In Figure 40, three PV panels are evaluated in five different scenarios. Implementing bypass diodes leads to a P-V curve with multiple power peaks, enhancing the overall performance of the PV installation. The maximum power dropped from 600 W to 440 W (one module shaded) and 300 W (two modules shaded) respectively (77).
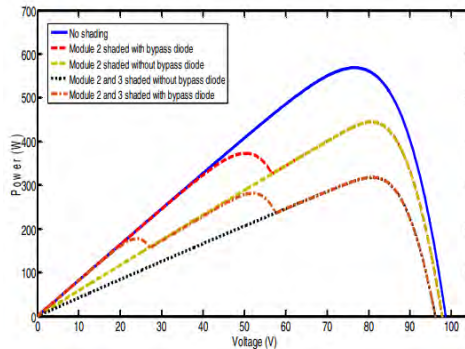


*Figure 40. P-V Curve: Bypass Diode Effect in Shading Conditions (77).*

### 2.4.2.4 Cell Mismatch

A cell mismatch is defined as a difference in the electrical characteristics of the installed PV panels. Photovoltaic cells are the elements that should be studied in detail. Industry research has defined mismatch values ranging from 0.01% up to 3%, depending on the string configuration and length of the strings.

Cell mismatch faults can be classified into different categories depending on the mismatch's time. The temporary mismatch is provoked by partial shading or temperature variation. The PV module can recover the initial behaviour without any permanent defect. The permanent mismatch is caused by soldering, degradation and hot spots. In this case, the default will be present for the remaining PV module life span (78).

Relative power loss (RPL) is a concept to calculate the electrical mismatch loss. RPL quantifies the discrepancy between the maximum power generated by individual cells, connected in series to form a PV module or string and the actual output power of that PV module or string (79).

In a recent study, a comparison was conducted between the condition of a PV panel with cell mismatches and the state of the PV panel after the cells were repaired. The electroluminescence image of the PV panel evaluated (a) before and (b) after the repair is shown in Figure 42.
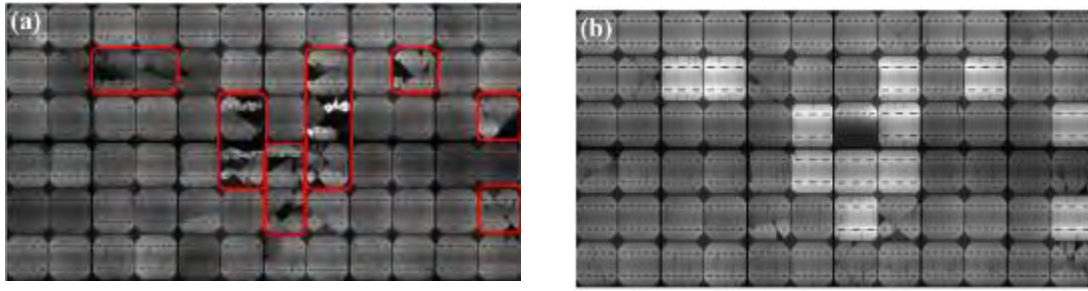
*Figure 42. EL Image (a) Before and (b) After the Repair (79).*

In both scenarios, the I-V and P-V curves were traced to illustrate the impact of cell mismatches. The I-V curve exhibits a characteristic stepped shape due to cell mismatches, shown in Figure 41. In the P-V curve, the mismatch results in the emergence of two peaks (79).
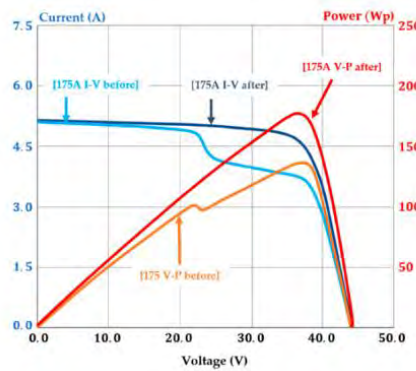


*Figure 41. I-V and P-V Characteristic Curves Before and After the repairment (79).*

Figure 43 illustrates that the power output is insignificant when the mismatch ratio exceeds 50%. With higher mismatch ratios, the power output difference increases rapidly (79).

### 2.4.2.5 Breakages and Cracks of PV Modules



*Figure 43. Chart of the Different Rates Compared to the Electrical Mismatch Ratio (79).*

In most cases, glass breakage defect occurs during the transportation, installation, and maintenance of modules. This defect typically does not directly lead to direct power degradation when using PV modules with EVA encapsulation to protect the PV cells (80). This defect increases the risk of electrical shock and moisture ingress, which can, in the long term, lead to other degradation modes such as corrosion, discolouration and delamination (81).

In recent years, to cut down on manufacturing costs and silicon usage, PV module thickness has been reduced, rendering the cells more delicate and prone to breakage, with a reduction from 330 μm to less than 100 μm in some cases (82). In addition, the cell surface has been increased too.

Generally, the only way to detect glass breakage and cracks is by using optical methods (83). Electroluminescence is the best method to identify cell cracks in a PV module (80). An example of cell cracks detected by electroluminescence is given in Figure 44.
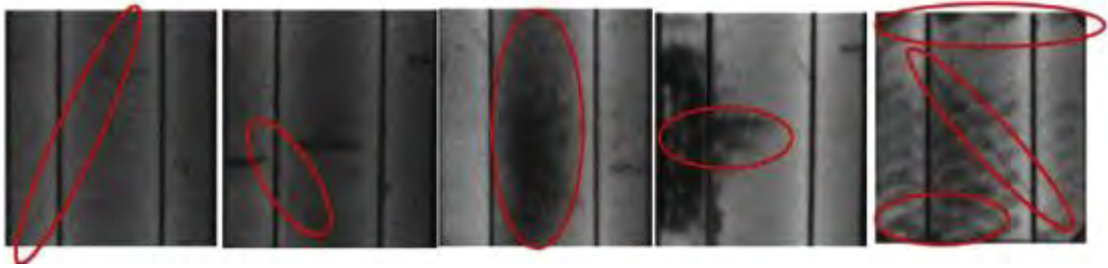


*Figure 44.Cell Cracks Detected by Electroluminescence (80).*

### 2.4.2.6 Potential Induced Degradation

In most PV installations, PV panels are connected in series to achieve a heightened voltage output. The module frames should be grounded as a safety precaution. The absence of a proper module frame ground can result in significant electric potential differences between the PV cell and the PV frame, potentially causing leakage currents from the PV cells to the PV panel frame or vice versa (84).

The most common leakage current path is through the surface of the front glass and the encapsulant (84). The surface conductivity of the front glass increases under high humidity and rain conditions (85). This phenomenon is defined as potential induced degradation, PID, and can lead to undesirable failures when the PV modules are exposed to outdoor conditions (86). The leakage current may be responsible for electrochemical corrosion (87), delamination (88) or breakdown of the original surface passivation (89).

Many factors influenced PID effects, such as the encapsulation materials (86), module construction (90) or the solar cell antireflective coating (91). Environmental stress (92), grounding conditions of the glass (93) and exposure to light influence PID development (94).

The electroluminescence image of a PV panel exhibiting PID and the corresponding I-V curve of cells with varying degrees of degradation are presented in Figure 46 and Figure 45.  PID effect is associated with a reduction of the parallel resistance ($R_P$) and a minor degradation of $I_{SC}$ (95). Both values defined before, $R_P$ and $I_{SC}$, decrease while $V_{OC}$ remains unaffected at first. The $V_{OC}$ degradation is a secondary effect of the $R_P$ reduction.
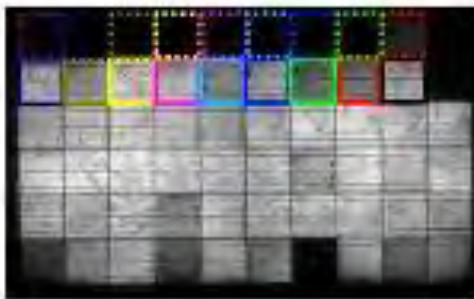


*Figure 46. EL image of PID affected module (95).*
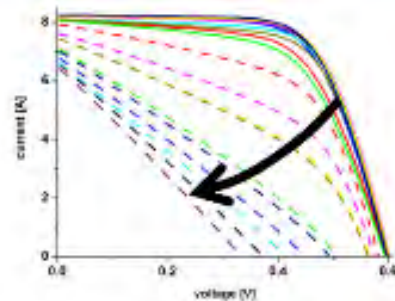


*Figure 45. I-V curve of individual cells degraded to different PID degrees (95).*

There are different methods to analyse PID at the PV panel level. The most common are the climate chamber PID testing and the PID testing with a conductive layer on top of the front glass. At a cell level, corona discharge assembly can be implemented (84).

### 2.4.2.7 Other Failures

Junction box failure, discolouration, corrosion and delamination are other failures that can appear in a PV module. All of these exhibit a degradation evolution over time unless junction box failure, which can potentially appear within the first three years of the PV system installation (96).

Many of the junction box failures are caused during the installation process (96). The primary failures in the junction box include inadequate securing, open or unsealed junction boxes, moisture penetration in the interconnections, and subpar wiring connections (75). These failures are depicted in Figure 47.



*Figure 47. Junction Box Failures. a) Open JB b) Poor fixing JB c) JB with Poor Wiring (75).*

Discolouration and delamination occurring in the encapsulant of the front glass, cells, back sheet, or the interconnecting ribbon are widespread failures in PV systems (97). In Figure 48 a) is shown a delamination around the PV cells while in b), a discolouration of the encapsulants. The concern of these phenomena is that they may create a void within the modules that can give rise to a suitable reservoir for gas accumulation and moisture (98). A 2013 study observed that discolouration and delamination caused a reduction in ISC and resulted in a power loss of approximately 18% in the PV modules compared to their initial value in the 25th year of installation (99). In a hot and humid climate, delamination is more common.
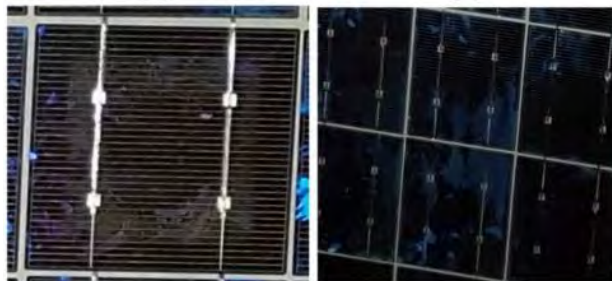


*Figure 48. a) Delamination around PV Cells. b) Discolouration of Encapsulants (97).*

Moisture ingress into the module through the lamination edges can lead to corrosion within the PV module (81). Corrosion attacks the metallic connections, causing performance loss and a deterioration of the adhesion between cells and the metallic frame (81). In Figure 49 is shown a corrosion attack in the edge and in the junction box.



*Figure 49. Corrosion of the a) Edge and b) Junction Box (81).*

# 3. PV System Simulator

The PV system simulator will be used to monitor, collect data and evaluate the performance of any PV installation. The system's remote access, flexibility and scalability make it very useful to be used as a training centre for students and industry professionals.

This PV system simulator will enable the evaluation of PV panels under different irradiance levels. The irradiated surface of the PV system simulator measures 1 meter in width and 2 meters in length, which provides limited space for the installation of PV panels. The system's restricted quantity of PV panels is not problematic since PV energy generation is scalable.

The system should be designed to implement different PV panel configurations, such as in series or parallel connections. In addition, the PV remote laboratory should be able to execute the proposed characterisation methods. All of which should be automated and remotely accessible.

The PV remote laboratory will consist of the following components:

- Six PV Panels
- DC/AC Inverter
- MPPT and PWM
- DC Power Supply
- DC Load
- Commutation Block

The number of PV panels and components is very limited. However, with the study and analysis of the PV panels available and with the different configurations proposed through the commutation block, any PV installation may be evaluated independently of the size and design.

The flowchart of the working path followed during the PV system simulator design is presented in Figure 50.
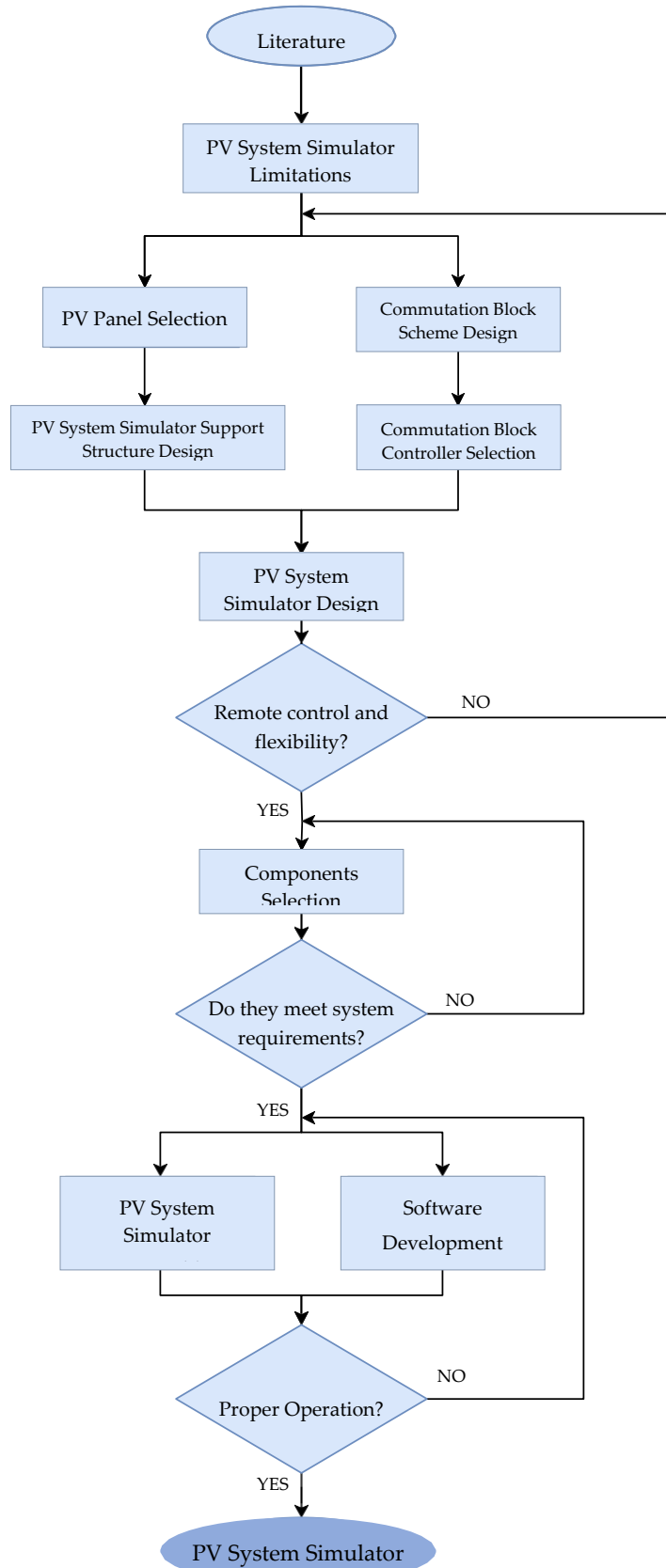


*Figure 50. Flowchart for PV System Simulator.*

## 3.1. PV Panels

Three distinct models of PV panels have been chosen for this project. The main parameters of the selected PV panels are shown in Table 3. PV Module Characteristics.

*Table 3. PV Module Characteristics.*

|  | SunPlus 100 | SunPlus S 50 | STP0309 |
|---|---|---|---|
| Maximum Power, Pmp | 100 W | 50 W | 30 W |
| Current at max power (Imp) | 2.78 A | 2.84 A | 1.15 A |
| Voltage at max power (Vmp) | 36 V | 17.6 V | 17.5 V |
| Short-circuit current (Isc) | 3 A | 3.07 A | 1.27 A |
| Open circuit voltage (Voc) | 43.2 V | 21.6 V | 22 V |
| Cells number \| type | 72 \| poly | 36 \| mono | 36 \| mono |
| Cell efficiency | 17.2 % | 18.4 % | 17 % |
| Module efficiency | 13.6 % | 15.2 % | 15.2 % |
| Surface | 734 x 1 001 x35 mm | 650x505 mm | 660x380x25 mm |
| Weight | 8.1 kg | 4.8 kg | 2.8 kg |

\*Standard Test Conditions: $T_a$ of the cell 25 °C, Irradiation 1 000 W/m2, Spectrum AM 1.5

Additional information about the PV panels can be found in their respective datasheets, located in **Appendix 3 – Components Datasheet**.

## 3.2. PV System Simulator Support Structure

The PV system simulator's support structure positions the PV panels and all the system's components. This design approach enables the entire assembly's mobility as a unified unit, achieved using wheels at the base.

The support structure of the PV remote lab is displayed in Figure 52. The base frame of the support structure frame is constructed of aluminium bars and features a rectangular shape with dimensions of 2.7 meters in length and 0.8 meters in width. Aluminium bars are installed on the base frame to support the PV panels in the desired configuration.
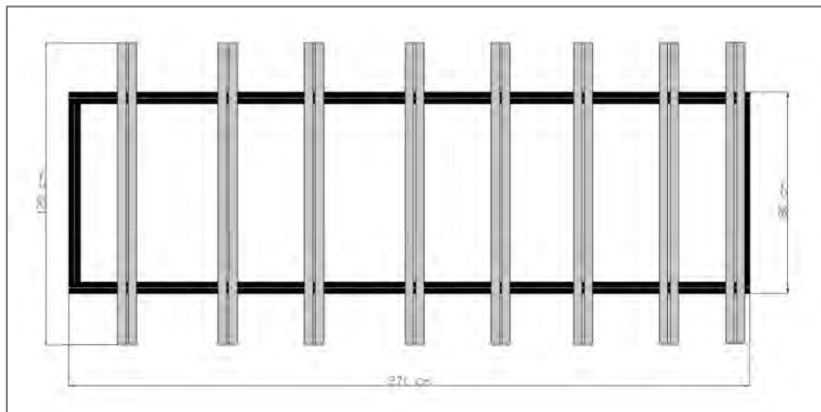


*Figure 52. PV System Simulator Support Structure.*

The PV system simulator is designed to provide an irradiated surface of 1 meter in width and 2 meters in length (2 m²). With this irradiation area, it's not feasible for the installed PV panels (2.62 m²) to receive total and direct irradiation.

Two different designs, the "Rotative design" and the "Overlapping design," have been proposed to address the issue.

### 3.2.1. Rotative Design

The rotative design encompasses the installation of all six PV panels on a rotating frame base, which can be pivoted to position all PV panels within the irradiated area. The PV panels installed will not have any modification regarding their position during the implementation of the distinct scenarios. This design provides two scenarios.

The first scenario aims to study all the PV panels except one, which has a capacity of 100 W. As depicted in Figure 53, the irradiated surface, indicated by the yellow square, encompasses the five defined PV panels.
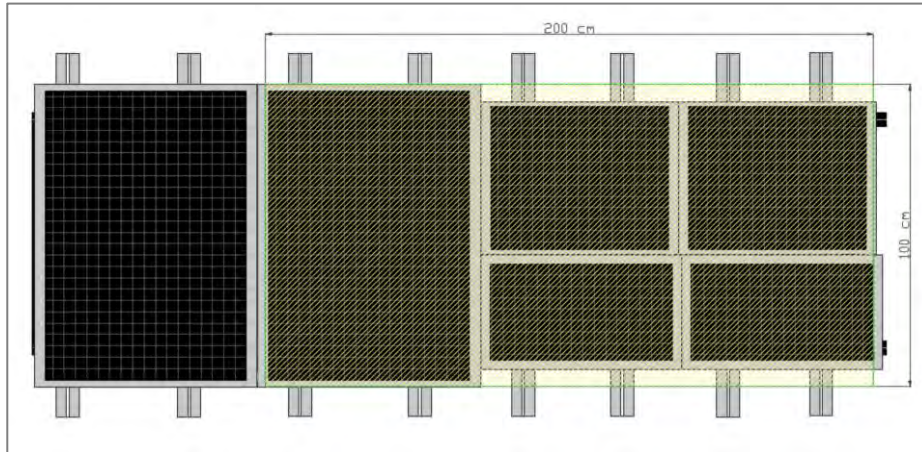


*Figure 53. Rotative Design: Scenario 1.*

In the second scenario, both PV panels with 100 W of power can be under analysis. As shown in Figure 54, the irradiated area covers both PV panels completely.
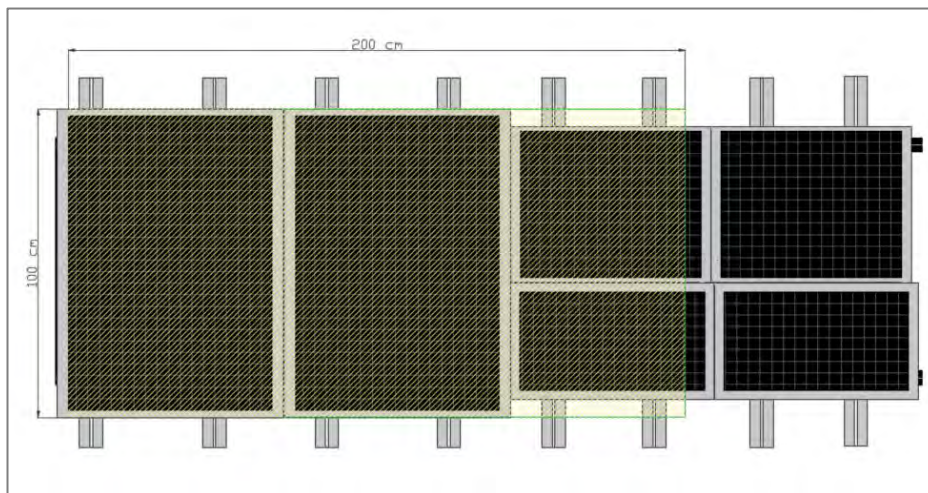


*Figure 54. Rotative Design: Scenario 2.*

### 3.2.2. Overlapping Design

This design entails the installation of five PV panels, with one having a capacity of 100 W. The remaining PV panel also rated at 100 W, can be evaluated by installing it over other already installed PV panels. The support structure does not have to be displaced. This design provides two scenarios.

As shown in Figure 55, evaluating 30 W PV panels, 50 W PV panels, and one of the 100 W PV panels simultaneously is feasible.
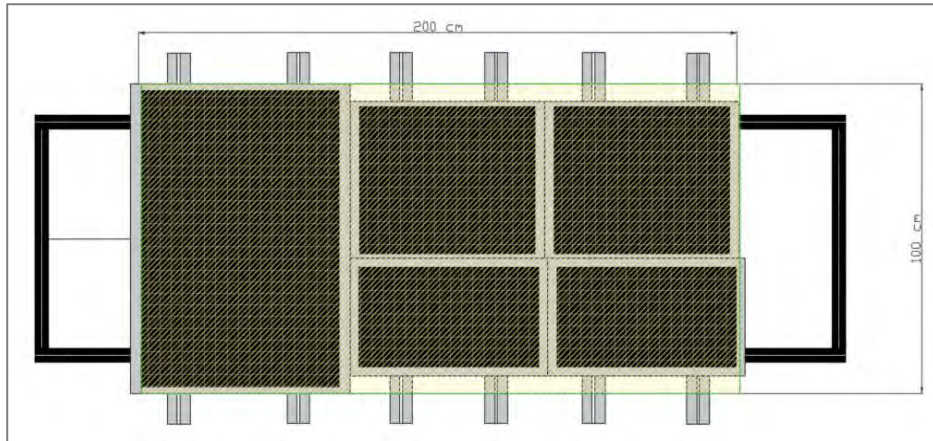


*Figure 55. Overlapping Design: Scenario 1.*

In the second scenario, as depicted in Figure 56, it is possible to study the behaviour of two 100 W PV panels. A second rack should be installed above the first to achieve an equal and uniform irradiation spectrum for both PV panels. This design allows for space on both sides of the support structure to accommodate the remaining components of the PV remote lab.
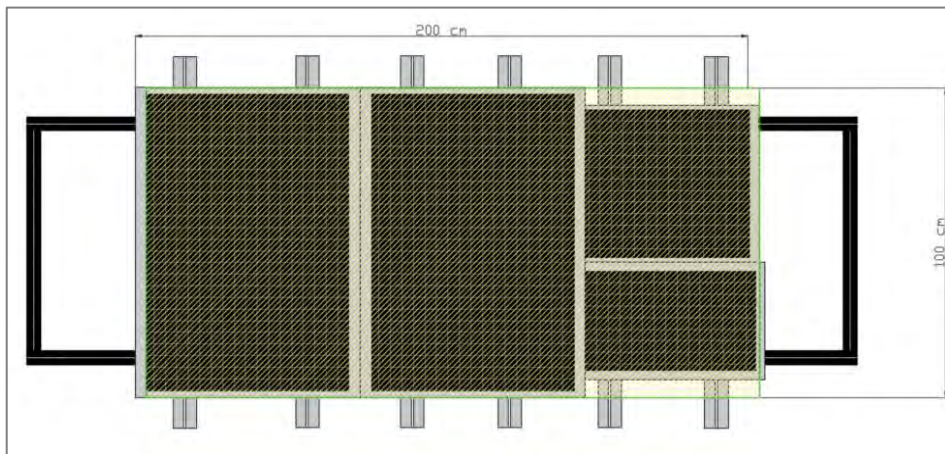


*Figure 56. Overlapping Design: Scenario 2.*

### 3.2.3. Support Structure Design Selection

The selected design for the PV system simulator is the Overlapping Design. This configuration enables the installation of all components of the PV remote laboratory in the support structure and allows for the assessment of numerous PV panel configurations. It offers a compact unit and configuration flexibility while considering the constraints of the PV system simulator.

## 3.3. Double PV String Commutation Block Scheme

A commutation block has been designed to dynamically evaluate different PV panel configurations by implementing the required characterisation methods. The commutation block is designed to automatically execute predefined scenarios, eliminating the necessity for manual adjustments, except when the second 100 W PV panel is evaluated.

The different scenarios defined will correspond to different PV panel configurations (series, parallel, etc.) and the application of different outputs (DC load, DC power supply, etc.) to allow the implementation of characterisation methods. The system will consist of two PV strings, allowing for the simultaneous evaluation of two different configurations of PV panels under the same environmental conditions (temperature and irradiation). Each of the PV strings will have its respective outputs. During the design process, two parts of the commutation block have been differentiated to simplify the defined scenarios. These parts are defined as:

- Commutation block of the PV system    - Commutation block of the system outputs

The commutation block of the PV system encompasses the PV panels and the necessary components to implement PV configuration changes. PV panels are listed to simplify their identification.

- STP0309 (30 W) → 01. 30 W                 - SunPlus S50 (50 W) → 04. 50 W
- STP0309 (30 W) → 02. 30 W                 - SunPlus 100 (100 W) → 05. 100 W
- SunPlus S50 (50 W) → 03. 50 W             - SunPlus 100 (100 W) → 06. 100 W

The outputs' commutation block includes the components for implementing the characterisation methods. The different outputs of the PV simulator are:

- DC load                                   - Inverter
- DC power supply                           - Solar charge controllers

DC load enables the I-V curve method, whereby the complete I-V curve can be plotted by varying the resistance, current, or voltage. The DC power supply is used to carry out the dark I-V curve and the electroluminescence method. The other outputs of the system are the inverter for AC conversion and two different solar charge controllers, PWM and MPPT, for DC conversion. This setup enables a potential comparison between different solar charge controller technologies.

Both parts of the system operate independently, and the configuration of one does not affect the performance of the other. As a result, both systems are complementary and can be proposed separately, yet they can be simultaneously applied and adjusted as needed.

### 3.3.1. Commutation Block Scheme Design

The main goal of the commutation block scheme (CBS) design is to provide a system able to perform the desired scenarios using the minimum components.

- CBS Design of the PV System

In addition to the PV panels, the components in Table 4 are part of the PV String commutation block.

*Table 4. Double PV String CBS Components: PV System*

| | | |
|---|---|---|
| —o⁄ o— | Single Pole Single Throuhg NO | 30 |
| —o⁄ o— | Single Pole Double Through | 6 |
| —▷|— | Diode | 2 |

The electromechanical relays are selected to control the current flow through the different PV panels. The diodes are installed in the PV panels with 30 W to perform tests related to shadowing conditions.

The CBS design of the PV system is presented in Figure 57.
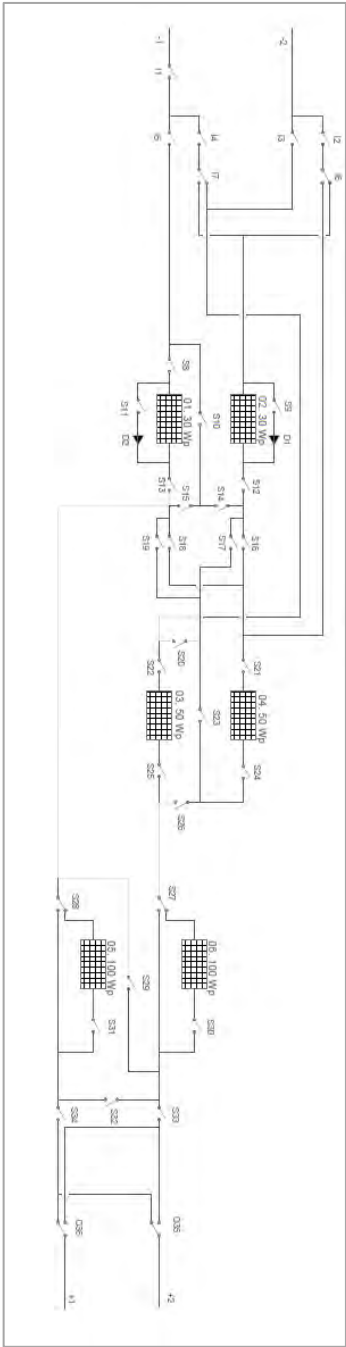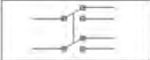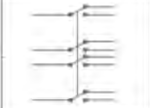


*Figure 57. CBS Design of the PV System.*

- CBS Design of the System Outputs

The components in Table 5 are installed in the commutation block of the system outputs.

*Table 5. Double PV String CBS Components: System Output.*

| | | |
|---|---|---|
| | Double Pole Double Through | 5 |
| | Four Pole Double Through | 2 |

The proposed system outputs will have eleven different outputs, as seen in Figure 58. The only difference between the two PV strings is the addition of a PWM solar charge controller in the first PV string. This will allow the MPPT and the PWM technologies to be compared simultaneously. The only component used in this part of the system is electromechanical relays, in particular, the following types:
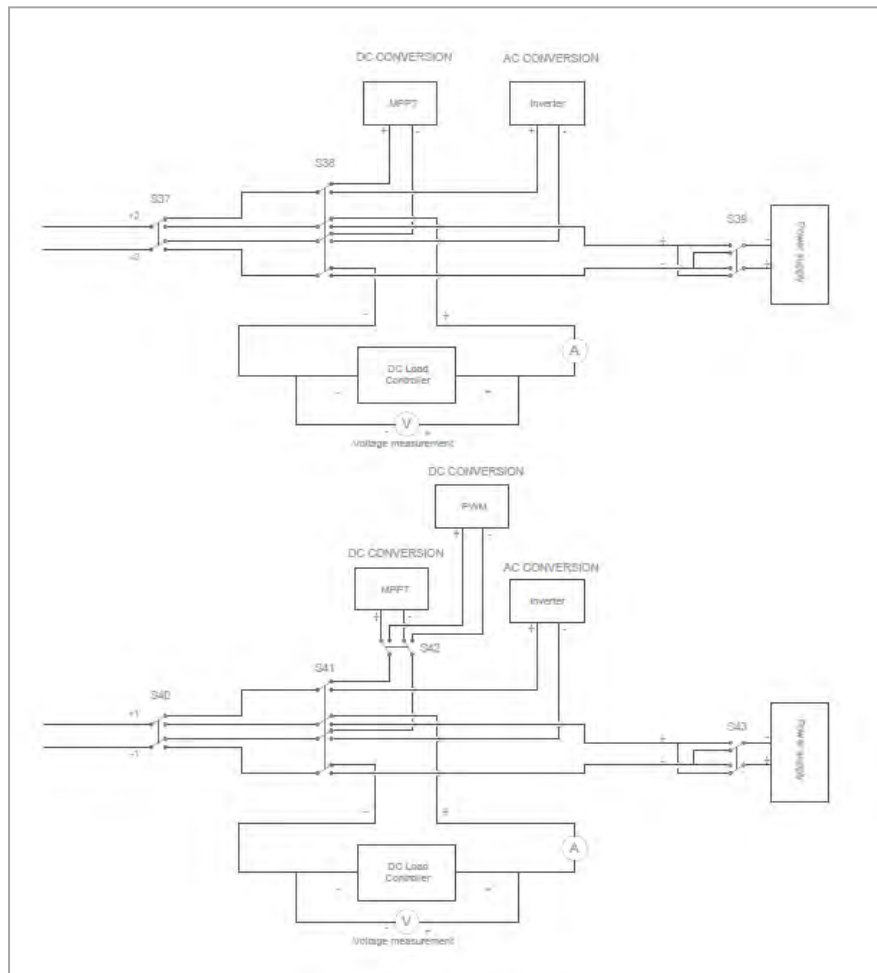


*Figure 58. CBS Design of Double PV String: System Outputs.*

- Complete CBS Design

The complete CBS design is presented in Figure 59.
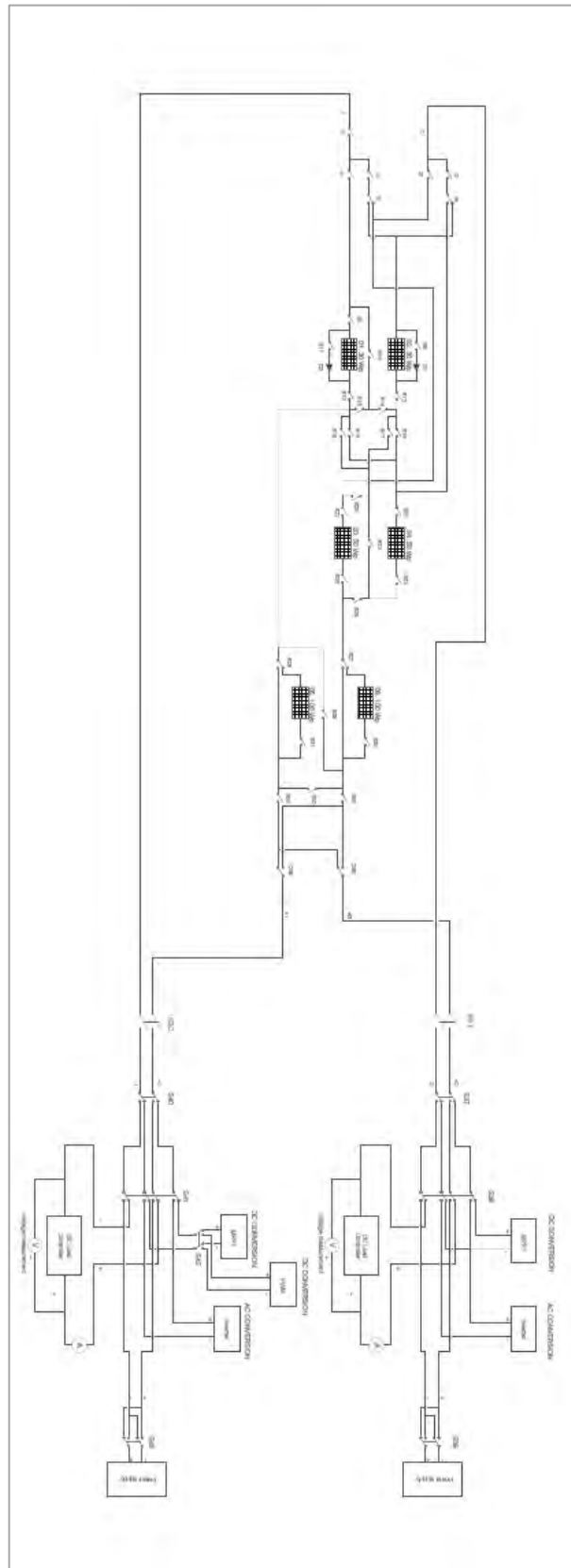


Figure 59. Complete CBS Design.

A contactor is installed in each string to regulate the current that flows through the PV strings and the outputs, ensuring the proper operation of both system parts.

### 3.3.2. Commutation Block Scenarios

The commutation block is designed to accommodate several scenarios relevant to the photovoltaic industry. The proposed design renders the PV remote lab highly flexible.

The scenarios of the two parts of the commutation block should be defined separately: the PV system and the system outputs. It should be remarked that both parts can be performed independently and are complementary.

- Commutation block scenarios of the PV system

The PV system scenarios refer to the scheme proposed in Figure 57.The total number of scenarios that can be performed in the PV system part of the double PV string commutation block rises to 41. These scenarios cover various PV panel configurations, including individual PV panels, series connections, parallel connections, etc. Most of them are scenarios that can be implemented in a PV installation, while others are designed to explain the electrical behaviour of the panels depending on the configuration.

Some examples of the scenarios that can be executed are presented in Figure 61 and Figure 60.
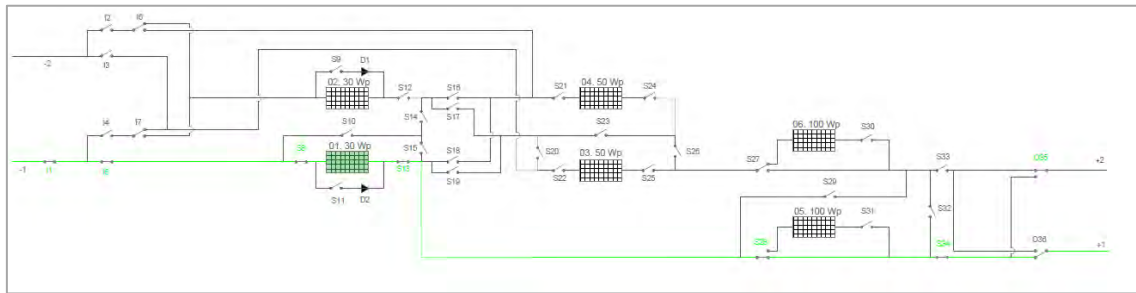


*Figure 61. Assessment of 01.30 W PV panel - PV String 1 (Scenario 1)*
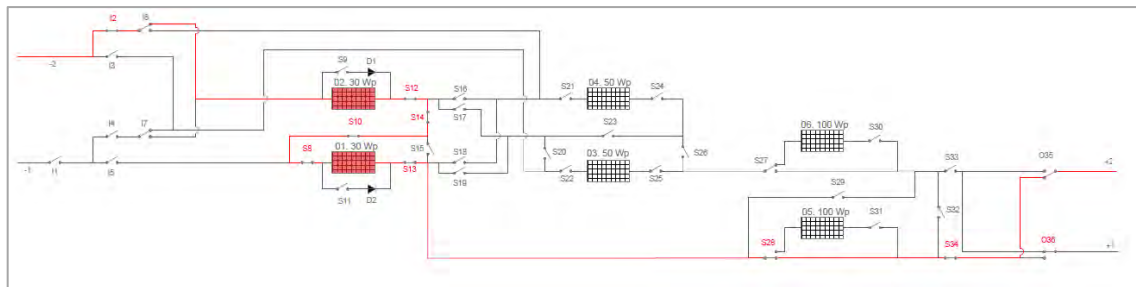


*Figure 60. Assessment of 01.30 W and 02.30 W PV panels – PV String 2 (Scenario 16)*

In **Appendix 1 – Scenarios Design of the Double PV String CBS**, the different scenarios drawings have been presented, showing for each scenario which relays should be closed and the resulting current circuit in the schematic. The schemes of this subsection are from Plan 2 to Plan 16.

A more detailed table with the definition of the PV panels under study, the PV string used, the configuration type, and the closed relays are attached in **Appendix 2 – Scenarios Configuration of the Double PV String CBS**.

- Commutation block scenarios of the system outputs

The system output scenarios refer to the proposed scheme proposed in Figure 58. The total number of scenarios that can be performed in the system outputs part of the double PV string commutation block rises to 11. These scenarios allow for implementing the I-V curve, dark I-V curve and electroluminescence method. Additionally, more tests can be performed with the inverter and solar charge controllers.

The scenarios that can be implemented in the first and second PV strings are defined in Table 6 and Table 7, respectively.

*Table 6. System Outputs - First PV String Scenarios*

|  | Proposed outputs – First PV String |
| --- | --- |
| *Scenario 1* | The PV system is connected to the MPPT - DC conversion. |
| *Scenario 2* | The PV system is connected to the PWM - DC conversion. |
| *Scenario 3* | The PV system is connected to the Inverter - AC conversion. |
| *Scenario 4* | The PV system is connected to the DC Load (I-V Curve method). |
| *Scenario 5* | The PV system is connected to the Power Supply (Dark I-V Curve and EL). |
| *Scenario 6* | The PV system is connected to the Power supply (Reverse Current). |

*Table 7. System Outputs - Second PV String Scenarios*

|  | Proposed outputs – Second PV String |
| --- | --- |
| *Scenario 1* | The PV system is connected to the MPPT - DC conversion. |
| *Scenario 2* | The PV system is connected to the Inverter - AC conversion. |
| *Scenario 3* | The PV system is connected to the DC Load (I-V Curve method). |
| *Scenario 4* | The PV system is connected to the Power Supply (Dark I-V Curve and EL). |
| *Scenario 5* | The PV system is connected to the Power supply (Reverse Current). |

The scenario when the MPPT is the output of the first PV string is presented in Figure 62.
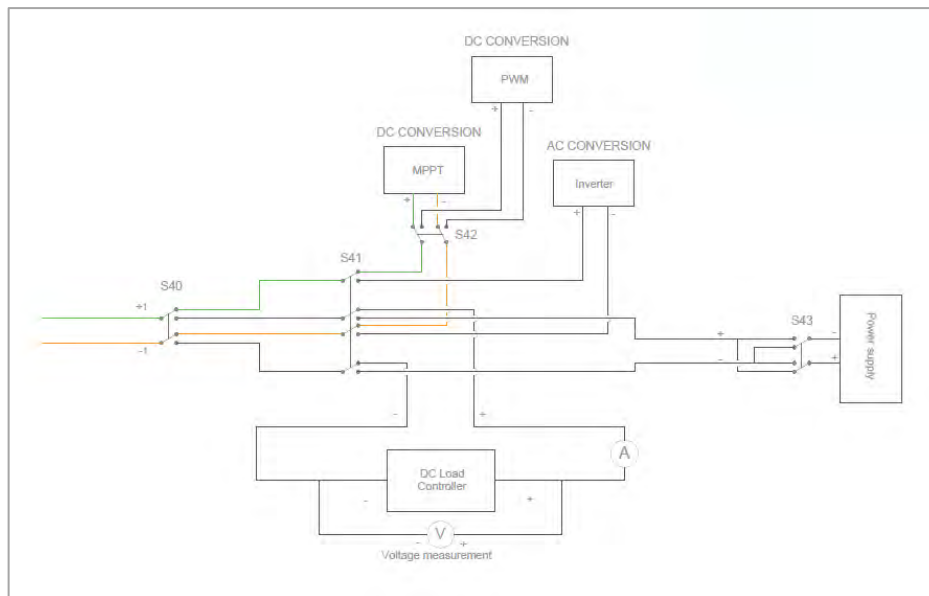


*Figure 62. First PV String – MPPT.*

**Appendix 1 – Scenarios Design of the Double PV String CBS** shows the current circuit scheme of the scenarios designed from Plan 17 to Plan 28. The closed relays and the final output implemented are defined in each scenario. A more detailed configuration table, where the outputs and the closed relays are defined in each scenario, is attached in **Appendix 2 – Scenarios Configuration of the Double PV String CBS**.

## 3.4. Commutation Block Controller

An Arduino should control the double PV string commutation block. The Arduino selected is the Mega 2560 microcontroller board. The Arduino Mega 2560 is chosen for its ample capabilities, offering 54 digital input/output pins and 16 analogue inputs, each providing a resolution of 10 bits. This Arduino model offers sufficient flexibility and control to effectively manage the double PV string commutation block.

The digital inputs/outputs of the Arduino Mega 2560 are utilised to control the system's electromechanical relays, contactors, and temperature sensors. The temperature sensors are connected to the Arduino by installing a digital communication cable (1 wire) to a digital input/output of the Arduino, which allows for connecting more than 20 sensors per line. To ensure the isolation and protection of the microcontroller board, a relay module will be implemented between the Arduino and the digital components connected.

Current and voltage sensors are connected to the analogue inputs of the Arduino. Eight analogue inputs will be dedicated to current measurements. The remaining eight will be used for voltage measurements. This approach allows precise monitoring.

The irradiance sensor will be directly connected to the computer thanks to the Modbus communication protocol implemented in the sensor.

A 5V and 24 V power supplies are used to power the system components. The 5V power supply provides the required energy to the Arduino Mega 2560 and the Channel Relay Module to operate effectively. The 24V power supply is connected to the electromechanical relays and contactors. This higher voltage supply is required to properly energise and control these components, allowing them to switch and control the electrical circuits as needed.

The simplified connection scheme, as shown in Figure 63 of the application diagram, provides an overview of the essential connections within the system.
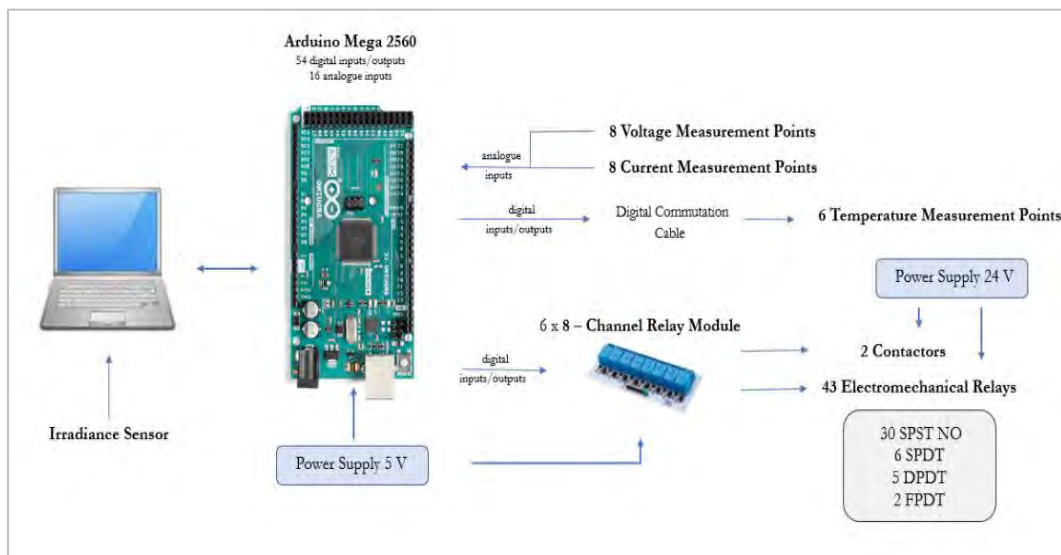


*Figure 63. Simplified Application Diagram for Arduino.*

## 3.5. Components Selection

The components that form the PV remote lab should be selected to accomplish the electrical parameters of the PV system. The components that need to have appropriate characteristics are:

- Electromechanical relays
- Contactor
- Bypass Diodes

- PV Branch Connectors
- Sensors
- Relay Module

### 3.5.1. Electromechanical Relays

The electromechanical relays play a crucial role in the commutation block switching on or off various system parts. They switch between the PV system scenarios or the system outputs scenarios previously defined.

Electromechanical relays consist of a coil, an armature mechanism, and electrical contacts, as shown in Figure 64. When the coil is energised, it generates a magnetic field that moves the armature, resulting in the opening or closing of the electrical contacts. The bidirectional relay covers the system requirements. However, it's important to note that electromechanical relays are generally slower than other relays. The switching and settling time for these relays typically range from 5 to 15 milliseconds.



*Figure 64. PCB Power Relay G2R-1-SNI.*

The key parameters necessary for sizing an electromechanical relay are:

- Contact configuration
- Coil rating

- Response time
- Switching capacity

All the relays used in the system will be based on a Single Pole Double Throw configuration. This choice ensures that all the relays in the system are the same model and have the same characteristics. Each relay will have a common terminal, a normally open terminal, and a normally closed terminal. The combination of multiple SPDT relays will form Double Pole Double Throw and Fourth Pole Double Throw relays. The total number of electromechanical relays needed in the system rises to 54 units.

The coil rating of the relay specifies the voltage needed to energise the coil and activate the contacts. A 24 VDC power supply has been designated to power the electromechanical relays.

The switching capacity of a relay is essential to ensure that it can safely handle the PV remote lab's maximum voltage and current levels. The maximum voltage is reached when the two 100 W PV panels are connected in series (86.4 V). The maximum current occurs when two 50 W PV panels are connected in parallel (6.14 A). Therefore, the selected relay should have a voltage rating exceeding 86.4 V and a current rating greater than 6.14 A.

The relay selected is the model **PCB Power Relay G2R-1-SNI**, with a coil rating of 24 V DC, a switching voltage of 125 V and a switching current of 10 A. The maximum set response time for the relays selected is 5 ms, and the maximum rest time is 15 ms for DC voltage.

This relay model is equipped with an LED indicator and a test button. The LED indicator provides visual feedback, while the test button allows for manual testing of the relay's functionality, providing a convenient way to verify its operation.

The relay's datasheet can be consulted in **Appendix 3 – Components Datasheet**.

### 3.5.2. Contactor

Contactors are electrically controlled switches used in applications requiring circuit making and breaking. An example of a contactor is shown in Figure 65. The operation of these elements is based on the closure of contacts in the contactor coils, achieved through the generation of a magnetic field by an external power supply.

In the PV remote lab, the primary function of the contactors is to switch off the system when no scenarios are being performed. Contactors provide electrical protection to prevent excessive currents, which could damage equipment. Contactors are strategically installed in the middle of both parts of the commutation block to ensure the system's safety.



*Figure 65. Contactor DILM7-10.*

The model selected is the **DILM7-10**, a 3–pole contactor with screw terminals. The maximum rating voltage of the element is 110 V, with 3 kW of maximum power and 20 A of operational current. The component has four contact sequences with a normally open configuration.

The contactor datasheet can be consulted in **Appendix 3 – Components Datasheet**.

### 3.5.3. Bypass Diodes

The bypass diodes installed in the PV panels are used to bypass the current of shaded photovoltaic cells, which ensures uninterrupted power production and optimises the power generated by the PV panels.

The 50 W and 100 W PV panels are equipped with bypass diodes. However, the 30 W PV panels do not have built-in bypass diodes. In these PV panels, bypass diodes will be installed with the capability to activate or deactivate their operation. The electromechanical relays will control the activation of the bypass diodes installed.

Selecting the appropriate rectifier diode for PV panels is crucial for efficient energy conversion. While silicon rectifier diodes are commonly used due to their availability and cost-effectiveness, the Schottky rectifier diode is more suitable for this application (100). The main advantage of the Schottky diode is its lower forward voltage drop, which results in improved energy conversion efficiency.

The selected diode should have a forward current rating of at least 2.54 A when 30 W PV panels are connected in parallel. The maximum reverse voltage rating should be at least 44 V when the 30 W panels are connected in series.

The Schottky rectifier diode selected is the model **MBR 2035 PT,** shown in Figure 66, with a maximum DC blocking voltage of 45 V, a maximum average forward rectified current of 30 A and a maximum reverse current of 20 mA. The diode's operating temperature ranges from - 65°C to + 150°C. The diode has three pins, two of which have a diode connected in parallel to the cathode and the remaining pin, the output, is in the middle.
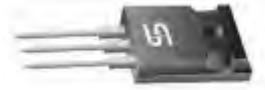


*Figure 66. Bypass Diode MBR 2035 PT.*

The diode datasheet can be consulted in **Appendix 3 – Components Datasheet**.

### 3.5.4. PV Branch Connector

PV branch connectors are single-contact electrical connectors used for PV panel connection in series. The MC4, a 4 mm multi-contact connector, is the standard connector used in the PV industry. As shown in Figure 67. Female and Male PV Branch Connectors., there is a female and



*Figure 67. Female and Male PV Branch Connectors.*

a male connector.

The model selected is the single-pole cable connector manufactured by Stäubli Electrical Connectors. The rated voltage of the connector is 1 000 V, and a rated current of 30 A, which matches the system requirements. The operating temperature of the connector ranges from - 40°C to + 90°C.

The PV branch connector datasheet can be consulted in **Appendix 3 – Components Datasheet**.

### 3.5.5. Relay Module

A relay module to decouple the control board from the power relays is required to control high-current relays. The relay module is typically used because it allows the control of components with high currents. In our case, the Arduino operates at low voltage logic and can be damaged by high currents. With the implementation of relays modules, the Arduino will be protected from the high current flowing through the electromechanical relays and the contactors, up to 6 A.



*Figure 68. Relay Module VMA436.*

The 8-channel relay module **VMA436** is selected. The Arduino directly controls this component.

The relay module datasheet is in Appendix 3 – Components Datasheet.

### 3.5.6. Sensors

The PV remote lab needs the implementation of sensors to measure and register the temperature, irradiance, current and voltage. Temperature and irradiance sensors are essential for measuring and recording the evolution of parameters during the PV panel assessments, which allows for recalculating the PV panel's electrical parameters to STC. Current and voltage sensors are crucial for measuring the data when the PV remote lab implements the I-V curve and dark I-V curve methods. Moreover, the sensors are also used to detect any abnormal situation.

The sensor distribution, Figure 69, is designed to achieve the objective of monitoring the entire PV system. Voltage and current sensors will be installed in all PV panels and in the middle of the two PV strings of the system. The temperature sensor will be placed on the aluminium frame of the PV panels. The PV system will only have one irradiance sensor as a reference.
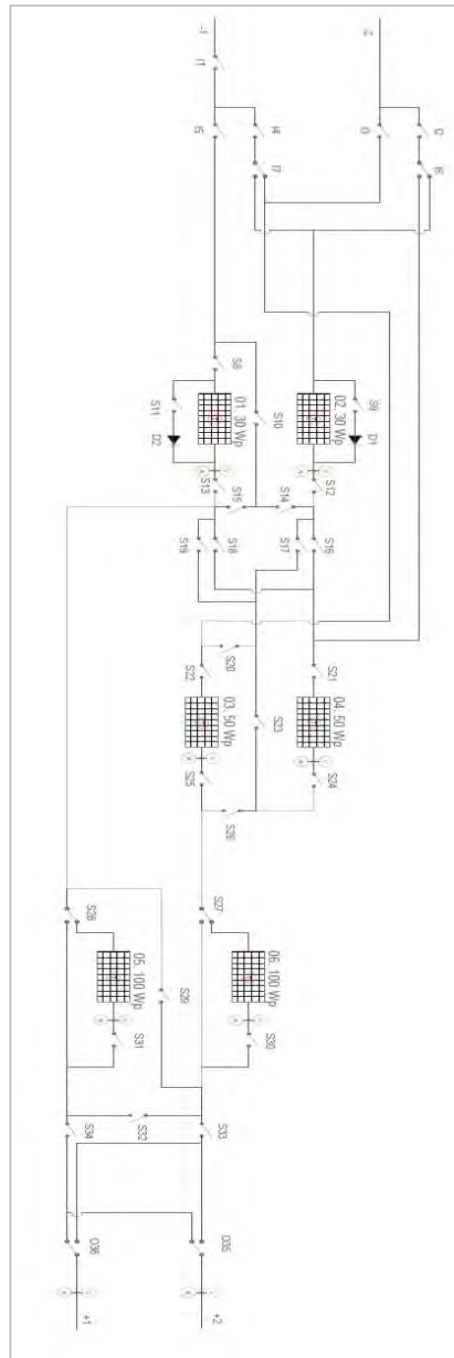


Figure 69. Measurement Points in the PV System.

The total number of measurement points in the system rises to 23. Eight points are dedicated to voltage measurement (marked in orange), another eight points for current measurement (marked in green), and six measurement points are temperature sensors (marked in red). The irradiation sensor is placed in one corner of the PV installation. This distribution allows comprehensive monitoring of the system's electrical and thermal parameters.

→ **Temperature Sensor**

The temperature sensors provide the PV panel temperature, allowing the recalculation of the different parameters to STC. Each PV panel will have a temperature sensor installed.

The **DS18B30** temperature sensor has been chosen for its suitability in meeting all the requirements for its intended application. The sensor selected has a rated temperature range of -55ºC to 125ºC and operates on a 3-5 VDC drive voltage. The sensor offers a resolution ranging from 9 to 12 bits, allowing for precise temperature measurements. The device's accuracy is ± 0.5 ºC, ensuring reliable and consistent results. The DS18B30 temperature sensor is well-suited for remote applications.

→ **Irradiance Sensor**

An irradiance sensor is employed to measure the level of solar irradiance absorbed by the surface of the PV panels during the tests. This data enables the recalculation of the parameters to STC.

The irradiance sensor selected is the **SR30-M2-D1** pyranometer, shown in Figure 70, a digital class A and high-quality pyranometer. The sensor measures a plane surface's solar irradiation received from a 180º field of view angle. The selected sensor has a calibration uncertainty lower than 1.2 %, and the rated operating temperature range is from - 40 ºC to + 80 ºC.



*Figure 70. Irradiance Sensor SR30-M2-D1.*

The datasheet of the irradiance sensor selected can be consulted in **Appendix 3 – Components Datasheet**.

→ **Current Sensor**

The current sensors installed in the system should measure the current values when I-V curve and dark I-V curve methods are implemented in the PV remote lab.

The sensor should cover currents up to the highest expected current in the system (6.14 A) and handle the maximum system voltage (86.4 V). A non-intrusive current sensor based on the Hall effect principle is required.

The model that accomplishes the requirements is the **ACS711 – Allegro Microsystems**, shown in Figure 71**,** which operates based on the Hall effect and is suitable for AC and DC applications. The model selected has an optimised accuracy range of -15.5 A to +15.5 A for output voltages below 100 V. The sensitivity of this model is 90 mV/A with a total output error of ± 5%.



*Figure 71. Current Sensor ACS711.*

The current sensor ACS711 – Allegro Microsystems datasheet is in **Appendix 3 – Components Datasheet**.

→ **Voltage Sensor**

The voltage sensors installed in the system should measure the voltage values when I-V curve and dark I-V curve methods are implemented in the PV remote lab.

The analogue input of the Arduino model selected has a DC voltage range from 0 to 5 V. A wider voltage range is required to trace the complete I-V curve of the PV panels. Therefore, a voltage divider should be implemented to increase the measurement voltage range. A voltage divider comprises two resistors that reduce the voltage measured to the desired and provide an affordable voltage to the Arduino analogue input.

Suitable voltage ranges should be defined for the different locations. The 30 W and 50 W PV panels have maximum voltages of 22 V and 21.6 V, respectively. Therefore, a voltage range from 0 V to 25 V is appropriate for these PV panels. The maximum voltage for the 100 W PV panels is 43.2 V. A voltage sensor ranging from 0 V to 50 V is adequate. The maximum voltage for the PV strings is 86.4 V. Hence, voltage sensors ranging from 0 V to 100 V would be needed.

In Figure 72, a voltage divider scheme is presented. Thanks to the schematic, the following equation can be obtained.

$$V_s = (R_1 + R_2) \times \frac{V_{out}}{R_2}$$

This verifies that the maximum voltage reaching the analogue pin of the Arduino is equal to or less than 3.3 V or 5 V. It is used to size the resistor value.

To calculate the voltage dropped by both resistors, the Kirchhoff law is used:

$$V_s = V_{R1} + V_{R2}$$

And following the Ohm law:

$$V_{R1} = I \times R_1 \qquad\qquad V_{R2} = I \times R_2$$

$$V_s = I \times R_1 + I \times R_2$$

$$I = \frac{V_s}{(R_1 + R_2)}$$

Considering that the current is equal in both resistors, the voltage dropped can be calculated for each resistor:

$$I_{R1} = \frac{V_{R1}}{R_1} = \frac{V_S}{R_1 + R_2} \qquad\qquad V_{R1} = V_S \left( \frac{R_1}{R_1 + R_2} \right)$$

$$I_{R2} = \frac{V_{R2}}{R_2} = \frac{V_S}{R_1 + R_2} \qquad\qquad V_{R2} = V_S \left( \frac{R_2}{R_1 + R_2} \right)$$

The power dissipated per each resistor is:

$$P_{R1} = I_{R1} \times V_{R1} \qquad\qquad P_{R2} = I_{R2} \times V_{R2}$$
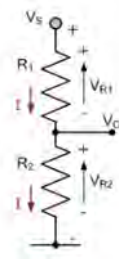


*Figure 72. Voltage Divider Scheme.*

The appropriate size and the relevant data using the equations defined are shown in Table 8.

*Table 8. Resistors calculation.*

|  | 30 W & 50 W | 100 W | PV String |
|---|---|---|---|
| V$_{out}$ | 5 V | 5 V | 5 V |
| V$_s$ | 25 V | 50 V | 100 V |
| R$_1$ | 10.20 kΩ | 24 kΩ | 30 kΩ |
| R$_2$ | 2.55 kΩ | 2.67 kΩ | 1.58 Kω |
| I | 1.961 mA | 1.873 mA | 3.165 mA |
| V$_{R1}$ | 20 V | 45 V | 95 V |
| V$_{R2}$ | 5 V | 5 V | 5 V |
| P$_{R1}$ | 0.018 W | 0.045 W | 0.112 W |
| P$_{R2}$ | 0.005 W | 0.005 W | 0.005 W |

All the resistors selected are from the same manufacturer, TT Electronics, and the same model, RC55Y, is chosen even though the resistance value differs. The RC55Y resistors are through-hole resistors with an axial leaded package with a voltage rating of 350 V and a tolerance of ± 0.1%. The resistor's power rating value is 250 mW for all of them except the 24 and 30 kΩ, which have a power rating of 500 mW. Considering the values calculated in Table 8, the resistors' operating voltage and power dissipation accomplish the PV system requirements.

The voltage sensor resolution should be defined. The Arduino has 10 bits resolution, which gives rise to 1023 steps. The Arduino resolution with an input of 5 V is 4.88 mV/step, which should be multiplied by the voltage divider value to define the resolution of the voltage divider. Following this reasoning, the resolution for the different voltage sensors is shown in Table 9.

*Table 9. Voltage sensor resolution.*

|  | 30 W & 50 W | 100 W | PV String |
|---|---|---|---|
| Sensor Resolution | 24.43 mV/step | 48.87 mV/step | 97.75 mV/step |

# 4. PV Remote Lab Assembly

An installation procedure has been followed to guarantee a correct assembling process. Firstly, installing the PV panels in the PV System Simulator Support Structure has been carried out according to the configuration selected, Overlapping Design. The result of the PV panels installation is shown in Figure 73.



*Figure 73. PV Panels Installation on the Support Structure.*

Subsequently, electromechanical relays, contactors, and connections are installed in a separate framework independent from the PV panel installation. The framework is composed of a DIN rail, where the components related to the PV system of the commutation block are installed in the inner section of the frame, and the components constituting the system outputs of the commutation block are positioned on the outer area of the DIN rail. The frame's height is minimised by employing the DIN rail's inner section and outer section, thus preventing potential shading effects on the PV panels.

The design result of the components assembling is shown in Figure 74 and Figure 75.
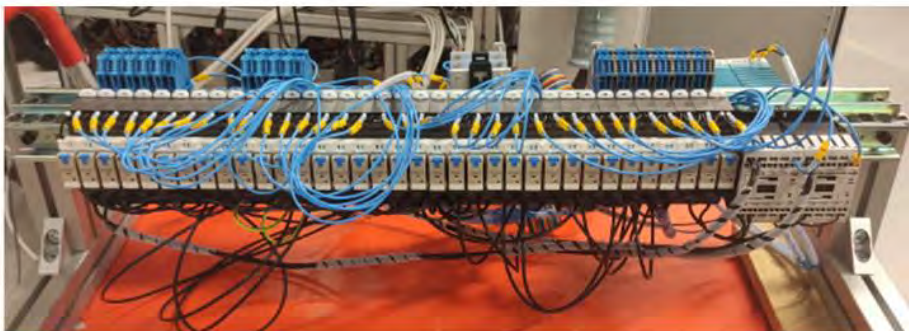


*Figure 74. Components Installed in the Interior of the DIN Rail.*
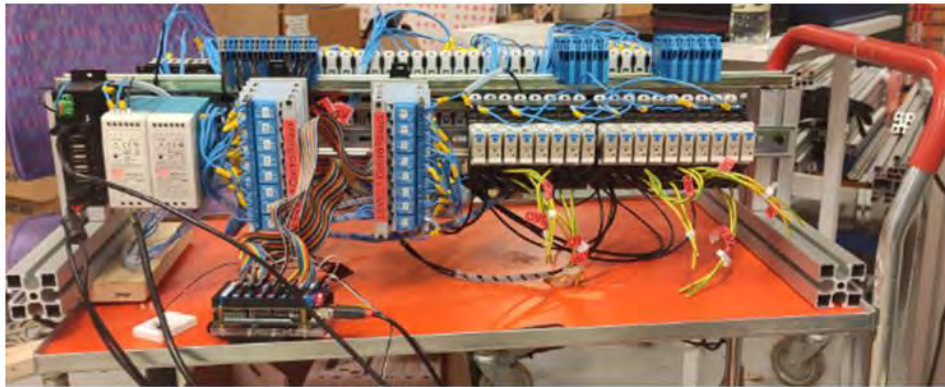
*Figure 75. Components Installed in the Exterior of the DIN Rail.*

The electromechanical relays are assigned numbers corresponding to the commutation block scheme to facilitate the rapid identification of devices. In contrast, the relay modules have been numbered according to the corresponding Arduino input number.

Then, the separate framework with the components is affixed to the PV panels' support structure. This integration ensured all the components in one unit, enhancing the system's portability when necessary. The comprehensive assembly of the PV system is visually depicted in Figure 76.



*Figure 76. Complete PV System Simulator Assembly.*

Upon the completion of the installation process, a series of tests have been conducted to confirm the proper functionality of the installation. These tests encompassed various assessments, including verifying relay responses to Arduino signals. Several errors were detected and promptly rectified throughout this testing phase, ensuring the system's optimal performance.

## 4.1. Software Development

The PV remote lab requires software to control the commutation block remotely. The software aims to provide a convenient and efficient way to manage and regulate the commutation block functions necessary to implement the desired scenario. LabVIEW, a robust and versatile tool utilised for testing, controlling, and designing hardware and software systems, has been employed to develop the PV remote lab system's environment.

A comprehensive set of three environments has been designed to effectively manage the component's functionalities. The first environment controls the electromechanical relays and contactors, allowing predetermined scenarios to be selected. The subsequent environment is tailored for overseeing the DC Load RND 320-KEL103 V3.10, a crucial element for implementing the I-V curve technique. The third environment is a control interface for the DC Power Supply RND 320-KD3305P, a component used for the dark I-V curve measurement and the electroluminescence test.

**Electromechanical Relays and Contactors Interface Control**

The interface depicted in Figure 77 enables complete control over the electromechanical relays and contactors. The left side of the image provides an overview of the relays and contactors integrated within the commutation block, indicating their activation status. These relays and contactors are strategically organised, distinguishing between those constituting the PV system and the system outputs.
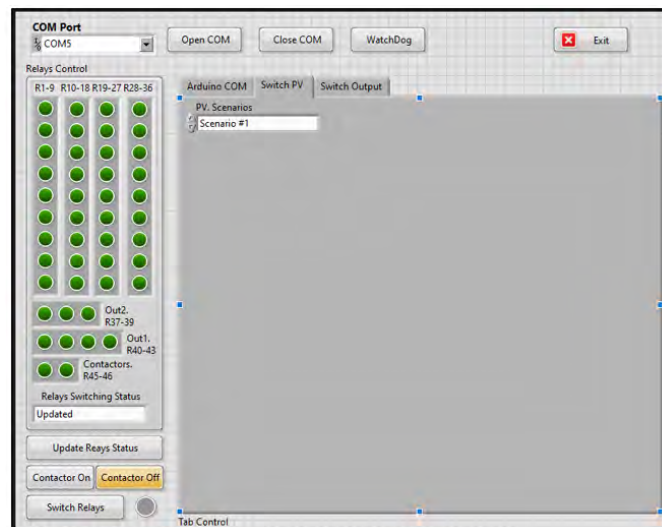


*Figure 77. Interface Control: Electromechanical Relays and Contactors.*

Utilising the developed interface enables the activation and deactivation of the intended relays and contactors. Distinct scenarios have been directly defined within the program to streamline development and enhance scenario flexibility. This approach eliminates the need to alter relays and contacts manually and ensures a seamless transition between scenarios.

**DC Load Interface Control**

The interface shown in  Figure 79 allows the control of the DC load implemented in the system. The connection status of the DC load can be visualised and controlled from the interface. The interface displays the established limits for the DC load regarding current, voltage, resistance, and power.
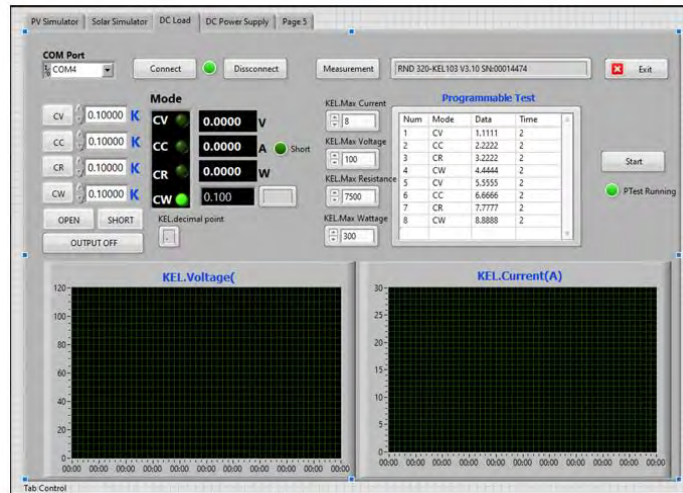


*Figure 79. Interface control: DC Load.*



*Figure 78. DC Load Front View.*

The interface sends a reference constant parameter (RCP) to the DC load to perform the desired measurement. In this case, four types of constant parameters can be sent:

- Resistance                                      - Voltage

- Current                                            - Power

The table in the right part of the interface shows the different constant parameters that will be sent to the DC load. These values can be changed for each measurement in the interface itself or employing an external file that should be loaded into the interface. The measurement time is the other value that can be modified. For the selected DC load, the minimum measurement time is 2 seconds.

The measurements' results can be displayed on the two graphs on the interface. In addition, an Excel file with the measured points is created.

**DC Power Supply Interface Control**

The interface presented in Figure 81 provides the means to control the selected DC power supply. The device's status and the option to connect or disconnect the device are available in the interface.
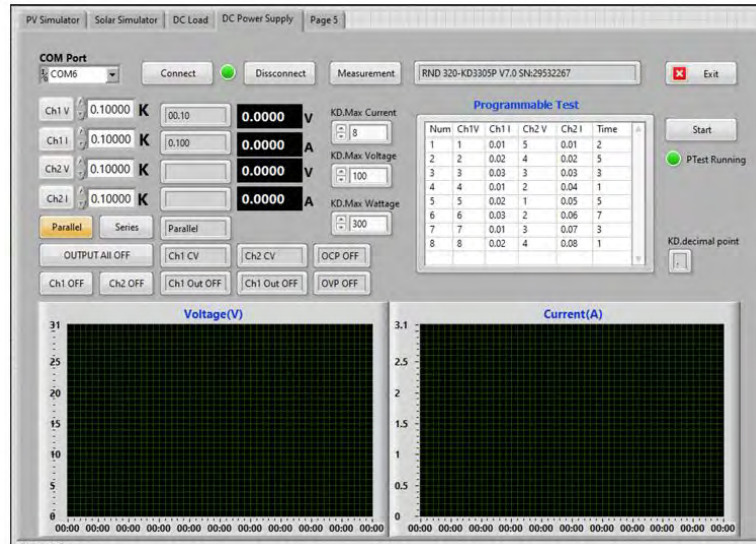


*Figure 81. Interface Control: DC Power Supply.*



*Figure 80. DC Power Supply Front View.*

As with the DC load, the interface shows the limit values of the DC power supply, maximum power, current and voltage. These values are limits and may not be exceeded. Regarding the connections, there are two channels to which the desired PV String can be connected. Only constant current and voltage values can be sent to the DC power supply to perform the measurement points.

The measurements' results can be displayed on the two graphs on the interface. In addition, an Excel file with the measured points is created.

# 5. Methods for PV Panels Characterisation

Assessing the performance of PV panels is crucial for understanding how they operate under different environmental conditions. The characterisation methods used help students and professionals better understand PV systems. The following method will be introduced and explained in detail:

1. I-V Curve Measurement
2. Dark I-V Curve Measurement
3. Electroluminescence Testing

Each method will be defined, including the equipment needed, the measurement setup, and the steps to be followed. These tests will provide valuable information about the PV system's performance, efficiency, and identification of degradation modes. Furthermore, additional technologies are defined to be implemented in the future.

Only the I-V curve and dark I-V curve measurements will be carried out in the present document due to some system constraints related to the budget and time availability.

## 5.1. I-V Curve Measurement

The I-V curve measurement is the method most used to analyse the state of a PV panel, which indicates the response of the PV module to different load conditions at a known radiation and temperature. This analysis aims to assess the performance and efficiency of the PV panels under varying temperature and irradiation conditions.

An irradiance source, such as a PV simulator or natural sunlight, and a DC load are required to implement this method. The irradiance source provides the necessary light intensity to simulate solar conditions. The DC load allows the load resistance to be adjusted to measure the points on the I-V curve of the PV panel.

The following steps need to be followed to obtain the I-V curve of a PV panel:

1. **Environmental Conditions Consideration**

The measurements of the I-V curve can be conducted under different conditions, the most pertinent being the STC. Additional calculations to adjust the results are required if measurements are carried out under different conditions from STC. In the case of a PV simulator, it is possible to achieve STC directly.

The parameters that should be measured to adjust the I-V curve to STC are the following:

- **Temperature**. The STC regarding the PV panel temperature is 25ºC. In the case of measuring a different value than the one provided by STC, the different temperature coefficients of the PV panels should be considered to adjust the I-V curve to STC in terms of current, voltage and power.

- **Irradiance**. The STC regarding the irradiance is 1 000 W/m$^2$. The PV simulator projects the desired irradiance for each experiment. However, we have decided not to perform the method with irradiance levels below 600 W/m$^2$, which is not recommended in standard industrial practice.

### 2. DC Load Selection & Connection

The DC load is a component used to modify the voltage and current of the PV panels by varying the resistive loads of the DC load controller itself. The most critical parameters that should be considered and studied to select an appropriate DC load for our system are the maximum applicable resistance, the maximum power dissipation, the system voltage and the system current.

Considering the four parameters that should be contemplated, the selected DC load is the RND 320-KEL103. The device has a maximum resistance of 7.5 kΩ, ensuring a wide resistive load range. The fixed DC load has a power dissipation of 300 W and can manage a system voltage of 120 V DC and a system current of up to 30 A. The DC load should be connected forward to trace the I-V curve.

### 3. Curve Measurement

This subsection describes the steps that should be followed to trace the curve. First, it is advisable to identify the $I_{SC}$ and $V_{OC}$ values of the PV panels. Once these parameters have been acquired, a sweep of measurement points should be performed to trace the complete I-V curve. Finally, the I-V curve obtained enables the extraction of $V_{MPP}$ and $I_{MPP}$ values for the studied PV panels.

#### 3.1. $I_{SC}$ and $V_{OC}$ Measurement

To determine the $V_{OC}$, the current in the PV panel should be set to zero. This value is reached by applying a constant current value of 0 A through the DC load. To obtain the $I_{SC}$, the voltage in the PV panel should be null. The DC load should apply a constant voltage value of 0 V to the PV panel.

#### 3.2. Point Sweep

To trace a detailed I-V curve, at least 100 data points are required, which should be acquired in the range of 20 and 100 ms to maintain the same conditions throughout the I-V curve trace (101). Nevertheless, the selected DC load in our system has a data acquisition time of 2 seconds, implying a significant delay in the overall testing period.

Depending on the kind of reference constant parameter sent by the DC load to the PV panels, it is possible to carry out the following procedures:

#### A. Resistance as the Reference Constant Parameter

The first procedure is based on having the resistance as the reference constant parameter. This procedure consists of 89 measurement points starting from 0 Ω up to the maximum DC load resistance value, 7 500 Ω. The measurement points are spaced at intervals of 0.2 Ω from 0 Ω to 10 Ω. After reaching 10 Ω, the interval increases to 200 Ω for each new measured point, starting from 100 Ω and progressing up to the maximum resistive load of the DC load, 7 500 Ω.

#### B. $V_{OC}$ and $I_{SC}$ as the Constant Reference Parameter

The second procedure uses the $V_{OC}$ and the $I_{SC}$ as the reference constant parameters. The process involves plotting 100 measurement points concerning $I_{SC}$ and $V_{OC}$. Firstly, 50 measurements according to the $V_{OC}$ are performed. The voltage sweep is from 0 V to $V_{OC}$. The spacing interval of the measurement points is $+V_{OC}/50$. Then, the measurement has as reference the $I_{SC}$. Another 50 measurement points are performed in the 0 A and $I_{SC}$ range. In this case, the measurement point variation is $+I_{SC}/50$.

The expected result of the point sweep is shown in Figure 82.
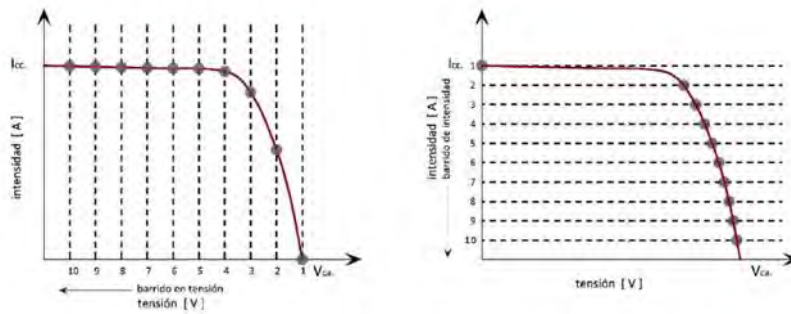


*Figure 82. Voltage and Current Sweep.*

Both graphs will be superimposed to obtain the complete I-V curve

### 3.3. I$_{MPPT}$ and V$_{MPPT}$ Obtention

To determine the I$_{MPP}$ and the V$_{MPP,}$ Ohm's Law (P = I x V) should be applied to each one of the values obtained. The I$_{MPP}$ and V$_{MPP}$ are deduced from the overall maximum power value.

### 4.  Data Visualisation

The I-V curve should be plotted in a graph with all the measurement points traced and the I$_{MPP}$ and V$_{MPP}$ defined. The current values are on the Y axis, while the voltage values are on the X axis. The shape of the graph will vary depending on the temperature and irradiance conditions during the test. The I-V curve graphs for different irradiation and temperature conditions are represented in Figure 84 and Figure 83.
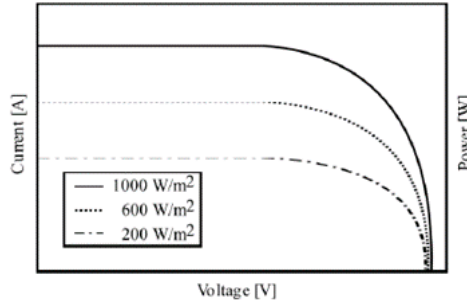


*Figure 84. I-V curve in Different Irradiance Conditions(50).*
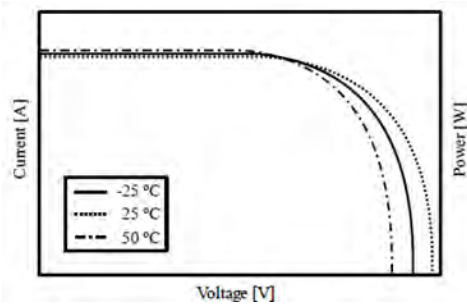


*Figure 83. I-V curve in Different Temperature Conditions(50).*

In monocrystalline silicon modules, the I$_{SC}$ is directly proportional to the solar irradiance and increases slightly with higher photovoltaic cell temperatures. The V$_{OC}$ logarithmically grows with higher solar irradiance levels and decreases linearly with cell temperature increase (102).

5. **STC Adjustment**

In the case of not performing the I-V Curve in STC, the current and voltage values should be adjusted to STC to check the correct operation of the PV panel. As presented in 2.2.3 Photovoltaic Cell Parameters, the following equations should be used to adjust the $I_{SC}$, $V_{OC}$ and all the pairs of current and voltage between the $I_{SC}$ and $V_{OC}$ (102) to STC. The equations to adjust the $I_{SC}$ and $V_{OC}$ are:

$$I_{SC(STD)} = \frac{G_{STD}}{G} \, I_{SC(measured)} + \alpha \, (T_{STD} - T_{cell})$$

$$V_{OC(STD)} = V_{OC(measured)} + \beta \, (T_{STD} - T_{cell}) + \frac{nKT_{cell}}{e} \ln\left(\frac{G_{STD}}{G}\right)$$

And for the rest of the measured points:

$$I_{(STD)} = I_{(measured)} + I_{SC(measured)} \left(\frac{G_{STD}}{G} - 1\right) + \alpha \, (T_{STD} - T_{cell})$$

$$V_{(STD)} = V_{(measured)} + \beta \, (T_{STD} - T_{cell}) - F_{CC} \, I_{(STD)}(T_{STD} - T_{cell}) - R_S(I_{STD} - I_{(measured)})$$

The $I_{SC}$ temperature coefficient ($\alpha$) and the $V_{OC}$ temperature coefficient ($\beta$) are required and are parameters listed in the datasheet. Moreover, the datasheet also shows the number of cells in series (N), the series resistance of the module ($R_S$) and the curve correction factor ($F_{CC}$).

6. **Data Visualisation in STC**

With all the measurement points adjusted to STC and the $I_{MPP}$ and $V_{MPP}$ defined by Ohm's Law, the I-V curve at STC can be plotted in a graph. The current values are on the Y axis, while the voltage values are on the X axis. Figure 85 represents a sample graph illustrating a PV panel's I-V & P-V curves.
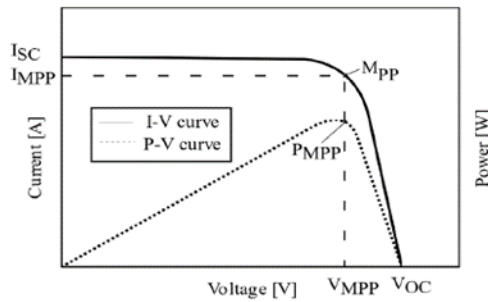


*Figure 85.I-V and P-V Curves of a PV Panel (50).*

## 5.2. Dark I-V Curve Measurement

The dark I-V curve evaluates PV panel performance and detects degradation modes in a low-light or dark environment. A dark I-V curve involves applying different voltage values to the PV panels using a DC power supply to measure the corresponding current responses. The following steps should be followed to obtain the I-V curve of a PV panel:

1.  **Environmental Conditions Consideration**

The PV panel under study should be placed in a dark environment. A layer can cover the PV panel cells, blocking any light-induced current. The temperature of the PV panel should be maintained around 25ºC, simulating the temperature at STC.

2.  **DC Power Supply Selection & Connection**

A DC power supply transforms AC power from a standard outlet into a consistent DC power source. This regulated direct current is subsequently employed to energise various devices, modules, or components. DC power supplies are available in diverse configurations, including input and output voltage levels, currents, and power ratings. The selected DC power supply RND 320-KD3305P has an operational voltage range from 0 V to 60 V, with a maximum operating current of 5 A. The rated power by the device is 150 W. With these characteristics, the selected DC power supply accomplishes the system requirements for the experiments carried out in this project.

The voltage and current supplied to the PV panel should be limited in the DC power supply to prevent surpassing the PV panel's limits and causing damage. Hence, it's recommended to set the maximum current value at 110% of the $I_{SC}$ and the maximum voltage value at 110% of the $V_{OC}$. Regarding the connection mode, the DC Power Supply should be connected to the PV panels in a forward configuration, providing a forward voltage.

3.  **Curve Measurement**

The $I_{SC}$ and $V_{OC}$ should be consulted in the PV panels datasheet or acquired in a previous I-V curve measurement at STC for the dark IV curve measurement. These parameters are crucial to be implemented in the DC power supply. This practice ensures that the PV panels remain within safe limits defined by the DC power supply, mitigating the risk of damage due to exceeding specified values.

The curve measurement involves varying the voltage the DC power supply provides, from 0 V to $V_{OC}$, in small increments and measuring the resultant current at each point. One hundred measurement points should be acquired. Two measurement ranges will be established to achieve a well-defined dark I-V curve on linear and logarithmic scales. The initial measurement range will span from 0 V to 10% of the $V_{OC}$. The spacing interval is $\frac{10\% \, x \, V_{OC}}{50}$. The subsequent range will extend from 10% of $V_{OC}$ to $V_{OC}$. In this case, the spacing interval is $\frac{90\% \, x \, V_{OC}}{50}$. Within each range, 50 measurement points will be captured. This approach ensures a comprehensive plot for linear and logarithmic graphs.

4. **Data Visualisation**

The measured data points from tracing the dark I-V curve can be plotted on a graph. The graph typically has voltage on the X-axis and current on the Y-axis. Each data point corresponds to a specific combination of the voltage provided and the resultant current measured.

As seen in Figure 87, the X-axis (current) is represented on a linear scale, which helps compare the dark I-V curve results with the I-V curve of the PV panel (54). With both curves traced, different degradation modes can be identified. A recent study evaluated a PV module with severe cell cracks (103). The results of the study are shown in Figure 86. Microcrack evaluation
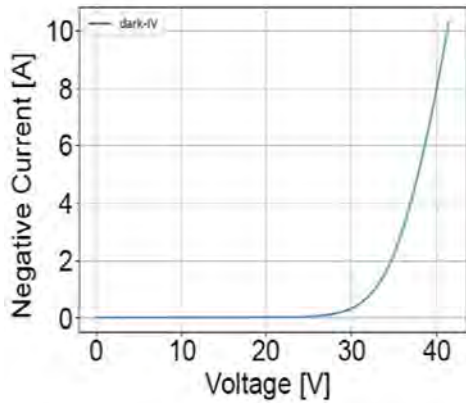


*Figure 87. Dark I-V curve (Current in a linear scale) (54).*
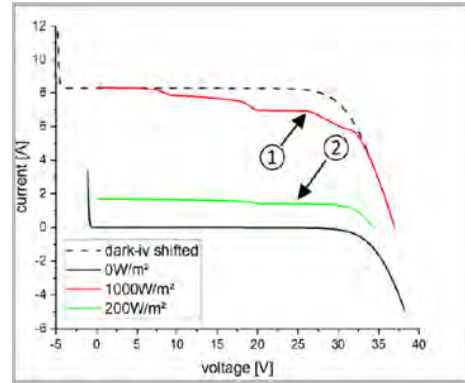


*Figure 86. Microcrack evaluation with I-V Curve & Dark I-V Curve (103).*

with I-V Curve & Dark I-V Curve (103)..

Figure 88 shows the y-axis (current) on a logarithmic scale. With the logarithmic scale, the current changes can be appreciated. Large curvature at low current levels (0,1 mA – 1 A) indicates low shunt resistance ($R_{sh}$). In higher current levels (1A - $V_{oc}$), the series resistance ($R_s$) is analysed. This approach retains the importance of tracing detailed points at very low current and high current levels. With this kind of graph, PID defects are identified (54).

5. **Dark Parameters Obtention**

The dark parameters of a PV panel are the series resistance, shunt resistance, diode factor and saturation current. They can be calculated through software such as MTR Software FitAll, which calculates the four parameters from the different measured points of the dark I-V curve. With them and software such as PVSIM, the PV panel's performance and state can be defined, calculating the actual value of the $V_{oc}$, $I_{MPP}$ and $V_{MPP}$.
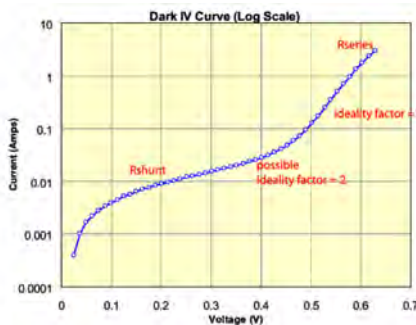


*Figure 88. Dark I-V curve (Current in a logarithmic scale) (54).*

## 5.3. Electroluminescence Method

The electroluminescence method is used to evaluate the performance of PV panels and detect potential degradation modes through a camera that captures the electroluminescent image, revealing the variations or anomalies in the PV panels. Therefore, it involves using a silicon CCD camera or an InGaAs camera. At the same time, a DC power supply provides a constant current to the PV panel under evaluation in a dark environment. The following steps need to be followed to obtain the electroluminescence image of a PV panel:

1. **Environmental Conditions Consideration**

The electroluminescence method is achieved in a dark environment. The PV panel under examination should be placed in a light-restricted climate to block any incident light that could generate current effectively. Maintaining the PV panel temperature close to 25ºC is essential, simulating the temperature at STC.

2. **DC Power Supply Selection & Connection**

The selected DC power supply RND 320-KD3305P has an operational voltage range from 0 V to 30 V, with a maximum operating current of 5 A. The rated power by the device is 150 W. It is crucial to ensure that the current supplied by the DC Power Supply is slightly limited above the Isc of the PV panel, mitigating the risk of potential damage to the cells. Regarding the connection mode, the DC Power Supply should be connected to the PV panels in a forward configuration.

3. **Camera Selection & Mounting**

A high-resolution imaging device should be positioned directly above the PV panel perpendicularly. The distance between the device and the PV panel should be adjusted to capture an image of the entire surface that will be evaluated. The emission spectra of the camera should have a peak at 1 150 nm (60). Moreover, the camera would have a high pixel resolution (650 x 900 pixels, for example) and 12-bit resolution (104). High-resolution imaging can acquire detailed information about the PV panel state and possible common failures (105).

4. **Image Acquisition**

The electroluminescence method should comply with IEC 60904-13, which requires a current equivalent applied to the short-circuit current to achieve module polarisation (104). Therefore, the DC power supply should deliver a constant current at Isc to the PV panel during the image acquisition. The camera's exposure time often depends on the quality of the camera itself. In one Sensovation digital camera test, the exposure time was approximately 300 seconds (58). In another test, the exposure time was 9 seconds (56).

5. *Expected Results*

Figure 90 and Figure 89 are images obtained by applying the EL method. PID and microcracks are the degradation modes identified.
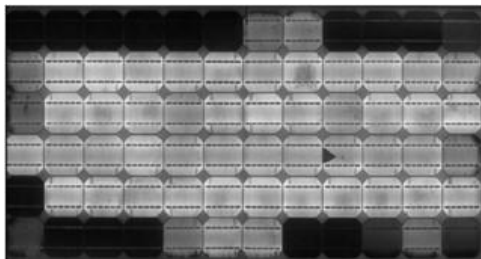


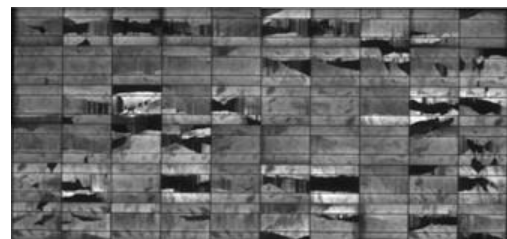*Figure 90. EL image of a PV module affected by PID (64).*



*Figure 89.EL image of a PV panel affected by Cracks (64).*

## 5.4. Solar Charge Controllers

The main objective of implementing solar charge controllers is to compare the performance of the two technologies most used in the field, PWM and MPPT, in terms of conversion efficiency. The input of the solar charge controllers is directly connected to the commutation block, which in turn is connected to the PV panels. The outputs of the solar charge controllers can be a DC or AC battery.

### 5.4.1. MPPT

The selected Maximum Power Point Tracker is the BlueSolar Charge Controller MPPT 75/10M - Light 12/24-10 of Victron, with two automatic detection battery voltage operational values, 12 V or 24 V. The rated charge current is 10 A with a maximum open circuit voltage of 75 V. The nominal PV power with 12 V operational battery voltage is 145 W, while with 24 V, it is 290 W. The PV voltage should exceed the battery voltage by 5 volts to start the operation of the controller.

The experimental tests that can be carried out with both operational modes are:

- With 12 V operational battery voltage, the PV panels with power ratings of 30 W and 50 W can be analysed individually and in parallel and series connections. The 100 W PV panel can be studied independently.
- PV panels can be connected in series with 24 V operational battery voltage, 30 W and 50 W power ratings. The 100 W PV panel can be analysed independently or connected in parallel or series with other panels.

### 5.4.2. PWM

The selected Pulse Width Modulation is the BlueSolar PWM -Light 12/24-10 of Victron, with two automatic detection battery voltage operational values, 12 V or 24 V. The rated charge current is 10 A with a maximum solar voltage of 28 V for a 12 V battery voltage or 55V with a 24 V battery voltage.

The experimental tests that can be carried out with both operational modes are:

- With a maximum solar voltage of 28 V, only the PV panels with 30 W and 50 W power ratings can be analysed individually or connected in parallel.
- With a maximum solar voltage of 55 V, the PV panels with 30 W and 50 W PV in series connection while the 100 W PV panels can be evaluated alone or in parallel connection.

## 5.5. Inverter

A DC to AC-inverter is also an element that can be very useful for comparing the solar charge controllers and the inverter. The selected microinverter is the DS3L by Altenergy Power Systems. It consists of two independent MPPT inputs with a peak efficiency of 97%. The recommended power range for connection is between 255 W and 550 W. However, lower-power PV panels can be connected due to the chosen panel's power rating. The operating voltage ranges from 16 V to 55 V, with a maximum input current of 18 A for each input. The nominal output voltage is 230 V with a current of 3.2 A.

With the chosen microinverter model, it is possible to analyse the 30 W and 50 W PV panels individually and connected in series or parallel. The 100 W PV panels can only be studied separately or connected in parallel.

# 6. Tests and Results

The PV remote lab has still not been put into operation because some components, such as the sensors, have not yet arrived, and due to the deadlines, it has not been possible to implement the characterisation methods in the PV remote laboratory on site. Nevertheless, it has been decided to implement the described characterisation methods in a PV panel to verify their correct approach. The I-V curve method follows the described procedure in an outdoor environment. Meanwhile, the dark I-V curve is carried out inside the laboratory following the defined instructions.

## 6.1. I-V Curve Tests

The I-V Curve method has been implemented with the following assembly:

The PV panel selected for the I-V curve test is the SunPlus 100. For the tests, this PV panel is placed at an angle of 30º to the ground. This setup is intended to capture the maximum available irradiation. Regarding the sensors, the irradiation sensor (SR30-M2-D1) is aligned in parallel to the PV panel and the sensor temperature (Fluke multimeter) is mounted on the PV panel surface without interfering with any cells. To complete the system, a DC load (RND 320-KEL103) and a computer are used to carry out the I-V curve method defined. Figure 91 illustrates the mounted system for the I-V curve measurement.



*Figure 91. Mounted System for the I-V Curve Measurement.*

Two distinct tests are conducted. The first test aims to determine which of the two procedures defined in "3.2. Point Sweep" for tracing the I-V curve is the most suitable. Two measurements are carried out in this test, one having the resistance as the reference constant parameter and the other having the $V_{OC}$ and $I_{SC}$ as the reference constant parameter. In the second test, the adequate constant reference parameter is used among those compared in the previous test, and the I-V curve is adjusted to STC.

### 6.1.1. Resistance Versus $V_{OC}$ & $I_{SC}$ as Reference Constant Parameter

This test was performed on the 28th of June of 2023 at 13:31 with a PV panel surface temperature of 39 ºC (Fluke multimeter) and an irradiance of 885 W/m² (SR30-M2-D1). The main goal of this test is to compare the two procedures defined in 5.1 I-V Curve Measurement in the subsection "3.2. Point Sweep".

With resistance as the reference constant parameter, 89 points have been defined. As described above, the measurement points are spaced at intervals of 0.2 Ω from 0 Ω to 10 Ω. After reaching 10 Ω, the interval increases to 200 Ω for each new measured point, starting from 100 Ω and progressing up to the maximum resistive load of the DC load, 7 500 Ω. These resistance values are applied to the PV panel using the DC load. The resultant graph of this procedure is shown in Figure 92.
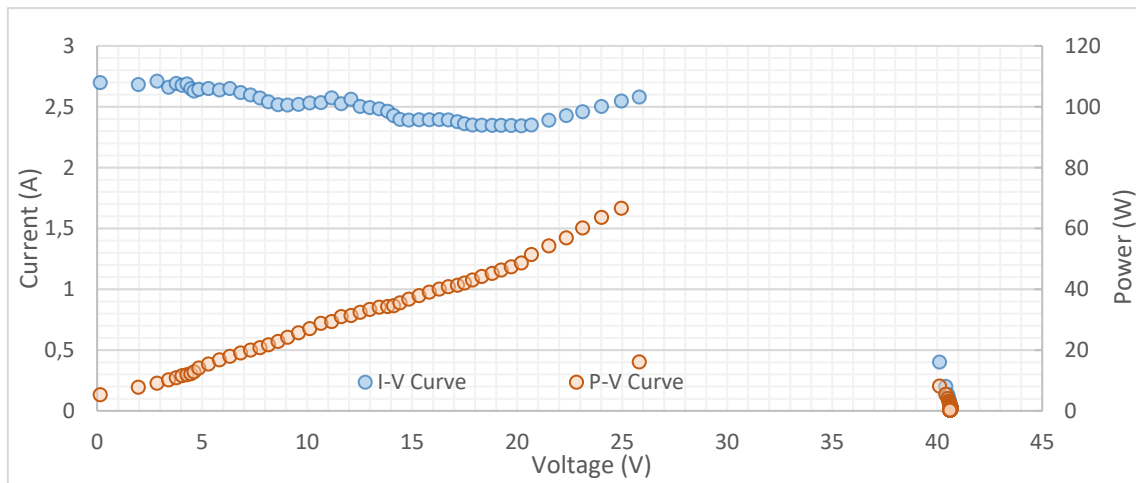


*Figure 92. First test: I-V Curve with the Resistance as RCP.*

With the $V_{OC}$ & the $I_{SC}$ as the reference constant parameter, 100 points are executed. In Figure 93, 50 measurements are performed according to the $V_{OC}$ (43.2 V). The voltage sweep is from 0 V to $V_{OC}$. The spacing interval of the measurement points is +$V_{OC}$/50. Then, the $I_{SC}$ (3 A) is the constant reference parameter.
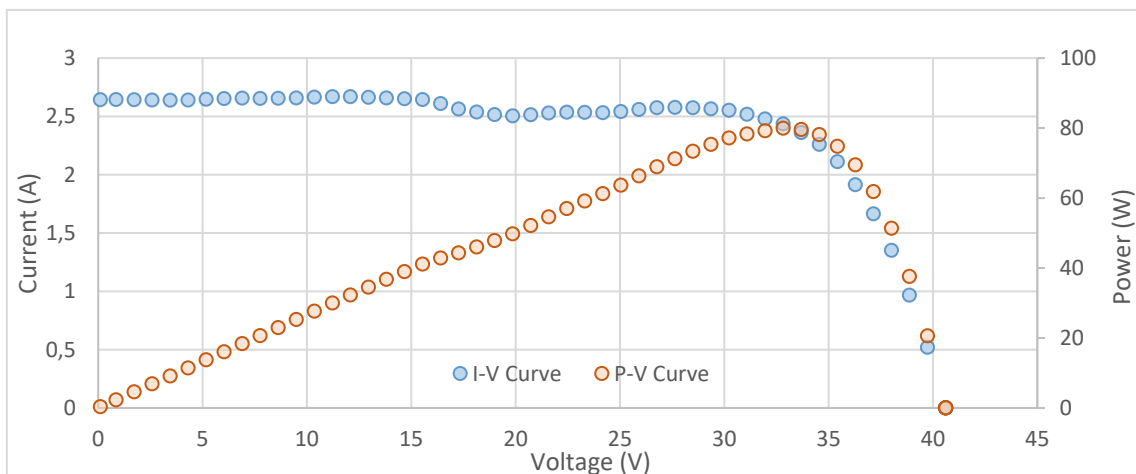


*Figure 93. First test: I-V Curve with the $V_{OC}$ as RCP.*

In Figure 94, 50 measurement points are performed in the 0 A and $I_{SC}$ range. In this case, the interval is +$I_{SC}$/50.
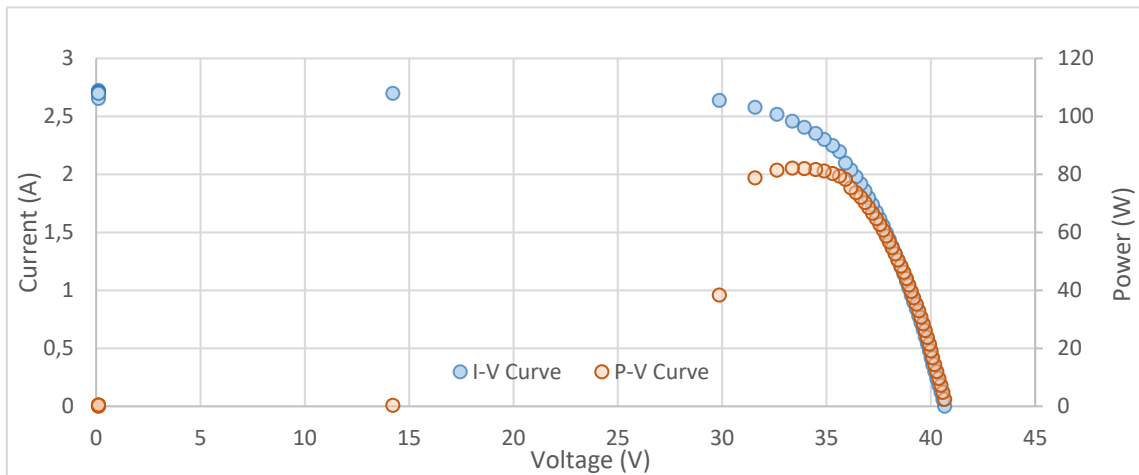
*Figure 94. First test: I-V Curve with the I$_{SC}$ as RCP.*

Superimposing the I-V Curve obtained with the V$_{OC}$ as the RCP and the I-V Curve obtained with the V$_{OC}$ as the RCP, the complete I-V curve is acquired.

Figure 95 illustrates the measurement conducted with I$_{SC}$ and V$_{OC}$ as RCP. The outcome of this process is a comprehensive I-V curve encompassing all the current and voltage values of the PV panel evaluated.
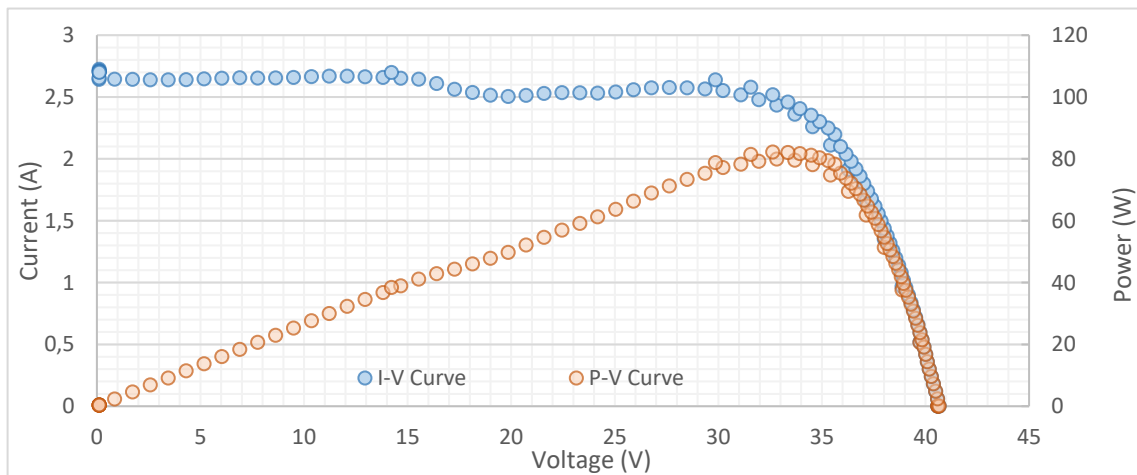


*Figure 95. First test: Complete I-V Curve with I$_{SC}$ and V$_{OC}$ as RCP.*

Figure 92. First test: I-V Curve with the Resistance as RCP. depicts the outcome when using resistance as the RCP. It is evident that the plotted I-V curve is not complete; an area of the graph, particularly within the 25 V to 40 V range (10 Ω to 300 Ω), requires more data points. Addressing this issue would entail modifying the defined resistance values. However, it is essential to note that for each PV panel, these resistance values will need to be adjusted because every PV panel has different I$_{SC}$ and V$_{OC}$ values. In addition, an anomaly can be seen in the measurement of the range between 15 V and 25 V. There is a drop and rise of the current that does not occur in the other graph.

Hence, we can deduce that the measurement conducted with I$_{SC}$ and V$_{OC}$ as RCP yields a more suitable outcome. The resultant plot is more comprehensive and without anomalies.

### 6.1.2. Complete I-V Curve Test

The primary aim of this test is to validate whether the proposed procedure aligns with the goals of the characteristic I-V curve method. The test has been executed to detect anomalies within the procedure method described.

The test was performed on the 29th of June 2 023 at 15:31 with a PV panel surface temperature of 38 ºC (Fluke multimeter), while the irradiance measured is 918 W/m² (SR30-M2-D1).

One hundred points were defined for this experiment, fifty referenced to the $V_{oc}$ (43.2 V) and fifty more to the $I_{sc}$ (3 A). The measurement started from 0 V, implementing a voltage interval of + 43.2 V / 50 to the DC load until the measurement reached $V_{oc}$, where the current would be 0 A. Then, the points sent to the DC load would begin to be measured, having as RCP the $I_{sc}$, with a variation of + 3 A / 50 until reaching $I_{sc}$.

Two graphs are displayed after performing two-point sweeps, one concerning $V_{oc}$, Figure 97 and the other regarding $I_{sc}$, Figure 96.
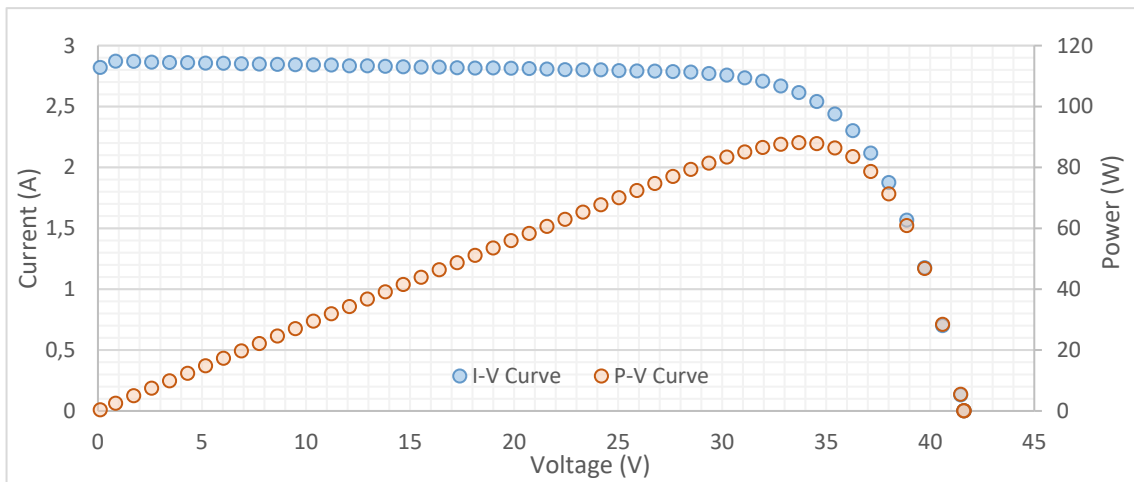


*Figure 97. Second test: I-V Curve with the $V_{oc}$ as RCP.*
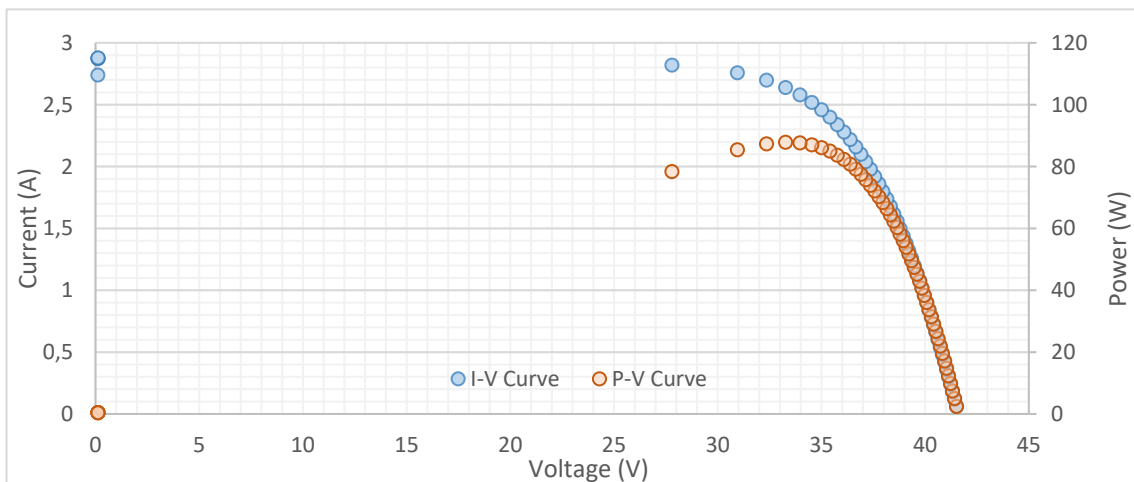


*Figure 96. Second test: I-V Curve with the $I_{sc}$ as RCP.*

Figure 98 illustrates the two graphs superimposed to get the complete I-V curve.
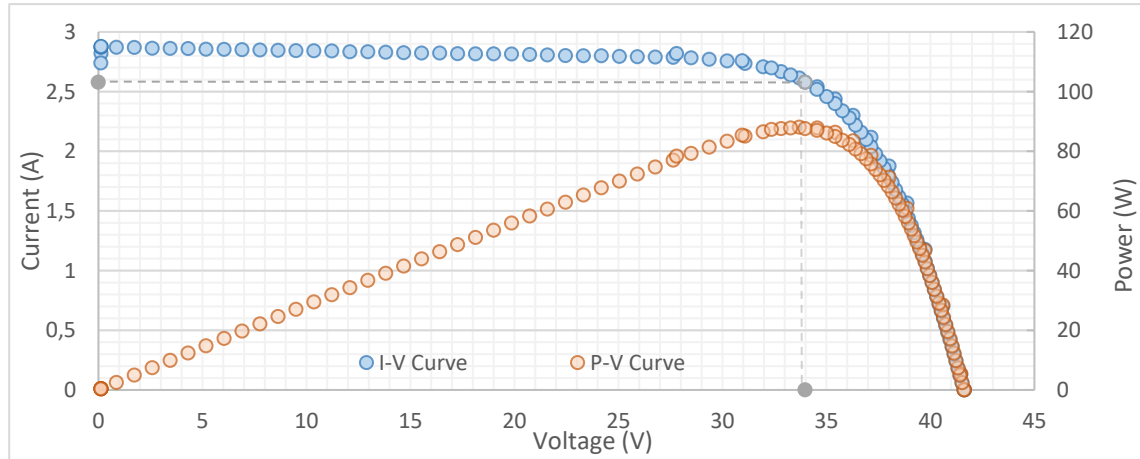


*Figure 98. Second test: Complete I-V Curve.*

The PV panel characteristics that can be obtained from the graph are:

V$_{OC}$: 40.72 V                                                        I$_{MPP}$: 2.51 A

I$_{SC}$: 2.80 A                                                         V$_{MPP}$: 33,10 V

P$_{MPP}$: 83.40 W

With these data, the fill factor value can be calculated:

$$FF = \frac{P_{MPP}}{V_{OC} \; I_{SC}} = \frac{83.40}{40.72 * 2.80} = 0.73$$

Then, to adjust the V$_{OC}$ and the I$_{SC}$ curve to the STC, the following equations should be used:

$$I_{SC(STD)} = \frac{G_{STD}}{G} \; I_{SC_{(measured)}} + \alpha \; (T_{STD} - T_{cell})$$

$$V_{OC(STD)} = V_{OC_{(measured)}} + \beta \; (T_{STD} - T_{cell}) + \frac{nKT_{cell}}{e} \ln\left(\frac{G_{STD}}{G}\right)$$

And for the rest of the measured points:

$$I_{(STD)} = I_{(measured)} + I_{SC_{(measured)}} \left(\frac{G_{STD}}{G} - 1\right) + \alpha \; (T_{STD} - T_{cell})$$

$$V_{(STD)} = V_{(measured)} + \beta \; (T_{STD} - T_{cell}) - F_{CC} \; I_{(STD)}(T_{STD} - T_{cell}) - R_S(I_{STD} - I_{(measured)})$$

For the PV panel selected, SunPlus 100, the I$_{SC}$ temperature coefficient ($\alpha$) is -0.33 % / ºC, and the V$_{OC}$ temperature coefficient ($\beta$) is 0,05 % / ºC. The number of cells in series (n) is 72. The datasheet does not specify the series resistance (R$_S$) and the curve correction factor (Fcc). Therefore, the typical values of these parameters have been taken: 1 $\Omega$ cm² for the R$_S$ (106) and 1.25 mW /ºC for the Fcc (102).

Figure 99 shows the I-V curve adjusted to STC.
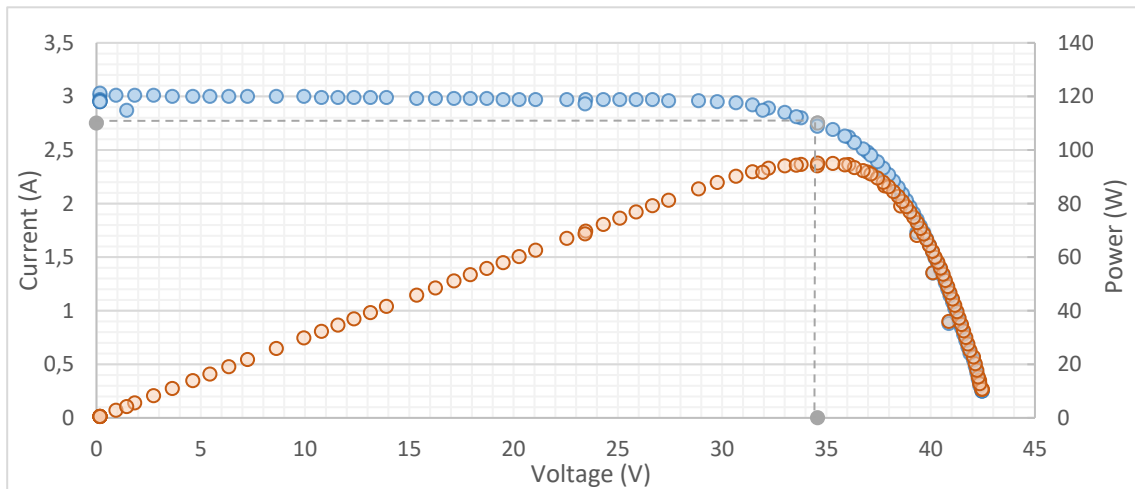


*Figure 99. Second test: Complete I-V Curve adjusted to STC.*

The PV panel characteristics obtained from the I-V curve adjusted to STC are the following:

$V_{OC}$: 42.48 V                                    $I_{MPP}$: 2.75 A

$I_{SC}$: 3.03 A                                    $V_{MPP}$: 34.58 V

$P_{MPP}$: 95.10 W

With these data, the fill factor value can be calculated:

$$FF = \frac{P_{MPP}}{V_{OC}\ I_{SC}} = \frac{95.10}{42.48 * 3.03} = 0.74$$

The obtained values closely match those specified in the panel datasheet. According to the datasheet, the $V_{OC}$ is 43.2 V, and the $I_{SC}$ is 3 A. The maximum power point is identified with a $V_{MPP}$ of 36 V and $I_{MPP}$ of 2.78 A, resulting in a maximum power point of 100 W.

87

## 6.2. Dark I-V Curve Test

The dark I-V curve measurement is conducted indoors at the KTH Laboratory. The PV panel evaluated is the SunPlus 100 W, and the selected DC power supply is defined in the 5.2 Dark I-V Curve Measurement. Due to not all the required sensors are available because their estimated arrival is not within the time frame of the work, the DC power supply is used to measure the current and voltage values.

The PV panel is completely covered in order not to have any interference in terms of irradiation, achieving a dark environment. During the dark I-V curve measurement, the temperature is 25.8 ºC. The setup for this experiment is shown in Figure 100.



*Figure 100. Dark I-C Curve Setup.*

The DC power supply is directly connected to the PV panel. The results obtained from the dark I-V curve measurement are plotted in Figure 101.
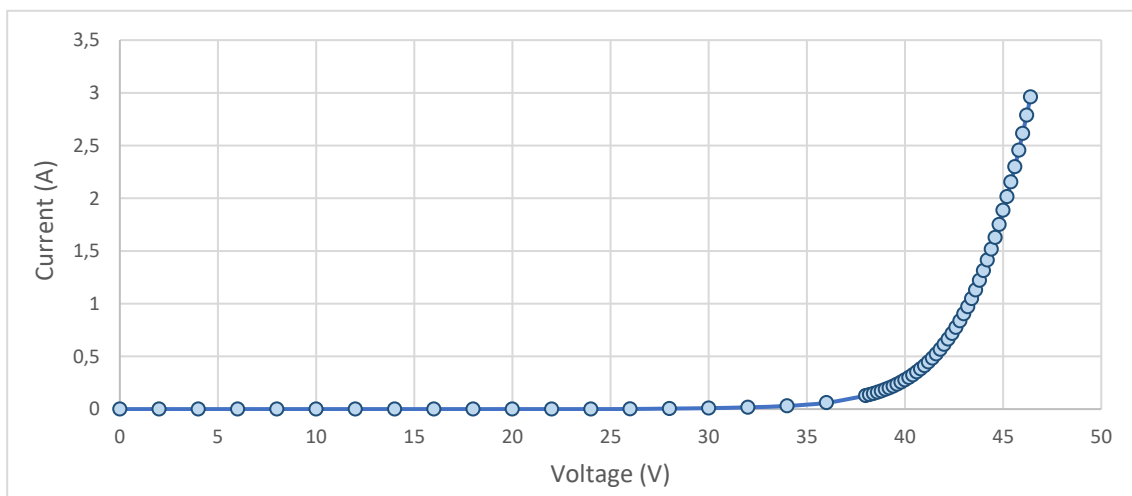


*Figure 101. First Experiment: Dark I-V Curve.*

During the data collection, a residual current measurement is taken at intervals of 2 V until reaching 38 V, where the current readings displayed more significant changes. Measurements are taken at intervals of 0.2 V starting from 38 V to accurately define the dark I-V curve, continuing

until 46.4 V. The final measurement is conducted because the resulting current reached 2.91 A, close to the I$_{SC}$, 3 A. The results for the PV panel analysed are the expected ones. The complete dark I-V curve is traced, showing that there is not any PID problem there.

A comparison between the dark I-V curve measured with the resultant I-V curve adjusted to STC realised in the complete I-V curve test can be achieved, as shown in Figure 102.
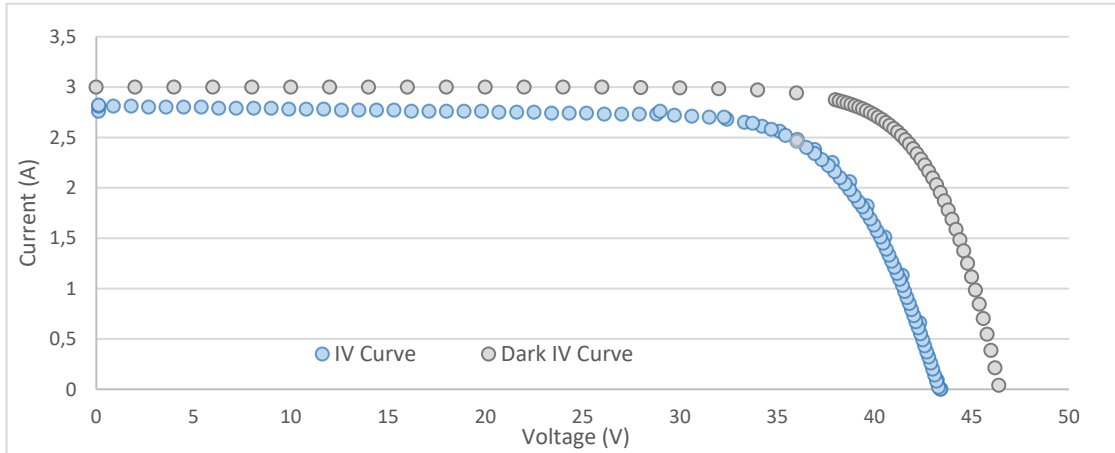


*Figure 102. Comparison among I-V Curve and Dark I-V Curve.*

The main difference between both curves is the higher voltages measured in the dark I-V curve provoked by the absence of photocurrent in the dark environment. Concerning the observed current behaviour, this could be attributed to cell deterioration or inadequate homogenisation of cell properties.

In addition, with the measurement points, another graph with a current logarithmic scale is presented where the values of R$_s$ and R$_{shunt}$ can be analysed.

As illustrated in Figure 103, the DC power supply records the lowest value at 26 V (0.001 A), while the remaining values are indicated as 0 A. Consequently, a device with increased sensibility within lower current ranges is necessary to generate a complete dark I-V curve on a logarithmic scale. Despite this limitation, the curve aligns with the anticipated results for this method.
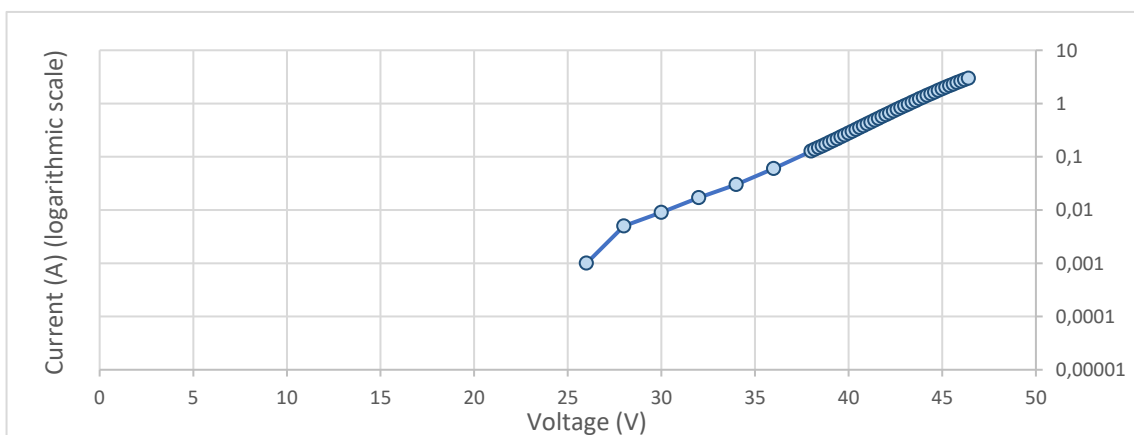


*Figure 103. Dark I-V Curve with Logarithmic Scale.*

# 7. User Control Interface

This chapter will provide an examination of the PV remote lab interface composition. The interface has been designed to facilitate comprehensive control and monitoring of the PV remote lab, encompassing everything from scenario selection to result visualisation. The interface comprises seven distinct windows.

## 7.1. Main Menu

The interface's main menu, shown in Figure 104, serves as the initial window from which six additional windows can be accessed. Within this menu, users can consult and access the following information and features:

**1. PV panel characteristics:** The different parameters of the PV panels installed in the system can be consulted.

**2. Scenarios of the PV system:** The possible configurations of the PV panels can be consulted and selected with the help of the scenarios schematics.

**3. Scenarios of the System Outputs:** The possible defined outputs of the system can be consulted and selected with the help of the scenarios schematics.

**4. Scenario Implemented:** The PV panel configuration and the selected outputs can be consulted, and the desired characterisation method should be chosen.

**5. Test results:** Shows the results of the implemented method with all relevant data.

**6. Direct Streaming:** Live broadcast of the PV remote lab simulator.
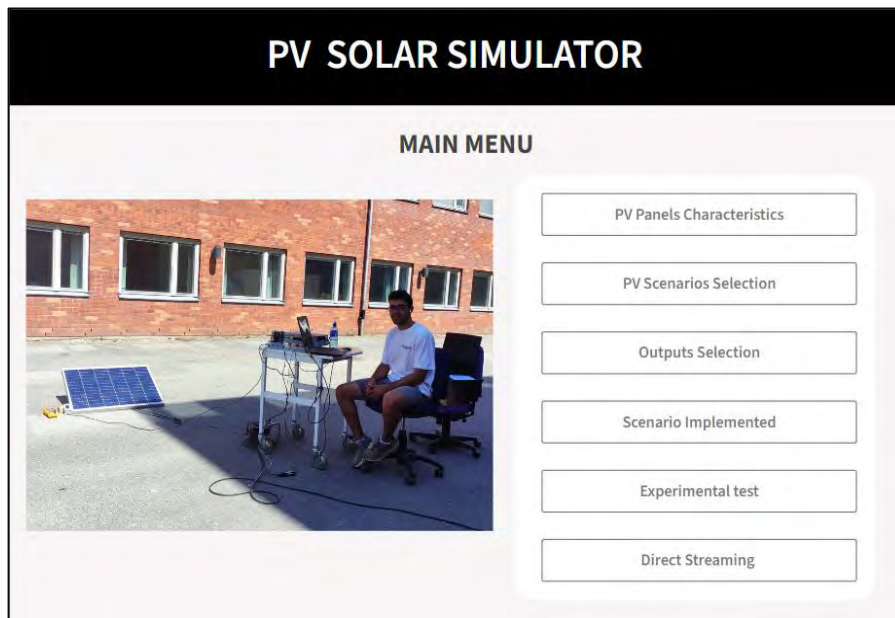


*Figure 104. Interface: Main Menu.*

## 7.2. PV Panel Characteristics

This interface displays the essential characteristics of the PV panels installed in the PV remote lab as can be consulted in Figure 105. The interface provides the maximum power point, $I_{SC}$ and $V_{OC}$. Additionally, it offers information of the number of cells connected in series and the PV panel and cell efficiency, all of which are critical data for conducting the characterisation of the PV panels.



| | SunPlus 100 | SunPlus S 50 | STP0309 |
|---|---|---|---|
| Maximum Power (Pmp) | 100 Wp | 50 Wp | 30 Wp |
| Current at max power (Imp) | 2.78 A | 2.84 A | 1.15 A |
| Voltage at max power (Vmp) | 36 V | 17.6 V | 17.5 V |
| Short-circuti current (Isc) | 3 A | 3.07 A | 1.27 A |
| Open Circuit Voltage (Voc) | 43.2 V | 21.6 V | 22 V |
| Cells number | type | 72 | poly | 36 | mono | 36 | mono |
| Cells Efficiency | 17.2 % | 18.4 % | 17 % |
| Module Efficiency | 13.6 % | 15.2 % | 15.2 % |
| Surface | 734 x 1001 x 35 mm | 650 x 505 mm | 660 x 380 x 25 mm |
| Weight | 8,1 kg | 4.8 kg | 2.8 kg |

Standard Test Conditions: Tcell 25 °C, Irradiation 1 000 W/m2, Spectrum AM 1.5

**PV Panel Identification**

- STP0309 (30 Wp) ⇒ 01. 30 Wp
- STP0309 (30 Wp) ⇒ 02. 30 Wp
- SunPlus S50 (50 Wp) ⇒ 03. 50 Wp
- SunPlus S50 (50 Wp) ⇒ 04. 50 Wp
- SunPlus 100 (100 Wp) ⇒ 05. 100 Wp
- SunPlus 100 (100 Wp) ⇒ 06. 100 Wp

Back to Main Menu

*Figure 105. Interface: PV Panels Characteristics.*

The interface also includes the identification of the PV panels based on the designed schemes. Moreover, users can return to the main menu, providing convenient navigation within the system.

## 7.3. Scenarios of the PV System

The interface presents a comprehensive list of the PV system scenarios created for the PV remote lab. When a user selects one of the scenarios from the dropdown menu, the corresponding circuit scheme for that scenario is displayed. This visual representation assists users in choosing the specific scenario they wish to implement. The selection made in this tab is instrumental in executing the chosen scenario within the PV remote lab.

Users can visit both PV panel scenario interfaces, Figure 107 and Figure 106 and return to the main menu, providing convenient navigation within the system.
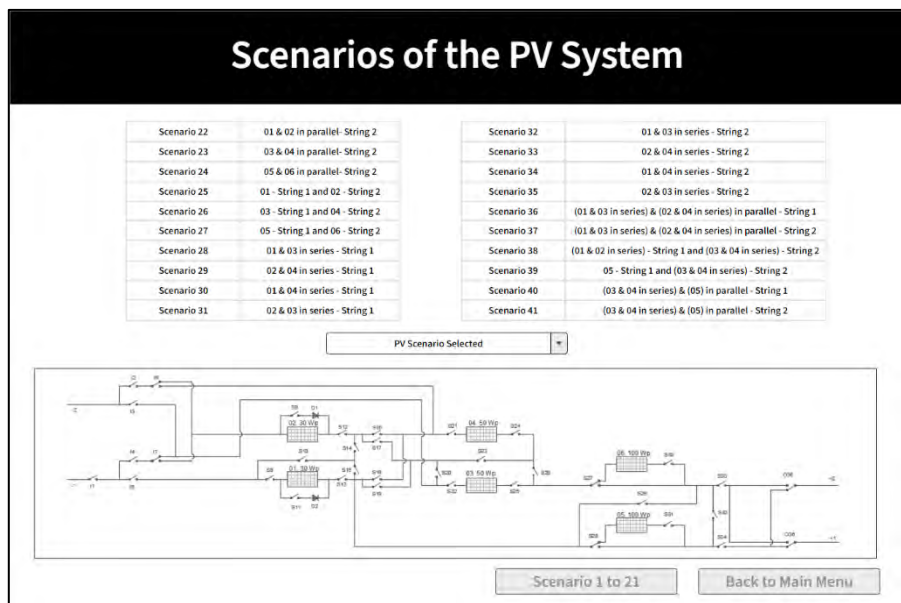


*Figure 107. Interface: Scenarios of the PV System (22 to 41).*
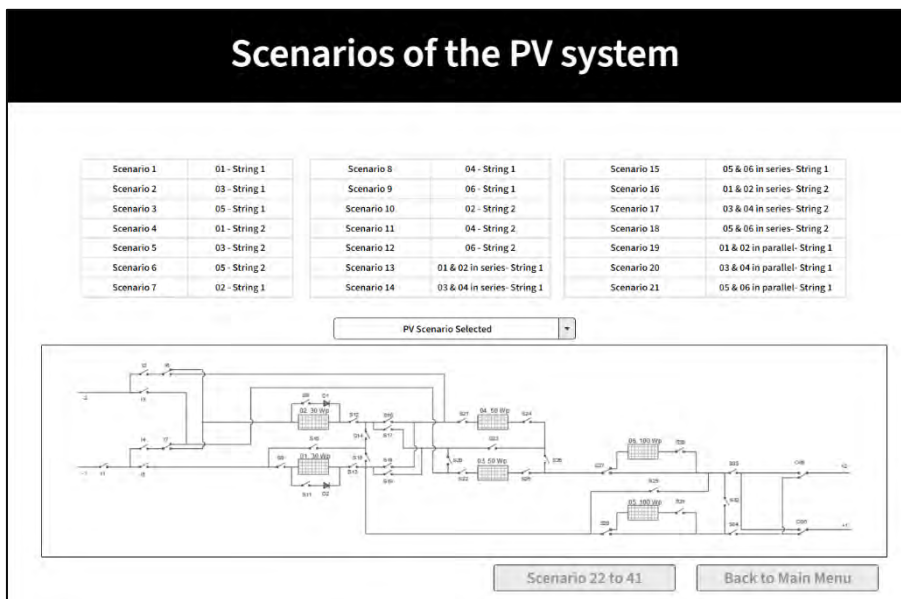


*Figure 106. Interface: Scenarios of the PV System (1 to 21).*

## 7.4. Scenarios of the System Outputs

Figure 108 shows the PV remote lab's different outputs for each PV string. Selecting the desired option in the drop-down tab displays the electrical circuit that will be implemented in the PV remote lab.
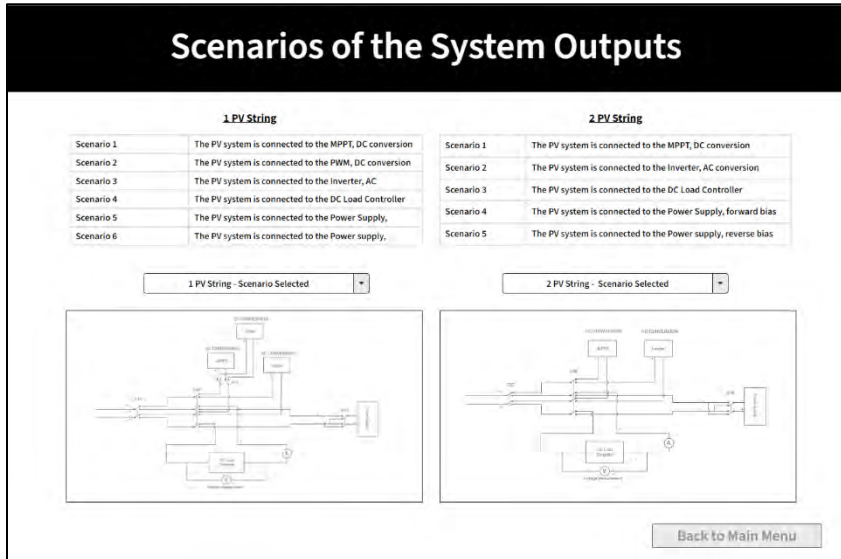


*Figure 108. Interface: Scenarios of the Outputs of the System.*

Users can return to the main menu, providing convenient navigation within the system.

## 7.5. Scenario Implemented

In this interface, Figure 109, are shown the PV system scenario and the system outputs scenarios selected previously. In addition to providing a final consultation for the chosen scenarios, users can select the preferred characterisation method. Users can select from three methods: the IV curve, the dark IV curve, or the electroluminescence method. Moreover, the desired irradiance level for the PV system simulator should be defined. Users can return to the main menu, providing convenient navigation within the system.
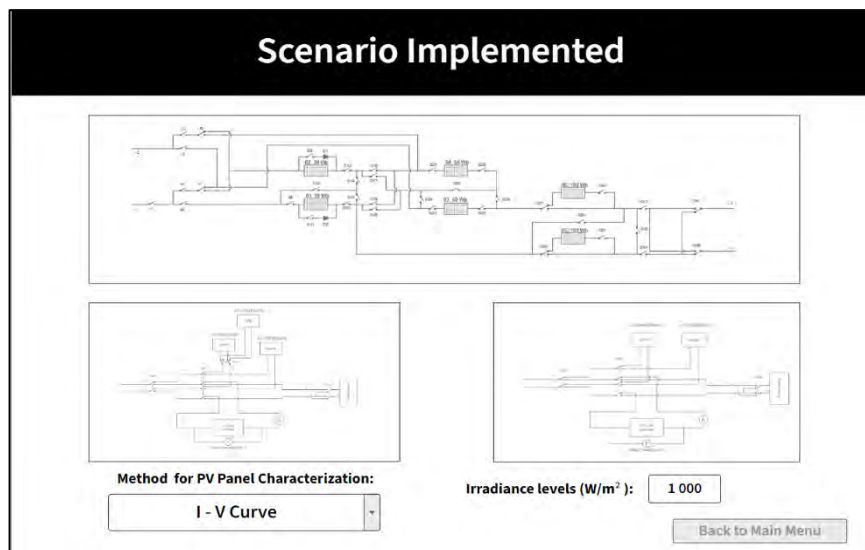


*Figure 109. Interface: Scenario Implemented.*

## 7.6. Test Results

Distinct windows will appear based on the method chosen for PV panel characterisation. Users can return to the main menu in all the windows, providing convenient navigation within the system.

### 7.6.1. I-V Curve Method

When the I-V curve method is employed within the system, the displayed window in Figure 110 is depicted. This window illustrates the selected scenarios and the associated environmental conditions during the test. It also provides a graphical representation of the I-V curve and the key parameters. Similarly, the same information is presented for the I-V curve adjusted to Standard Test Conditions (STC) and the corresponding parameters.
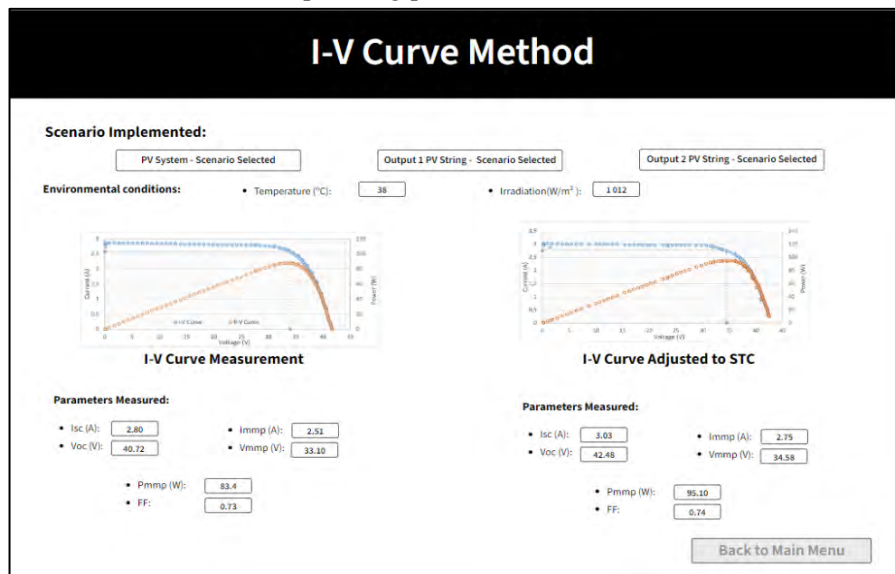


*Figure 110. Interface: I-V Curve Method.*

### 7.6.2. Dark I-V Curve Method

In the case of a dark I-V curve method, the interface displays the selected scenarios and the corresponding environmental conditions for the test, as can be consulted in Figure 111. The window further provides graphical representations of the dark I-V curve in linear and
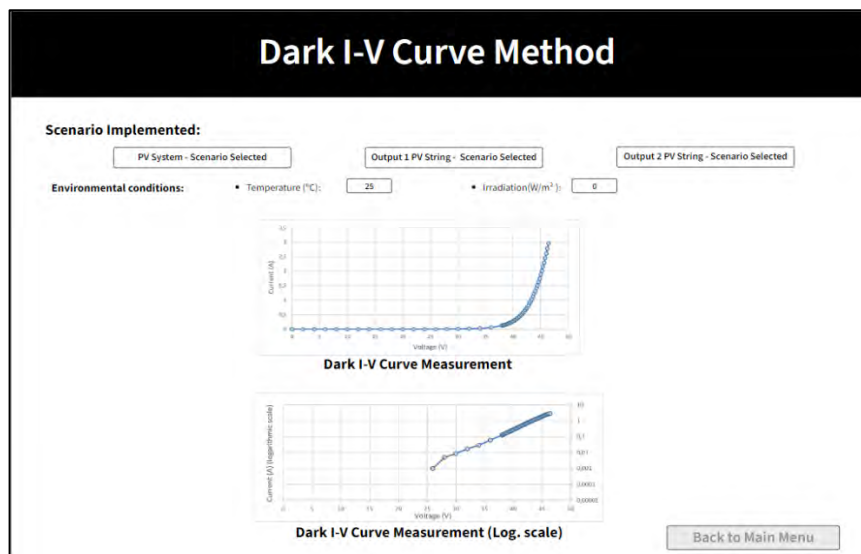


*Figure 111. Interface: Dark I-V Curve Measurement.*

94

logarithmic scales. The availability of these two representations is crucial for analysing the PV panels.

### 7.6.3. Electroluminescence Method

When utilising the electroluminescence method, the interface showcases the chosen scenarios and provides information about the environmental conditions during image acquisition. The electroluminescence method interface is shown in Figure 112. Moreover, it presents the electroluminescence image, allowing users to assess the evaluated PV panel's state visually.
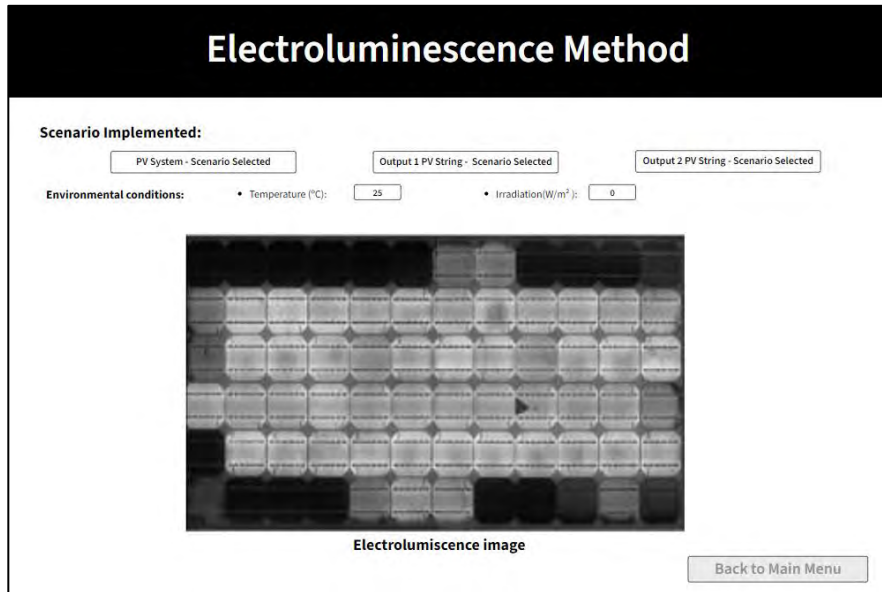


*Figure 112. Electroluminescence Method.*

## 7.7. Direct Streaming

Within this window, Figure 113, users can monitor the real-time status of the PV remote lab. This feature allows immediate access to the lab's current conditions and operations. Users can return to the main menu, providing convenient navigation within the system.
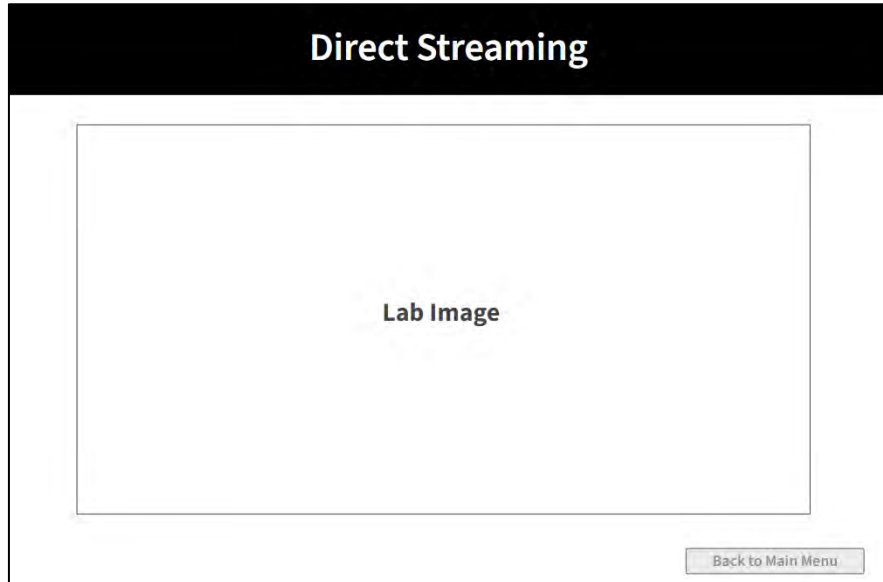


*Figure 113. Direct Streaming.*

# 8. Conclusion

The literature review presented at the beginning of the document has greatly assisted in developing a PV system simulator that fulfils the objectives defined. Describing the functions of each element, characterisation methods and the degradation modes of PV panels has been instrumental in appropriately shaping the PV system simulator.

The implemented commutation block facilitates system flexibility and scalability assurance, enabling the practical realisation of numerous scenarios and replicating the desired PV configuration. All components constituting the PV system simulator have been dimensioned according to the system's requirements and limitations. The PV solar simulator is efficiently integrated within the same support structure, allowing for convenient mobility. The user control interface can also remotely control the PV system simulator.

The tests performed to validate the defined characterisation methods have yielded successful results. The pending tests on the PV system simulator will be conducted once the remaining components have been received.

After checking the successful operation of the proposed system, it becomes evident that the PV system simulator can play a pivotal role in facilitating educational initiatives and enhancing industry professionals' skills. This simulator can serve as a comprehensive training centre, offering a valuable resource for KTH students and a practical tool for individuals working in the PV industry. The multifunctional capabilities of the PV remote lab make it an ideal platform for hands-on learning and skill development in photovoltaics, further bridging the gap between academic knowledge and practical industry application

# 9. Next Steps

Once all the requisite components are accessible, conducting a thorough PV system simulator evaluation becomes imperative. This entails adhering to the characterisation techniques elucidated earlier. Upon the availability of the electroluminescence camera, it is crucial to execute the verification of the process. Furthermore, a comparative analysis between solar chargers and inverters can be conducted.

After confirming the accurate functionality of the PV system simulator, subsequent tests can be executed to identify various degradation modes.

Figure 114 delineates the characterisation methods that can effectively pinpoint prevalent degradation modes in solar panels. Incorporating these tests in the simulator in the future would enhance its educational and practical value. Students and industry professionals would then have the opportunity to observe the repercussions of these degradation modes.
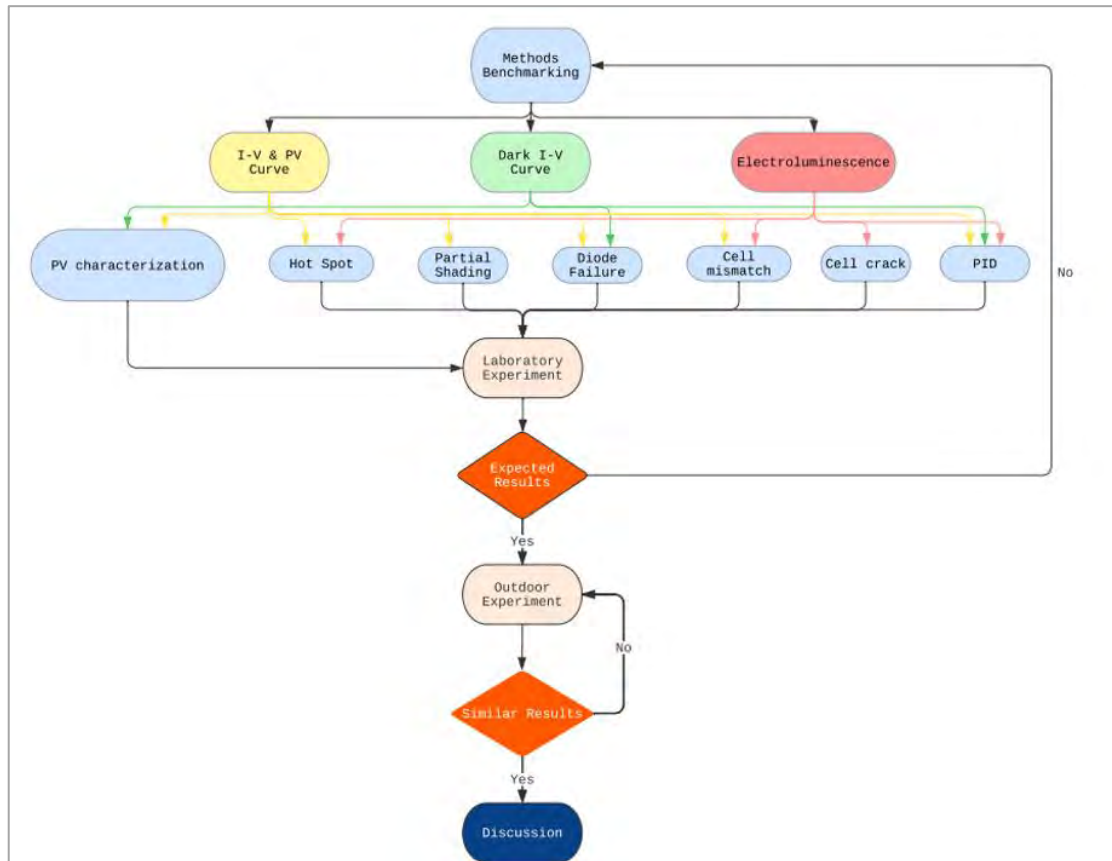


*Figure 114. Degradation Modes Test Identification.*

## References

1.  United Nations. Kyoto protocol to the United Nations framework convention on climate change [Internet]. 1997. Available from: https://unfccc.int/kyoto_protocol

2.  United Nations. Paris Agreement [Internet]. 2015. Available from: https://unfccc.int/process-and-meetings/the-paris-agreement

3.  International Energy Agency [Internet]. 2021. Net Zero by 2050. Available from: https://www.iea.org/reports/net-zero-by-2050

4.  International Energy Agency [Internet]. [cited 2023 Jan 25]. Net zero by 2050 hinges on a global push to increase energy efficiency – Analysis. Available from: https://www.iea.org/articles/net-zero-by-2050-hinges-on-a-global-push-to-increase-energy-efficiency

5.  International Energy Agency. World Energy Outlook 2022. Available from: https://www.iea.org/reports/world-energy-outlook-2022

6.  International Energy Agency [Internet]. [cited 2023 Jan 25]. Renewable Electricity – Analysis. Available from: https://www.iea.org/reports/renewable-electricity

7.  Use of hydrogen - U.S. Energy Information Administration (EIA) [Internet]. [cited 2023 Feb 8]. Available from: https://www.eia.gov/energyexplained/hydrogen/use-of-hydrogen.php

8.  Ohl R. Ligh sensitive electric device. US patent No. 2,402; 1941. 662 p.

9.  Our World in Data [Internet]. [cited 2023 Feb 1]. Solar photovoltaic (PV) module prices. Available from: https://ourworldindata.org/grapher/solar-pv-prices

10. MIT News | Massachusetts Institute of Technology [Internet]. 2018 [cited 2023 Feb 3]. Explaining the plummeting cost of solar power. Available from: https://news.mit.edu/2018/explaining-dropping-solar-cost-1120

11. Infographic: Competitiveness of Renewables Continued amid Fossil Fuel Crisis [Internet]. 2022 [cited 2023 Feb 3]. Available from: https://www.irena.org/News/articles/2022/Jul/Competitiveness-of-Renewables-Continued-Amid-Fossil-Fuel-Crisis

12. IEA [Internet]. [cited 2023 Feb 8]. Solar PV – Analysis. Available from: https://www.iea.org/reports/solar-pv

13. Sarkar S, Rahman M. Power-Energy Optimization of Solar Photovoltaic Device Modeling. In: 2018 IEEE Electron Devices Kolkata Conference (EDKCON) [Internet]. Kolkata, India: IEEE; 2018 [cited 2023 Feb 9]. p. 541–6. Available from: https://ieeexplore.ieee.org/document/8770431/

14. Al-Ezzi AS, Ansari MNM. Photovoltaic Solar Cells: A Review. ASI. 2022 Jul 8;5(4):67.

15. Awogbemi O, Oluwaleye IO, Komolafe CA. A Survey Of Solar Energy Utilization For Sustainable Development In Nigeria. JMEST.

16. Hashim ET, Abbood AA. Temperature Effect on Power Drop of Different Photovoltaic Modules. Journal of Engineering. 2016;22(5).

17.  Zhu Y, Xiao W. A comprehensive review of topologies for photovoltaic I–V curve tracer. Solar Energy. 2020 Jan;196:346–57.

18.  American Society for Testing and Materials, 1985, 'Standard Methods of Testing Electrical Performance of Nonconcentrator Terrestrial Photovoltaic Modules and Arrays Using Reference Cells: E 1036', Philadelphia, 10 p.

19.  Associação Brasileira de Normas Técnicas, 1991, 'Dispositivos fotovoltaicos – Correção das curvas características corrente versus tensão (IxV), em função da temperatura e radiação: NB-1386', Rio de Janeiro, 3 p.

20.  Sugianto S. Comparative Analysis of Solar Cell Efficiency between Monocrystalline and Polycrystalline. Intek. 2020 Dec 4;7(2):92.

21.  IEA [Internet]. [cited 2024 Mar 12]. Solar. Available from: https://www.iea.org/energy-system/renewables/solar-pv

22.  International Technology Roadmap for Photovoltaic (ITRPV) - vdma.org - VDMA [Internet]. [cited 2023 Feb 20]. Available from: https://www.vdma.org/international-technology-roadmap-photovoltaic

23.  Szabo L. The history of using solar energy. In: 2017 International Conference on Modern Power Systems (MPS) [Internet]. Cluj-Napoca, Romania: IEEE; 2017 [cited 2023 Feb 3]. p. 1–8. Available from: http://ieeexplore.ieee.org/document/7974451/

24.  Fraunhofer Institute for Solar Energy Systems ISE [Internet]. 2022 [cited 2023 Feb 3]. Fraunhofer ISE Develops the World's Most Efficient Solar Cell with 47.6 Percent Efficiency - Fraunhofer ISE. Available from: https://www.ise.fraunhofer.de/en/press-media/press-releases/2022/fraunhofer-ise-develops-the-worlds-most-efficient-solar-cell-with-47-comma-6-percent-efficiency.html

25.  Mismatch for Cells Connected in Parallel | PVEducation [Internet]. [cited 2023 Mar 16]. Available from: https://www.pveducation.org/pvcdrom/modules-and-arrays/mismatch-for-cells-connected-in-parallel

26.  Kyritsis A, Papanikolaou N, Christodoulou C, Gonos I, Tselepis S. Installation Guidelines. In: McEvoy's Handbook of Photovoltaics [Internet]. Elsevier; 2018 [cited 2023 Feb 9]. p. 891–914. Available from: https://linkinghub.elsevier.com/retrieve/pii/B9780128099216000240

27.  Ko SW, Ju YC, Hwang HM, So JH, Jung YS, Song HJ, et al. Electric and thermal characteristics of photovoltaic modules under partial shading and with a damaged bypass diode. Energy. 2017 Jun;128:232–43.

28.  Technology E. Electrical Technology. 2019 [cited 2023 Mar 16]. What is Blocking Diode and Bypass Diode in Solar Panel Junction Box? Available from: https://www.electricaltechnology.org/2019/10/blocking-bypass-diode-solar-panel-junction-box.html

29.  Rabbani MA. Solar power systems and DC to AC inverters. 2022; Available from: https://www.researchgate.net/publication/348371201_SOLAR_POWER_SYSTEMS_AND_DC_TO_AC_INVERTERS

30. Abed AN, Kasim NK, Al-Saleem H. Performance Improvement of CIGS PV Solar Grid Tied System Using Planer Concentrators, Case Study : Baghdad. 2020 [cited 2023 Feb 20]; Available from: http://rgdoi.net/10.13140/RG.2.2.33172.73604

31. Weckend S, Wade A, Heath G. End of Life Management: Solar Photovoltaic Panels [Internet]. 2016 Aug [cited 2023 Feb 20] p. NREL/TP-6A20-73852, 1561525. Report No.: NREL/TP-6A20-73852, 1561525. Available from: https://www.osti.gov/servlets/purl/1561525/

32. Ai-Habahbeh OM, Al-Hrout BA, Al-Hiary EM, Al-Fraihat SA. Reliability investigation of photovoltaic cell using finite element modelling. In: 2013 9th International Symposium on Mechatronics and its Applications (ISMA) [Internet]. Amman, Jordan: IEEE; 2013 [cited 2023 Feb 20]. p. 1–5. Available from: https://ieeexplore.ieee.org/document/6547391/

33. Kalejs J. Junction box wiring and connector durability issues in photovoltaic modules. In: Dhere NG, Wohlgemuth JH, Jones-Albertus R, editors. San Diego, California, United States; 2014 [cited 2023 Feb 21]. p. 91790S. Available from: http://proceedings.spiedigitallibrary.org/proceeding.aspx?doi=10.1117/12.2063488

34. Design and Implementation of PWM Charge Controller and Solar Tracking System. IJSR. 2015 May 5;5(5):1214–7.

35. Acharya PS, Aithal PS. A Comparative Study of MPPT and PWM Solar Charge Controllers and their Integrated System. J Phys: Conf Ser. 2020 Dec 1;1712(1):012023.

36. Thounaojam W, Ebenezer V, Balekundri A. Design and Development of Microcontroller Based Solar Charge Controller. IJETAE.

37. Awale KS, Kumbhar AU, Kole VA, Kamate JB. Arduino Based MPPT Solar Charge Controller. J Electr Electron Syst [Internet]. 2017 [cited 2023 Mar 17];06(02). Available from: https://www.omicsgroup.org/journals/arduino-based-mppt-solar-charge-controller-2332-0796-1000221.php?aid=89246

38. Islam MS. Thin Film Solar Charge Controller: A Research Paper for Commercialization of Thin Film Solar Cell. Advances in Energy and Power. 2015 May;3(2):29–60.

39. Technical-Information-Which-solar-charge-controller-PWM-or-MPPT.pdf [Internet]. [cited 2023 Oct 12]. Available from: https://www.victronenergy.com/upload/documents/Technical-Information-Which-solar-charge-controller-PWM-or-MPPT.pdf

40. Patrao I, Figueres E, González-Espín F, Garcerá G. Transformerless topologies for grid-connected single-phase photovoltaic inverters. Renewable and Sustainable Energy Reviews. 2011 Sep;15(7):3423–31.

41. Ikkurti HP, Saha S. A comprehensive techno-economic review of microinverters for Building Integrated Photovoltaics (BIPV). Renewable and Sustainable Energy Reviews. 2015 Jul;47:997–1006.

42. Pisano M, Bizzarri F, Brambilla A, Gruosso G, Gajani GS. Micro-inverter for solar power generation. In: International Symposium on Power Electronics Power Electronics, Electrical Drives, Automation and Motion [Internet]. Sorrento, Italy: IEEE; 2012 [cited 2023 Mar 17]. p. 109–13. Available from: http://ieeexplore.ieee.org/document/6264547/

43. Adda R, Ray O, Mishra SK, Joshi A. Synchronous-Reference-Frame-Based Control of Switched Boost Inverter for Standalone DC Nanogrid Applications. IEEE Trans Power Electron. 2013 Mar;28(3):1219–33.

44. Patil AA, Bhosale Y. Development of Bi-directional energy meter for a grid-connected PV system with power quality improvement using D-STATCOM. In: 2019 International Conference on Computation of Power, Energy, Information and Communication (ICCPEIC) [Internet]. Melmaruvathur, Chennai, India: IEEE; 2019 [cited 2023 Feb 23]. p. 130–4. Available from: https://ieeexplore.ieee.org/document/9082363/

45. Oyelami S, Nurudeen A. A Pyranometer for Solar Radiation Measurement-Review. 2020.

46. Seven Sensor [Internet]. 2020 [cited 2023 Mar 15]. Comparison of Pyranometers Vs. Reference Cell Solar Irradiance Sensors | Seven Sensor | sevensensor.com. Available from: https://www.sevensensor.com/comparison-of-pyranometers-vs-reference-cell-solar-irradiance-sensors

47. Azouzoute A, Merrouni AA, Bennouna EG, Gennioui A. Accuracy Measurement of Pyranometer vs Reference cell for PV resource assessment. Energy Procedia. 2019 Jan;157:1202–9.

48. Solar Module Temperature Sensor-MSPT-100 | Online Store | Buy Now | TrackSo [Internet]. [cited 2023 Mar 17]. Available from: https://trackso.in/shop/product/surface-module-temperature-mspt-100/

49. van Dyk EE, Gxasheka AR, Meyer EL. Monitoring current–voltage characteristics and energy output of silicon photovoltaic modules. Renewable Energy. 2005 Mar;30(3):399–411.

50. Morales-Aragonés JI, Dávila-Sacoto M, González LG, Alonso-Gómez V, Gallardo-Saavedra S, Hernández-Callejo L. A Review of I–V Tracers for Photovoltaic Modules: Topologies and Challenges. Electronics. 2021 May 27;10(11):1283.

51. Duran E, Piliougine M, Sidrach-de-Cardona M, Galan J, Andujar JM. Different methods to obtain the I-V Curve of PV modules: A review. In: 2008 33rd IEEE Photovolatic Specialists Conference [Internet]. San Diego, CA, USA: IEEE; 2008 [cited 2023 Feb 14]. p. 1–6. Available from: https://ieeexplore.ieee.org/document/4922578

52. Khatib T, Elmenreich W, Mohamed A. Simplified I-V Characteristic Tester for Photovoltaic Modules Using a DC-DC Boost Converter. Sustainability. 2017 Apr 20;9(4):657.

53. Marquez JMA, M. A. Bohórquez, J. M. Enrique, E. Durán, M. Sidrach, J.A. Carretero. Analysis and failures monitoring in PV panels by means of I-V and P-V curves using dc-dc converters. 2005 [cited 2023 Feb 16]; Available from: http://rgdoi.net/10.13140/RG.2.1.3825.8966

54. IEA-PVPS. Qualification of Photovoltaic (PV) Power Plants using Mobile Test Equipment 2021. 2021.

55. Bouzidi K, Chegaar M, Aillerie M. Solar Cells Parameters Evaluation from Dark I-V Characteristics. Energy Procedia. 2012;18:1601–10.

56. Owen-Bellini M, Sulas-Kern DB, Perrin G, North H, Spataru S, Hacke P. Methods for *In Situ* Electroluminescence Imaging of Photovoltaic Modules Under Varying Environmental Conditions. IEEE J Photovoltaics. 2020 Sep;10(5):1254–61.

57. International Electrotechnical Commission. IEC 60904-1: Photovoltaic devices – Part 1: Measurement of photovoltaic current-voltage characteristics. 2006.

58. Berardone I, Lopez Garcia J, Paggi M. Analysis of electroluminescence and infrared thermal images of monocrystalline silicon photovoltaic modules after 20 years of outdoor use in a solar vehicle. Solar Energy. 2018 Oct;173:478–86.

59. Kropp T, Berner M, Stoicescu L, Werner JH. Self-Sourced Daylight Electroluminescence From Photovoltaic Modules. IEEE J Photovoltaics. 2017 Sep;7(5):1184–9.

60. Fuyuki T, Kondo H, Yamazaki T, Takahashi Y, Uraoka Y. Photographic surveying of minority carrier diffusion length in polycrystalline silicon solar cells by electroluminescence. Appl Phys Lett. 2005 Jun 27;86(26):262108.

61. Jahn U, Herz M, Köntges M, Parlevliet D, Paggi M, Tsanakas I. Review on infrared and electroluminescence imaging for PV field applications: International Energy Agency Photovoltaic Power Systems Programme: IEA PVPS Task 13, Subtask 3.3: report IEA-PVPS T13-12:2018. Paris: International Energy Agency; 2018. 94 p.

62. Potthoff T, Bothe K, Eitner U, Hinken D, Köntges M. Detection of the voltage distribution in photovoltaic modules by electroluminescence imaging: Voltage distribution in pv modules by el imaging. Prog Photovolt: Res Appl. 2010 Mar;18(2):100–6.

63. Gabor AM, Ralli M, Montminy S, Alegria L, Bordonaro C, Woods J, et al. Soldering Induced Damage to Thin Si Solar Cells. 2006;

64. Dirk C. Jordan, Timothy J. Silverman, John H. Wohlgemuth, Sarah R. Kurtz, Kaitlyn VanSant. Photovoltaic failure and degradation modes. 2017; Available from: https://www.researchgate.net/publication/313113081_Photovoltaic_failure_and_degradati on_modes_PV_failure_and_degradation_modes

65. Balasubramani G, Thangavelu V, Chinnusamy M, Subramaniam U, Padmanaban S, Mihet-Popa L. Infrared Thermography Based Defects Testing of Solar Photovoltaic Panel with Fuzzy Rule-Based Evaluation. Energies. 2020 Mar 13;13(6):1343.

66. Kim J, Rabelo M, Padi SP, Yousuf H, Cho EC, Yi J. A Review of the Degradation of Photovoltaic Modules for Life Expectancy. Energies. 2021 Jul 15;14(14):4278.

67. Deng S, Zhang Z, Ju C, Dong J, Xia Z, Yan X, et al. Research on hot spot risk for high-efficiency solar module. Energy Procedia. 2017 Sep;130:77–86.

68. Alqaisi Z, Mahmoud Y. Comprehensive Study of Partially Shaded PV Modules With Overlapping Diodes. IEEE Access. 2019;7:172665–75.

69. Identification of faults on PV systems using thermography [Internet]. [cited 2023 Mar 16]. Available from: https://kitawa.de/en/thermography-pv-systems

70. Wendlandt S, Giese A, Drobisch A, Tornow D, Hanusch M, Berghold J, et al. The Temperature as the Real Hot Spot Risk Factor at PV-Modules. 27th European Photovoltaic Solar Energy Conference and Exhibition; 3553-3557. 2012;5 pages, 7896 kb.

71. Zhang Z, Hu G, Chen Q, Yan Z. Correntropy-based parameter estimation for photovoltaic array model considering partial shading condition. IET Renewable Power Generation. 2019 Jun;13(8):1309–16.
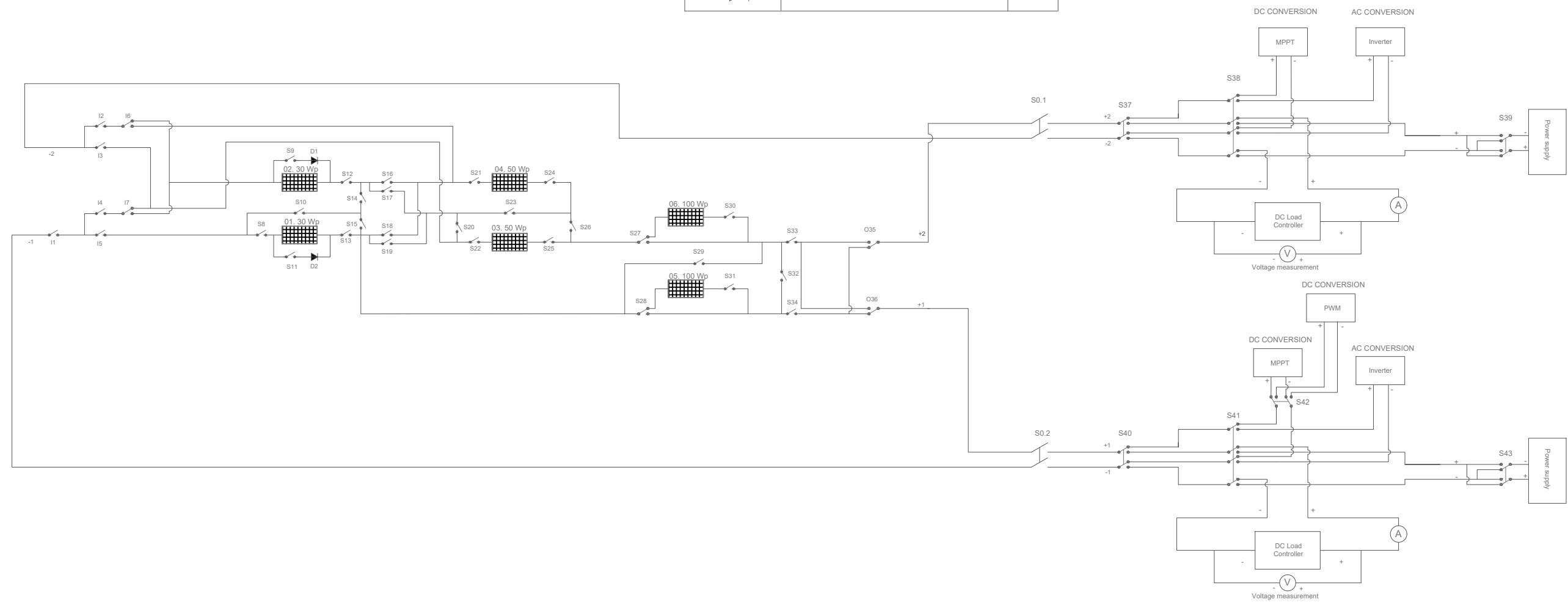
72. Kim KA, Seo GS, Cho BH, Krein PT. Photovoltaic Hot-Spot Detection for Solar Panel Substrings Using AC Parameter Characterization. IEEE Trans Power Electron. 2016 Feb;31(2):1121–30.

73. Khodapanah M, Ghanbari T, Moshksar E, Hosseini Z. Partial shading detection and hotspot prediction in photovoltaic systems based on numerical differentiation and integration of the $P − V$ curves. IET Renewable Power Generation. 2023;17(2):279–95.

74. Rajput P, Malvoni M, Kumar NM, Sastry OS, Tiwari GN. Risk priority number for understanding the severity of photovoltaic failure modes and their impacts on performance degradation. Case Studies in Thermal Engineering. 2019 Dec;16:100563.

75. Köntges M, Altmann S, Heimberg T, Jahn U, Berger KA. Mean degradation rates in pv systems for various kinds of pv module failures.

76. Xiao C, Hacke P, Johnston S, Sulas-Kern DB, Jiang C, Al-Jassim M. Failure analysis of field-failed bypass diodes. Prog Photovolt Res Appl. 2020 Sep;28(9):909–18.

77. Ahmed B, Necaibia A, Slimani A, Dabou R, Ziane A, Sahouane N. A Demonstrative Overview of Photovoltaic Systems Faults. In: 2019 1st Global Power, Energy and Communication Conference (GPECOM) [Internet]. Nevsehir, Turkey: IEEE; 2019 [cited 2023 Mar 17]. p. 281–5. Available from: https://ieeexplore.ieee.org/document/8778567/

78. Dhass AD, Beemkumar N, Harikrishnan S, Ali HM. A Review on Factors Influencing the Mismatch Losses in Solar Photovoltaic System. Álvarez-Gallegos A, editor. International Journal of Photoenergy. 2022 Feb 14;2022:1–27.

79. Park S, Cho Y, Kim S, Lee K, Yi J. Effect of Cell Electrical Mismatch on Output of Crystalline Photovoltaic Modules. Energies. 2022 Oct 10;15(19):7438.

80. Hajjaj C, Bouaichi A, Zitouni H, Alami Merrouni A, Ghennioui A, Ikken B, et al. Degradation and performance analysis of a monocrystalline PV system without EVA encapsulating in semi-arid climate. Heliyon. 2020 Jun;6(6):e04079.

81. Ndiaye A, Charki A, Kobi A, Kébé CMF, Ndiaye PA, Sambou V. Degradations of silicon photovoltaic modules: A literature review. Solar Energy. 2013 Oct;96:140–51.

82. Dallas W, Polupan O, Ostapenko S. Resonance ultrasonic vibrations for crack detection in photovoltaic silicon wafers. Meas Sci Technol. 2007 Mar 1;18(3):852–8.

83. Rueland, E., Herguth, A., Trummer, A.D., Wansleben, S., & Fath, P. (2005). OPTICAL μ-CRACK DETECTION IN COMBINATION WITH STABILITY TESTING FOR IN-LINE-INSPECTION OF WAFERS AND CELLS. Optical μ-crack detection in combination with stability testing for in-line-inspection of wafers and cells. 2005;

84. Pingel S, Frank O, Winkler M, Daryan S, Geipel T, Hoehne H, et al. Potential Induced Degradation of solar cells and panels. In: 2010 35th IEEE Photovoltaic Specialists Conference [Internet]. Honolulu, HI, USA: IEEE; 2010 [cited 2023 Mar 17]. p. 002817–22. Available from: http://ieeexplore.ieee.org/document/5616823/

85. Dhere NG, Shiradkar NS, Schneller E. Evolution of Leakage Current Paths in MC-Si PV Modules From Leading Manufacturers Undergoing High-Voltage Bias Testing. IEEE J Photovoltaics. 2014 Mar;4(2):654–8.

86. Berghold J, Koch S, Pingel S, Janke S, Ukar A, Grunow P, et al. PID: from material properties to outdoor performance and quality control counter measures. In: Dhere NG, Wohlgemuth JH, Jones-Albertus R, editors. San Diego, California, United States; 2015 [cited 2023 Mar 17]. p. 95630A. Available from: http://proceedings.spiedigitallibrary.org/proceeding.aspx?doi=10.1117/12.2188464

87. Mon G, Wen L, Meyer J. Electrochemical and galvanic corrosion efffcts in thin-film photovoitaic modules.

88. Dhere NG, Pandit MB. 17th European Photovoltaic Solar Energy Conference, Munich, Germany, 22-26 October 200.

89. Swanson R, Cudzinovic M, DeCeuster D, Desai V, Jürgens J, Kaminar N, et al. The surface polarization effect in high- efficiency silicon solar cells.

90. R. Doumane, M. Balistrou, P.O. Logerais, J.F. Durastanti. A model to estimate the efficiency loss of a photovoltaic module with aging. In 2012.

91. Pingel S, Frank O, Winkler M, Daryan S, Geipel T, Hoehne H, et al. Potential Induced Degradation of solar cells and panels. In: 2010 35th IEEE Photovoltaic Specialists Conference [Internet]. Honolulu, HI, USA: IEEE; 2010 [cited 2023 Mar 17]. p. 002817–22. Available from: http://ieeexplore.ieee.org/document/5616823/

92. Hacke P, Smith R, Terwilliger K, Perrin G, Sekulic B, Kurtz S. Development of an IEC test for crystalline silicon modules to qualify their resistance to system voltage stress: IEC test for c-Si modules. Prog Photovolt: Res Appl. 2014 Jul;22(7):775–83.

93. Chandril S, P V V RV, S R. On-site Detection and Mitigation of Potential Induced Degradation at Photovoltaic Power Plants – Case Study. Academia Letters [Internet]. 2021 Aug 1 [cited 2023 Mar 17]; Available from: https://www.academia.edu/50914916/On_site_Detection_and_Mitigation_of_Potential_Induced_Degradation_at_Photovoltaic_Power_Plants_Case_Study

94. Koentopp MB, Krober M, Taubitz C. Toward a PID Test Standard: Understanding and Modeling of Laboratory Tests and Field Progression. IEEE J Photovoltaics. 2016 Jan;6(1):252–7.

95. Schutze M, Junghanel M, Koentopp MB, Cwikla S, Friedrich S, Muller JW, et al. Laboratory study of potential induced degradation of silicon photovoltaic modules. In: 2011 37th IEEE Photovoltaic Specialists Conference [Internet]. Seattle, WA, USA: IEEE; 2011 [cited 2023 Mar 17]. p. 000821–6. Available from: http://ieeexplore.ieee.org/document/6186080/

96. Maoyi Chang, Chienyu Chen, Hsueh CH, Hsieh WJ, Yen E, Ho KL, et al. The reliability investigation of PV junction box based on 1GW worldwide field database. In: 2015 IEEE 42nd Photovoltaic Specialist Conference (PVSC) [Internet]. New Orleans, LA: IEEE; 2015 [cited 2023 Mar 17]. p. 1–4. Available from: http://ieeexplore.ieee.org/document/7356130/

97. Segbefia OK, Imenes AG, Sætre TO. Moisture ingress in photovoltaic modules: A review. Solar Energy. 2021 Aug;224:889–906.

98. Durability and Reliability of Polymers and Other Materials in Photovoltaic Modules - 1st Edition [Internet]. [cited 2023 Mar 17]. Available from: https://www.elsevier.com/books/durability-and-reliability-of-polymers-and-other-materials-in-photovoltaic-modules/yang/978-0-12-811545-9

99.  Park NC, Jeong JS, Kang BJ, Kim DH. The effect of encapsulant discoloration and delamination on the electrical characteristics of photovoltaic module. Microelectronics Reliability. 2013 Sep;53(9–11):1818–22.

100. Mohan N, Undeland TM, Robbins WP. Power electronics: converters, applications, and design. 2nd ed. New York: Wiley; 1995. 802 p.

101. Guidelines for the assessment of photovoltaic plants.

102. Hecktheuer, L. A., Krenzinger, A., & Prieb, C. W. M.. Methodology for Photovoltaic Modules Characterization and Shading Effects Analysis. Journal of the Brazilian Society of Mechanical Sciences, 24(1), 26–32 [Internet]. 2022; Available from: https://doi.org/10.1590/S0100-73862002000100004

103. Froebel J, Jaeckel B, Pander M, Zeller U. DARK IV-CURVES AS A METHOD FOR IN SITU MODULE CHARACTERISATION.

104. Guada M, Moretón Á, Rodríguez-Conde S, Sánchez LA, Martínez M, González MÁ, et al. Daylight luminescence system for silicon solar panels based on a bias switching method. Energy Sci Eng. 2020 Nov;8(11):3839–53.

105. DNV [Internet]. [cited 2023 Jun 1]. Electroluminescence (EL): a detailed technique to visualize PV module failures. Available from: https://www.dnv.com/article/electroluminescence-el-a-detailed-technique-to-visualize-pv-module-failures-188329

106. Green. Accuracy of Analytical Expressions for Solar Cell Fill Factors. Solar Cells. 1982;7:337–40.

# Appendix 1 – Scenarios Design of the Double PV String CBS

| | | |
|---|---|---|
| ⊞ | Photovoltaic Module | 6 |
| ⚬／⚬ | Single Pole Single Throuhg NO | 30 |
| ⚬／⚬ | Single Pole Double Through | 6 |
| | Double Pole Double Through | 5 |
| | Four Pole Double Through | 2 |
| | Contactor | 2 |
| ▷⏐ | Diode | 2 |

DC CONVERSION
AC CONVERSION
MPPT
Inverter
S38
S0.1
S37
+2
-2
S39
Power supply
-
+
DC Load Controller
-     +
V   Voltage measurement
A

S9  D1
02. 30 Wp
S12   S16
S14   S17
S21   04. 50 Wp   S24
S23
S8   01. 30 Wp   S15   S18
S13   S19
S20   03. 50 Wp
S22   S25   S26
S11  D2

I2  I6
-2
I3
I4  I7
I1  I5
-1

06. 100 Wp   S30
S27   S29
S33   O35   +2
S31   S32
05. 100 Wp
S28   S34   O36   +1

DC CONVERSION
PWM
DC CONVERSION   AC CONVERSION
MPPT   S42   Inverter
S41
S0.2   S40
+1
-1
S43
Power supply
-
+
DC Load Controller
-     +
V   Voltage measurement
A

| Project: | Development of Photovoltaic System Simulator: PV Remote Lab | Plan Number: | Escale: |
|---|---|---|---|
| Plan Title: | Double PV String Commutation Block Scheme | 001 | S/N |
| Author: Jesús Querol Puchal | Supervisor: Taras Koturbash | Date: 28/04/2023 | |

KTH
VETENSKAP OCH KONST

| | Photovoltaic Module | 6 |
|---|---|---|
| | Single Pole Single Throuhg NO | 30 |
| | Single Pole Double Through | 6 |
| | Diode | 2 |

| Project: | Development of Photovoltaic System Simulator: PV Remote Lab | | Plan Number: | | Escale: | |
|---|---|---|---|---|---|---|
| Plan Title: | Double PV String Commutation Block Scheme: PV System | | 002 | | S/N | |
| Author: Jesús Querol Puchal | | Supervisor: Taras Koturbash | | Date: | 28/04/2023 | |

# Wire 1 - 01. 30 W



# Wire 1 - 03. 50 W
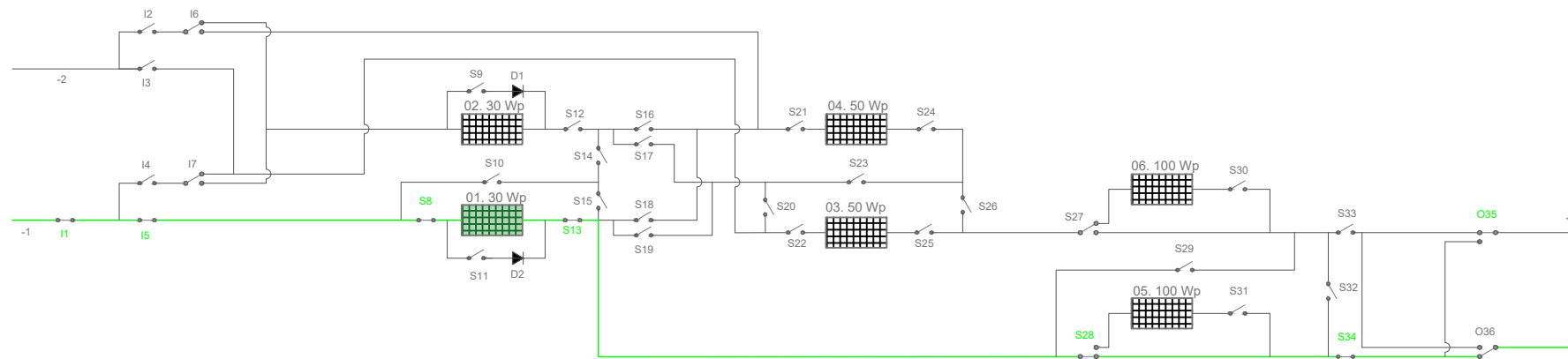


# Wire 1 - 05. 100 W



## SCENARIO 1

| Relays closed |
|---|
| I1 - I5 - S8 - S13 - S28 - S34 - O35 |
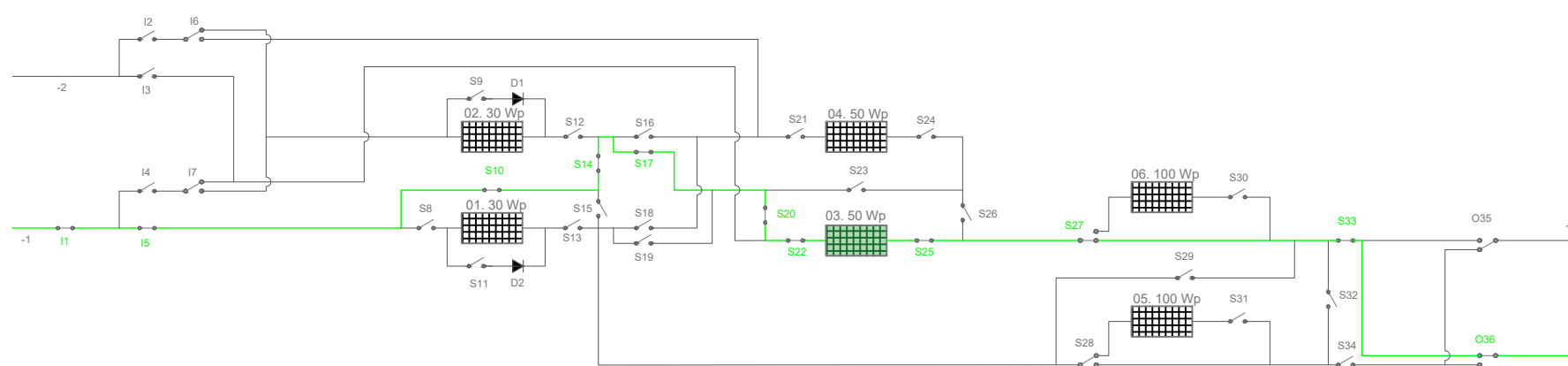
## SCENARIO 2

| Relays closed |
|---|
| I1 - I5 - S10 - S14 - S17 - S20 - S22 - S25 - S27 - S33 - O36 |
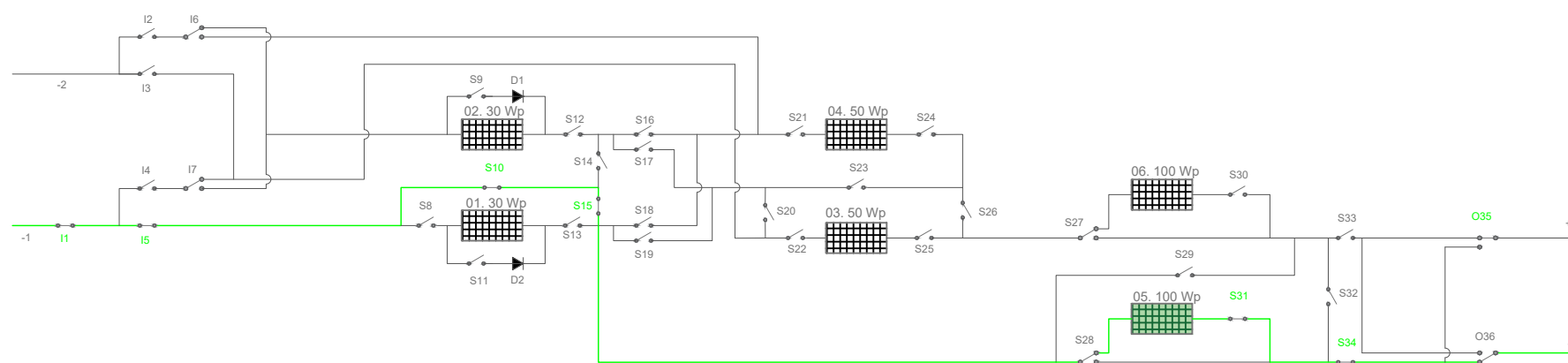
## SCENARIO 3

| Relays closed |
|---|
| I1 - I5 - S10 - S15 - S31 - S34 - O35 |

| Project: | Development of Photovoltaic System Simulator: PV Remote Lab | Plan Number: | Escale: | |
|---|---|---|---|---|
| | | 003 | S/N | KTH VETENSKAP OCH KONST |
| Plan Title: | Double PV String CBS: PV Panels 01, 03, 05 Alone Under Study - PV String 1 | | | |
| Author: Jesús Querol Puchal | Supervisor: Taras Koturbash | Date: 28/04/2023 | | |

# Wire 2 - 01. 30 W



## SCENARIO 4

| Relays closed |
|---|
| I2 - I6 - S16 - S14 - S10 - S8 - S13 - S28 - S34 - O36 |

# Wire 2 - 03. 50 W
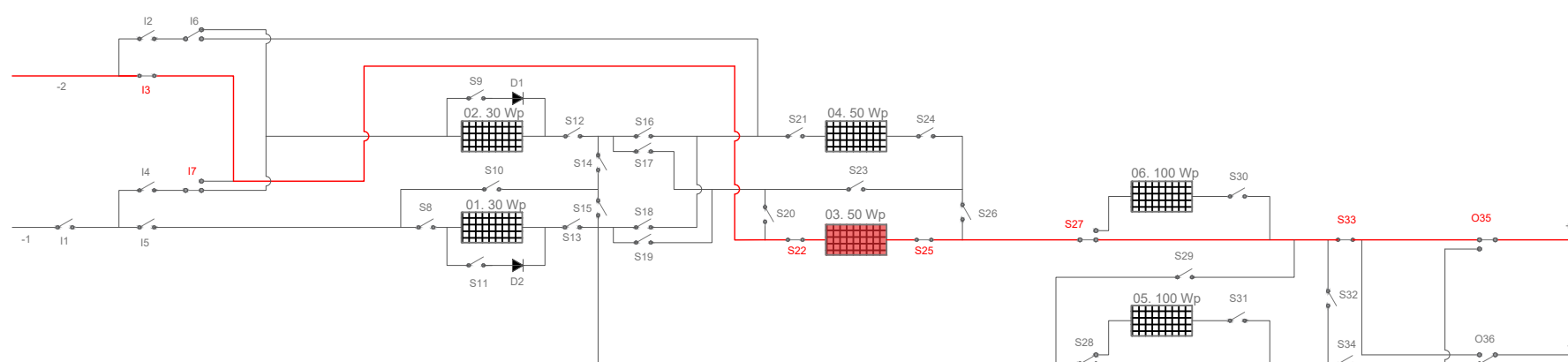


## SCENARIO 5

| Relays closed |
|---|
| I3 - I7 - S22 - S25 - S27 - S33 - O35 |

# Wire 2 - 05. 100 W
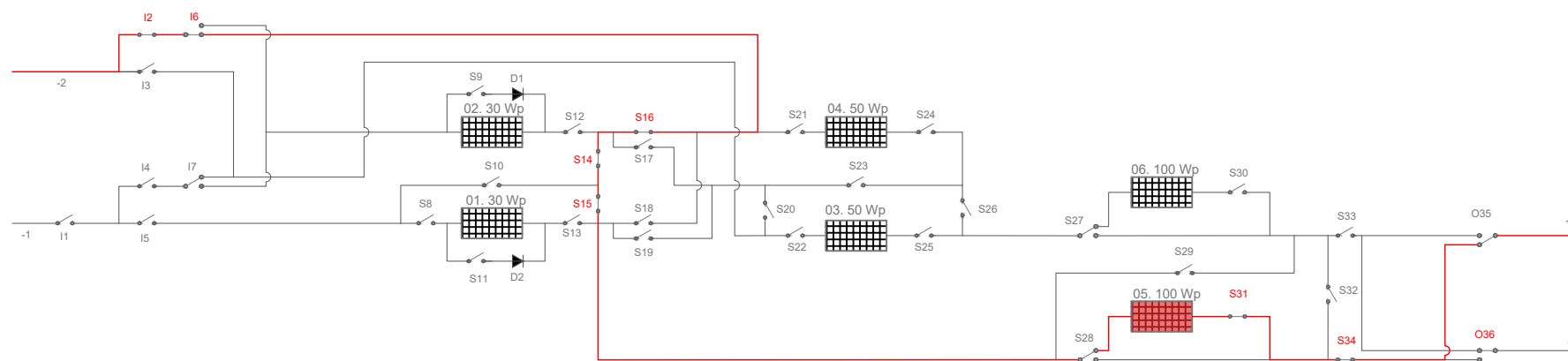


## SCENARIO 6

| Relays closed |
|---|
| I2 - I6 - S16 - S14 - S15 - S31 - S34 - O36 |

| Project: | Development of Photovoltaic System Simulator: PV Remote Lab | Plan Number: | Escale: |
|---|---|---|---|
| | | 004 | S/N |
| Plan Title: | Double PV String CBS: PV Panels 01, 03, 05 Alone Under Study - PV String 2 | | |
| Author: Jesús Querol Puchal | Supervisor: Taras Koturbash | Date: 28/04/2023 | |

# Wire 1 - 02. 30 W
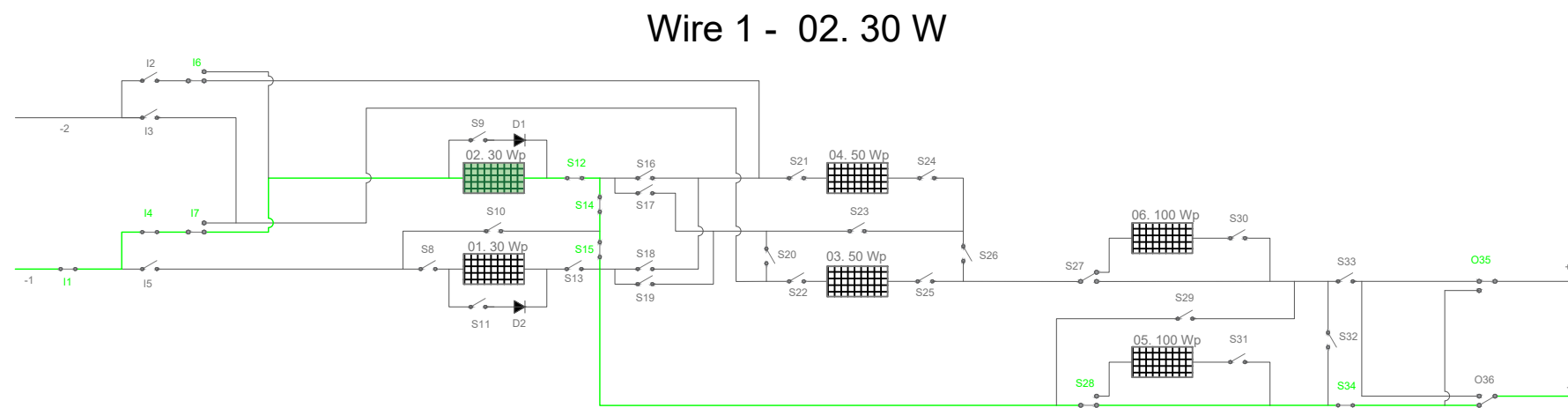


## SCENARIO 7

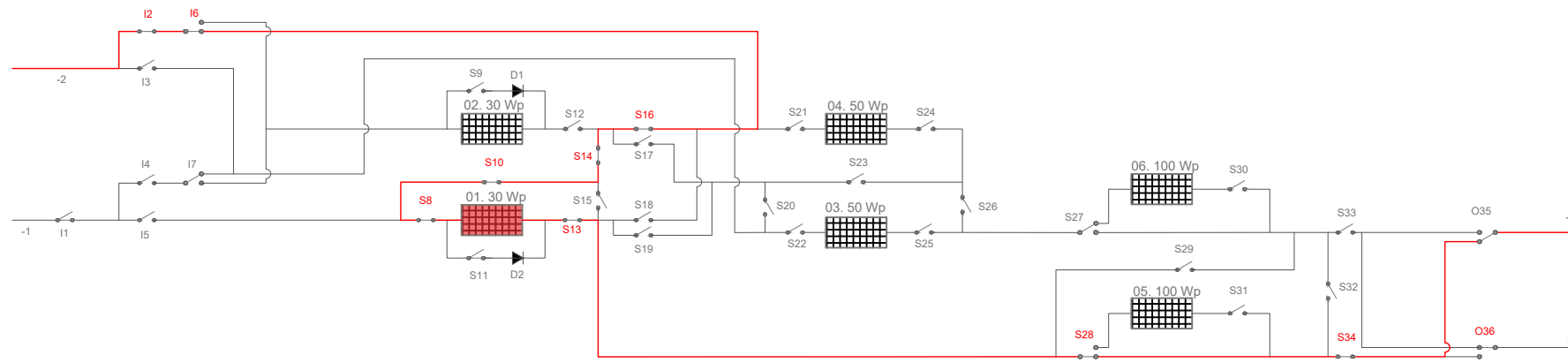| Relays closed |
|---|
| I1 - I4 - I7 - I6 - S12 - S14 - S15 - S28 - S34 - O35 |

# Wire 1 - 04. 50 W
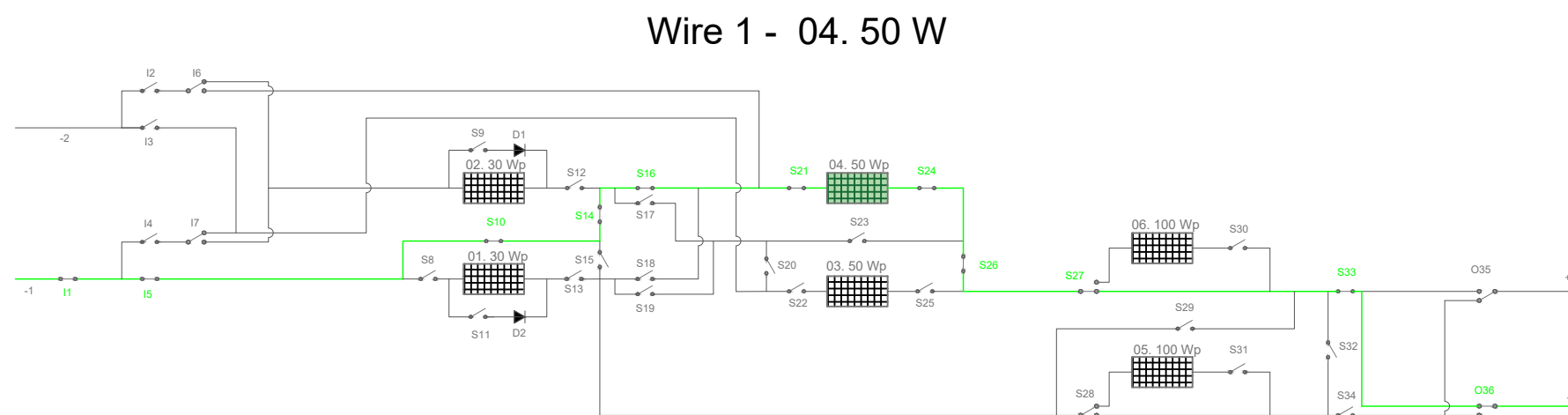


## SCENARIO 8

| Relays closed |
|---|
| I1 - I5 - S10 - S14 - S16 - S21 - S24 - S26 - S27 - S33 - O36 |

# Wire 1 - 06. 100 W
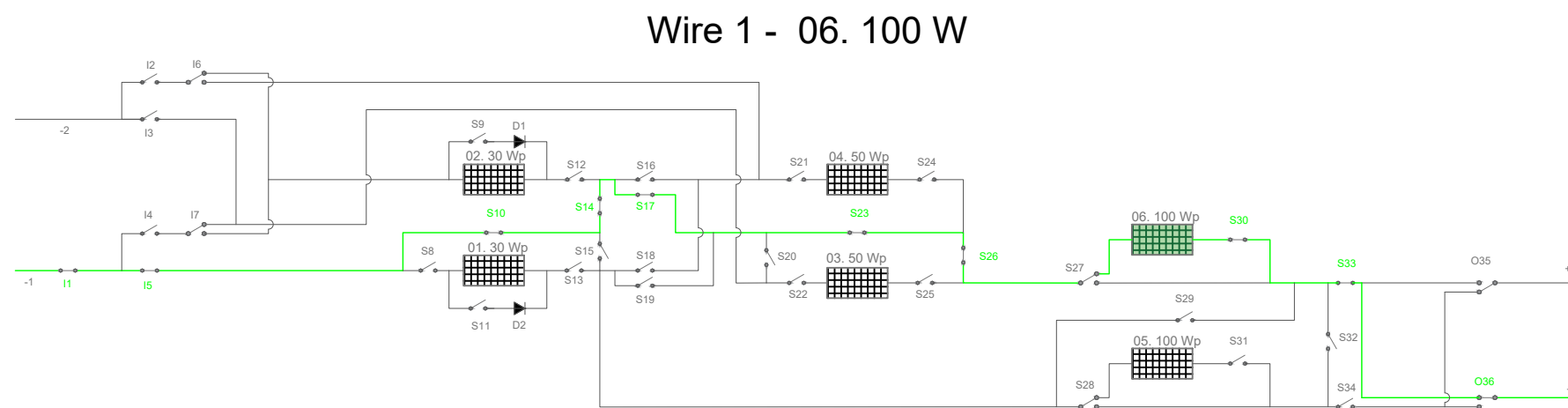


## SCENARIO 9

| Relays closed |
|---|
| I1 - I5 - S10 - S14 - S17 - S23 - S26 - S30 - S33 - O36 |

| Project: | Development of Photovoltaic System Simulator: PV Remote Lab | Plan Number: | Escale: | |
|---|---|---|---|---|
| | | 005 | S/N | |
| Plan Title: | Double PV String CBS: PV Panels 02, 04 and 06 Alone Under Study - PV String 1 | | | |
| Author: Jesús Querol Puchal | Supervisor: Taras Koturbash | Date: 28/04/2023 | | KTH VETENSKAP OCH KONST |

# Wire 2 - 02. 30 W
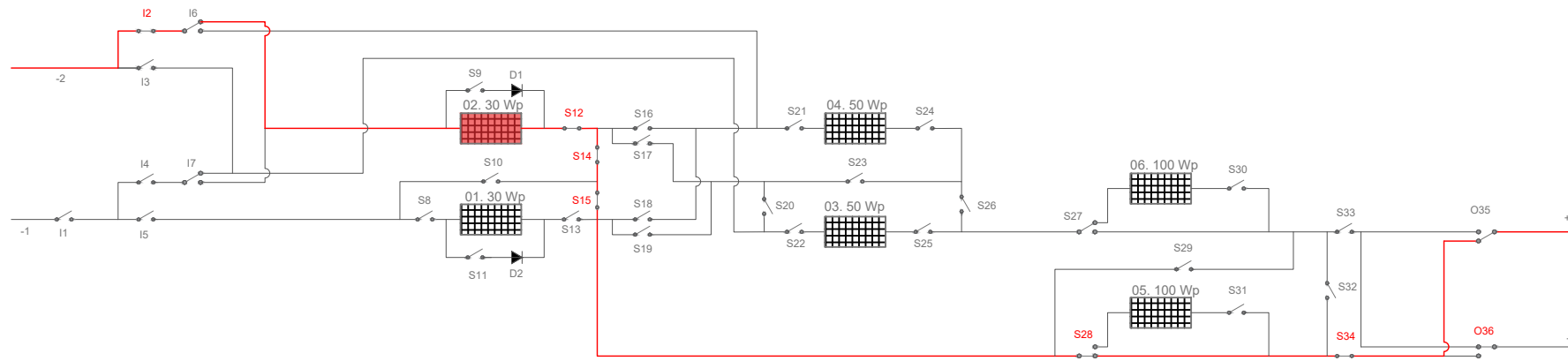


## SCENARIO 10

| Relays closed |
| --- |
| I2 - S12 - S14 - S15 - S28 - S34 - O36 |

# Wire 2 - 04. 50 W
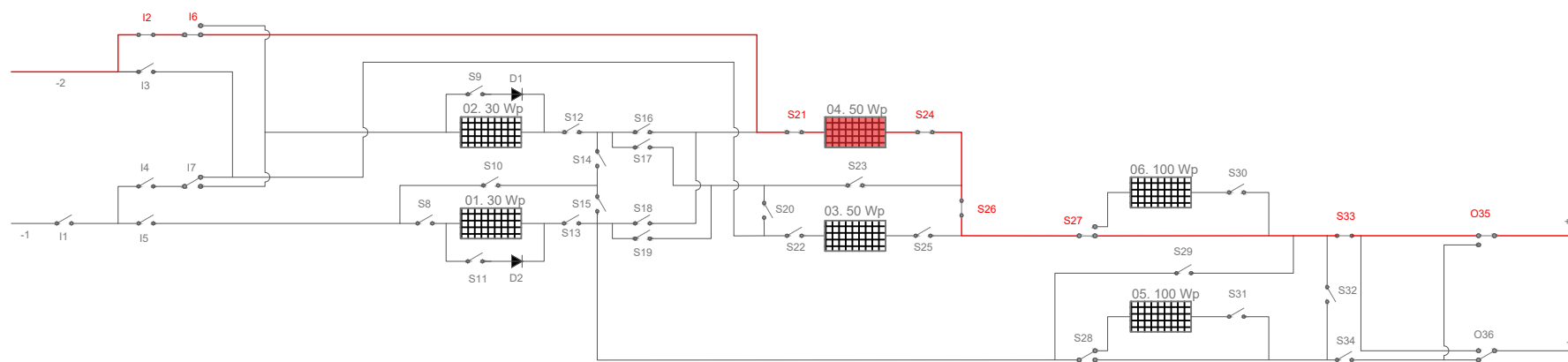


## SCENARIO 11

| Relays closed |
| --- |
| I2 - I6 - S21 - S24 - S26 - S27 - S33 - O35 |

# Wire 2 - 06. 100 W
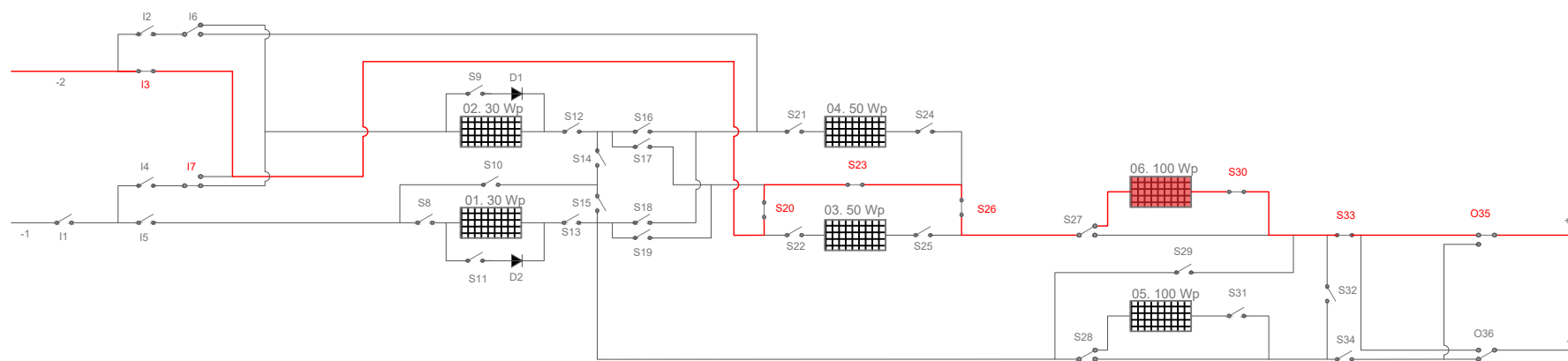


## SCENARIO 12

| Relays closed |
| --- |
| I3 - I7 - S20 - S23 - S26 - S30 - S33 - O35 |

| Project: | Development of Photovoltaic System Simulator: PV Remote Lab | Plan Number: | Escale: |
| --- | --- | --- | --- |
| Plan Title: | Double PV String CBS: PV Panels 02, 04 and 06 Alone Under Study - PV String 2 | 006 | S/N |
| Author: Jesús Querol Puchal | Supervisor: Taras Koturbash | Date: 28/04/2023 | |

# Wire 1 - 30 W PV Panels in series

# Wire 1 - 50 W PV Panels in series



## SCENARIO 14

| Relays closed |
| --- |
| I1 - I5 - I7 - S10 - S14 - S16 - S21 - S24 - S23 - S20 - S22 - S25 - S27 - S33 - O36 |

# Wire 1 - 100 W PV Panels in series
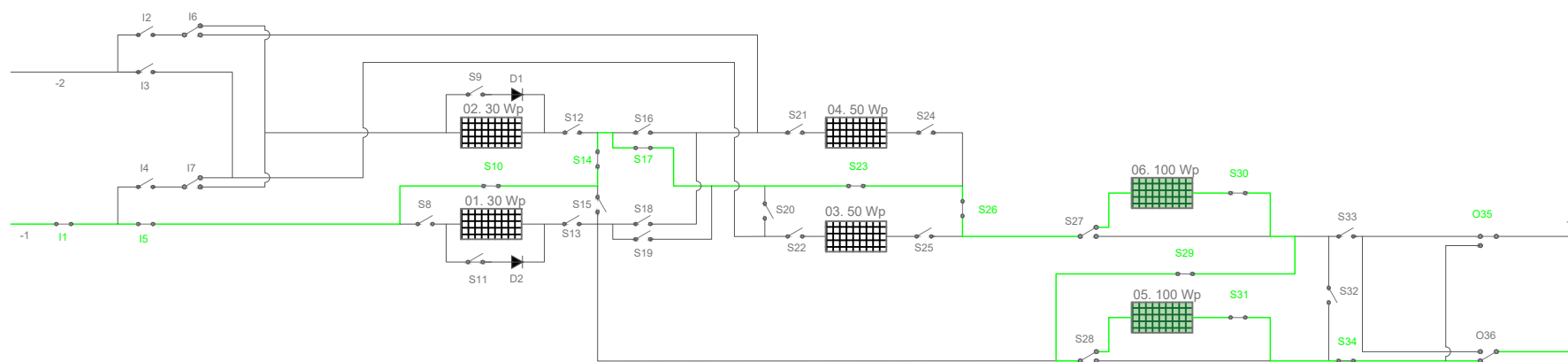


## SCENARIO 15

| Relays closed |
| --- |
| I1 - I5 - S10 - S14 - S17 - S23 - S26 - S30 - S29 - S31 - S34 - O35 |

| Project: | Development of Photovoltaic System Simulator: PV Remote Lab | Plan Number: | Escale: | |
| --- | --- | --- | --- | --- |
| | | 007 | S/N | |
| Plan Title: | Single PV String CBS: PV Panels with the Same Power in Series - PV String 1 | | | |
| Author: Jesús Querol Puchal | Supervisor: Taras Koturbash | Date: 28/04/2023 | | KTH VETENSKAP OCH KONST |

# Wire 2 - 30 W PV Panels in series
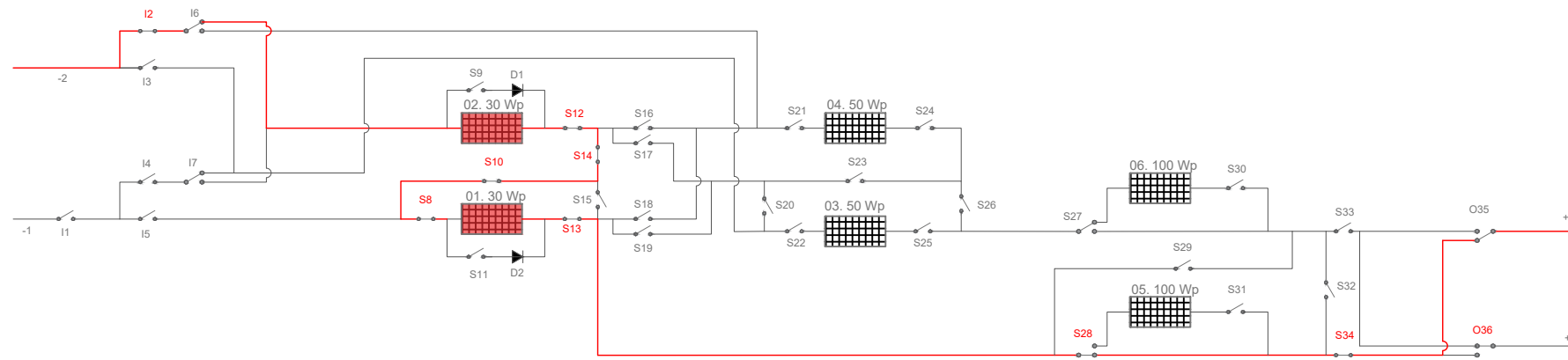
## SCENARIO 16

| Relays closed |
|---|
| I2 - S12 - S14 - S10 - S8 - S13 - S28 - S34 - O36 |

# Wire 2 - 50 W PV Panels in series
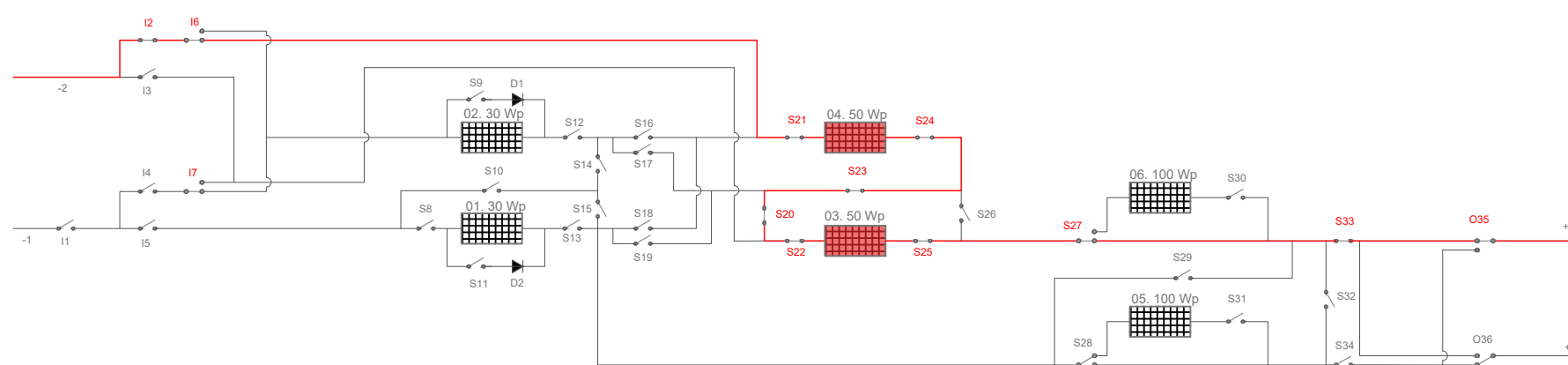
## SCENARIO 17

| Relays closed |
|---|
| I2 - I6 - I7 - S21 - S24 - S23 - S20 - S22 - S25 - S27 - S33 - O35 |

# Wire 2 - 100 W PV Panels in series
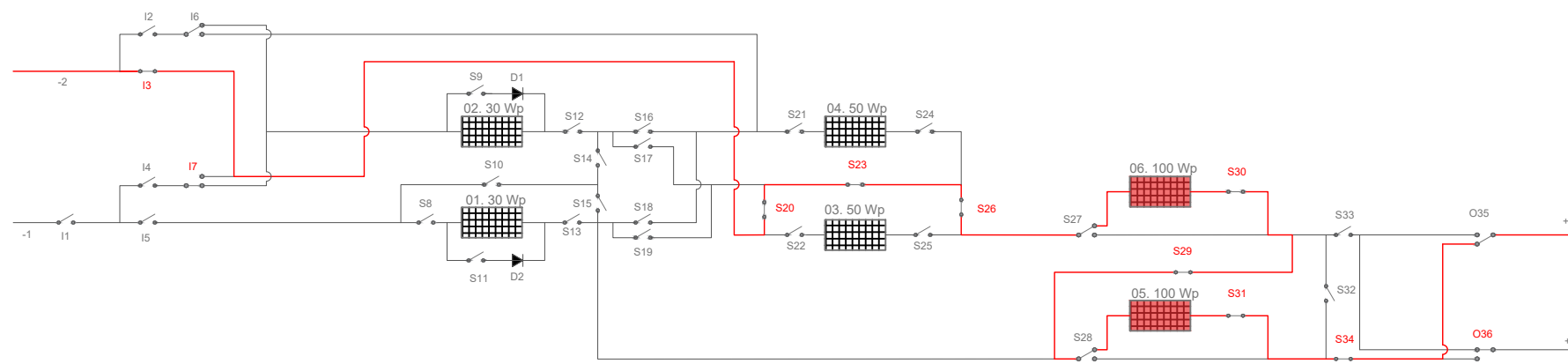
## SCENARIO 18

| Relays closed |
|---|
| I3 - I7 - S20 - S23 - S26 - S30 - S29 - S31 - S34 - O36 |

| Project: | Development of Photovoltaic System Simulator: PV Remote Lab | | Plan Number: | Escale: | |
|---|---|---|---|---|---|
| | | | 008 | S/N | KTH VETENSKAP OCH KONST |
| Plan Title: | Single PV String CBS: PV Panels with the Same Power in Series - PV String 2 | | | | |
| Author: Jesús Querol Puchal | Supervisor: Taras Koturbash | | Date: 28/04/2023 | | |

# Wire 1 - 30 W PV Panels in parallel
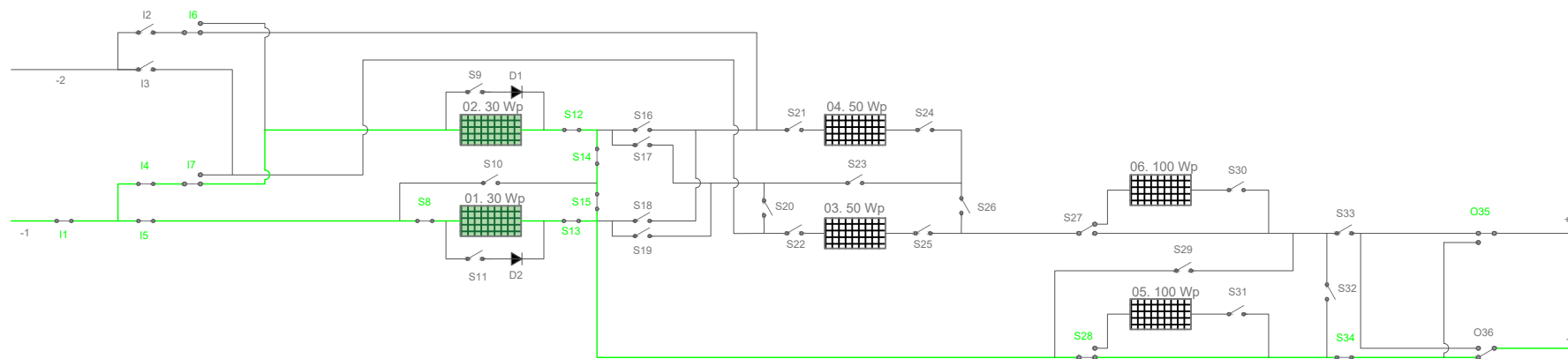


## SCENARIO 19

| Relays closed |
| --- |
| I1 - I4 - I5 - I6 - I7 - S12 - S14 - S8 - S13 - S15 - S28 - S34 - O35 |

# Wire 1 - 50 W PV Panels in parallel
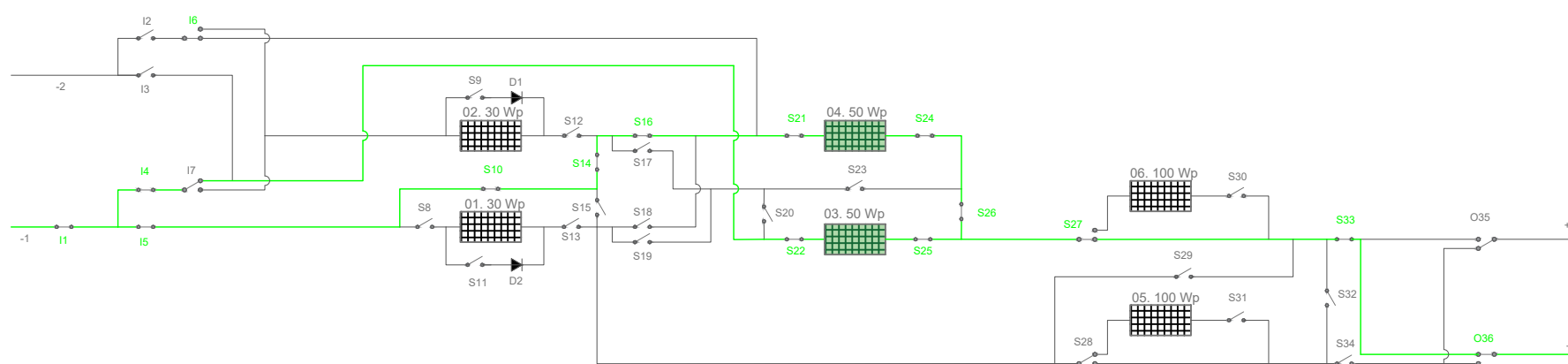


## SCENARIO 20

| Relays closed |
| --- |
| I1 - I4 - I5 - I6 - S10 - S14 - S16 - S21 - S24 - S22 - S25 - S26 - S27 - S33 - O36 |

# Wire 1 - 100 W PV Panels in parallel
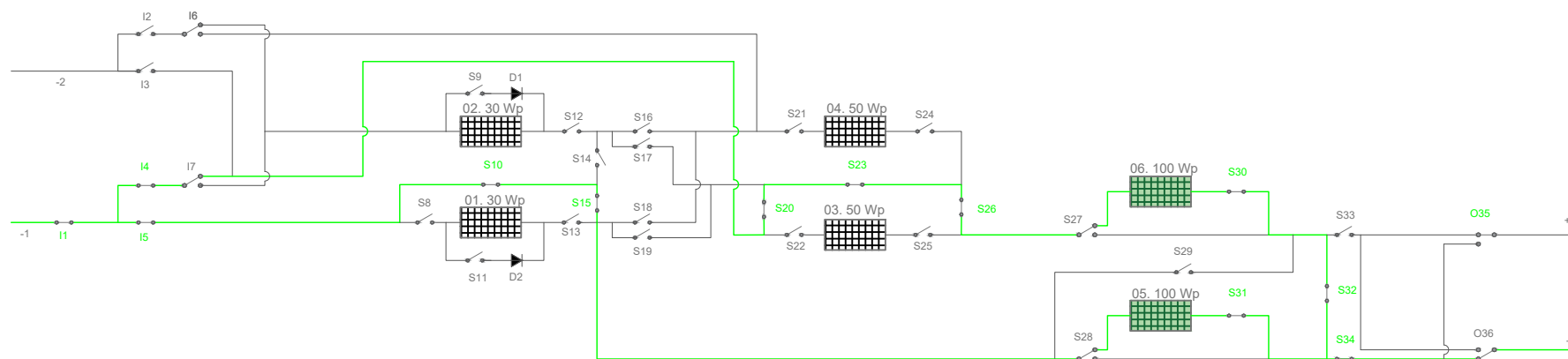


## SCENARIO 21

| Relays closed |
| --- |
| I1 - I4 - I5 - S10 - S15 - S20 - S23 - S26 - S30 - S31 - S32 - S34 - O35 |

| Project: | Development of Photovoltaic System Simulator: PV Remote Lab | Plan Number: | Escale: |
| --- | --- | --- | --- |
| | | 009 | S/N |
| Plan Title: | Single PV String CBS: PV Panels with the Same Power in Parallel - PV String 1 | | |
| Author: Jesús Querol Puchal | Supervisor: Taras Koturbash | Date: 28/04/2023 | KTH VETENSKAP OCH KONST |

# Wire 2 - 30 W PV Panels in parallel
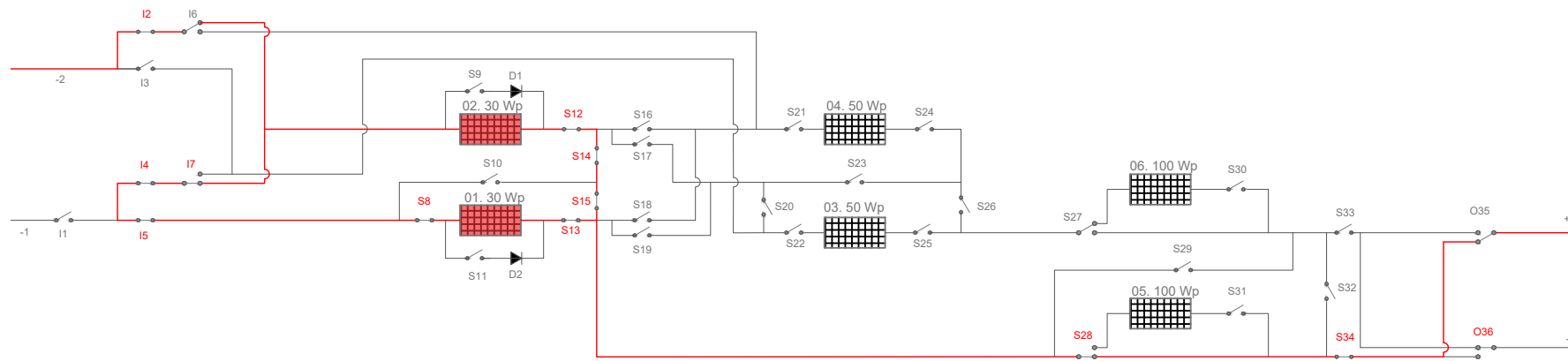


## SCENARIO 22

| Relays closed |
|---|
| I2 - I4 - I5 - I7 - S12 - S14 - S8 - S15 - S13 - S28 - S34 - O36 |

# Wire 2 - 50 W PV Panels in parallel
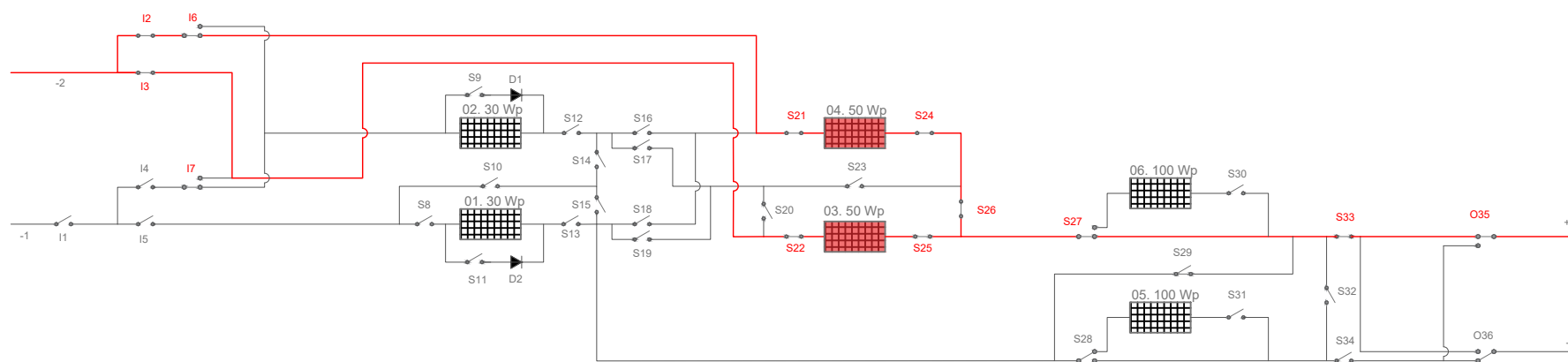


## SCENARIO 23

| Relays closed |
|---|
| I2 - I3- I6 - I7 - S21 - S22 - S24 - S25 - S26 - S27 - S33 - O35 |

# Wire 2 - 100 W PV Panels in parallel
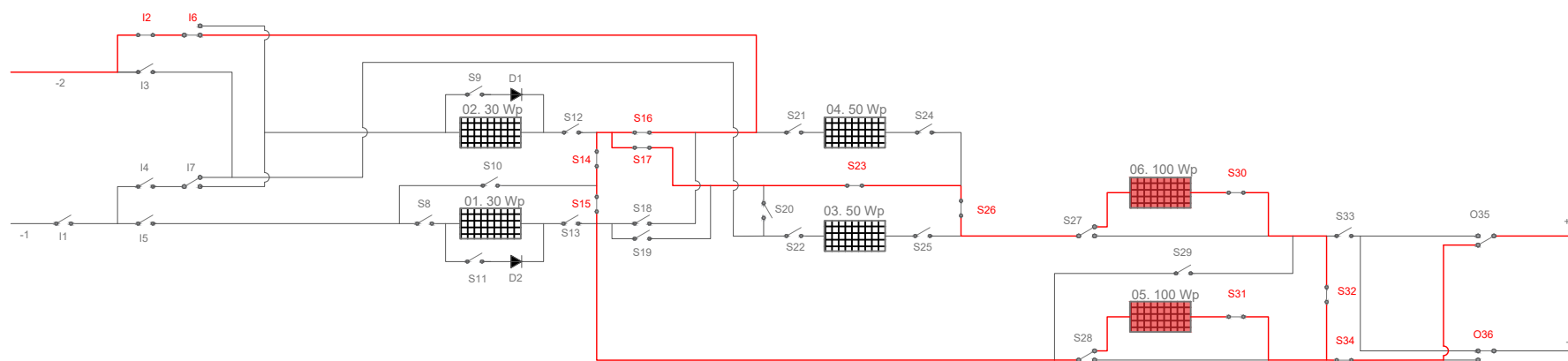


## SCENARIO 24

| Relays closed |
|---|
| I2 - I6 - S16 - S14 - S15 - S17 - S23 - S26 - S30 - S31 - S32 - S34 - O36 |

| Project: | Development of Photovoltaic System Simulator: PV Remote Lab | Plan Number: | Escale: |
|---|---|---|---|
| Plan Title: | Single PV String CBS: PV Panels with the Same Power in Parallel - PV String 2 | 010 | S/N |
| Author: Jesús Querol Puchal | Supervisor: Taras Koturbash | Date: 28/04/2023 | KTH VETENSKAP OCH KONST |

# 01. 30 W - Wire 1 & 02. 30 W - Wire 2
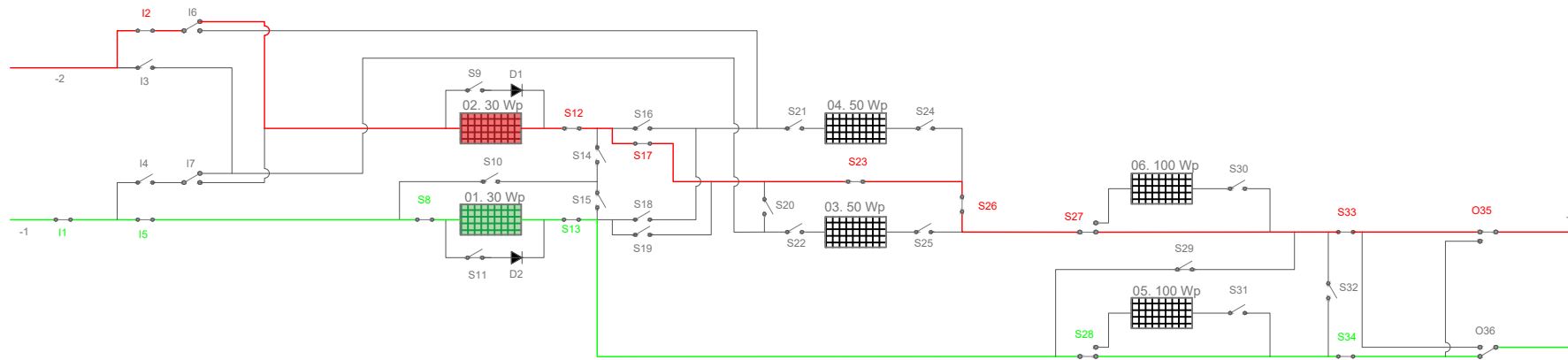
## SCENARIO 25

| Relays closed |
|---|
| I1 - I2 - I5 - S8 - S12 - S13 - S17 - S23 - S26 - S27 - S28 - S33 - S34 - O35 |

# 03. 50 W - Wire 1 & 04. 50 W - Wire 2
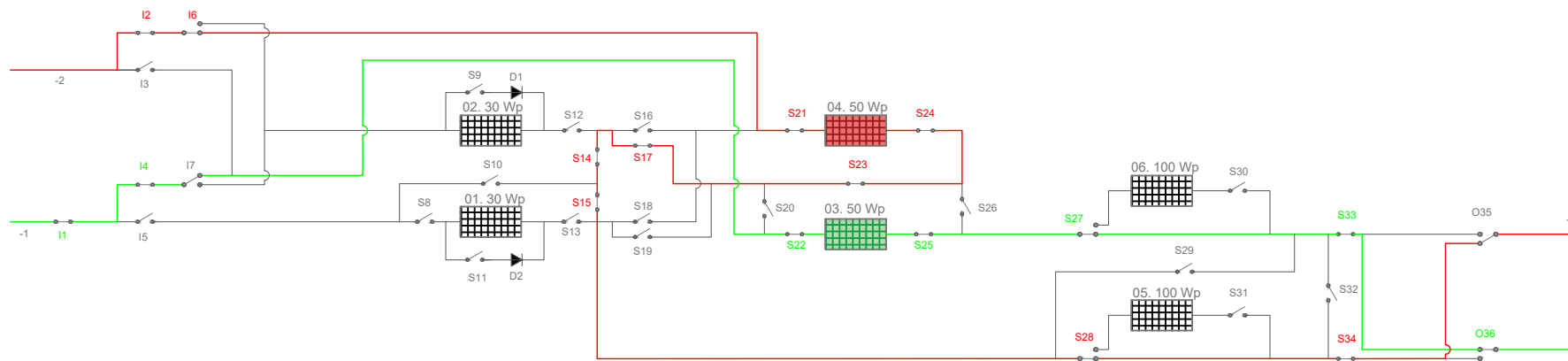
## SCENARIO 26

| Relays closed |
|---|
| I1 - I2 - I4 - I6 - S21 - S24 - S23 - S17 - S14 - S15 - S22 - S25 - S27 - S28 - S33 - S34 - O36 |

# 05. 100 W - Wire 1 & 06. 100 W - Wire 2
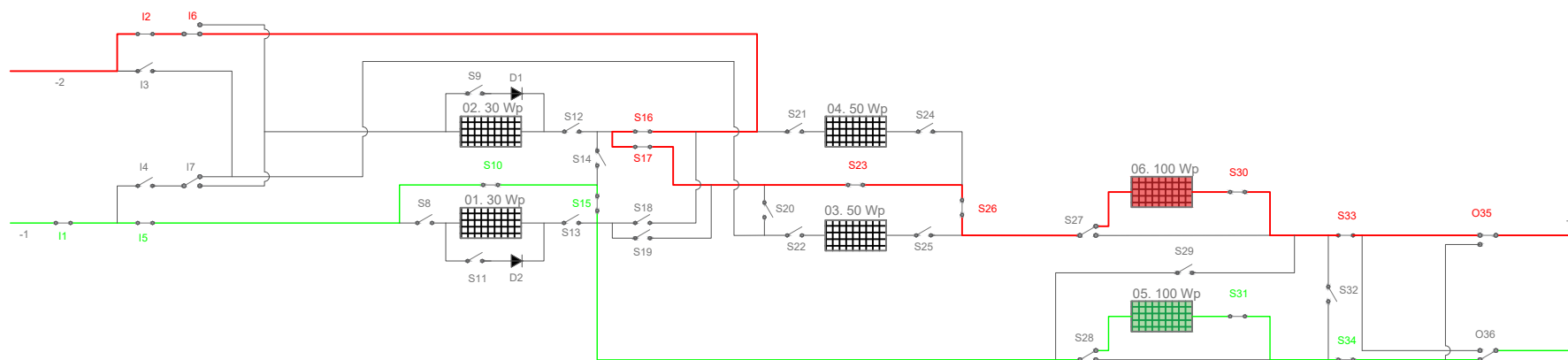
## SCENARIO 27

| Relays closed |
|---|
| I1 - I2 - I5 - I6 - S10 - S15 - S16 - S17 - S23 - S26 - S30 - S31 - S33 - S34 - O35 |

| Project: | Development of Photovoltaic System Simulator: PV Remote Lab | Plan Number: | Escale: |
|---|---|---|---|
| Plan Title: | Single PV String CBS: PV Panels with the Same Power through Diferent Strings | 011 | S/N |
| Author: Jesús Querol Puchal | Supervisor: Taras Koturbash | Date: 28/04/2023 | |

## 01. 30 Wp & 03. 50 Wp - Wire 1



## SCENARIO 28

| Relays closed |
|---|
| I1 - I5 - S8 - S13 - S19 - S20 - S22 - S25 - S27 - S33 - O36 |
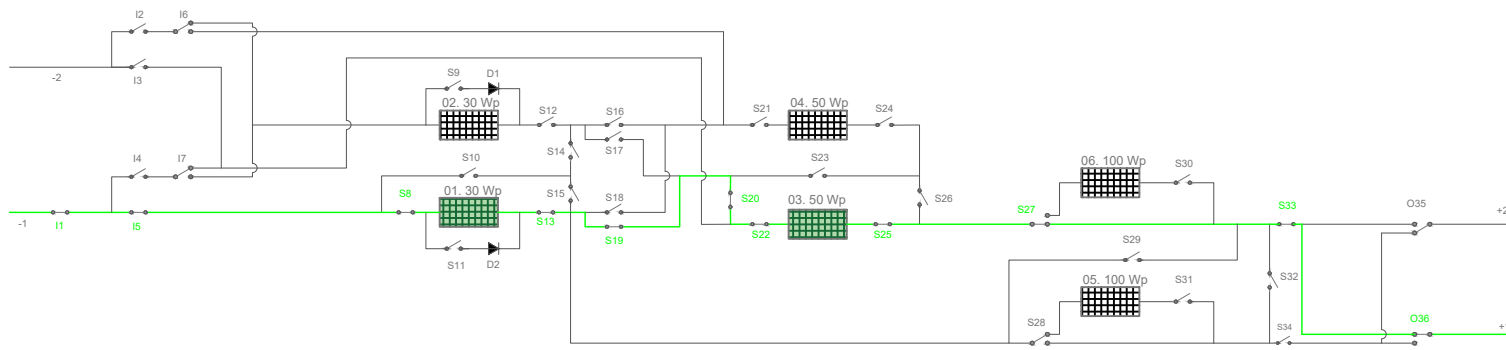
## SCENARIO 29

| Relays closed |
|---|
| I1 - I4 - I7 - S12 - S16 - S21 - S24 - S26 - S27 - S33 - O36 |

## 02. 30 Wp & 04. 50 Wp - Wire 1



## 01. 30 Wp & 04. 50 Wp - Wire 1
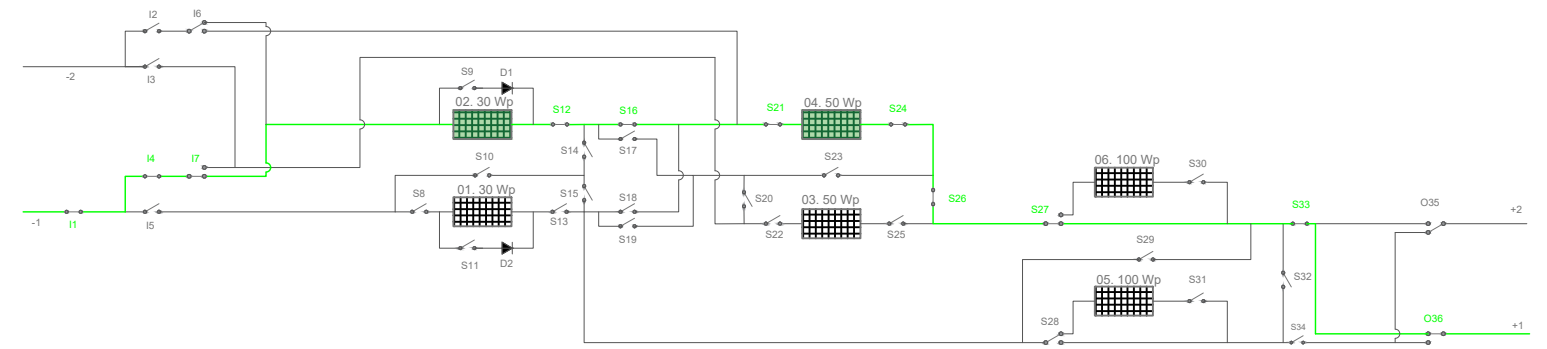


## SCENARIO 30

| Relays closed |
|---|
| I1 - I5 - S8 - S13 - S18 - S21 - S24 - S26 - S27 - S33 - O36 |
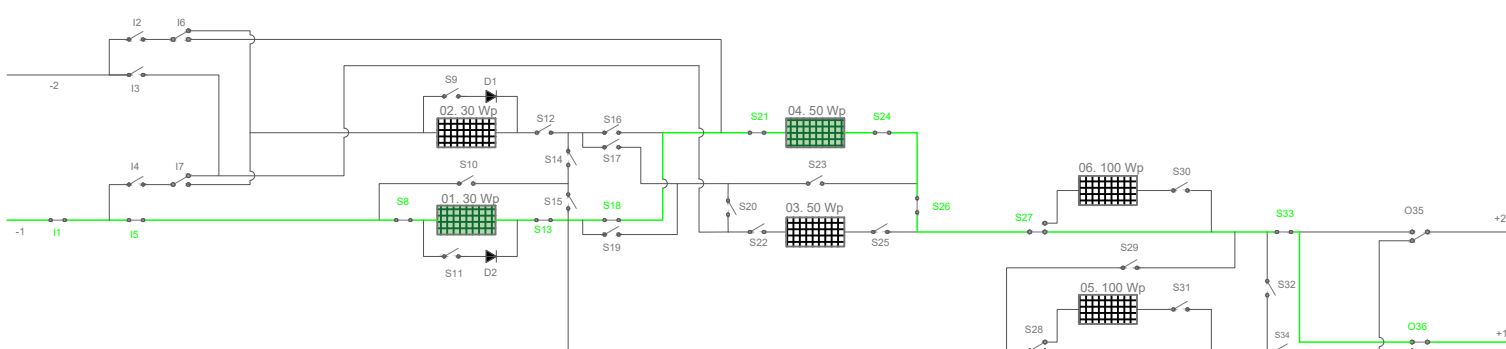
## SCENARIO 31

| Relays closed |
|---|
| I1 - I4 - I7 - S12 - S17 - S20 - S22 - S25 - S27 - S33 - O36 |

## 02. 30 Wp & 03. 50 Wp - Wire 1
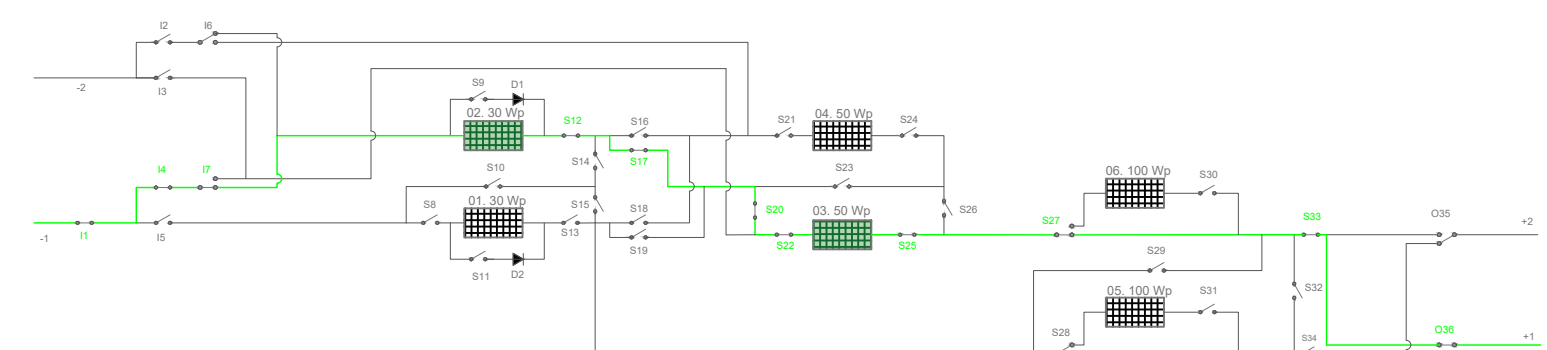


| Project: | Development of Photovoltaic System Simulator: PV Remote Lab | | Plan Number: | Escale: |
|---|---|---|---|---|
| Plan Title: | Single PV String CBS: Mix 30 Wp & 50 Wp - PV String 1 | | 012 | S/N |
| Author: Jesús Querol Puchal | Supervisor: Taras Koturbash | | Date: 28/04/2023 | |

## 01. 30 Wp & 03. 50 Wp - Wire 2
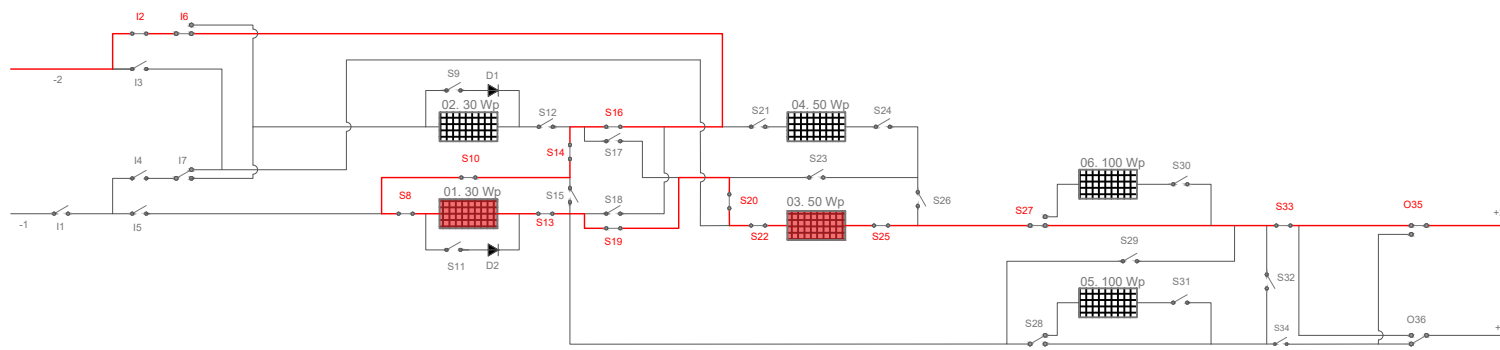


## SCENARIO 32

| Relays closed |
| --- |
| I2 - I6 - S16 - S14 - S10 - S8 - S13 - S19 - S20 - S22 - S25 - S27 - S33 - O34 |

## SCENARIO 33

| Relays closed |
| --- |
| I2 - S12 - S16 - S21 - S24 - S26 - S27 - S33 - O34 |

## 02. 30 Wp & 04. 50 Wp - Wire 2



## 01. 30 Wp & 04. 50 Wp - Wire 2
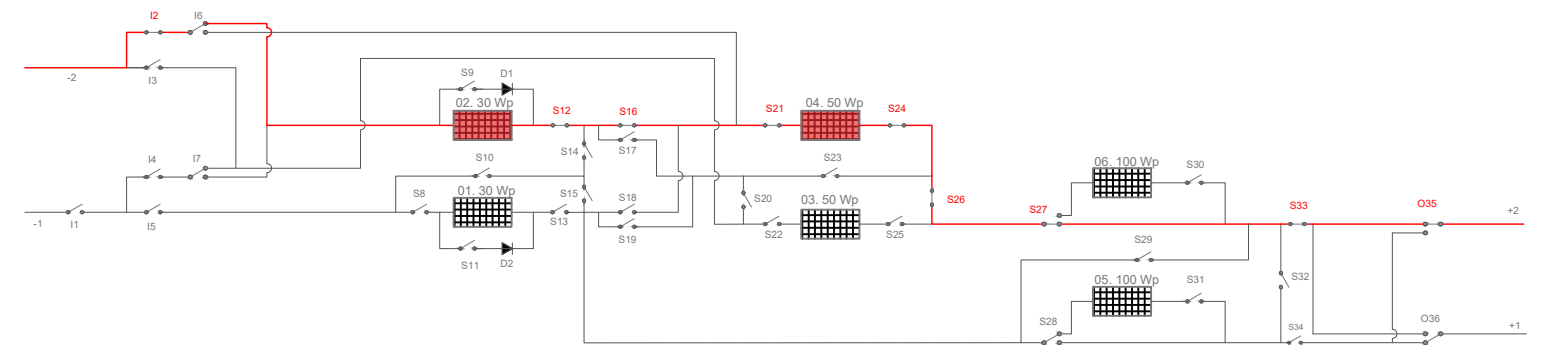


## SCENARIO 34

| Relays closed |
| --- |
| I3 - I4 - I5 - S8 - S13 - S18 - S21 - S24 - S26 - S27 - S33 - O34 |
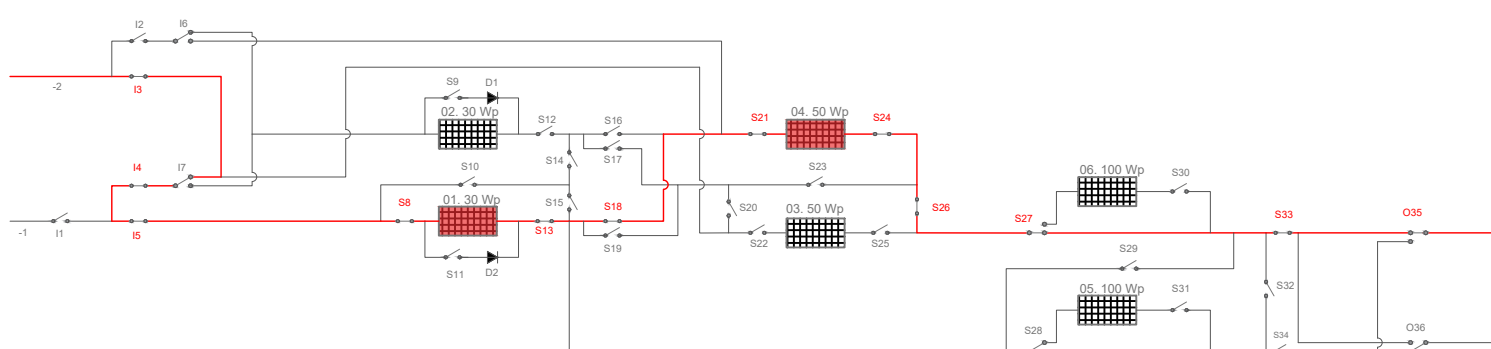
## SCENARIO 35

| Relays closed |
| --- |
| I2 - S12 - S17 - S20 - S22 - S25 - S27 - S33 - O34 |

## 02. 30 Wp & 03. 50 Wp - Wire 2
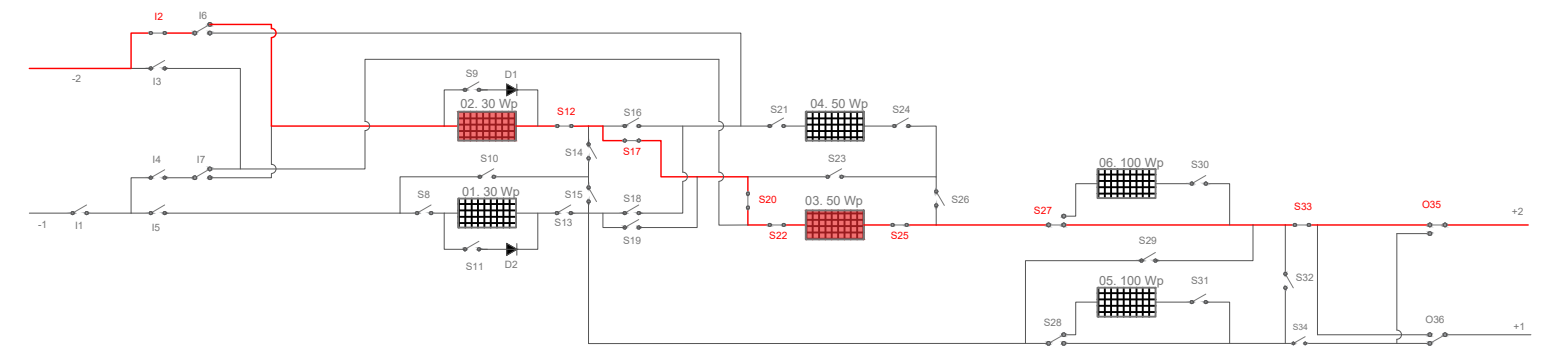


| Project: | Development of Photovoltaic System Simulator: PV Remote Lab | | Plan Number: | | Escale: | |
| --- | --- | --- | --- | --- | --- | --- |
| | | | 013 | | S/N | |
| Plan Title: | Single PV String CBS: Mix 30 Wp & 50 Wp - PV String 2 | | | | | |
| Author: Jesús Querol Puchal | | Supervisor: Taras Koturbash | | Date: 28/03/2023 | | |

# Mix 30 Wp & 50 Wp in parallel - Wire 1
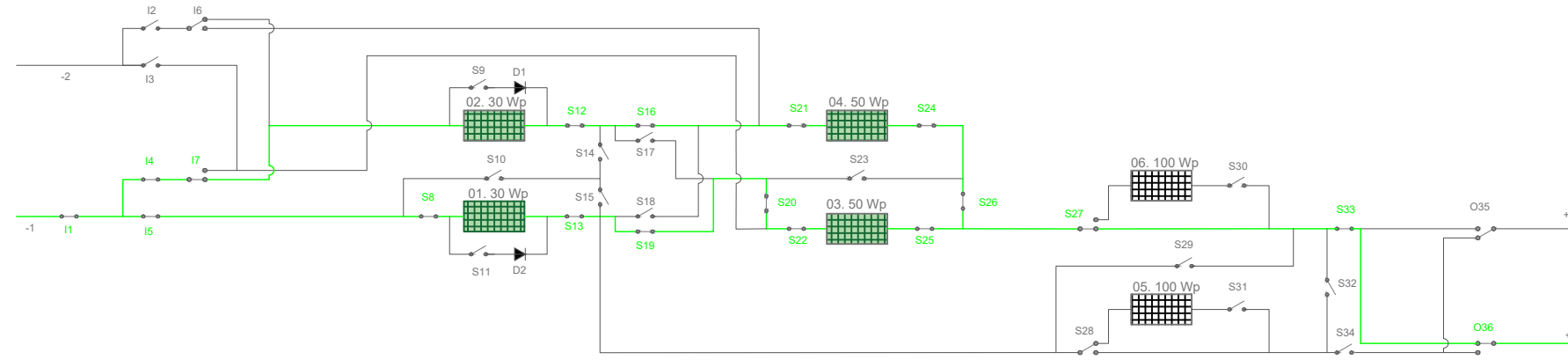
## SCENARIO 36

| Relays closed |
| --- |
| I1 - I4 - I5 - I7 - S12 - S16 - S8 - S13 - S16 - S19 - S20 - S21 - S22 - S24 - S25 - S26 - S27 - S33 - O36 |

# Mix 30 Wp & 50 Wp in parallel - Wire 2
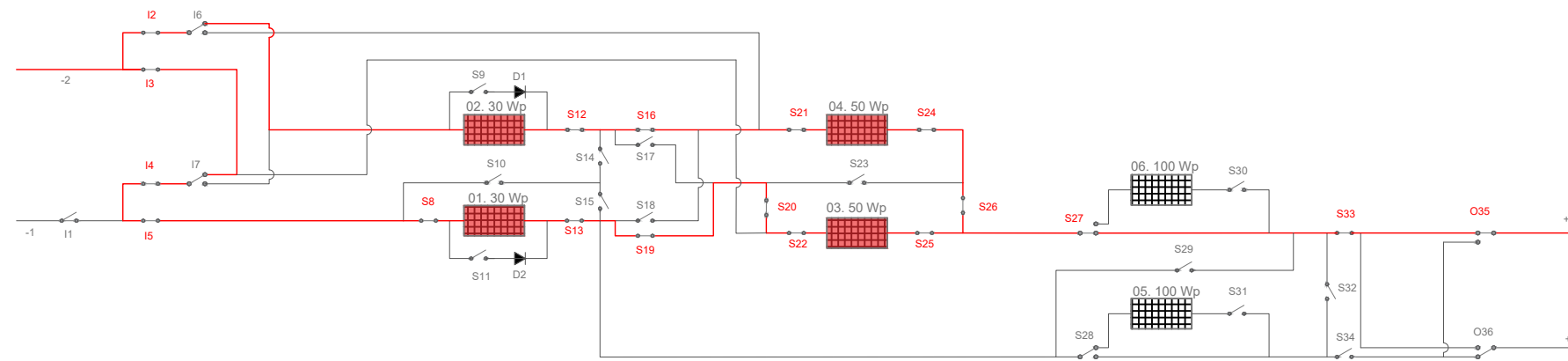
## SCENARIO 37

| Relays closed |
| --- |
| I2 - I3 - I4 - I5 - S8 - S12 - S13 - S16 - S19 - S21 - S20 - S22 - S24 - S25 - S26 - S27 - S33 - O35 |

| Project: | Development of Photovoltaic System Simulator: PV Remote Lab | Plan Number: | Escale: |
| --- | --- | --- | --- |
| Plan Title: | Single PV String CBS: 30 Wp & 50 Wp in series & parallel | 014 | S/N |
| Author: Jesús Querol Puchal | Supervisor: Taras Koturbash | Date: 28/04/2023 | |

# 30 W PV panels in series - Wire 1 & 50 W PV panels in series - Wire 2
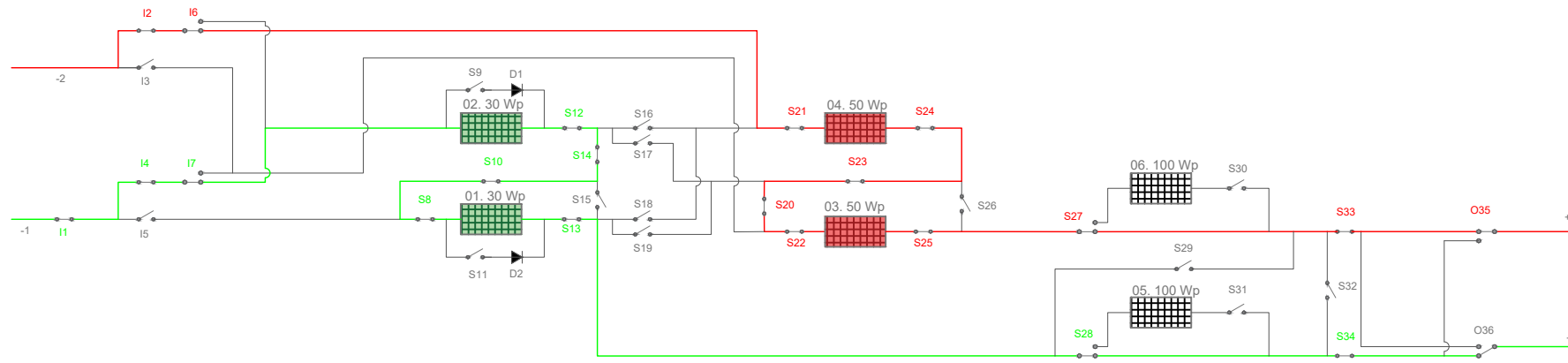
| Relays closed |
|---|
| I2 - I6 - I1 - I4 - I7 - S12 - S14 - S10 - S8 - S13 - S21 - S24 - S23 - S20 - S22 - S25 - S27 - S28 - S33 - S34 - O35 |

# 100 W PV panel - Wire 1 & 50 W PV panels in series - Wire 2
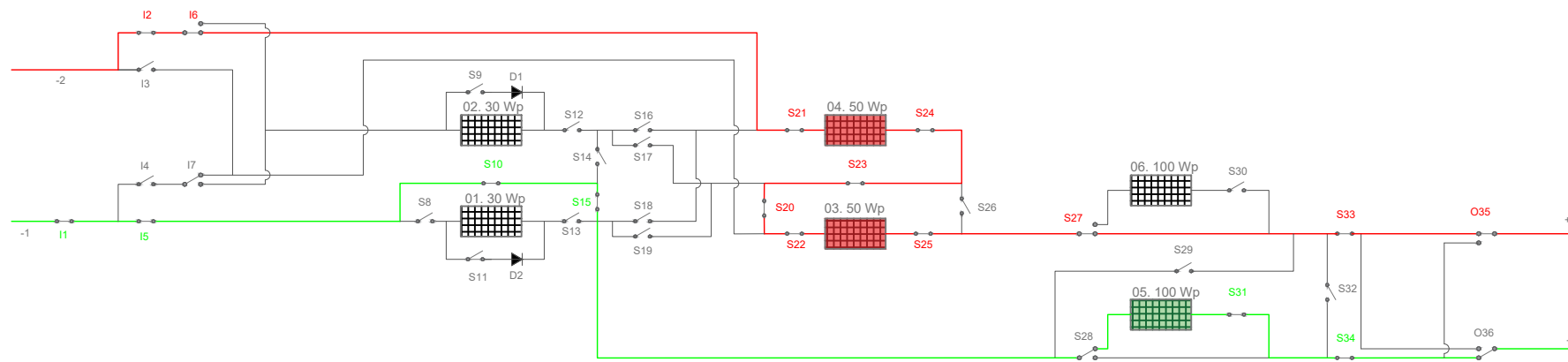
| Relays closed |
|---|
| I2 - I6 - I1 - I5 - S10 - S15 - S21 - S24 - S23 - S20 - S22 - S25 - S27 - S31 - S33 - S34 - O35 |

| Project: | | Plan Number: | Escale: | |
|---|---|---|---|---|
| Development of Photovoltaic System Simulator: PV Remote Lab | | 015 | S/N | |
| Plan Title: | Single PV String CBS: PV Panels Mix | | | |
| Author: Jesús Querol Puchal | Supervisor: Taras Koturbash | Date: 28/04/2023 | | |

**50 W & 100 W in parallel - Wire 1**
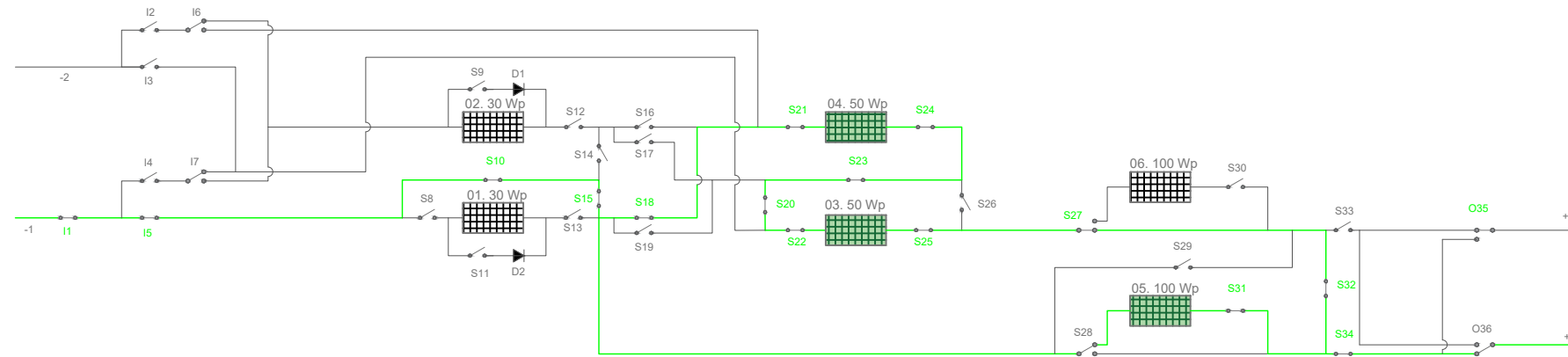
**50 W & 100 W in parallel - Wire 2**

## SCENARIO 41

| Relays closed |
|:---:|
| I2 - I6 - S16 - S14 - S15 - S21 - S24 - S23 - S20 - S22 - S25 -  S27 - S31 - S32 - S34 - O36 |

| Project: | Development of Photovoltaic System Simulator: PV Remote Lab | | Plan Number: | Escale: | |
|---|---|---|---|---|---|
| | | | **016** | S/N | |
| Plan Title: | Single PV String CBS: 50 Wp & 100 Wp in parallel | | | | |
| Author: Jesús Querol Puchal | Supervisor: Taras Koturbash | | Date: 28/04/2023 | | |

DC CONVERSION — MPPT
AC CONVERSION — Inverter
S38
S37
+2
-2
S39
Power supply
DC Load Controller
A
V
Voltage measurement

DC CONVERSION — PWM
DC CONVERSION — MPPT
AC CONVERSION — Inverter
S41
S42
S40
+1
-1
S43
Power supply
DC Load Controller
A
V
Voltage measurement
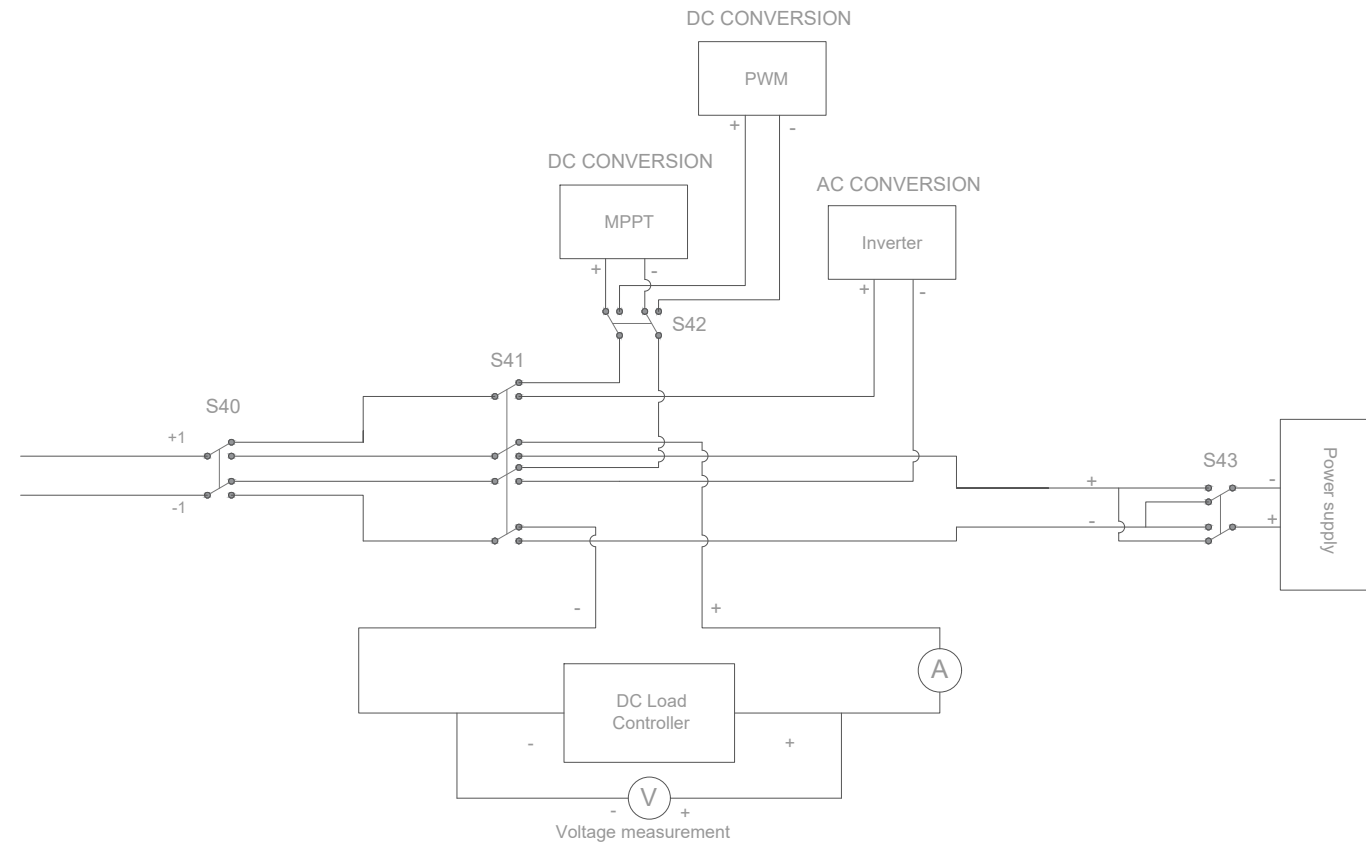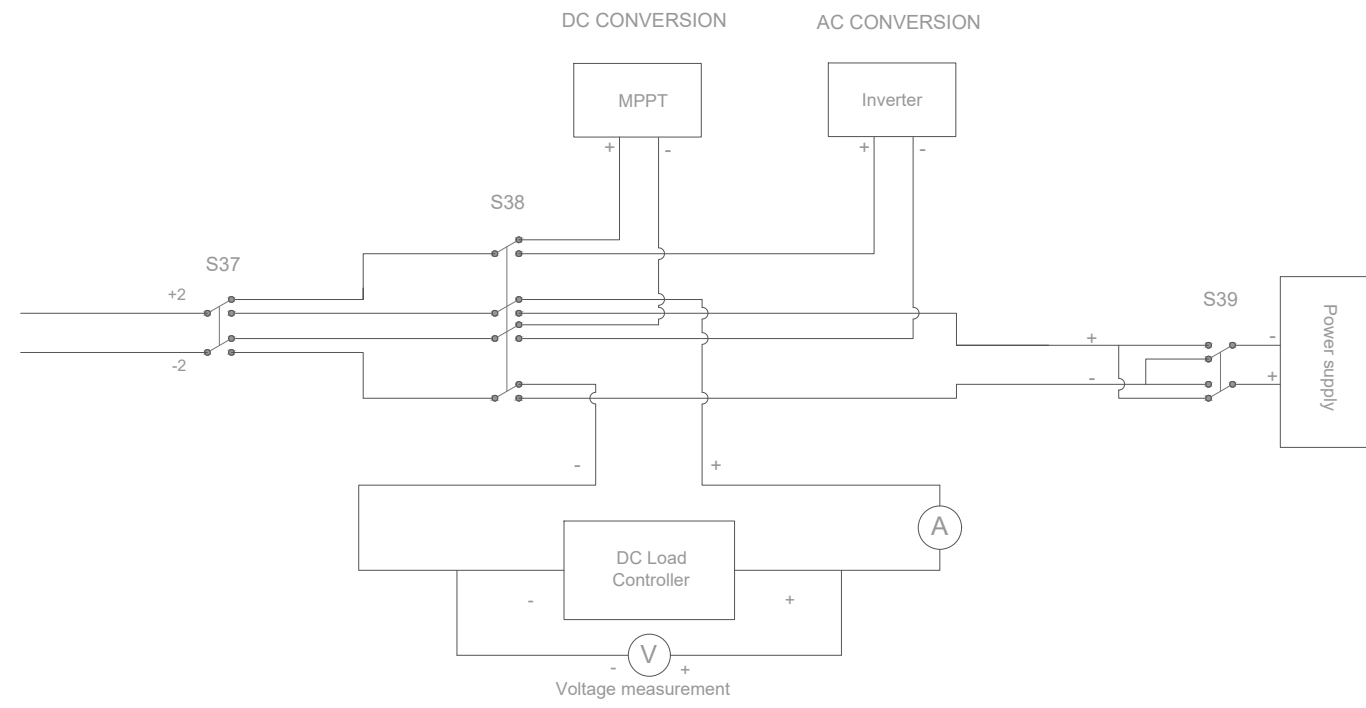
| | Double Pole Double Through | 5 |
|---|---|---|
| | Four Pole Double Through | 2 |

| Project: | Development of Photovoltaic System Simulator: PV Remote Lab | Plan Number: | Escale: |
|---|---|---|---|
| Plan Title: | Double PV String Complete Block Scheme: Outputs of the System | 017 | S/N |
| Author: Jesús Querol Puchal | Supervisor: Taras Koturbash | Date: 28/04/2023 | |

KTH
VETENSKAP OCH KONST

Relays closed

No one

DC CONVERSION

PWM

+ -

DC CONVERSION

MPPT

AC CONVERSION

Inverter

+ -

+ -

S42

S41

S40

+1

-1

S43

+ -

- +

Power supply

-

+

DC Load
Controller

- +

A

V

- +

Voltage measurement
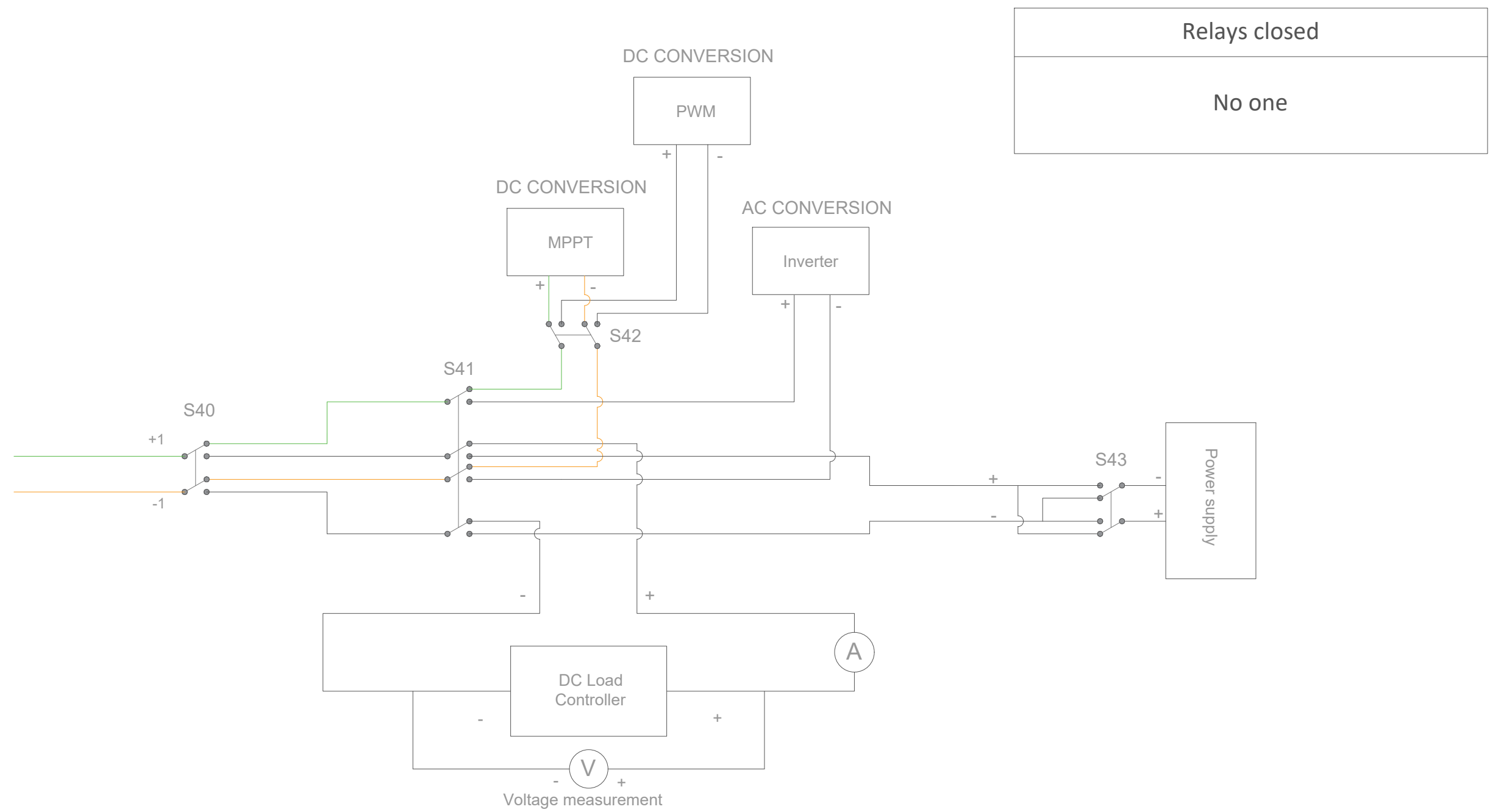
| Project: | Development of Photovoltaic System Simulator: PV Remote Lab | | Plan Number: | Escale: | |
|---|---|---|---|---|---|
| Plan Title: | Double PV String CBS: 1 String - MPPT | | 018 | S/N | |
| Author: | Jesús Querol Puchal | Supervisor: Taras Koturbash | Date: | 28/04/2023 | |

KTH
VETENSKAP
OCH KONST

| Relays closed |
|---|
| S41 |

DC CONVERSION

PWM

+   -

DC CONVERSION

MPPT

+   -

AC CONVERSION

Inverter

+   -

S42

S41

S40

+1

-1

S43

Power supply

-

+

A

DC Load
Controller

-

+

V

-   +

Voltage measurement
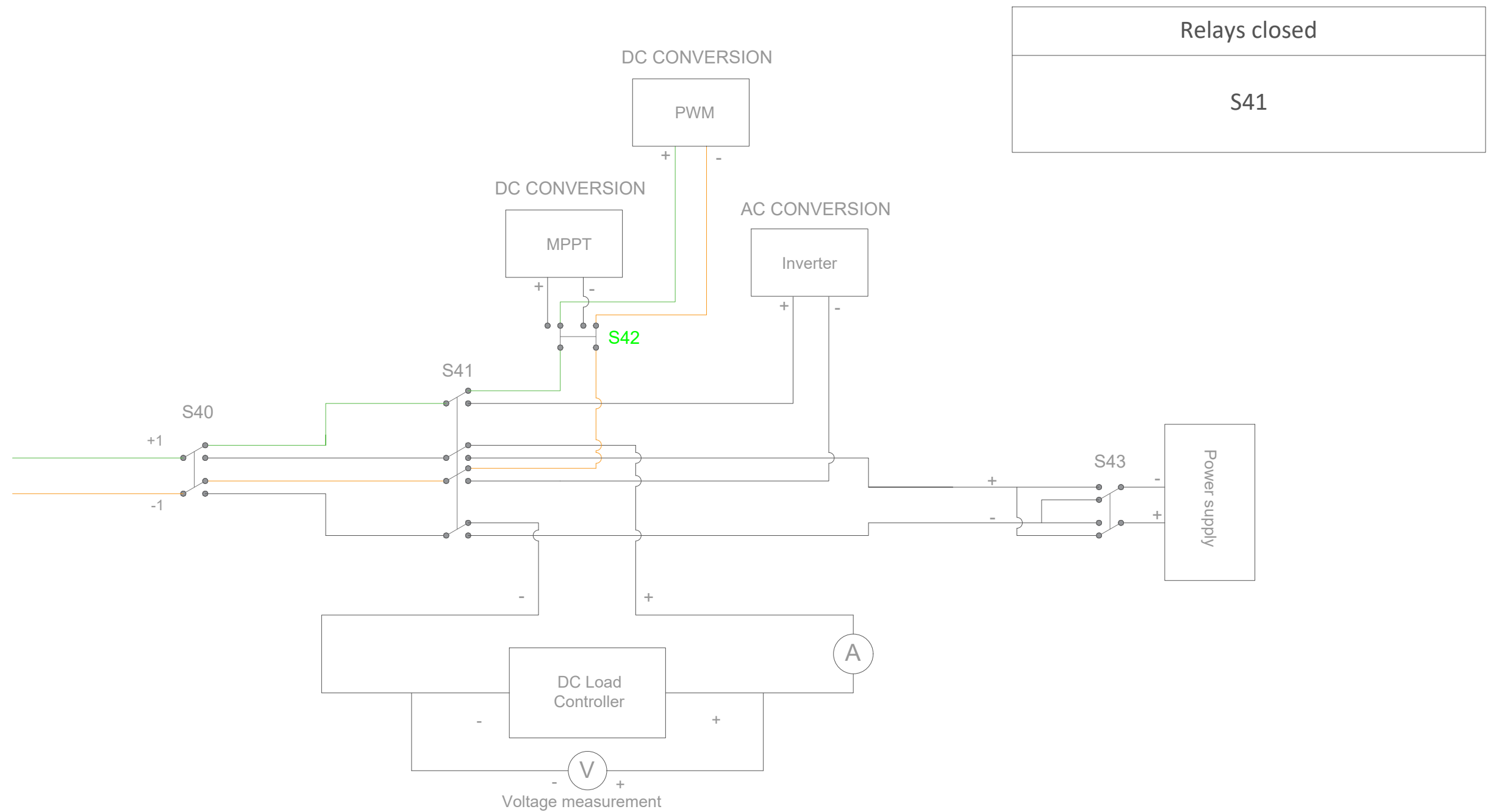
| Project: | Development of Photovoltaic System Simulator: PV Remote Lab | Plan Number: | Escale: |
|---|---|---|---|
| Plan Title: | Double PV String CBS:  1 PV String - PWM | 019 | S/N |
| Author: Jesús Querol Puchal | Supervisor: Taras Koturbash | Date: 28/04/2023 | |
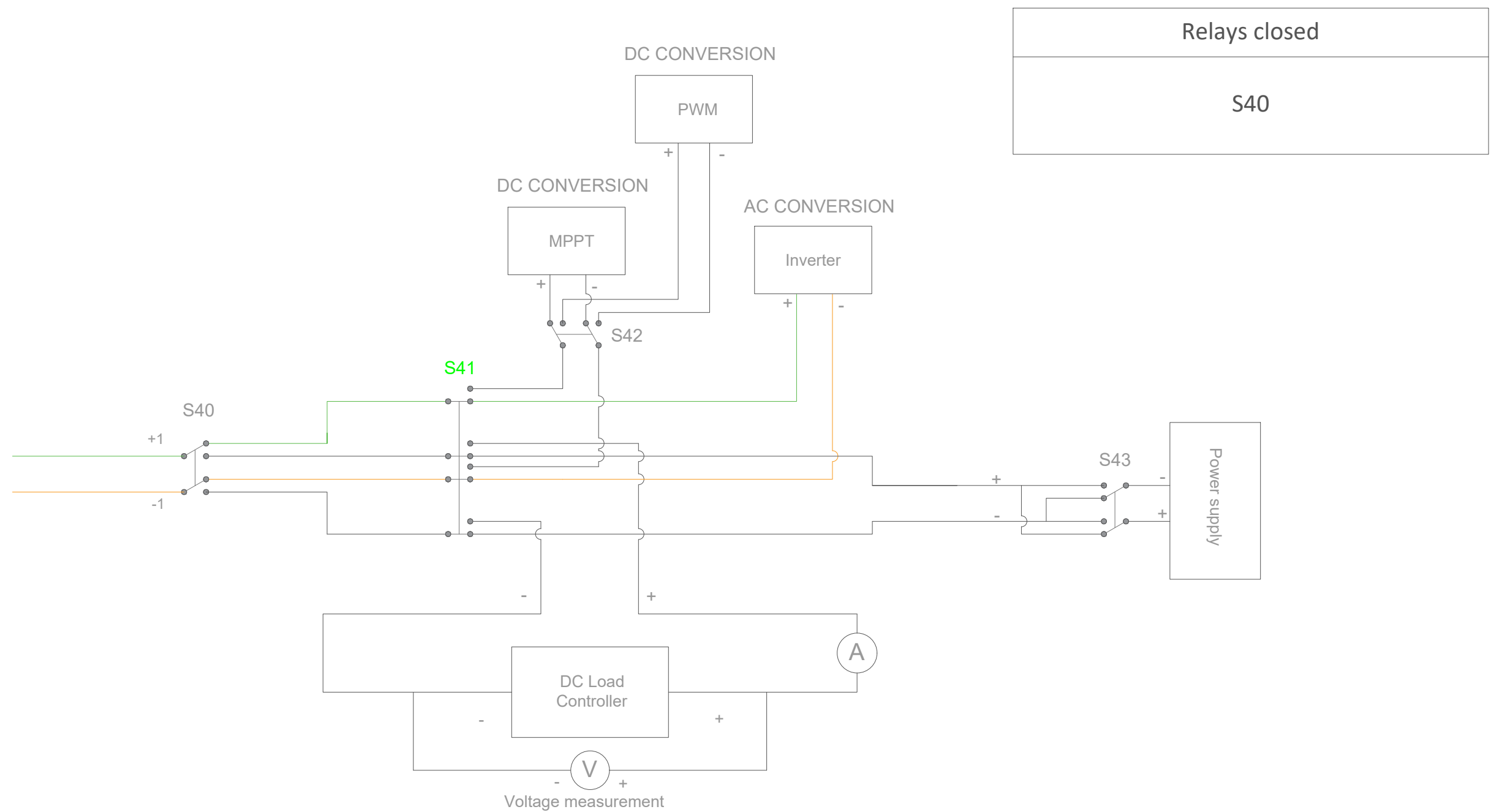
KTH
VETENSKAP
OCH KONST

Relays closed

S40

DC CONVERSION

PWM

+ -

DC CONVERSION

MPPT

AC CONVERSION

Inverter

+ -

+

S42

S41

S40

+1

-1

S43

Power supply

+

-

-

+

-

+

DC Load
Controller

-

+

A

-

+

V

- +

Voltage measurement

| Project: | Development of Photovoltaic System Simulator: PV Remote Lab | Plan Number: | Escale: |
|---|---|---|---|
| Plan Title: | Double PV String CBS: 1 PV String - Inverter | 020 | S/N |
| Author: Jesús Querol Puchal | Supervisor: Taras Koturbash | Date: 28/04/2023 | |
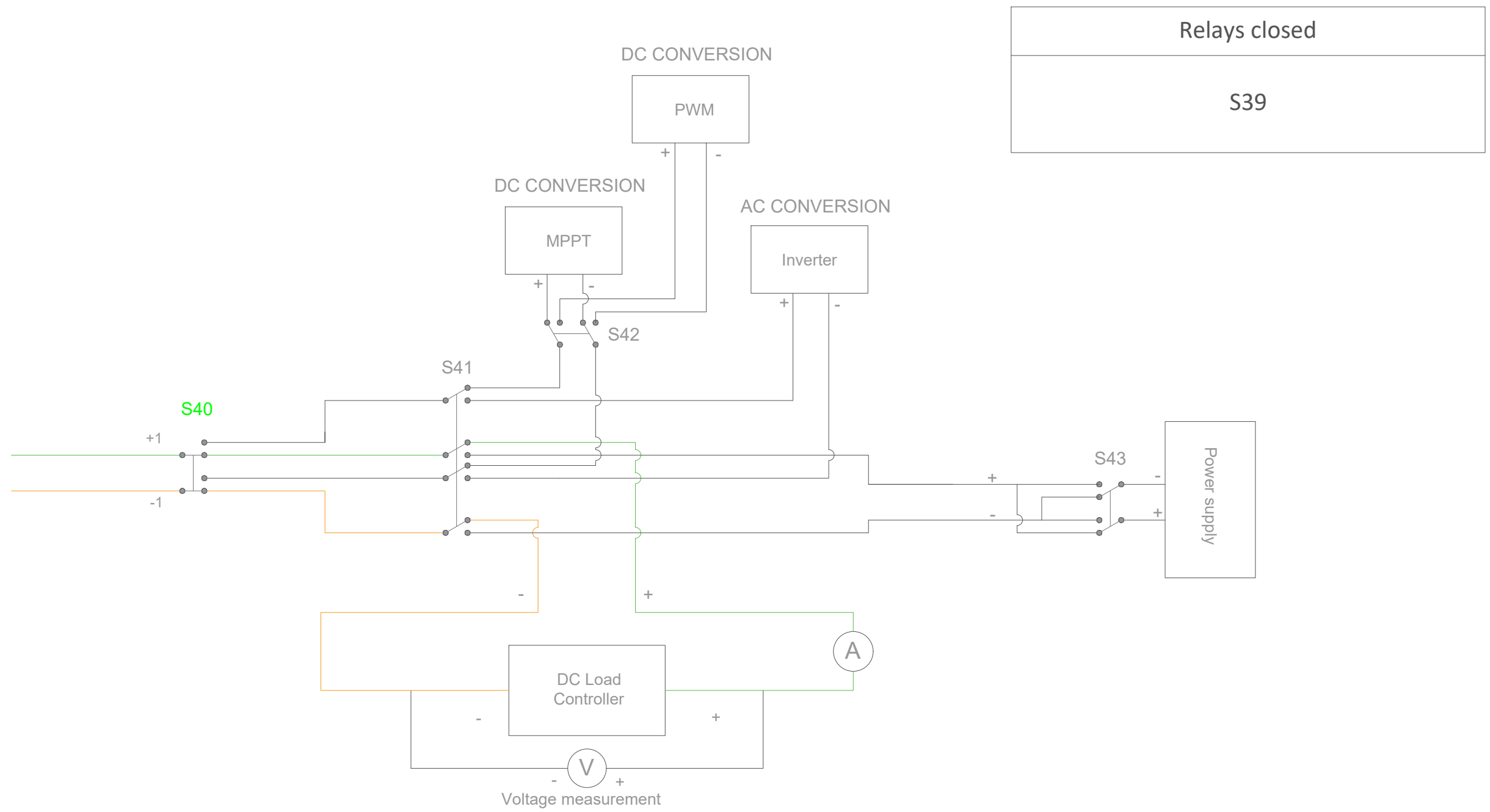
KTH
VETENSKAP
OCH KONST

SCENARIO 4

| Relays closed |
|---|
| S39 |

DC CONVERSION

PWM

+    -

DC CONVERSION

MPPT

+    -

AC CONVERSION

Inverter

+    -

S42

S41

S40

+1

-1

S43

Power supply

+    -

-    +

A

DC Load
Controller

-         +

V

-    +

Voltage measurement

| Project: | Development of Photovoltaic System Simulator: PV Remote Lab | Plan Number: | Escale: |
|---|---|---|---|
| | | 021 | S/N |
| Plan Title: | Double PV String CBS: 1 PV String - DC Load Controller | | |
| Author: Jesús Querol Puchal | Supervisor: Taras Koturbash | Date: 28/04/2023 | |

KTH
VETENSKAP
OCH KONST

| Relays closed |
|---|
| S39 - S40 |

DC CONVERSION

PWM

+    -

DC CONVERSION

MPPT

AC CONVERSION

Inverter

+    -

+    -

S42

S41

S40

+1

-1

S43

Power supply

+

-

+

-

-    +

DC Load
Controller

-    +

A

-    +

V

Voltage measurement

| Project: | Development of Photovoltaic System Simulator: PV Remote Lab | | Plan Number: | Escale: |
|---|---|---|---|---|
| | | | 022 | S/N |
| Plan Title: | Double PV String CBS: 1 PV String - Power Supply | | | |
| Author: Jesús Querol Puchal | Supervisor: Taras Koturbash | | Date: 28/04/2023 | |

KTH
VETENSKAP
OCH KONST

| Relays closed |
|---|
| S39 - S40 - S42 |

DC CONVERSION

PWM

+  -

DC CONVERSION

MPPT

+  -

AC CONVERSION

Inverter

+  -

S42

S41

S40

+1

-1

S43

Power supply

+

-

+

-

A

DC Load
Controller

-  +

V

-  +

Voltage measurement

| Project: | Development of Photovoltaic System Simulator: PV Remote Lab | Plan Number: | | Escale: |
|---|---|---|---|---|
| | | 023 | | S/N |
| Plan Title: | Double PV String CBS: 1 PV String - Power Supply (Reverse Current) | | | |
| Author: | Jesús Querol Puchal | Supervisor: Taras Koturbash | Date: | 28/04/2023 |

KTH
VETENSKAP
OCH KONST

Relays closed

No one

DC CONVERSION

AC CONVERSION

MPPT

Inverter

S38

S37

+2

-2

S39

Power supply

-

+

DC Load
Controller

A

-

+

V

-   +

Voltage measurement

| Project: | Development of Photovoltaic System Simulator: PV Remote Lab | Plan Number: | Escale: |
|---|---|---|---|
| Plan Title: | Double PV String CBS: 2 PV String - MPPT | 024 | S/N |
| Author: Jesús Querol Puchal | Supervisor: Taras Koturbash | Date: 28/04/2023 | |

KTH
VETENSKAP
OCH KONST

| Relays closed |
|:---:|
| S37 |

DC CONVERSION   AC CONVERSION

MPPT

Inverter

+   -

+

S38

S37

+2

-2

S39

Power supply

+

-

+

-

+

-

+

-

-

+

DC Load
Controller

-   +

A

-   +

V

Voltage measurement

| Project: | Development of Photovoltaic System Simulator: PV Remote Lab | | Plan Number: | Escale: | |
|:---|:---:|:---|:---:|:---:|:---:|
| | | | 025 | S/N | |
| Plan Title: | Double PV String CBS: 2 PV String - Inverter | | | | |
| Author: | Jesús Querol Puchal | Supervisor: Taras Koturbash | Date: 28/04/2023 | | KTH VETENSKAP OCH KONST |

| Relays closed |
|:---:|
| S36 |

DC CONVERSION

AC CONVERSION

MPPT

Inverter

+ -

+ -

S38

S37

+2

-2

S39

- +

Power supply

- +

A

-

+

DC Load Controller

-

+

- +

V

Voltage measurement
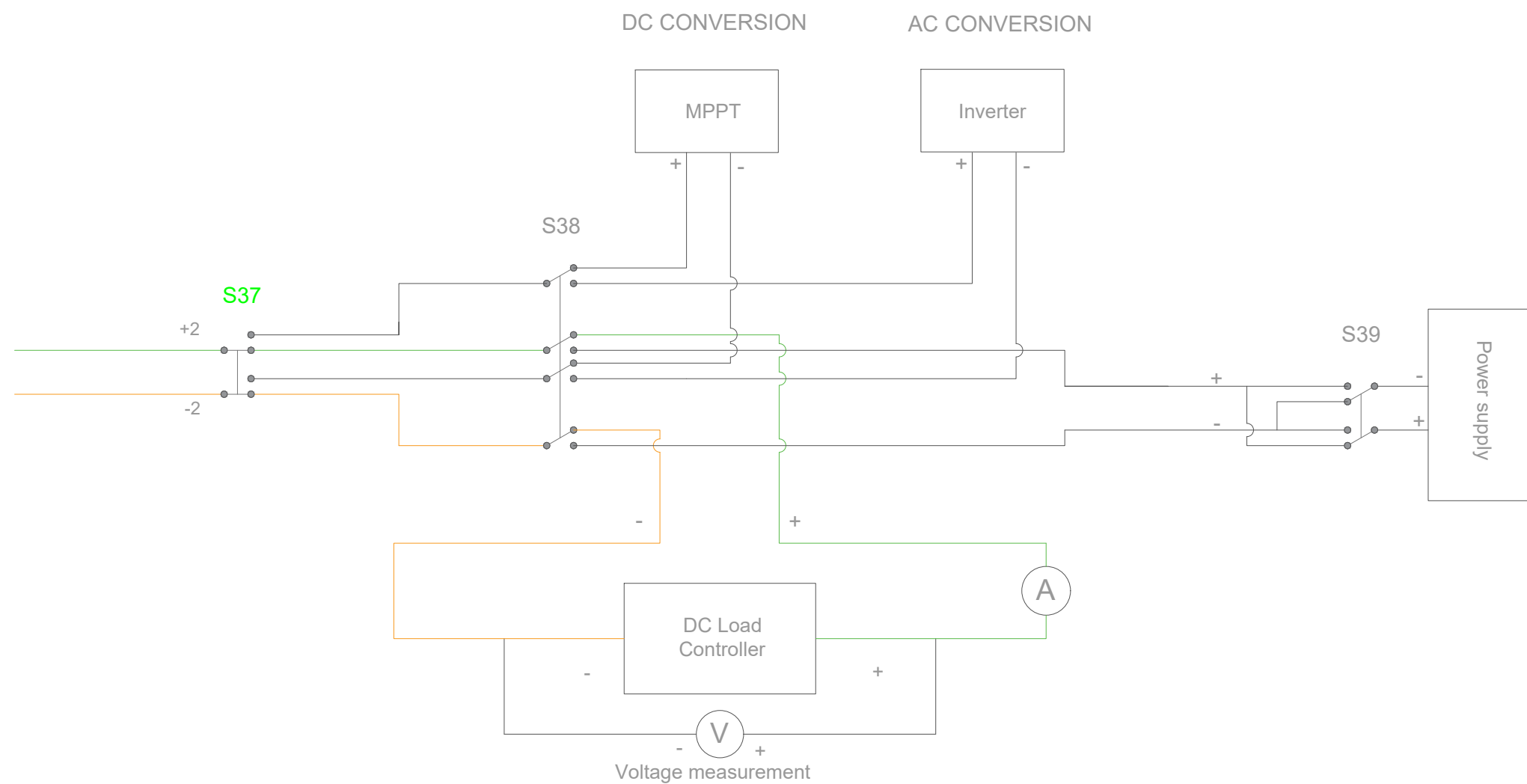
| Project: | Development of Photovoltaic System Simulator: PV Remote Lab | Plan Number: | Escale: |
|---|---|---|---|
| Plan Title: | Double PV String CBS: 2 PV String - DC Load Controller | 026 | S/N |
| Author: Jesús Querol Puchal | Supervisor: Taras Koturbash | Date: 28/04/2023 | |

KTH
VETENSKAP
OCH KONST

# SCENARIO 4

| Relays closed |
|---|
| S36 - S37 |

DC CONVERSION

AC CONVERSION

MPPT

Inverter

+  -

+  -

S38

S37

+2

-2

S39

Power supply

+

-

-

+

-

+

-

+

A

DC Load
Controller

-

+

V

-  +

Voltage measurement

Relays closed

S36 - S37 - S38

DC CONVERSION

AC CONVERSION

MPPT

Inverter

S38

S37

S39

+2

-2

Power supply

A

DC Load
Controller

V

Voltage measurement

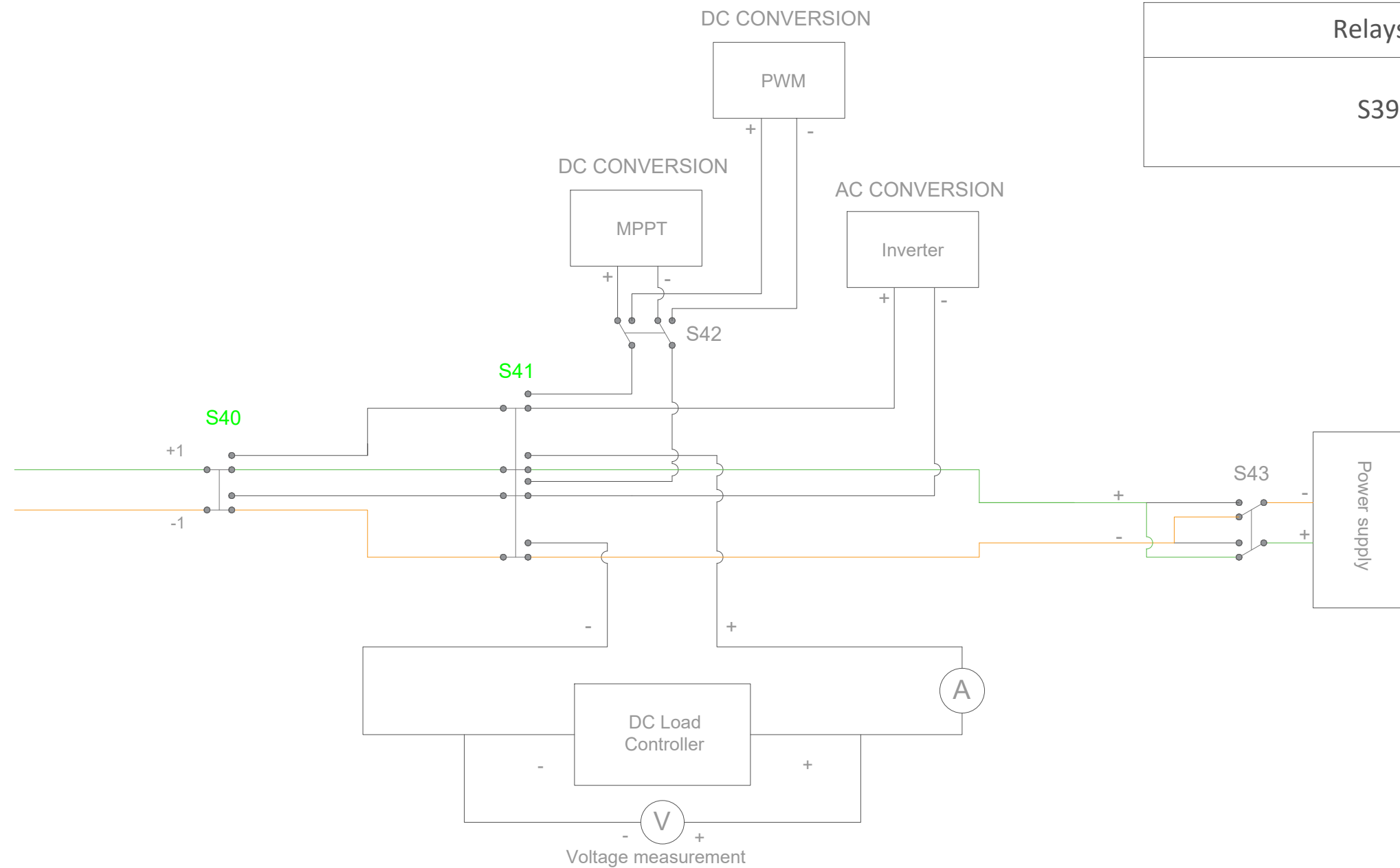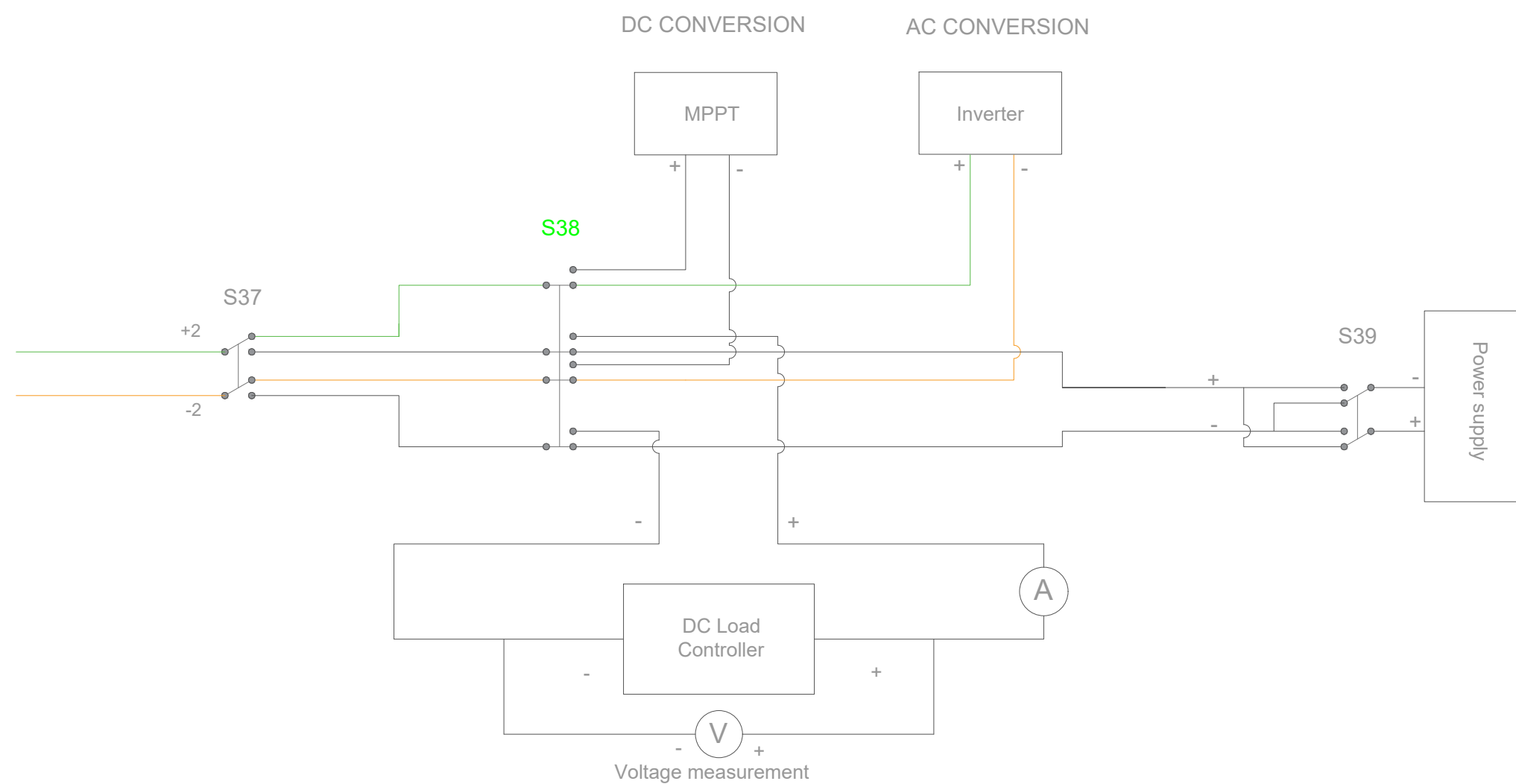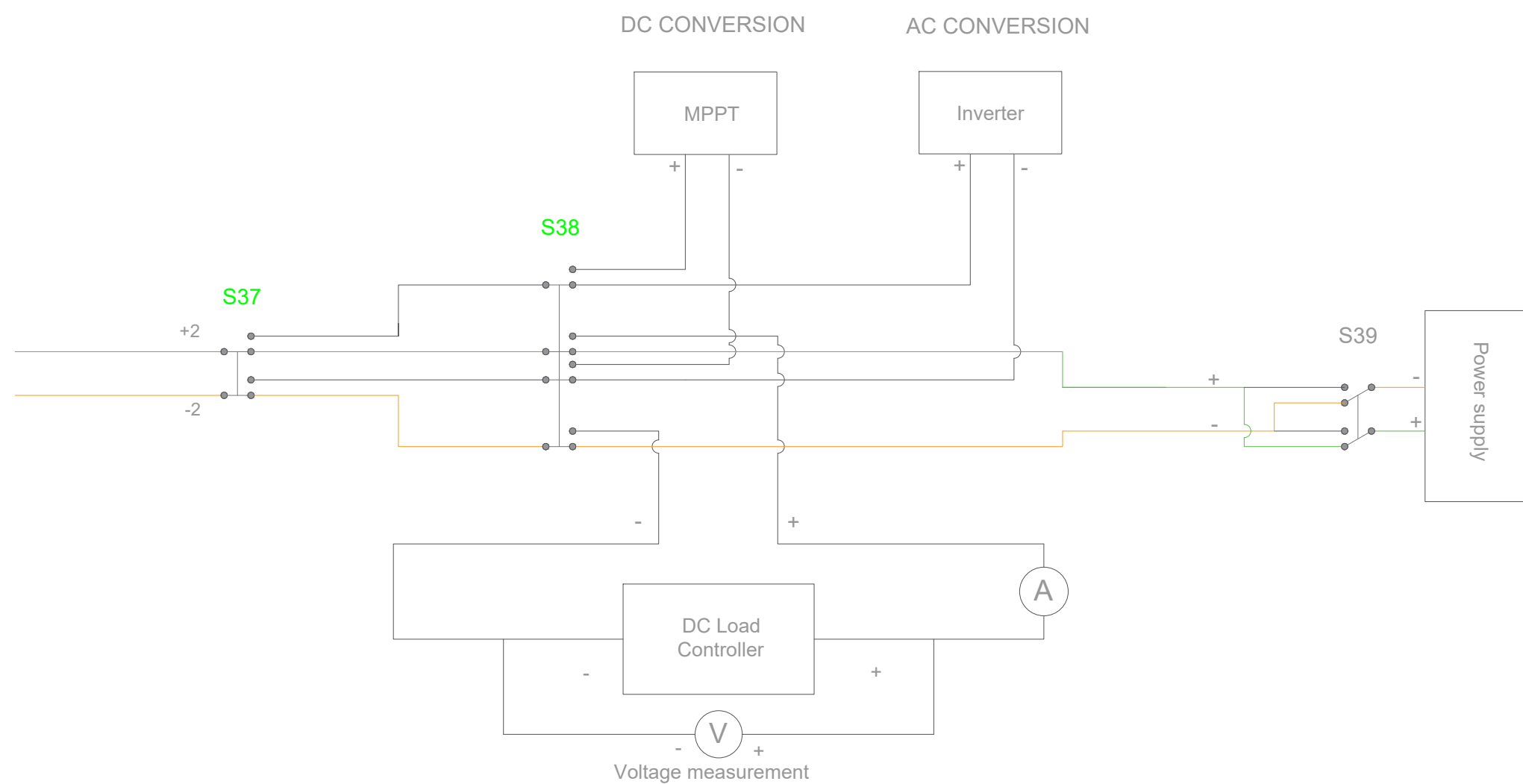| Project: | Development of Photovoltaic System Simulator: PV Remote Lab | Plan Number: | Escale: |
|---|---|---|---|
| Plan Title: | Double PV String CBS: 2 PV String - Power Supply (Reverse Current) | 028 | S/N |
| Author: Jesús Querol Puchal | Supervisor: Taras Koturbash | Date: 28/04/2023 | |

KTH
VETENSKAP
OCH KONST

# Appendix 2 – Scenarios Configuration of the Double PV String CBS

Double PV String Commutation Block Scheme Configuration of the PV System

| | PV panels | String. Num. | Configuration | Relays closed | | Output |
| | | | | Input | System | |
|---|---|---|---|---|---|---|
| Scenario 1 | 01 | 1 | The PV panel is studied alone. | I1 - I5 | S8 - S13 - S28 | O34 |
| Scenario 2 | 03 | 1 | The PV panel is studied alone. | I1 - I5 | S10-S14-S17-S20-S22-S25-S27-S33 | O35 |
| Scenario 3 | 05 | 1 | The PV panel is studied alone. | I1 - I5 | S10 - S15 - S31 | O34 |
| Scenario 4 | 01 | 2 | The PV panel is studied alone. | I2 - I6 | S16 - S14 - S10 - S8 - S13 - S28 | O35 |
| Scenario 5 | 03 | 2 | The PV panel is studied alone. | I3 - I7 | S22 - S25 - S27 - S33 | O34 |
| Scenario 6 | 05 | 2 | The PV panel is studied alone. | I2 - I6 | S16 - S14 - S15 - S31 | O35 |
| Scenario 7 | 02 | 1 | The PV panel is studied alone. | I1 - I4 - I7 - I6 | S12 - S14 - S15 - S28 | O34 |
| Scenario 8 | 04 | 1 | The PV panel is studied alone. | I1 - I5 | S10 - S14 - S16 - S21 - S24 - S26 - S27 - S33 | O35 |
| Scenario 9 | 06 | 1 | The PV panel is studied alone. | I1 - I5 | S10 - S14 - S17 - S23 - S26 - S30 - S33 | O35 |
| Scenario 10 | 02 | 2 | The PV panel is studied alone. | I2 | S12 - S14 - S15 - S28 | O35 |
| Scenario 11 | 04 | 2 | The PV panel is studied alone. | I2 - I6 | S21 - S24 - S26 - S27 - S33 | O34 |
| Scenario 12 | 06 | 2 | The PV panel is studied alone. | I3 - I7 | S20 - S23 - S26 - S30 - S33 | O34 |
| Scenario 13 | 01 & 02 | 1 | The PV panels are connected in series | I1 - I4 - I6 - I7 | S12 - S14 - S10 - S8 - S13 - S28 | O34 |
| Scenario 14 | 03 & 04 | 1 | The PV panels are connected in series | I1 - I5 - I7 | S10 - S14 - S16 - S21 - S24 - S23 - S20 - S22 - S25 - S27 - S33 | O35 |
| Scenario 15 | 05 & 06 | 1 | The PV panels are connected in series | I1 - I5 | S10 - S14 - S17 - S23 - S26 - S30 - S29 - S31 | O34 |
| Scenario 16 | 01 & 02 | 2 | The PV panels are connected in series | I2 | S12 - S14 - S10 - S8 - S13 - S28 | O35 |
| Scenario 17 | 03 & 04 | 2 | The PV panels are connected in series | I2 - I6 -I7 | S21 - S24 - S23 - S20 - S22 - S25 - S27 - S33 | O34 |
| Scenario 18 | 05 & 06 | 2 | The PV panels are connected in series | I3 - I7 | S20 - S23 - S26 - S30 - S29 - S31 | O35 |
| Scenario 19 | 01 & 02 | 1 | The PV panels are connected in parallel | I1 - I4 - I5 - I6 -I7 | S12 - S14 - S8 - S13 - S15 - S28 | O34 |
| Scenario 20 | 03 & 04 | 1 | The PV panels are connected in parallel | I1 - I4 - I5 - I6 | S10 - S14 - S16 - S21 - S24 - S22 - S25 - S26 - S27 - S33 | O35 |
| Scenario 21 | 05 & 06 | 1 | The PV panels are connected in parallel | I1 - I4 - I5 | S10 - S15 - S20 - S23 - S26 - S30 - S31 - S32 | O34 |
| Scenario 22 | 01 & 02 | 2 | The PV panels are connected in parallel | I2 - I4 - I5 - I7 | S12 - S14 - S8 - S15 - S13 - S28 | O35 |
| Scenario 23 | 03 & 04 | 2 | The PV panels are connected in parallel | I2 - I3- I6 - I7 | S21 - S22 - S24 - S25 - S26 - S27 - S33 | O34 |

| | PV panels | String. Num. | Configuration | Relays closed | | Output |
|---|---|---|---|---|---|---|
| | | | | Input | System | |
| Scenario 24 | 05 & 06 | 2 | The PV panels are connected in parallel | I2 - I6 | S16 - S14 - S15 - S17 - S23 - S26 - S30 - S31 - S32 | O35 |
| Scenario 25 | 01 & 02 | Both Strings | 01 - 1 String & 02 - 2 String | I1 - I2 - I5 | S8 - S12 - S13 - S17 - S23 - S26 - S27 - S28 - S33 | O34 |
| Scenario 26 | 03 & 04 | Both Strings | 03 - 1 String & 04 - 2 String | I1 - I2 - I4 - I6 | S21 - S24 - S23 - S17 - S14 - S15 - S22 - S25 - S27 - S28 - S33 | O35 |
| Scenario 27 | 05 & 06 | Both Strings | 05 - 1 String & 06 - 2 String | I1 - I2 - I5 - I6 | S10 - S15 - S16 - S17 - S23 - S26 - S30 - S31 - S33 | O34 |
| Scenario 28 | 01 & 03 | 1 | The PV panels are connected in series | I1 - I5 | S8 - S13 - S19 - S20 - S22 - S25 - S27 - S33 | O35 |
| Scenario 29 | 02 & 04 | 1 | The PV panels are connected in series | I1 - I4 - I7 | S12 - S16 - S21 - S24 - S26 - S27 - S33 | O35 |
| Scenario 30 | 01. & 04 | 1 | The PV panels are connected in series | I1 - I5 | S8 - S13 - S18 - S21 - S24 - S26 - S27 - S33 | O35 |
| Scenario 31 | 02 & 03 | 1 | The PV panels are connected in series | I1 - I4 - I7 | S12 - S17 - S20 - S22 - S25 - S27 - S33 | O35 |
| Scenario 32 | 01 & 03 | 2 | The PV panels are connected in series | I2 - I6 | S16 - S14 - S10 - S8 - S13 - S19 - S20 - S22 - S25 - S27 - S33 | O34 |
| Scenario 33 | 02 & 04 | 2 | The PV panels are connected in series | I2 | S12 - S16 - S21 - S24 - S26 - S27 - S33 | O34 |
| Scenario 34 | 01 & 04 | 2 | The PV panels are connected in series | I3 - I4 - I5 | S8 - S13 - S18 - S21 - S24 - S26 - S27 - S33 | O34 |
| Scenario 35 | 02 & 03 | 2 | The PV panels are connected in series | I2 | S12 - S17 - S20 - S22 - S25 - S27 - S33 | O34 |
| Scenario 36 | 30 Wp & 50 Wp | 1 | ( 01 & 03 in series) & ( 02 & 04 in series) in parallel | I1 - I4 - I5 - I7 | S12 - S16 - S8 - S13 - S19 - S20 - S21 - S22 - S24 - S25 - S26 - S27 - S33 | O35 |
| Scenario 37 | 30 Wp & 50 Wp | 2 | ( 01 & 03 in series) & ( 02 & 04 in series) in parallel | I2 - I3 - I4 - I5 | S8 - S12 - S13 - S16 - S19 - S21 - S20 - S22 - S24 - S25 - S26 - S27 - S33 | O34 |
| Scenario 38 | 30 Wp & 50 Wp | Both Strings | (01 & 02 in series) - 1 String & (03 & 04 in series) - 2 String | I2 - I6 - I1 - I4 - I7 | S12 - S14 - S10 - S8 - S13 - S21 - S24 - S23 - S20 - S22 - S25 - S27 - S28 - S33 | O34 |
| Scenario 39 | 50 Wp & 05 | Both Strings | 05 - 1 String & (03 & 04 in series) - 2 String | I2 - I6 - I1 - I5 | S10 - S15 - S21 - S24 - S23 - S20 - S22 - S25 - S27 - S31 - S33 | O34 |
| Scenario 40 | 50 Wp & 100 Wp | 1 | ( 03 & 04 in series) & ( 05) in parallel | I1 - I5 | S10 - S15 - S18 - S21 - S24 - S23 - S20 - S22 - S25 - S27 - S31 - S32 | O34 |
| Scenario 41 | 50 Wp & 100 Wp | 2 | ( 03 & 04 in series) & ( 05) in parallel | I2 - I6 | S16 - S14 - S15 - S21 - S24 - S23 - S20 - S22 - S25 - S27 - S31 - S32 | O35 |

Double PV String Commutation Block Scheme Configuration of the Outputs

| | Outputs proposed – 1 PV String | Relays closed |
|---|---|---|
| Scenario 1 | The PV system is connected to the MPPT, DC conversion | - |
| Scenario 2 | The PV system is connected to the PWM, DC conversion | S41 |
| Scenario 3 | The PV system is connected to the Inverter, AC conversion | S40 |
| Scenario 4 | The PV system is connected to the DC Load Controller | S39 |
| Scenario 5 | The PV system is connected to the Power Supply, forward bias | S39 - S40 |
| Scenario 6 | The PV system is connected to the Power supply, reverse bias | S39 - S40 - S42 |

| | Outputs proposed – 2 PV String | Relays closed |
|---|---|---|
| Scenario 1 | The PV system is connected to the MPPT, DC conversion | - |
| Scenario 2 | The PV system is connected to the Inverter, AC conversion | S37 |
| Scenario 3 | The PV system is connected to the DC Load Controller | S36 |
| Scenario 4 | The PV system is connected to the Power Supply, forward bias | S36 - S37 |
| Scenario 5 | The PV system is connected to the Power supply, reverse bias | S36 - S37 - S38 |

# Appendix 3 – Components Datasheet

# Solar Modules
# **Sun Plus**

Solar Modules Sun Plus are designed for industrial and professional applications using scratch resistant anodised aluminum with a twin wall frame. The junction box is borrowed from large sized modules and support a user friendly and outdoor proof field installation. Crystalline cells are sandwiched between tempered low iron solar glass sheets and double layered highly resistant foil.

Please find the technical data on the next page.

Die Solarmodule Sun Plus eignen sich für die industrielle und private Anwendung. Durch die doppelte Rahmung mit anodisiertem Aluminium sind sie besonders kratzfest. Die Anschlussdose gleicht der von großen Modulen und ist somit besonders nutzerfreundlich und eignet sich für Installationen auch unter harschen Bedingungen. Die kristallinen Zellen sind in eisenoxidarmes Kristallglas und doppelschichtige hochresistente Folie eingebunden.

Die technischen Daten finden Sie auf der nächsten Seite.

| Technical Data | Technische Daten | | | Sun Plus 100_24 | Sun Plus 150_24 | Sun Plus 200_5 |
|---|---|---|---|---|---|---|
| System voltage | Systemspannung | VDC | V | | 24 | |
| Power | Nennleistung | Pmp | W | 100 | 150 | 200 |
| Voltage at max. power | Spannung bei Max. Leistung | Vmp | V | 36,0 | 36,0 | 35,6 |
| Current at max. power | Strom bei Maximalleistung | Imp | A | 2,78 | 4,16 | 5,62 |
| Open circuit voltage | Leerlaufspannung | Voc | V | 43,2 | 43,2 | 44,6 |
| Short circuit current | Kurzschlußstrom | Isc | A | 3,00 | 4,49 | 6,07 |
| Cell | Zellen | | | 72 x poly | 72 x poly | 72 x mono |
| Cell efficiency | Zellen Wirkungsgrad | | % | 17,1 | 17,1 | 17,8 |
| Module efficiency | Modul Wirkungsgrad | | % | 13,6 | 14,8 | 15,7 |
| Max. tolerance | Max. Leistungstoleranz | | % | | +/-3 % | |
| Max. system voltage | Max. Systemspannung | | V | | 600 | |
| Operating module temp. | Min. Betriebstemperatur | | °C | | -40 … +85 | |
| Front | Vorderseite | | | | tempered glass \| gehärtetes Glas | |
| Frame | Rahmen | | | | clear anodized aluminium \| silber eloxiertes Aluminium | |
| Junction box protection | Anschlussdose Schutzklasse | | | | IP65 | |
| Module cable | cross section | Modulkabel | Querschnitt | mm² | | 4 | |
| | length | | Länge | l | mm | | 900 | |
| | connector | | Stecker | | | Standard4 | |
| Dimension | Abmessung | X x Y x Z | mm | 734 x 1001 x 35 | 1025 x 985 x 40 | 1580 x 808 x 40 |
| Mounting holes pitch | Befestigungslöcher | x1/y/x2 | mm | 400 / 966 / 699 | 800 / 945 / 985 | 800 / 789 / 1300 |
| Mounting hole Ø | Befestigungslöcher Ø | d1 | mm | 9 x 14 | 6 x 9 | 9 x 14 |
| Weight | Gewicht | | kg | 8,1 | 10,5 | 15,9 |
| By-Pass diode number | By-Pass Dioden Anzahl | | | 2 | 2 | 3 |
| Temperature coefficient | Power | Temperaturkoeffizient | Leistung | TC_P | %/°C | -0,430 | − 0,450 | -0,430 |
| | Voc | | Voc | TC_Voc | %/°C | -0,330 | − 0,370 | -0,310 |
| | Isc | | Isc | TC_Isc | %/°C | | 0,081 | 0,044 |
| Package type | Verpackungstyp | | | | single \| einzeln | |
| Certificates | Zertifikate | | | | CE, RoHs | |
| **Article Number** | **Artikelnummer** | | | **310306** | **310220** | **310269** |

# Solar Modules
## Sun Plus
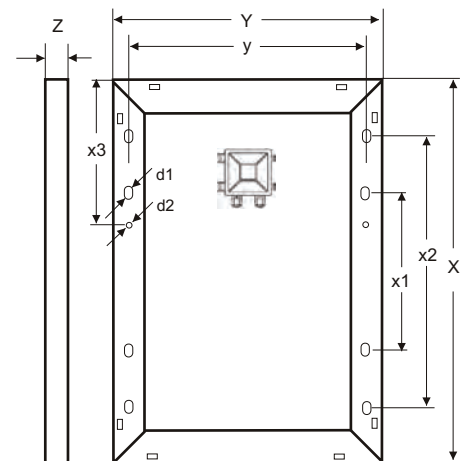
Solar Modules Sun Plus are designed for industrial and professional applications using scratch resistant anodised aluminum with a twin wall frame.The junction box is borrowed from large sized modules and support a user friendly and outdoor proof field installation. Crystalline cells are sandwiched between tempered low iron solar glass sheets and double layered highly resistant foil.

Please find the technical data on the next page.

Die Solarmodule Sun Plus eignen sich für die industrielle und private Anwendung. Durch die doppelte Rahmung mit anodisiertem Aluminium sind sie besonders kratzfest. Die Anschlussdose gleicht der von großen Modulen und ist somit besonders nutzerfreundlich und eignet sich für Installationen auch unter harschen Bedingungen. Die kristallinen Zellen sind in eisenoxidarmes Kristallglas und doppelschichtige hochresistente Folie eingebunden.

Die technischen Daten finden Sie auf der nächsten Seite.

| Technical Data | Technische Daten | | | Sun Plus S 50 | Sun Plus 80 | Sun Plus S 100 | Sun Plus 150_24 |
|---|---|---|---|---|---|---|---|
| Systemvoltage | Systemspannung | (VDC) | [V] | 12 | 12 | 12 | 24 |
| Power | Nennleistung | (Pmp) | [W] | 50 | 80 | 100 | 150 |
| Voltage at max. power | Spannung bei Max. Leistung | (Vmp) | [V] | 17,6 | 17,8 | 17,6 | 36,0 |
| Current at max. power | Strom bei Maximalleistung | (Imp) | [A] | 2,84 | 4,49 | 5,68 | 4,16 |
| Open circuit voltage | Leerlaufspannung | (Voc) | [V] | 21,6 | 22,3 | 21,6 | 43,2 |
| Short circuit voltage | Kurzschlußstrom | (Isc) | [A] | 3,07 | 4,85 | 6,14 | 4,49 |
| Cell | Zellen | | | 36 x mono | 36 x mono | 36 x mono | 72 x poly |
| Cell efficiency | Zellen Wirkungsgrad | | | 18,4 | 18,3 | 17,8 | 17,1 |
| Module efficiency | Modul Wirkungsgrad | | [%] | 15,2 | 14,6 | 15,4 | 14,8 |
| Max. tolerance | Max. Leistungstoleranz | | [%] | +/−3 | | | |
| Max. system voltage | Max. Systemspannung | | [V] | 70 | 600 | 600 | 600 |
| Operating module temp. | Min. Betriebstemperatur | | [°C] | −40 … +85 | | | |
| Front | Vorderseite | | | tempered glass | gehärtetes Glas | | | |
| Frame | Rahmen | | | clear anodized aluminium (colour: silver) | silber eloxiertes Aluminium | | | |
| Junction box protection | Anschlussdose Schutzklasse | | | IP65 | | | |
| Module cable | cross section | Modul-kabel | Querschnitt | [mm²] | 2,5 | 4 | 4 | 4 |
| | length | | Länge | [mm] | 900 | 900 | 900 | 900 |
| | connector | | Stecker | | Standard4 | Standard4 | Standard4 | Standard4 |
| Dimension (l x w x h) | Abmessung (L x B x H) | | [mm] | 650 x 505 x 35 | 806 x 680 x 34 | 1200 x 540 x 35 | 1025 x 985 x 40 |
| Mounting holes pitch | Befestigungslöcher | (y/x1/x2) | [mm] | 325 / 465 / − | 400 / 640 / − | 600 / 500 / − | 800 / 945 / 985 |
| Mounting hole Ø | Befestigungslöcher Ø | | [mm] | 6 x 9 | 6 x 9 | 9 x 14 | 6 x 9 |
| Weight | Gewicht | | [kg] | 4,8 | 6,2 | 8,2 | 10,5 |
| By-Pass diode number | By-Pass Dioden Anzahl | | | 1 | 2 | 2 | 2 |
| Temperature coefficient | Power | Temperaturkoeffizient | Leistung | [%] | −0,44 | −0,44 | −0,44 | −0,44 |
| | Voc | | Voc | [%] | −0,35 | −0,35 | −0,35 | −0,35 |
| | Isc | | Isc | [%] | −0,06 | −0,06 | −0,06 | −0,06 |
| Package type | Verpackungstyp | | | single box | einzeln | | | |
| Certificates | Zertifikate | | | CE, RoHS | | | |
| **Article Number** | **Artikelnummer** | | | **310200** | **310221** | **310214** | **310220** |

## BENEFITS

### Reliable and Robust Design

Proven materials, tempered front glass, and a sturdy anodized frame allow panels to operate reliably in multiple mounting configurations.

### Classic Design

Combines high efficiency and attractive crystalline cells give an elegant appearance.

### More Power

Using industry leading 17.0% efficiency solar cells delivers incredible performance.

(10WP Panel shown)

# MONO & POLY-CRYSTALLINE (12 VOLT) SILICONE SOLAR CELL MODULES

## 5WP – 150WP

### Features

- Modules are designed in accordance with IEC61215:1993 standards, manufactured with proven materials and tested to ensure electrical performance and service life.

- SiN film deposited on the front surface by PECVD acts as anti- reflection coating and gives a uniform dark blue appearance.

- Cells are laminated between highly transparent low-iron 3mm tempered glass, TPT and two layers of EVA to prevent moisture penetrating the module.

- Heavy duty anodized aluminium frame provides high wind resistance and convenient mounting access.

- Waterproof junction box and terminals allows for quick and simple connection.

- Modules will either be supplied with no cable, cable supplied but not connected to the junction box or fully fitted – depending on the option selected. Supplied cables guarantee excellent power transmission throughout the year.

- There is no current requirement for the STI Solar Modules to comply with ROHS.

- 20 year power output transferable warranty

## PV MODULES MADE WITH IEC 61215 CERTIFICATION

| Model | Output Wp | Size mm | Weight Kgm | Pmax W | Vmp V | Imp A | Voc V | Isc A |
|---|---|---|---|---|---|---|---|---|
| STP005P | 5 | 306 x 218 x 25 | 1.0 | 5 | 16.8 | 0.3 | 21 | 0.39 |
| STP010P | 10 | 397 x 280 x 25 | 1.5 | 10 | 16.8 | 0.59 | 21 | 0.66 |
| STP020P | 20 | 638 x 278 x 25 | 2.2 | 20 | 17.5 | 1.15 | 22 | 1.27 |
| STP030P | 30 | 660 x 380 x 25 | 2.8 | 30 | 17.5 | 1.72 | 22 | 1.90 |
| STP045P | 45 | 634 x 535 x 25 | 4.5 | 45 | 17.5 | 2.58 | 22 | 2.86 |
| STP060P | 60 | 685 x 670 x 35 | 6.0 | 60 | 17.2 | 3.49 | 21.6 | 3.97 |
| STP080P | 80 | 815 x 670 x 35 | 7.8 | 80 | 17.2 | 4.65 | 21.6 | 5.00 |
| STP100P | 100 | 1055 x 670 x 35 | 8.0 | 100 | 19.55 | 5.12 | 23.15 | 5.45 |
| STP120P | 120 | 1250 x 670 x 35 | 12.0 | 120 | 17.2 | 6.98 | 21.6 | 7.93 |
| STP150P | 150 | 1490 x 670 x 35 | 15.2 | 150 | 17.2 | 8.72 | 21.6 | 9.72 |

## CERTIFICATIONS

| | |
|---|---|
| ISO9001 (2008) | 1014QMO5 |
| TUV / IEC61215 | PV60040905 |
| IEC61710 (Salt Mist Corrosion Test) | 4786191107-NABL-S1 |
| CE | G4M20301-0199-E-16 |

## MATERIALS

| | |
|---|---|
| Frame | Aluminium 6063 T5 |
| Front Cover | High-transmission Glass |

## ABSOLUTE MAXIMUM LIMITS

| PARAMETERS | RATING | UNIT |
|---|---|---|
| Operating temperature | –40 to +85 | °C |
| Storage temperature | –40 to +85 | °C |
| Dielectric voltage withstood | 3000max | V-DC |
| NOCT | 48 | °C |

## TEMPERATURE COEFFICIENTS

| | | |
|---|---|---|
| Current temperature coefficient | dIsc/dT | +0.003A/K |
| Voltage temperature coefficient | dVoc/dT | – 0.13V/K |
| Power temperature coefficient | dPm/dT | – 0.675W/K |

## WARRANTY

All Solar Technology International solar modules are supplied with a 20 year limited peak power warranty. The warranty claim will deemed to be valid if within 20 years any solar module exhibits power output at less than 80% of minimum 'Peak Power Standard Test Conditions' as noted on the data plate of each module and/or any fault is determined to be the cause of defects in materials and workmanship but not where interference with the module/s by an unauthorised person (of Solar Technology International) has caused the fault or defect. The warranty includes any call outs, labour and other expenses associated with the repair or replacement of the defective part module. Solar Technology International may, at its discretion offer one of the following remedies in the event of a successful claim against the module performance warranty: 1) to replace the defective module/s 2) refund the percentage of the cost of the module to the customer representing the percentage of the power output less than 80% of the minimum. Solar Technology International endeavours to but is not bound by its commitment to rectify any fault within 7 days of notification.

## IV CURVE



Legend: STC | 800W/m² | 600W/m² | STCPV | STC PV 800W/m² | STCPV 600W/m²
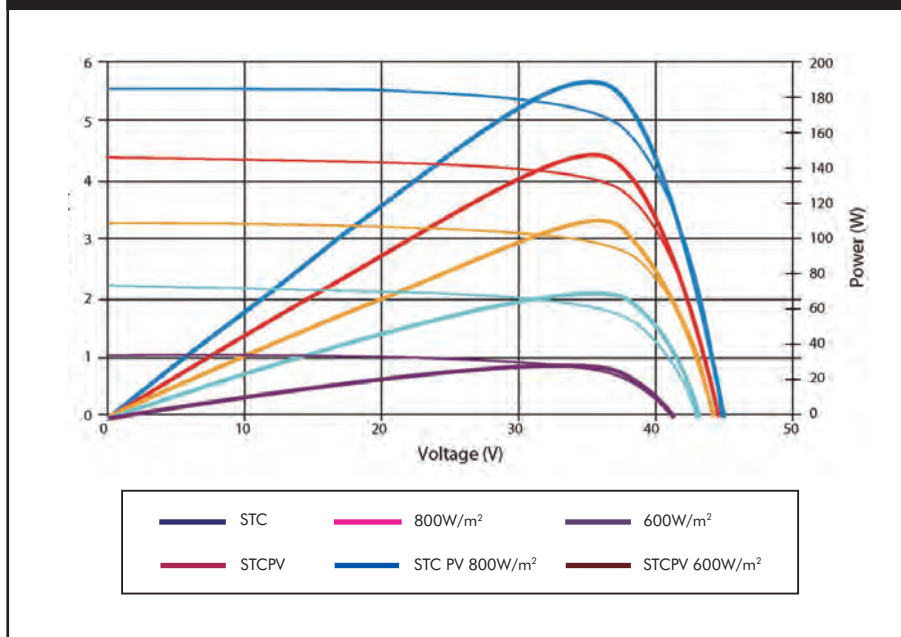
ALL FIGURES TAKEN UNDER THE FOLLOWING STANDARD TEST CONDITIONS:
IRRADIANCE 1000W/M², MODULE TEMPERATURE 25°C, AM=1.5
(All technical data subject to changes without prior notice)

PV LOGIC

Solar Technology Internation Ltd, Unit 6 Station Drive, Bredon, Glos. GL20 7HH
Tel: 01684 774000   Email: sales@solartechnology.co.uk   Online: www.solartechnology.co.uk
PV Logic is a brand of Solar Technology International Ltd

# General-purpose Relay
# G2R-□-S (S)

## Slim and Space-saving Power Plug-in Relay

■ Reduces wiring work by 60% when combined with the
   P2RF-□-PU Push-In Plus Socket
   (according to actual OMRON measurements).
■ Lockable test button models available.
■ Built-in mechanical operation indicator.
■ Provided with nameplate.
■ AC type is equipped with a coil-disconnection self-diagnostic
   function (LED type).
■ High switching power (1-pole: 10 A).
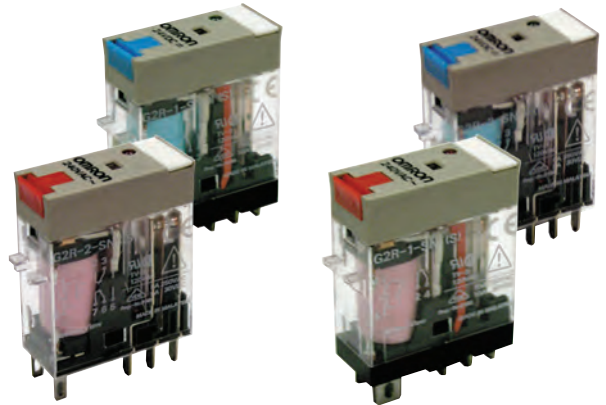
For the most recent information on models that have been certified for safety standards, refer to your OMRON website.

## Model Number Structure

### Model Number Legend

G2R - □ - S □ □ (S)
      1  2  3  4  5

**1. Number of Poles**
  1:    1 pole
  2:    2 poles

**2. Terminals**
  S:    Plug-in

**3. Classification**
  Blank:  General-purpose
  N:      LED indicator
  D:      Diode
  ND:    LED indicator and diode
  NI:     LED indicator with test button
  NDI:  LED indicator and diode with test button

**Note:** Contact your OMRON representative for Relays with gold-plated contacts.

**4. Rated Coil Voltage**

**5. Mechanical operation indicator and Nameplate**
  (S):    Models with mechanical operation indicator and Nameplate

## Ordering Information

When your order, specify the rated voltage.

### List of Models

| Classification | Coil ratings | Contact form | |
|---|---|---|---|
| | | **SPDT** | **DPDT** |
| General-purpose | AC 24, 110, 120, 230, 240 DC 6, 12, 24, 48 | **G2R-1-S (S)** | **G2R-2-S (S)** |
| LED indicator | | **G2R-1-SN (S)** | **G2R-2-SN (S)** |
| LED indicator with test button | | **G2R-1-SNI (S)** | **G2R-2-SNI (S)** |
| Diode | DC 6, 12, 24, 48 | **G2R-1-SD (S)** | **G2R-2-SD (S)** |
| LED indicator and diode | | **G2R-1-SND (S)** | **G2R-2-SND (S)** |
| LED indicator and diode with test button | | **G2R-1-SNDI (S)** | **G2R-2-SNDI (S)** |

**Note: 1.** The standard models are compliant with UL/CSA and VDE standards. Also, an EC compliance declaration has been made for combinations with the P2RF-□-E, P2RF-□-S and P2RF-□-PU. The Relays bear the CE Marking.
      **2.** Refer to *Connecting Sockets*, below, for applicable Socket models.
      **3.** When ordering, add the rated coil voltage and "(S)" to the model number. Rated coil voltages are given in the coil ratings table.
          Example: G2R-1-S 12 VDC (S)
                      └── Rated coil voltage

OMRON

**1**

## Accessories (Order Separately)
### Connecting Sockets

| Applicable Relay model | | Track/surface-mounting Socket | | Back-mounting Socket | |
|---|---|---|---|---|---|
| | | Push-In Plus Terminal Blocks | Screw terminals * | PCB terminals | Solder terminals |
| No. of poles | | Model | Models | Models | Model |
| 1 pole | G2R-1-S (S) | P2RF-05-PU | P2RF-05<br>P2RF-05-E | P2R-05P<br>P2R-057P | P2R-05A |
| 2 poles | G2R-2-S (S) | P2RF-08-PU | P2RF-08<br>P2RF-08-E | P2R-08P<br>P2R-087P | P2R-08A |

* The structure of P2RF-□-E models provides finger protection. Round terminals cannot be used. Use forked crimp terminals.

### Accessories for Push-In Plus Terminal Block Sockets (P2RF-□-PU)
#### Short Bars

| Pitch | No. of poles | Colors | Model ✱ | Minimum order (quantity) |
|---|---|---|---|---|
| 7.75 mm | 2 | Red (R)<br>Blue (S)<br>Yellow (Y) | PYDN-7.75-020□ | 10 |
| | 3 | | PYDN-7.75-030□ | |
| | 4 | | PYDN-7.75-040□ | |
| | 20 | | PYDN-7.75-200□ | |
| 15.5 mm | 8 | | PYDN-15.5-080□ | |

**Note:** Use the Short Bars for crossover wiring within one Socket or between Sockets.
* Replace the box (□) in the model number with the code for the covering color.

#### Labels

| Model | Minimum order (sheet) (quantity per sheet) |
|---|---|
| XW5Z-P4.0LB1 | 5<br>1 sheet (60 pieces) |

### Mounting Tracks

| Applicable Socket | Description | | Model | Minimum order (quantity) |
|---|---|---|---|---|
| Track-connecting Socket | Mounting track | 50 cm (ℓ) × 7.3 mm (t): | PFP-50N | --- |
| | | 1 m (ℓ) × 7.3 mm (t): | PFP-100N | |
| | | 1 m (ℓ) × 16 mm (t): | PFP-100N2 | |
| | End plate *1 | | PFP-M | 10 |
| | Spacer | | PFP-S | |
| Back-connecting Socket | Mounting plate *2 | | P2R-P | 1 |

*1. When mounting DIN rail, please use End Plate (PFP-M).
*2. Used to mount several P2R-05A and P2R-08A Connecting Sockets side by side.

# Specifications

## Coil Ratings

| Rated voltage | | Rated current* | | Coil resistance | Coil inductance (H) (ref. value) | | Must operate voltage | Must release voltage | Max. voltage | Power consumption (approx.) |
|---|---|---|---|---|---|---|---|---|---|---|
| | | 50 Hz | 60 Hz | | Armature OFF | Armature ON | % of rated voltage | | | |
| AC | 24 V | 43.5 mA | 37.4 mA | 253 Ω | 0.81 | 1.55 | 80% max. | 30% max. | 110% | 0.9 VA at 60 Hz |
| | 110 V | 9.5 mA | 8.2 mA | 5,566 Ω | 13.33 | 26.83 | | | | |
| | 120 V | 8.6 mA | 7.5 mA | 7,286 Ω | 16.13 | 32.46 | | | | |
| | 230 V | 4.4 mA | 3.8 mA | 27,172 Ω | 72.68 | 143.90 | | | | |
| | 240 V | 3.7 mA | 3.2 mA | 30,360 Ω | 90.58 | 182.34 | | | | |

| Rated voltage | | Rated current* | Coil resistance | Coil inductance (H) (ref. value) | | Must operate voltage | Must release voltage | Max. voltage | Power consumption (approx.) |
|---|---|---|---|---|---|---|---|---|---|
| | | | | Armature OFF | Armature ON | % of rated voltage | | | |
| DC | 6 V | 87.0 mA | 69 Ω | 0.25 | 0.48 | 70% max. | 15% min. | 110% | 0.53 W |
| | 12 V | 43.2 mA | 278 Ω | 0.98 | 2.35 | | | | |
| | 24 V | 21.6 mA | 1,113 Ω | 3.60 | 8.25 | | | | |
| | 48 V | 11.4 mA | 4,220 Ω | 15.2 | 29.82 | | | | |

**Note: 1.** The rated current and coil resistance are measured at a coil temperature of 23°C with tolerances of +15%/-20% for the AC rated current and ±10% for the DC coil resistance.
**2.** The AC coil resistance and inductance values are reference values only (at 60 Hz).
**3.** Operating characteristics were measured at a coil temperature of 23°C.
**4.** The maximum voltage is the maximum possible value of the voltage that can be applied to the relay coil.
It is not the maximum voltage that can be applied continuously.

## Contact Ratings

| Number of poles | 1 pole | | 2 poles | |
|---|---|---|---|---|
| Load | Resistive load (cosφ = 1) | Inductive load (cosφ = 0.4; L/R = 7 ms) | Resistive load (cosφ = 1) | Inductive load (cosφ = 0.4; L/R = 7 ms) |
| Rated load | 10 A at 250 VAC; 10 A at 30 VDC | 7.5 A at 250 VAC; 5 A at 30 VDC | 5 A at 250 VAC; 5 A at 30 VDC | 2 A at 250 VAC; 3 A at 30 VDC |
| Rated carry current | 10 A | | 5 A | |
| Max. switching voltage | 440 VAC, 125 VDC | | 380 VAC, 125 VDC | |
| Max. switching current | 10 A | | 5 A | |
| Max. switching power | 2,500 VA, 300 W | 1,875 VA, 150 W | 1,250 VA, 150 W | 500 VA, 90 W |
| Failure rate (reference value) * | 100 mA at 5 VDC | | 10 mA at 5 VDC | |

**Note:** P level: $\lambda_{60}$ = 0.1 x 10$^{-6}$/operation
* This value was measured at a switching frequency of 120 operations per minute.

## Characteristics

| Item | 1 pole | 2 poles |
|---|---|---|
| Contact configration | SPDT | |
| Contact structure | Single | |
| Contact resistance | 100 mΩ max. | |
| Operate (set) time | 15 ms max. | |
| Release (reset) time | AC: 10 ms max.; DC: 5 ms max. (w/built-in diode: 20 ms max.) | AC: 15 ms max.; DC: 10 ms max. (w/built-in diode: 20 ms max.) |
| Max. operating frequency | Mechanical: 18,000 operations/hr<br>Electrical: 1,800 operations/hr (under rated load) | |
| Insulation resistance | 1,000 MΩ min. (at 500 VDC) | |
| Dielectric strength * | 5,000 VAC, 50/60 Hz for 1 min between coil and contacts;<br>1,000 VAC, 50/60 Hz for 1 min between contacts of same polarity | 5,000 VAC, 50/60 Hz for 1 min between coil and contacts;<br>3,000 VAC, 50/60 Hz for 1 min between contacts of different polarity<br>1,000 VAC, 50/60 Hz for 1 min between contacts of same polarity |
| Vibration resistance | Destruction: 10 to 55 to 10 Hz, 0.75 mm single amplitude (1.5 mm double amplitude)<br>Malfunction: 10 to 55 to 10 Hz, 0.75 mm single amplitude (1.5 mm double amplitude) | |
| Shock resistance | Destruction: 1,000 m/s$^2$<br>Malfunction: 200 m/s$^2$ when energized; 100 m/s$^2$ when not energized | |
| Endurance | Mechanical: AC coil: 10,000,000 operations min.;<br>DC coil: 20,000,000 operations min. (at 18,000 operations/hr)<br>Electrical: 100,000 operations min. (at 1,800 operations/hr under rated load) | |
| Ambient temperature | Operating: −40°C to 70°C (with no icing or condensation) | |
| Ambient humidity | Operating: 5% to 85% | |
| Weight | Approx. 20 g | |

**Note:** Values in the above table are the initial values.
* These values are relay only. Prease refer to the "Products Related to Common Sockets and DIN Tracks Data Sheet" for connecting sockets.

## Approved Standards

### UL 508 (File No. E41643)

| Model | Contact form | Coil ratings | Contact ratings | Opera-tions |
|---|---|---|---|---|
| G2R-1-S (S) | SPDT | 5 to 110 VDC 6 to 240 VAC | 10 A, 30 VDC (resistive)<br>10 A, 250 VAC (general use) | 100 × 10$^3$ |
| | | | TV-3 (NO contact only) | 25 × 10$^3$ |
| G2R-2-S (S) | DPDT | | 5 A, 30 VDC (resistive)<br>5 A, 250 VAC (general use) | 100 × 10$^3$ |
| | | | TV-3 (NO contact only) | 25 × 10$^3$ |

### CSA 22.2 No.0, No.14 (File No. LR31928)

| Model | Contact form | Coil ratings | Contact ratings | Opera-tions |
|---|---|---|---|---|
| G2R-1-S (S) | SPDT | 5 to 110 VDC 6 to 240 VAC | 10 A, 30 VDC (resistive)<br>10 A, 250 VAC (general use) | 100 × 10$^3$ |
| | | | TV-3 (NO contact only) | 25 × 10$^3$ |
| G2R-2-S (S) | DPDT | | 5 A, 30 VDC (resistive)<br>5 A, 250 VAC (general use) | 100 × 10$^3$ |
| | | | TV-3 (NO contact only) | 25 × 10$^3$ |

### IEC/VDE (Certificate No. 40015012 EN 61810-1)

| Contact form | Coil ratings | Contact ratings | Operations |
|---|---|---|---|
| 1 pole | 6, 12, 24, 48 VDC 24, 110, 120, 230, 240 VAC | 5 A, 440 VAC (cosφ = 1.0)<br>10 A, 250 VAC (cosφ = 1.0)<br>10 A, 30 VDC (0 ms) | 100 × 10$^3$ |
| 2 poles | 6, 12, 24, 48 VDC 24, 110, 120, 230, 240 VAC | 5 A, 250 VAC (cosφ =1.0)<br>5 A, 30 VDC (0 ms) | 100 × 10$^3$ |

### LR

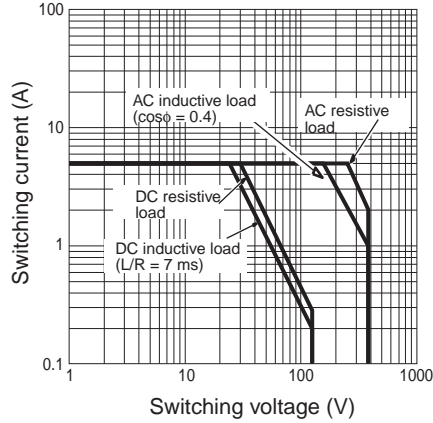| Number of poles | Coil ratings | Contact ratings | Operations |
|---|---|---|---|
| 1 pole | 5 to 110 VDC 6 to 240 VDC | 10 A, 250 VAC (general use)<br>7.5 A, 250 VAC (PF0.4)<br>10 A, 30 VDC (resistive)<br>5A, 30VDC (L/R=7ms) | 100 × 10$^3$ |
| 2 poles | 5 to 110 VDC 6 to 240 VDC | 5 A, 250 VAC (general use)<br>2 A, 250 VAC (PF0.4)<br>5 A, 30 VDC (resistive)<br>3A, 30VDC (L/R=7ms) | 100 × 10$^3$ |

# Engineering Data
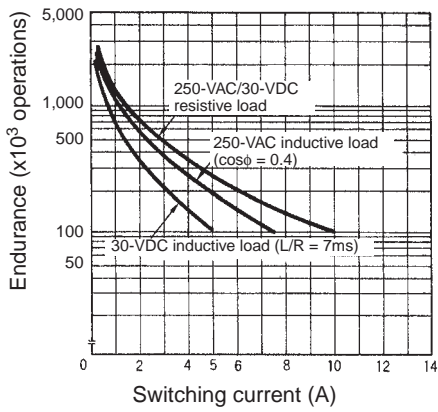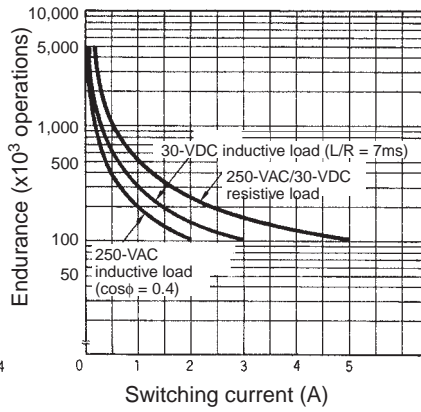
## Maximum Switching Power

**G2R-1-S (S)**
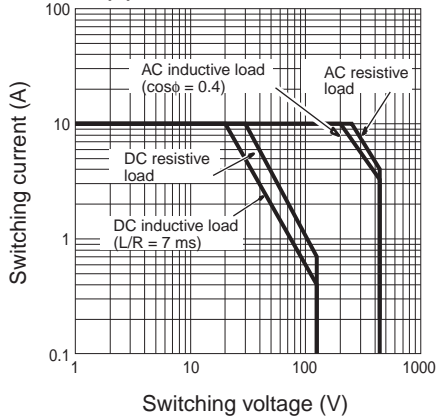


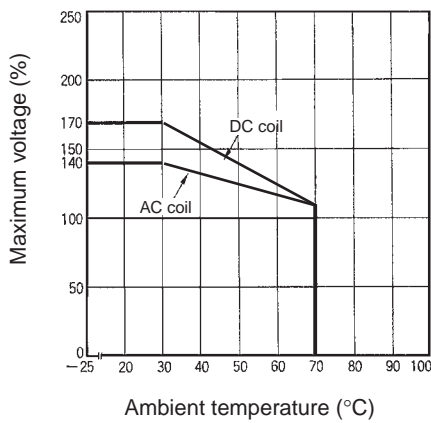**G2R-2-S (S)**



## Endurance

**G2R-1-S (S)**



**G2R-2-S (S)**



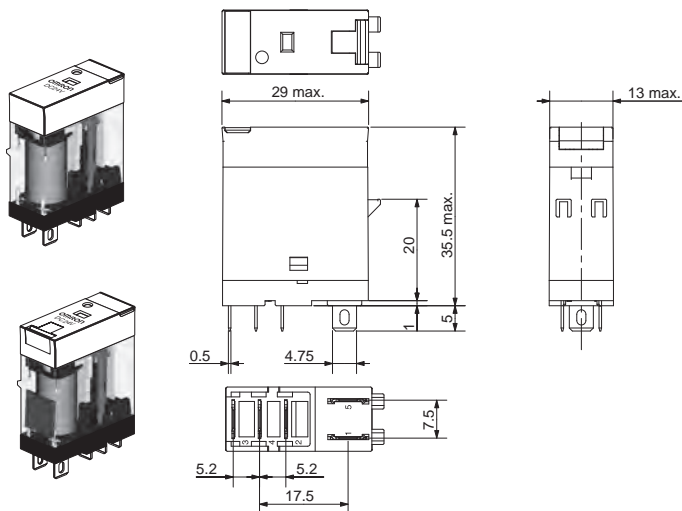## Ambient Temperature vs Maximum Coil Voltage

# Dimensions

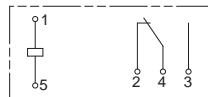**Note:** All units are in millimeters unless otherwise indicated.

### SPDT Relays

**G2R-1-S (S), G2R-1-SN (S), G2R-1-SNI (S)**
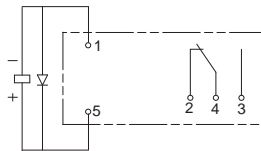**G2R-1-SD (S), G2R-1-SND (S), G2R-1-SNDI (S)**
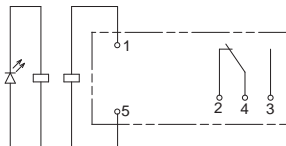
**Terminal Arrangement/Internal Connections
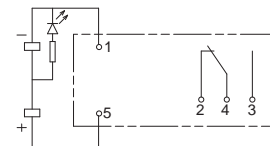(Bottom View)**

29 max.

13 max.

35.5 max.

20

5

1

0.5    4.75

7.5

5.2    5.2

17.5

**G2R-1-S (S)**



**G2R-1-SD (S) (DC)**



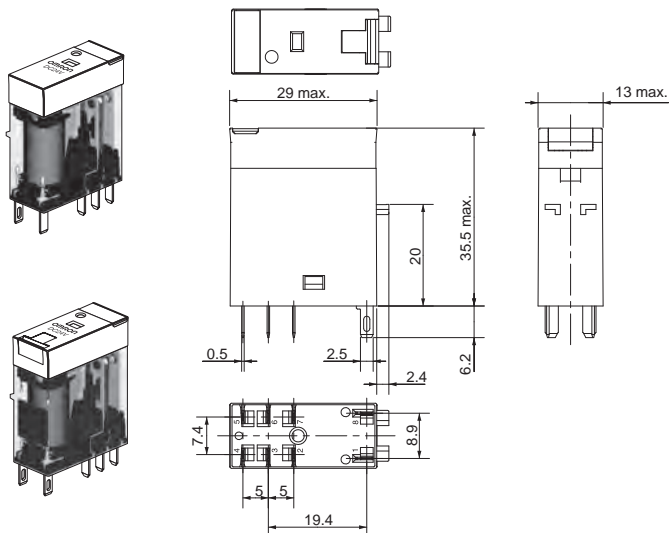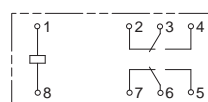**G2R-1-SN (S), G2R-1-SNI (S) (AC)**



**G2R-1-SN (S), G2R-1-SNI (S) (DC)**



**G2R-1-SND (S), G2R-1-SNDI (S) (DC)**
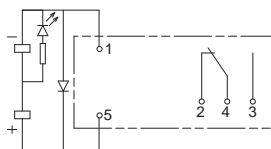


### DPDT Relays

**G2R-2-S (S), G2R-2-SN (S), G2R-2-SNI (S)**
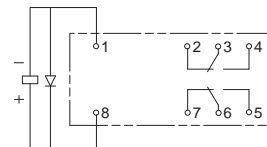**G2R-2-SD (S), G2R-2-SND (S), G2R-2-SNDI (S)**
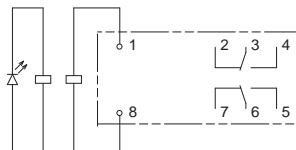
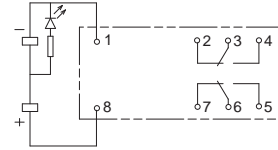**Terminal Arrangement/Internal Connections
(Bottom View)**

29 max.

13 max.

35.5 max.

20

6.2

0.5    2.5

2.4

7.4    8.9

5    5
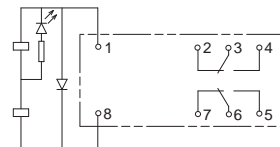
19.4

**G2R-2-S (S)**



**G2R-2-SD (S) (DC)**
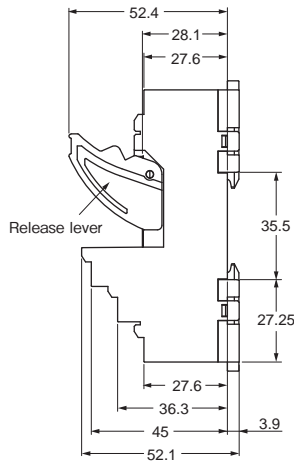


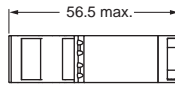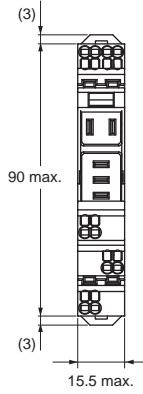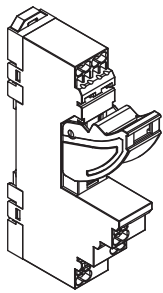**G2R-2-SN (S), G2R-2-SNI (S) (AC)**



**G2R-2-SN (S), G2R-2-SNI (S) (DC)**



**G2R-2-SND (S), G2R-2-SNDI (S) (DC)**

## Track/Surface Mounting Sockets
### P2RF-05-PU

56.5 max.

52.4
28.1
27.6

(3)

90 max.

Release lever

35.5

27.25

(3)

15.5 max.

27.6
36.3
45          3.9
52.1

**Terminal Arrangement/
Internal Connection Diagram
(Top View)**

A2 (1)    A1 (5)

12 (2)

14 (3)

11 (4)

**Note:** The numbers in parentheses are traditionally used terminal numbers.

**Mounting Hole Dimensions**

Two M4 screw holes or two 4-dia. holes

108
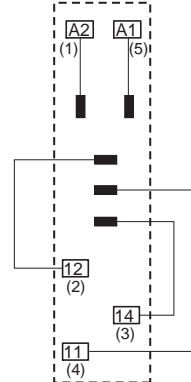
**Note:** Pull out the hooks to mount the Relay with screws.

### P2RF-08-PU
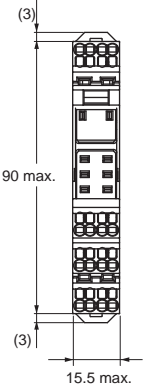
56.5 max.

52.4
28.1
27.6

(3)

90 max.

Release lever

35.5

27.25

(3)

15.5 max.

27.6
36.3
45          3.9
52.1

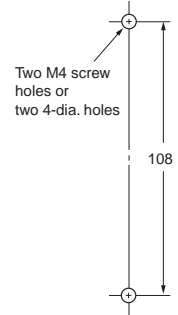**Terminal Arrangement/
Internal Connection Diagram
(Top View)**

A2 (1)    A1 (8)

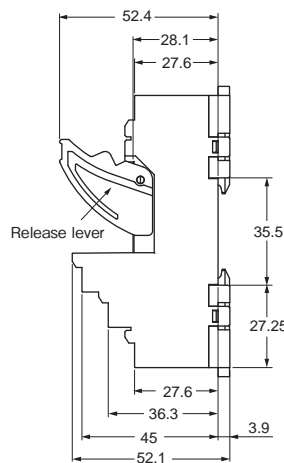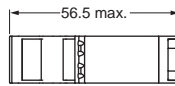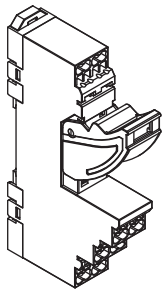12 (2)    22 (7)

14 (4)    24 (5)

11 (3)    21 (6)

**Note:** The numbers in parentheses are traditionally used terminal numbers.
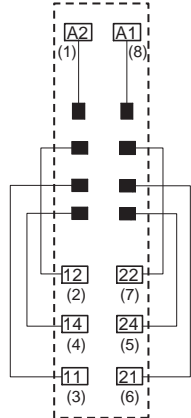
**Mounting Hole Dimensions**

Two M4 screw holes or two 4-dia. holes

108
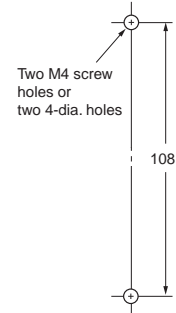
**Note:** Pull out the hooks to mount the Relay with screws.

## Accessories for P2RF-□-PU
### Short Bars
### PYDN-7.75-□□ (7.75 mm)

3.90

L

18.5

12

2.25          1.57

### PYDN-15.5-080□ (15.5 mm)

115.85

3.90

18.5

12

2.25          1.57
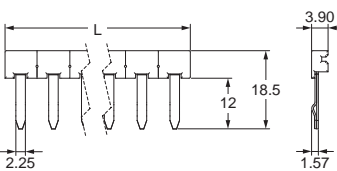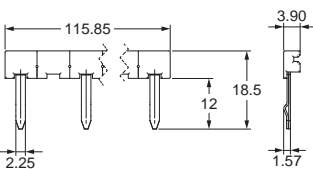
| Application | Pitch | No. of poles | L (Length) | Colors | Model * | Maximum carry current |
|---|---|---|---|---|---|---|
| For Contact terminals (common) | 7.75 mm | 2 | 15.1 | Red (R) Blue (S) Yellow (Y) | **PYDN-7.75-020□** | 20 A |
| | | 3 | 22.85 | | **PYDN-7.75-030□** | |
| | | 4 | 30.6 | | **PYDN-7.75-040□** | |
| | | 20 | 154.6 | | **PYDN-7.75-200□** | |
| For Coil terminals | 15.5 mm | 8 | 115.85 | | **PYDN-15.5-080□** | |

*Replace the box (□) in the model number with the code for the covering color.

**Note: 1.** Use the Short Bars for crossover wiring within one Socket or between Sockets.
**2.** When using short bar to coil terminals of P2RF-□□-PU, A1 terminal cannot be used. In case crossover wiring of A1 terminal side is needed, crossover wiring using A1 terminals by wire is possible.

**Short bar correspondence table**

| | Contact terminal (Common) | Coil terminal | |
|---|---|---|---|
| | | A1 | A2 |
| P2RF-□□-PU | Available | --- | ○ |

## P2RF-05-E

Five, M3.5´7

85.5 max.

3.5-dia. hole

7 ±0.2

2

48 max.

39.5

35.5

4

16.0 max.

11.5

61 max.

**Terminal Arrangement (Top View)**

④ (11)

(12) ②

③ (14)

⑤

(A1)

(A2) ①

**Mounting Holes (for Surface Mounting)**

3.2-dia. hole

39.5±0.1

M3 or 3.5-dia. hole
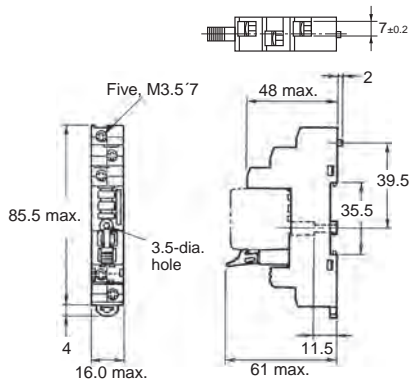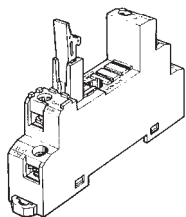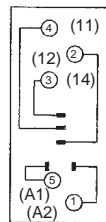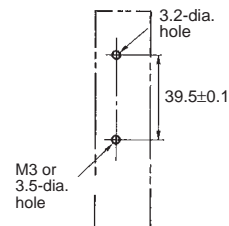
**Note:** Pin numbers in parentheses apply to DIN standard.

## P2RF-08-E
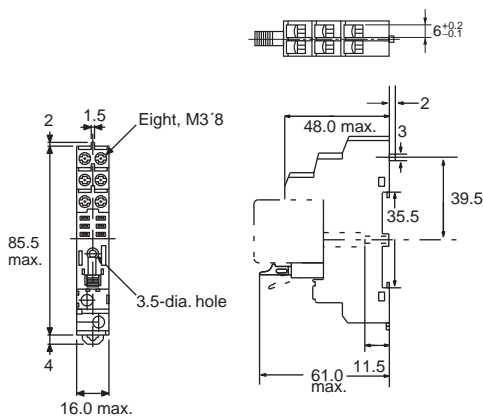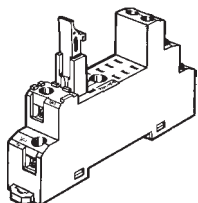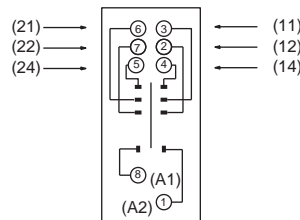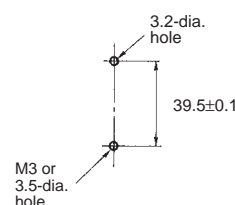
$6^{+0.2}_{-0.1}$

2

1.5

Eight, M3´8

85.5 max.

3.5-dia. hole

4

16.0 max.

48.0 max.

2

3

39.5

35.5

61.0 max.

11.5

**Terminal Arrangement (Top View)**
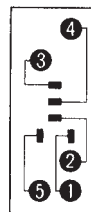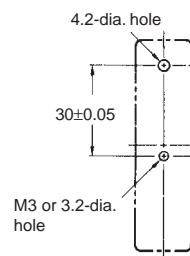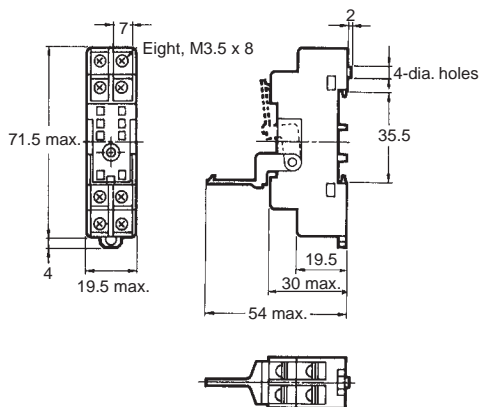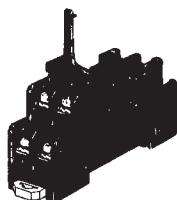
(21) → ⑥ ③ ← (11)

(22) → ⑦ ② ← (12)

(24) → ⑤ ④ ← (14)

⑧ (A1)

(A2) ①

**Mounting Holes (for Surface Mounting)**

3.2-dia. hole

39.5±0.1

M3 or 3.5-dia. hole

## P2RF-05

7

Five, M3.5 x 8

71.5 max.

4

19.5 max.

2

4-dia. holes

35.5

19.5

30 max.

54 max.

**Terminal Arrangement (Top View)**

④

③

②

⑤ ①

**Mounting Holes (for Surface Mounting)**

4.2-dia. hole

30±0.05

M3 or 3.2-dia. hole

## P2RF-08

7

Eight, M3.5 x 8

71.5 max.

4

19.5 max.

2

4-dia. holes

35.5

19.5

30 max.

54 max.

**Terminal Arrangement (Top View)**

⑥ ③

⑤ ④

⑦ ②

⑧ ①

**Mounting Holes (for Surface Mounting)**

4.2-dia. hole

30±0.05

M3 or 3.2-dia. hole
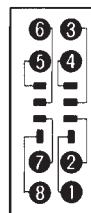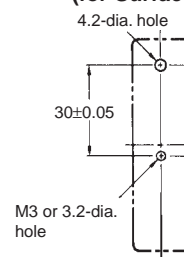
## Mounting Height of Relay with Track/Surface Mounting Sockets

**P2RF-05-PU**



G2R-□-S (S)
Relay

63.6

28.1

(3.9)

**P2RF-08-PU**



G2R-□-S (S)
Relay

63.6

28.1

(3.9)

**P2RF-□**



G2R-□-S (S)
Relay

P2RF
Socket

66.5   62.0

**P2RF-□-E**



G2R-□-S (S)
Relay

P2RF-□-E
Socket

67.0  70.5
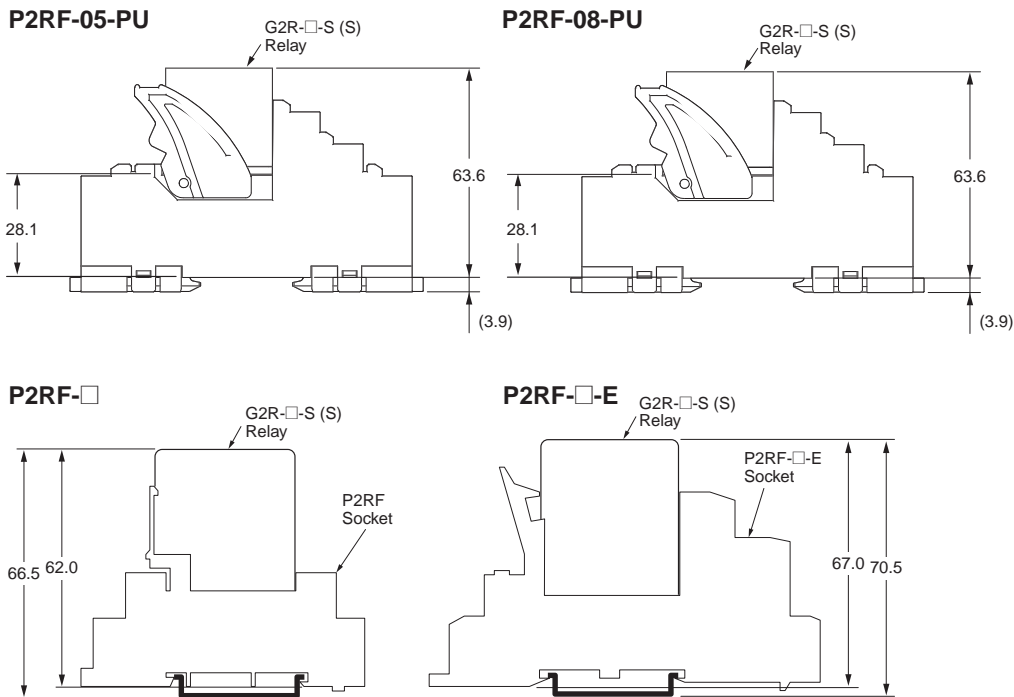
## Back-connecting Sockets

**P2R-05P (1-pole)**



14.5 max.

35.5 max.

36.5 max.

1  4  7
6
4.5
15
1.2
4
3.5
1.5
7  4

**Terminal Arrangement (Bottom View)**

❸
❹
❷
❶  ❺

**Mounting Holes**

Tolerance: ±0.1

4

Five, 1.6-dia. holes

6
4.5
15
4
(5)
7

**P2R-08P (2-pole)**



14.5 max.

35.5 max.

36.5 max.

4  7
0.3
5
5
20
1
2.8
1.5
7.5

Terminal plate thickness: 0.3

**Terminal Arrangement (Bottom View)**

❹  ❺
❸  ❻
❷  ❼
❶  ❽

**Mounting Holes**

7.5   Eight, 1.3-dia. holes

5
5
20
(4.3)

## P2R-05A (1-pole)

4.5
7.5
1.2
0.3
6.7
3.8
16.7
5
14.5 max.
35.5 max.

6

Five, 3 x 1.8-dia. holes

Terminal plate thickness: 0.3
36.5 max.

**Terminal Arrangement (Bottom View)**

3
4
2
1   5

**Panel Cutout**

13.6±0.1
30.5±0.2

## P2R-08A (2-pole)

6.5   7.5
1.2
0.3
5
5
20
2.6
2.8
1.5
14.5 max.
35.5 max.

Eight, 3 x 1.2-dia. holes

7.5

Terminal plate thickness: 0.3
36.5 max.

4   5
3   6
2   7
1   8

Recommended thickness of the panel is 1.6 to 2.0 mm

## P2R-057P (1-pole)
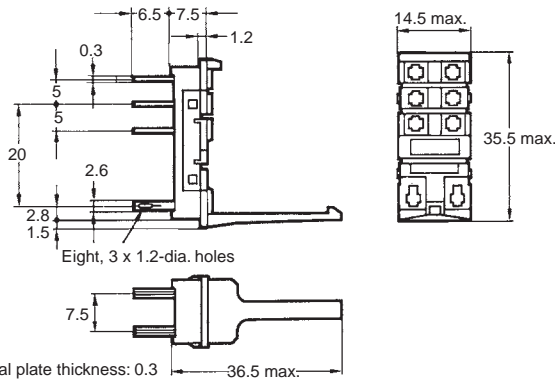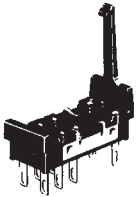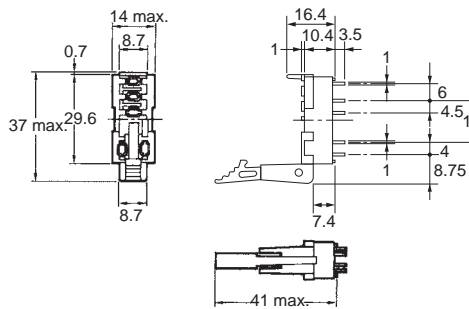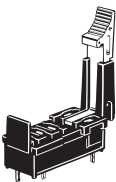
14 max.
0.7
8.7
37 max.
29.6
8.7

16.4
10.4   3.5
1
6
4.5
15
4
1
8.75
7.4
41 max.

**Terminal Arrangement (Bottom View)**

3
4
2
1
5

**Mounting Holes**

4±0.1
Five, 1.6-dia. holes
6±0.1
4.5±0.1   15±0.1
4±0.1
5
7±0.1

## P2R-087P (2-pole)

14 max.
7.5
37 max.   29.1
8.9

16.4
10.4   3.5
1
0.3
5
5
20
1
8.1
7.4
41 max.

**Terminal Arrangement (Bottom View)**

4   5
3   6
2   7
1   8

**Mounting Holes**

7.5
Eight, 1.3-dia. holes
5
5
20
(8.1)
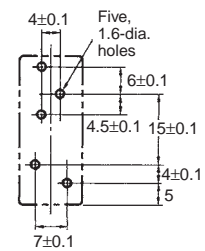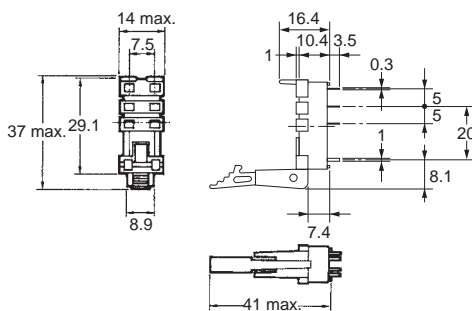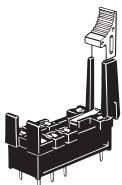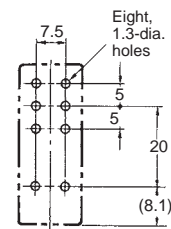
## Mounting Height of Relay with Back-connecting Sockets

### P2R-□P

44.5

G2R-□-S (S) Relay
P2R-□P Socket

### P2R-□A

38.0

G2R-□-S (S) Relay
P2R-□A Socket

### P2R-□7P

47.5

G2R-□-S (S) Relay
P2R-□7P Socket
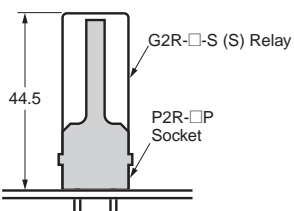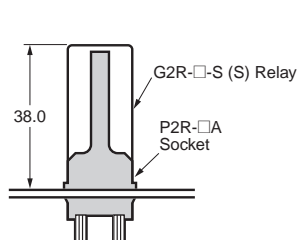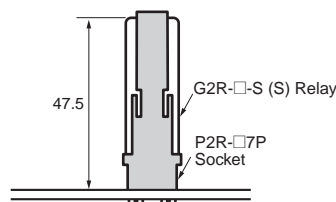
## Mounting Tracks

**PFP-100N, PFP-50N**
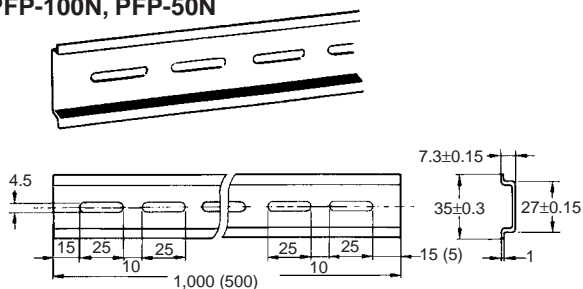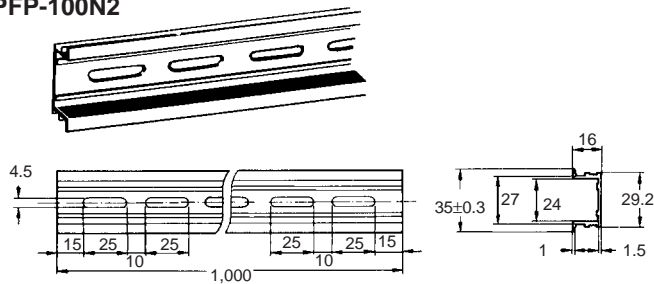


It is recommended to use a panel 1.6 to 2.0 mm thick.

**PFP-100N2**



## End Plate

**PFP-M**



M4 x 8 pan head screw
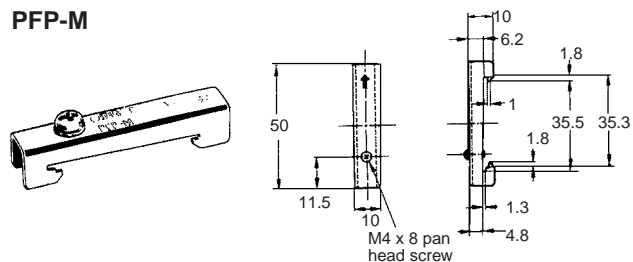
## Spacer

**PFP-S**
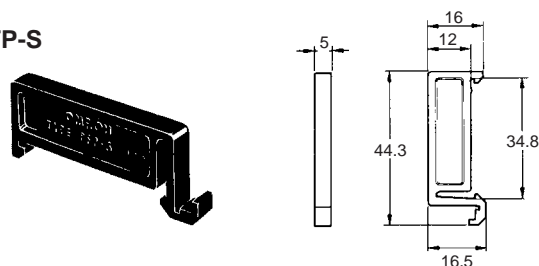


## Mounting Plate

**P2R-P**



Square hole

t=1.6 mm
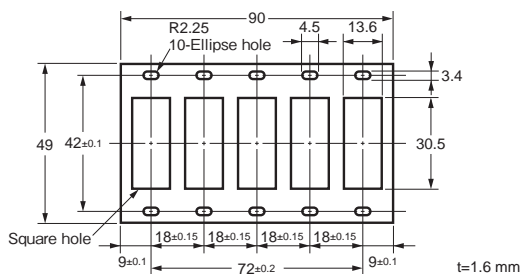
# Safety Precautions

Be sure to read the *Common Precautions for All Relay* in the website at the following URL:
http://www.ia.omron.com/.
Refer to *Products Related to Common Sockets and DIN Tracks* for precautions on the applicable Sockets.
Refer to *PYF-□□-PU/P2RF-□□-PU* for precautions on Push-In Plus Terminal Block Sockets.

## Warning Indications

| ⚠ CAUTION | Indicates a potentially hazardous situation which, if not avoided, may result in minor or moderate injury or in property damage. |
|---|---|

### ⚠ Cation

- Do not use the test button for any purpose other than testing. Be sure not to touch the test button accidentally as this will turn the contacts ON. Before using the test button, confirm that circuits, the load, and any other connected item will operate safely.
- Check that the test button is released before turning ON relay circuits.
- If the test button is pulled out too forcefully, it may bypass the momentary testing position and go straight into the locked position.
- Use an insulated tool when you operate the test button.

## Terms and Conditions Agreement

2016.4

**In the interest of product improvement, specifications are subject to change without notice.**

## OMRON Corporation
**Industrial Automation Company**

http://www.ia.omron.com/

Advanced Contact Technology

**Multi-Contact** MC
*STÄUBLI GROUP*

## MA231 (de_en)
## Montageanleitung

**PV-Kupplungsstecker PV-KST4/...-UR***
**PV-Kupplungsbuchse PV-KBT4/...-UR***

## MA231 (de_en)
## Assembly instructions

**PV male cable coupler PV-KST4/...-UR***
**PV female cable coupler PV-KBT4/...-UR***

### Inhalt

### Content

Kupplungsbuchse / Female cable coupler

**PV-KBT4/2.5.../PV-KBT4/6...**

Kupplungsstecker / Male cable coupler

**PV-KST4/2.5.../PV-KST4/6**

**PV-KBT4/8II-UR**

**Optional**
**PV-SSH4**
Sicherungshülse / Safety lock clip

**PV-KST4/8II-UR**

* UL file E343181                    (siehe / see www.multi-contact.com --> MA252)

### Technische Daten

### Technical data

| | | |
|---|---|---|
| Steckverbindersystem | Connector system | **Ø 4 mm** |
| TÜV-zertifiziert nach EN 50521 | TÜV certified according to EN 50521 | **Zertifikat / Certificate R 60028286** |
| UL-zertifiziert nach UL standard 6073 | UL certified according to UL standard 6703 | **Zertifikat / Certificate E343181** |
| Bemessungsspannung | Rated voltage | **1000 V DC (IEC)**<br>**1000 V DC (UL)**<br>**1500 V DC[1]** |
| Bemessungsstrom IEC (90°C) | Rated current IEC (90°C) | **17 A (1,5 mm²)**<br>**22,5 A(2,5 mm², 14 AWG)**<br>**30 A (4 mm², 6 mm², 10 AWG)**<br>**43 A (10 mm², 8 AWG)** |
| Bemessungsstrom IEC (85°C) | Rated current IEC (85°C) | **39 A (4 mm²)**<br>**45 A (6 mm²)** |
| Prüfspannung | Test voltage | **6 kV (50 Hz, 1 min.)** |
| Umgebungstemperaturbereich | Ambient temperature range | **-40 °C...+90 °C (IEC)**<br>**-40 °C...+75 °C (UL)**<br>**-40 °C...+70 °C (UL: 14 AWG)** |
| Obere Grenztemperatur | Upper limiting temperature | **105 °C (IEC)** |
| Schutzart, gesteckt<br>ungesteckt | Degree of protection, mated<br>unmated | **IP68 (1 m/1 h)**<br>**IP2X** |
| Überspannungskat./Verschmutzungsgrad | Overvoltage category/Pollution degree | **CATIII/3** |
| Kontaktwiderstand der Steckverbinder | Contact resistance of plug connectors | **0,35 mΩ** |
| Schutzklasse | Safety class | **II** |
| Kontaktwiderstand | Contact resistance | **0,35 mOhm** |

**[1]** 2PFG2330: Nur für Zugangsbeschränkte Standorte zugelassen / Only for use in PV-systems with restricted access locations

## Sicherheitshinweise

Die Montage und Installation der Produkte darf nur durch qualifiziertes und trainiertes Fachpersonal unter Berücksichtigung aller anwendbaren gesetzlichen Sicherheitsbestimmungen und Regelungen erfolgen.
Multi-Contact (MC) lehnt jegliche Haftung infolge Nichteinhaltung dieser Warnhinweise ab.

Benutzen Sie nur die von MC angegebenen Einzelteile und Werkzeuge. Weichen Sie nicht von den hier beschriebenen Vorgängen zur Vorbereitung und Montage ab, da sonst bei der Selbstkonfektionierung weder die Sicherheit noch die Einhaltung der technischen Daten gewährleistet ist. Ändern Sie das Produkt nicht in irgend einer Weise ab.

Nicht von MC hergestellte Steckverbindungen, die mit MC-Elementen steckbar sind und von den Herstellern manchmal auch als „MC-kompatibel" bezeichnet werden, entsprechen nicht den Anforderungen für eine sichere, langzeitstabile elektrische Verbindung und dürfen aus Sicherheitsgründen nicht mit MC-Elementen gesteckt weren. MC übernimmt daher keine Haftung, falls diese von MC nicht freigegebenen Steckverbindungen mit MC-Elementen gesteckt werden und deshalb Schäden entstehen.

⚡ **Die hier beschriebenen Arbeiten dürfen nicht an stromführenden oder unter Spannung stehenden Teilen durchgeführt werden.**

⚡ **Der Schutz vor einem elektrischen Schlag muss durch das Endprodukt gegeben sein und vom Anwender sichergestellt werden.**

⚡ **Die Steckverbindungen dürfen nicht unter Last getrennt werden. Das Stecken und Trennen unter Spannung ist zulässig.**

⚠ **Die Steckverbinder sind wasserdicht gemäss IP-Schutzart. Sie sind aber nicht geeignet für einen dauerhaften Gebrauch unter Wasser. Legen Sie die Steckverbinder nicht direkt auf die Dachhaut auf.**

⚠ **Nicht gesteckte Steckverbinder sind mit einer Verschlusskappe (MC4 Artikel Nr. 32.0716 für Buchsen und 32.0717 für Stecker) vor Feuchtigkeit und Schmutz zu schützen. Die Steckverbinder dürfen nicht im verschmutzten Zustand miteinander gesteckt werden.**

⚠ **Die Steckverbindung darf nie einer dauerhaft mechanischen Zugbelastung ausgesetzt sein. Das Kabel sollte mit Kabelbindern befestigt werden.**

⚠ **MC untersagt aus Sicherheitsgründen, weder PVC-Kabel noch unverzinnte Kabel vom Typ H07RN-F zu verwenden.**

ℹ **Weitere technische Daten entnehmen Sie bitte dem Produktkatalog.**

## Safety Instructions

The products may be assembled and installed only by suitably qualified and trained specialists with due observance of all applicable safety regulations.
Multi-Contact (MC) declines any liability in the event of failure to observe these warnings.

Use only the components and tools specified by MC. Do not deviate from the preparation and assembly procedures described here, since in this event, in the event of self-assembly, no guarantee can be given as to safety or conformity with the technical data. Do not modify the product in any way.

Connectors not made by MC which can be mated with MC elements and in some cases are also described as "MC-compatible" do not conform to the requirements for safe electrical connection with long-term stability, and for safety reasons must not be plugged together with MC elements. MC can therefore accept no liability for damage which occurs as a result of mating these connectors which lack MC approval with MC elements.

⚡ **The work described here must not be carried out on live or load-carrying parts.**

⚡ **Protection from electric shock must be assured by the end product and its user.**

⚡ **The plug connections must not be disconnected under load. Plugging and unplugging when live is permitted.**

⚠ **The plug connectors are watertight in accordance with IP protection class. However, they are not suitable for continuous operation under water. Do not place the plug connectors directly on the roof membrane.**

⚠ **Unmated plug connectors must be protected from moisture and dirt with a sealing cap (MC4 Article No. 32.0716 for sockets and 32.0717 for plugs). The male and female parts must not be plugged together when soiled.**

⚠ **The plug connection must not be subjected to continuous mechanical tension. The cable should be fixed with cable binders.**

⚠ **For safety reasons MC prohibits the use of either PVC cables or untinned cables of type H07RN-F.**

ℹ **For further technical data please see the product catalogue.**

---

## Erklärung der Symbole

⚡ **Warnung vor gefährlicher elektrischer Spannung**

⚠ **Warnung vor einer Gefahrenstelle**

ℹ **Nützlicher Hinweis oder Tipp**

## Explanation of the symbols

⚡ **Warning of dangerous voltages**

⚠ **Warning of a hazard area**

ℹ **Useful hint or tip**

## Erforderliches Werkzeug

**(ill. 1)**
Abisolierzange **PV-AZM...** inkl. ein-gebauten Abisolier-Messern sowie Sechskantschlüssel SW2,5.

Leiterquerschnitt: 1,5/2,5/4/6 mm²
Typ: **PV-AZM-1.5/6**
Bestell-Nr. **32.6029-156**

Leiterquerschnitt: 4/6/10 mm²
Typ: **PV-AZM-4/10**
Bestell-Nr. **32.6027-410**

**(ill. 2)**
Crimpzange **PV-CZM...** inkl. Locator und eingebautem Crimpeinsatz.

Crimpbereich:
1,5/2,5/4mm² (14/12 AWG)
Typ: **PV-CZM-18100**
Bestell-Nr. **32.6020-18100**

Crimpbereich:
2,5/4/6mm² (12/10 AWG)
Typ: **PV-CZM-19100**
Bestell-Nr. **32.6020-19100**

Crimpbereich: 4/10 mm² (12 AWG)
Typ: **PV-CZM-20100**
Bestell-Nr. **32.6020-20100**

Crimpbereich: 12/10/8 AWG
Typ: **PV-CZM-22100**
Bestell-Nr. **32.6020-22100**

**(ill. 3)**
**PV-MS** Montageschlüssel,
1 Set = 2 Stück
Bestell-Nr.: **32.6024**

**(ill. 4)**
**PV-WZ-AD/GWD** Steckschlüssel zum Anziehen
Bestell-Nr. **32.6006**

**(ill. 5)**
**PV-SSE-AD4** Steckschlüssel zum Kontern
Bestell-Nr. **32.6026**

**(ill. 6)**
**PV-PST** Prüfstift
Bestell-Nr. **32.6028**

## Tools required

**(ill. 1)**
Stripping pliers **PV-AZM...** incl. built-in blade as well as hexagonal screwdriver A/F 2,5mm.

Cable cross section: 1,5/2,5/4/6 mm²
Type: **PV-AZM-1.5/6**
Order No. **32.6029-156**

Cable cross section: 4/6/10 mm²
Type: **PV-AZM-4/10**
Order No. **32.6027-410**

**(ill. 2)**
Crimping pliers **PV-CZM...** incl. Locator and built-in crimping insert.

Crimping range:
1,5/2,5/4mm² (14/12 AWG)
Type: **PV-CZM-18100**
Order No. **32.6020-18100**

Crimping range:
2,5/4/6mm² (12/10 AWG)
Type: **PV-CZM-19100**
Order No. **32.6020-19100**

Crimping range: 4/10 mm² (12 AWG)
Type: **PV-CZM-20100**
Order No. **32.6020-20100**

Crimping range: 12/10/8 AWG
Typ: **PV-CZM-22100**
Bestell-Nr. **32.6020-22100**

**(ill. 3)**
Open-end spanner **PV-MS**,
1 Set = 2 pieces
Order No.: **32.6024**

**(ill. 4)**
**PV-WZ-AD/GWD** socket wrench insert to tighten
Order No. **32.6006**

**(ill. 5)**
**PV-SSE-AD4** socket wrench insert to secure
Order No. **32.6026**

**(ill. 6)**
Test plug **PV-PST**
Order No. **32.6028**

**(ill. 7)**
SW15 Gabelschlüssel

**(ill. 7)**
Open-end spanner A/F 15 mm



**(ill. 8)**
SW12 Drehmomentschlüssel

**(ill. 8)**
Torque screwdriver A/F 12 mm

## Vorbereitung der Leitung

## Cable preparation

Anschlussleitungen mit einem Litzen-aufbau der Klassen 5 und 6 können angeschlossen werden.

Cables with a strand construction of classes 5 and 6 can be connected.

> ⚠ **Achtung:**
> Verwenden Sie keine blanken oder bereits oxidierten Leiter. Verzinnte Leiter sind vorteilhaft. Sämtliche Solarkabel von MC haben hochwertige, verzinnte Leiter.

> ⚠ **Attention:**
> Use no uncoated or already oxidised conductors. It is recommended to use tinned conductors. All MC solar cables have high-quality, tinned conductors.



**(ill. 9, Tab. 1)**
Kontrollieren Sie die Masse A und b gemäss Illustration 9 und Tabelle 1.

**(ill. 9, Tab. 1)**
Check dimensions A and b in accordance with illustration 9 and table 1.

**Tab. 1**

| b: Kontrollmass b:Control dimension | Leiterquerschnitt Conductor cross section | | | A: Ø-Bereich Leitung mm A: Ø range of the cable mm | | |
|---|---|---|---|---|---|---|
| | | For termination to USE-2, 600 V wire | For termination to UL4703 PV wire, 600 V or 1000 V | | | For termination to UL4703PV wire, 600V or 1000V |
| | | | | 3 – 6 | 5,5 – 9 | 6,7 – 8,9 |
| mm | mm² (stranding) | AWG (stranding) | AWG (stranding) | Typ/Type | | |
| ~ 3 | 1,5 – 2,5 (klassen/class 5 or 6) | 14 (19 to 37) | 14 (19 to 49) | PV-K...T4/2,5I | | PV-K...T4/2,5II |
| ~ 5 | 4 – 6 (klassen/class 5 or 6) | 12, 10 (19 to 37) | 12, 10 (19 to 56) | PV-K...T4/6I | | PV-K...T4/6II |
| ~ 7,2 | 10 (klassen/class 5 or 6) | | | | PV-K...T4/10II | |
| ~ 4,4 | | 8 (7 to 164) | 8 (7 to 164) | | | PV-K...T4/8II |



**(ill. 10)**
Kontrollieren Sie die Masse L gemäss Illustration 10 und Tabelle 2.

**(ill. 10)**
Check dimensions L accordance with illustration 10 and table 2.

**Tab. 2**

| Typ/Type | Masse/Lengh "L" |
|---|---|
| PV-K...T4/2,5I | 6 – 7,5 mm |
| PV-K...T4/6I | 6 – 7,5 mm |
| PV-K...T4/10II | 6 – 7,5 mm |
| PV-K...T4/8II | 8,5 – 10 mm |

> ⚠ **Achtung:**
> Schneiden Sie beim Abisolieren keine Einzeldrähte ab!

> ⚠ **Attention:**
> Do not cut individual strands at stripping

> ℹ *Hinweis:*
> *Die Bedienung der Abisolierzange PV-AZM... sowie das Auswechseln von Messersätzen entnehmen Sie bitte der Bedienungsanleitung MA267 auf www.multi-contact.com*

> ℹ *Note:*
> *For directions on the operation of stripping pliers PV-AZM... and changing blade sets, see operating instruction MA267 at www.multi-contact.com*
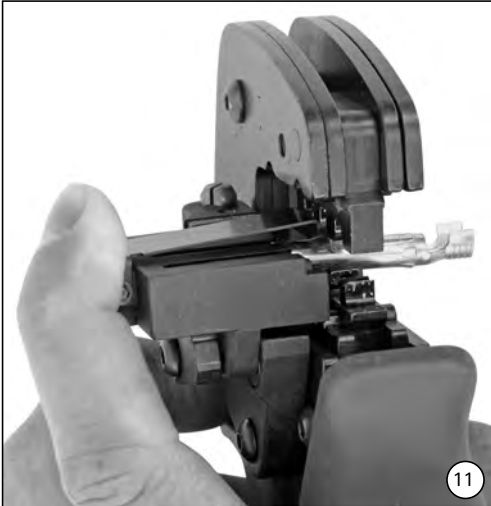
## Crimpen

**(ill. 11)**
Öffnen Sie den Klemmbügel (K) und halten Sie ihn fest. Legen Sie den Kontakt in den passenden Querschnittsbereich. Drehen Sie die Crimplaschen nach oben. Lassen Sie den Klemmbügel (K) los. Der Kontakt ist fixiert.

## Crimping

**(ill. 11)**
Open the clamp (K) and hold. Place the contact in the appropriate cross-section range.
Turn the crimp lugs upwards. Release the clamp (K). The contact is fixed.
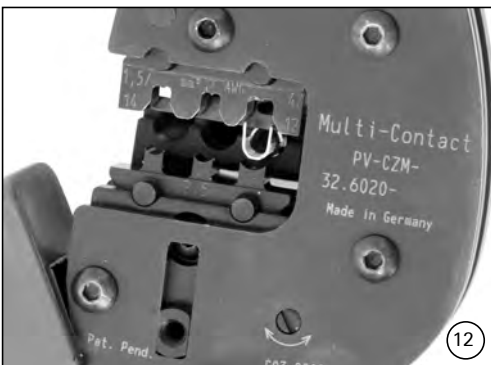


**(ill. 12)**
Drücken Sie die Zange leicht zusammen, bis die Crimplaschen sicher innerhalb der Crimp-Matritze liegen.

**(ill. 12)**
Press the pliers gently together until the crimp lugs are properly located within the crimping die.
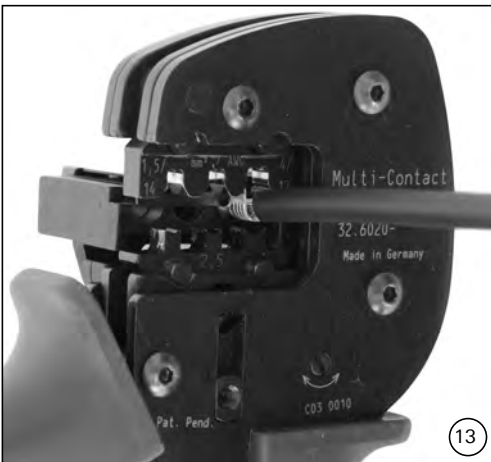


**(ill. 13)**
Führen Sie das abisolierte Kabel ein, bis die Isolation am Crimp-Einsatz anschlägt. Schliessen Sie die Crimpzange ganz.

**(ill. 13)**
Insert the stripped cable end until the insulation comes up against the crimp insert. Completely close the crimping pliers.



**(ill. 14)**
Kontrollieren Sie die Vercrimpung visuell.

> **Hinweis:**
> *Die Handhabung der Crimpzange entnehmen Sie bitte der Bedienungsanleitung MA251 auf www.multi-contact.com*

**(ill. 14)**
Visually check the crimp.

> **Note:**
> *For directions on the operation of the crimping tool, please see operating instructions MA251 at www.multi-contact.com*



## Montage-Prüfung

**(ill. 15)**
Führen Sie den angecrimpten Kontakt von hinten in die Stecker- bzw. Buchsenisolation ein bis zum Einrasten. Prüfen Sie durch leichtes Ziehen an der Leitung, ob das Metallteil richtig eingerastet ist.

## Assembly check

**(ill. 15)**
Insert the crimped-on contact into the insulator of the male or female coupler until it clicks into place. Pull gently on the lead to check that the metal part is correctly engaged.

**(ill. 16)**
Stecken Sie den Prüfstift mit der entsprechenden Seite in die Buchse bzw. in den Stecker bis zum Anschlag. Bei richtig montiertem Kontakt muss die weisse Markierung am Prüfstift noch sichtbar sein.

Die Kräfte dürfen keine sichtbare Verformung im Dichtbereich der Isolation aufweisen.
Beachten Sie die Spezifikationen des Leitungsherstellers betreffend Biegeradius.

**(ill. 16)**
Insert the appropriate end of the test pin into the male or female coupler as far as it will go. If the contact is correctly located, the white mark on the test pin must still be visible.

The forces must not create a visible deformation in the sealing portion of the insulation.
Refer to cable manufacturers specification for minimum bending radius.
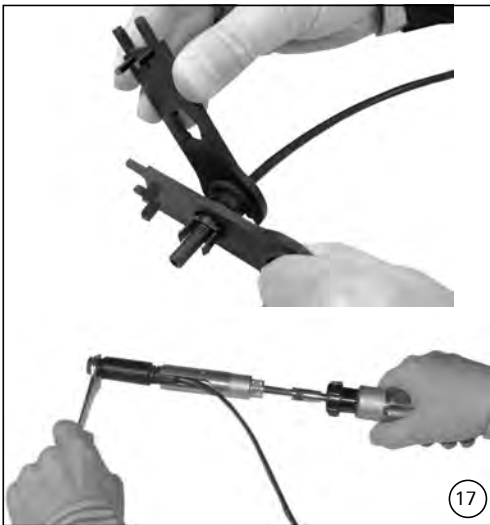
**(ill. 17)**
Ziehen Sie die Leitungsverschraubung mit den Werkzeugen **PV-MS** handfest an

oder

ziehen Sie die Leitungsverschraubung mit den Werkzeugen
**PV-WZ-AD/GWD** und **PV-SSE-AD4** an.

**In beiden Fällen gilt:**
Das Anzugsdrehmoment muss auf die konkret verwendeten Solarleitungen abgestimmt werden. Typische Werte liegen im Bereich von 2,5 Nm bis 3 Nm.

**(ill. 17)**
Screw up the cable gland hand-tight with the tools **PV-MS**

or

tighten the cable gland with the tools **PV-WZ-AD/GWD** and **PV-SSE-AD4**.

**In both cases:**
The tightening torque must be appropriate for the solar cables used. Typical values are between 2,5 Nm and 3 Nm.

### Stecken und Trennen der Kabelkupplung ohne Sicherungshülse PV-SSH4

**Stecken**
**(ill. 18)**
Stecken Sie die Kabelkupplung zusammen bis zum Einrasten. Kontrollieren Sie das korrekte Einrasten durch Ziehen an der Kabelkupplung.

### Plugging and unplugging the cable coupler without safety lock clip PV-SSH4

**Plugging**
**(ill. 18)**
Plug the parts of the cable coupler together until they click in place. Check that they have engaged properly by pulling on the cable coupler.
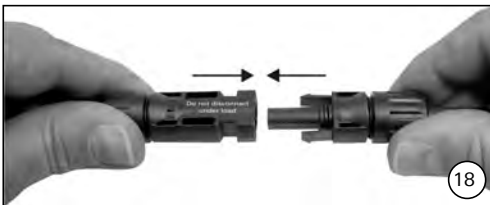
**Trennen**
**(ill. 19)**
Zum Trennen der Kontakte drücken Sie die Einrastlaschen (X) entweder von Hand oder mit dem Werkzeug PV-MS zusammen und ziehen Sie die Kabelkupplung auseinander.

**Unplugging**
**(ill. 19)**
To disconnect the contacts, press the latches (X) together either by hand or with the tool PV-MS and pull the halves of the cable coupler apaart.

PV-SSH4



20
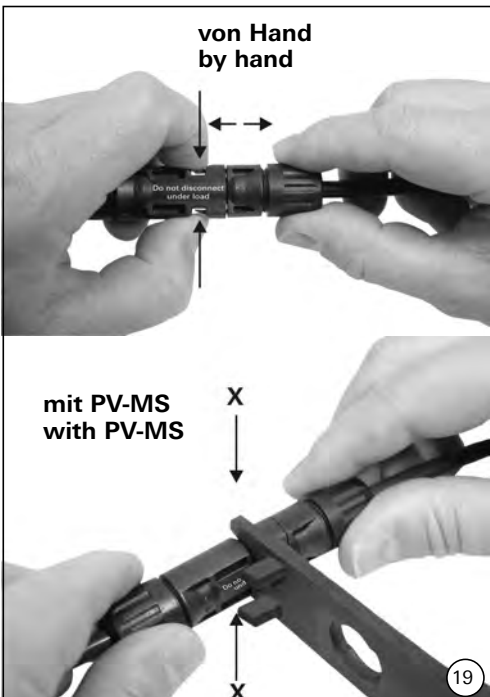
**Stecken**

**(ill. 20)**

Stecken Sie die Kabelkupplung zusammen bis zum Einrasten. Kontrollieren Sie das korrekte Einrasten durch Ziehen an der Kabelkupplung.

**Trennen**

Die Kabelkupplung kann nur noch mit dem Werkzeug PV-MS getrennt werden. Drücken Sie die Einrastlaschen (X) mit dem Werkzeug PV-MS zusammen und ziehen Sie die Kabelkupplung auseinander.

**Leitungsführung**

Die Kräfte dürfen keine sichtbare Verformung im Dichtbereich der Isolation aufweisen.
Beachten Sie die Spezifikationen des Leitungsherstellers betreffend Biegeradius.

**Plugging**

**(ill. 20)**

Plug the parts of the cable coupler together until they click in place. Check that they have engaged properly by pulling on the cable coupler.

**Unplugging**

The cable coupler can be disconnected only with the tool PV-MS. Press the latches (X) together with the tool PV-MS and pull the halves of the coupler apart.

**Cable routing**

The forces must not create a visible deformation in the sealing portion of the insulation.
Refer to cable manufacturers specification for minimum bending radius.



20mm

20mm

**Notizen / Notes:**

**Pb** **RoHS COMPLIANCE**
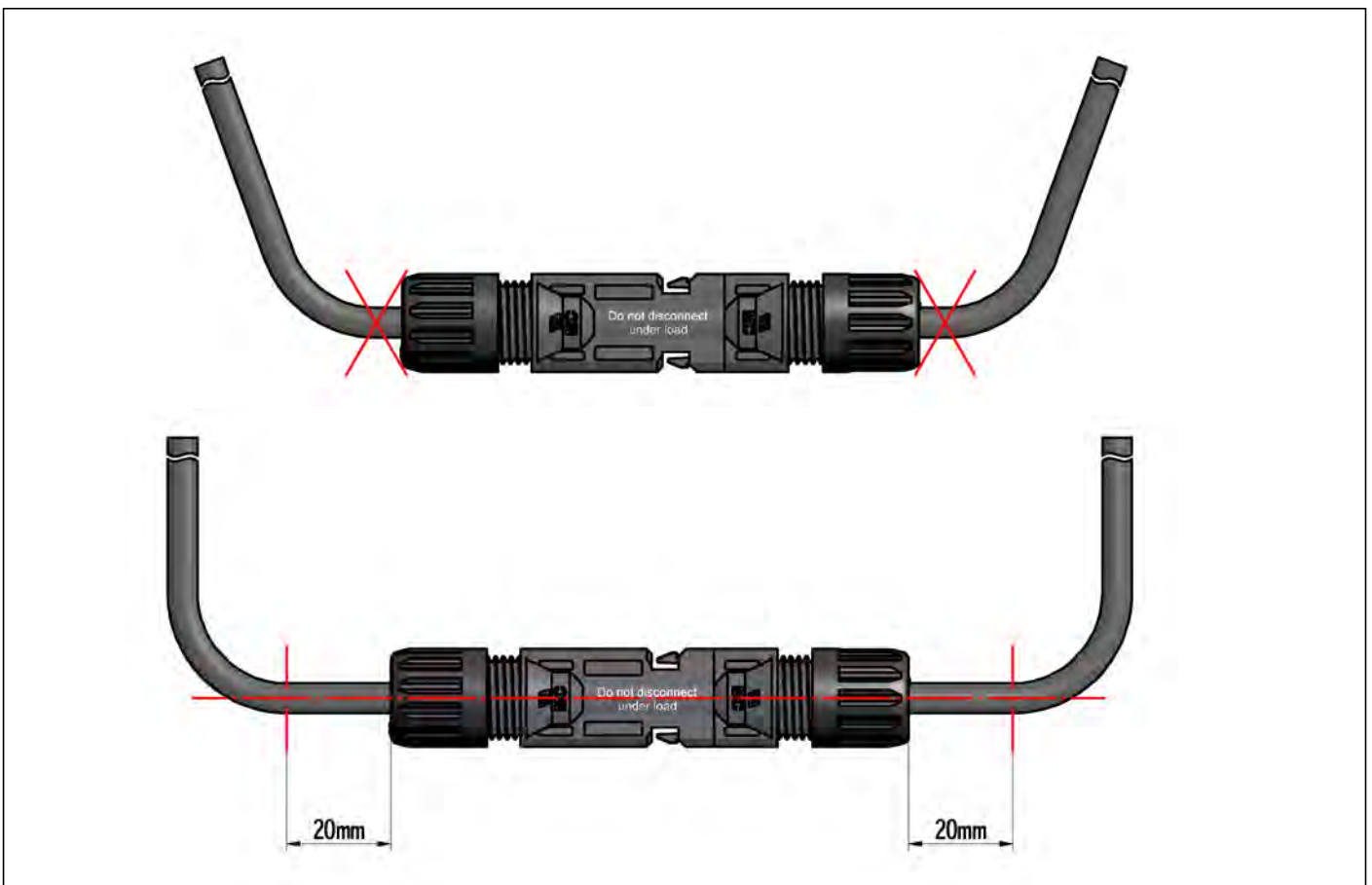
# MBR3035PT - MBR30150PT

## 30.0 AMPS. Schottky Barrier Rectifiers

### TO-3P/TO-247AD

## Features

✧ Plastic material used carries Underwriters Laboratory Classifications 94V-0
✧ Metal silicon junction, majority carrier conduction
✧ Low power loss, high efficiency
✧ High current capability, low forward voltage drop
✧ High surge capability
✧ For use in low voltage, high frequency inverters, free wheeling, and polarity protection applications
✧ Guardring for overvoltage protection
✧ High temperature soldering guaranteed: 260°C/10 seconds,0.17"(4.3mm)from case
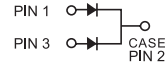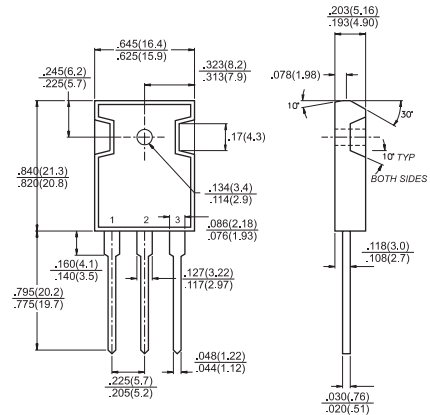
## Mechanical Data

✧ Cases: JEDEC TO-3P/TO-247AD molded plastic body
✧ Terminals: Pure tin plated, lead free. solderable per MIL-STD-750, Method 2026
✧ Polarity: As marked
✧ Mounting position: Any
✧ Mounting torque: 10 in. - lbs. max
✧ Weight: 0.2 ounce, 5.6 grams

PIN 1
PIN 3
CASE PIN 2

**Dimensions in inches and (millimeters)**

## Maximum Ratings and Electrical Characteristics

Rating at °C ambient temperature unless otherwise specified.
Single phase, half wave, 60 Hz, resistive or inductive load.
For capacitive load, derate current by 20%

| Type Number | Symbol | MBR 3035 PT | MBR 3045 PT | MBR 3050 PT | MBR 3060 PT | MBR 3090 PT | MBR 30100 PT | MBR 30150 PT | Units |
|---|---|---|---|---|---|---|---|---|---|
| Maximum Recurrent Peak Reverse Voltage | $V_{RRM}$ | 35 | 45 | 50 | 60 | 90 | 100 | 150 | V |
| Maximum RMS Voltage | $V_{RMS}$ | 24 | 31 | 35 | 42 | 63 | 70 | 105 | V |
| Maximum DC Blocking Voltage | $V_{DC}$ | 35 | 45 | 50 | 60 | 90 | 100 | 150 | V |
| Maximum Average Forward Rectified Current (SEE F1G. 1) | $I_{(AV)}$ | 30 | | | | | | | A |
| Peak Repetitive Forward Current (Rated $V_R$, Square Wave, 20KHz) at Tc=105°C | $I_{FRM}$ | 30 | | | | | | | A |
| Peak Forward Surge Current, 8.3 ms Single Half Sine-wave Superimposed on Rated Load (JEDEC method ) | $I_{FSM}$ | 200 | | | | | | | A |
| Peak Repetitive Reverse Surge Current (Note 2) | $I_{RRM}$ | 2.0 | | | 1.0 | | | | A |
| Maximum Instantaneous Forward Voltage at (Note 1) $I_F$=15A, Tc=25°C $I_F$=15A, Tc=125°C $I_F$=30A, Tc=25°C $I_F$=30A, Tc=125°C | $V_F$ | — 0.60 0.82 0.72 | | 0.75 0.65 — — | | 0.85 0.75 — — | | 0.95 0.92 1.02 0.98 | V |
| Maximum Instantaneous Reverse Current @ Tc=25 °C at Rated DC Blocking Voltage Per Leg(Note 2) @ Tc=125 °C | $I_R$ | 1.0 | | | | 0.5 | | | mA |
| | | 20 | | 15 | | 10 | | | mA |
| Voltage Rate of Change at (Rated $V_R$) | dV/dt | 10,000 | | 1,000 | | | | | V/uS |
| Maximum Thermal Resistance Per Leg(Note 3) | $R_{\theta JC}$ | 1.4 | | | | | | | °C/W |
| Operating Junction Temperature Range | $T_J$ | -65 to +150 | | | | | | | °C |
| Storage Temperature Range | $T_{STG}$ | -65 to +175 | | | | | | | °C |

Notes:  1. 2.0us Pulse Width, f=1.0 KHz
2. Pulse Test: 300us Pulse Width, 1% Duty Cycle
3. Thermal Resistance from Junction to case Per Leg

Version: A06

# RATINGS AND CHARACTERISTIC CURVES (MBR3035PT THRU MBR30150PT)

### FIG.1- FORWARD CURRENT DERATING CURVE

RESISTIVE OR INDUCTIVE LOAD

MBR3035PT-MBR3045PT
MBR3050PT-MBR30150PT

AVERAGE FORWARD CURRENT. (A)
CASE TEMPERATURE. ($^{\circ}$C)
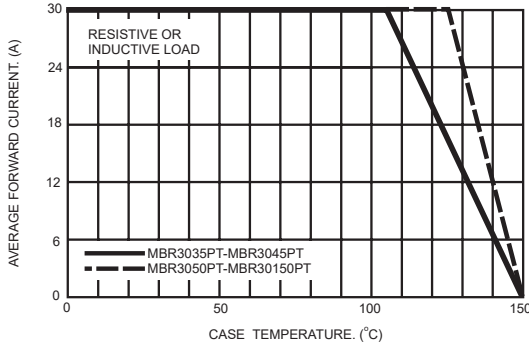
### FIG.2- MAXIMUM NON-REPETITIVE FORWARD SURGE CURRENT PER LEG

Tj=Tj max.
8.3ms Single Half Sine Wave
JEDEC Method

PEAK FORWARD SURGE CURRENT. (A)
NUMBER OF CYCLES AT 60Hz
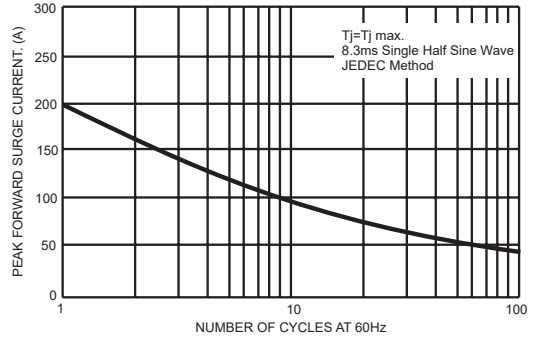
### FIG.3- TYPICAL INSTANTANEOUS FORWARD CHARACTERISTICS PER LEG

Tj=150$^{\circ}$C

Pulse Width=300$\mu$s
1% Duty Cycle

Tj=25$^{\circ}$C

MBR3035PT-MBR3045PT
MBR3050PT & MBR3060PT
MBR3090PT-MBR30150PT

INSTANTANEOUS FORWARD CURRENT. (A)
FORWARD VOLTAGE. (V)
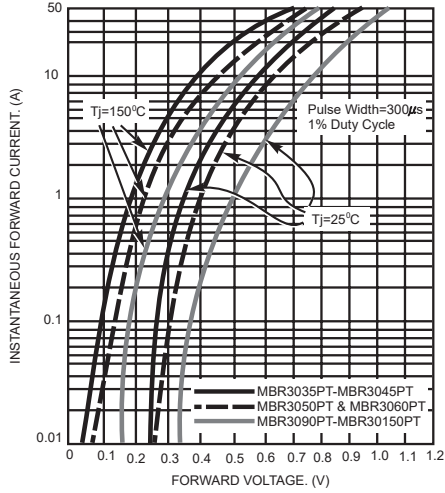
### FIG.4- TYPICAL REVERSE CHARACTERISTICS PER LEG

Tj=125$^{\circ}$C

Tj=25$^{\circ}$C

MBR3035PT-MBR3045PT
MBR3050PT-MBR30150PT

INSTANTANEOUS REVERSE CURRENT. (mA)
PERCENT OF RATED PEAK REVERSE VOLTAGE. (%)
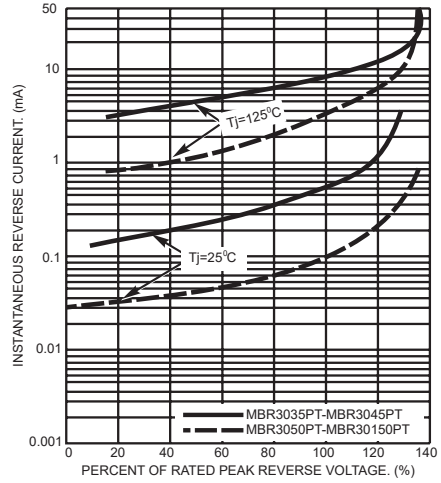
### FIG.5- TYPICAL JUNCTION CAPACITANCE PER LEG

Tj=25$^{\circ}$C
f=1.0MHz
Vsig=50mVp-p

MBR3035PT-MBR3045PT
MBR3050PT & MBR3060PT
MBR3090PT-MBR30150PT

JUNCTION CAPACITANCE. (pF)
REVERSE VOLTAGE. (V)
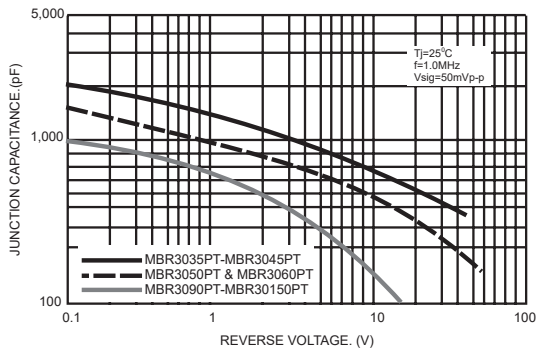
### FIG.6- TYPICAL TRANSIENT THERMAL IMPEDANCE PER LEG

TRANSIENT THERMAL IMPEDANCE. ($^{\circ}$C/W)
T, PULSE DURATION. (sec)

Version: A06

# DATASHEET - DILM7-10(230V50HZ,240V60HZ)
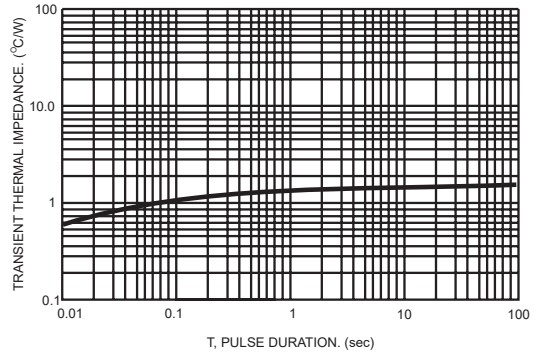
Contactor, 3 pole, 380 V 400 V 3 kW, 1 N/O, 230 V 50 Hz, 240 V 60 Hz, AC operation, Screw terminals

**EAT·N**
Powering Business Worldwide™
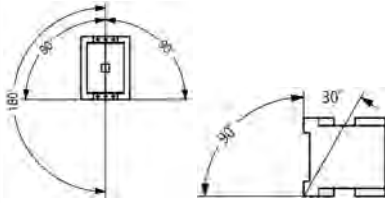
| | |
|---|---|
| **Part no.** | DILM7-10(230V50HZ,240V60HZ) |
| **Catalog No.** | 276550 |
| **Alternate Catalog No.** | XTCE007B10F |
| **EL-Nummer (Norway)** | 4130261 |

## Delivery program

| Product range | | Contactors |
|---|---|---|
| Application | | Contactors for Motors |
| Subrange | | Contactors up to 170 A, 3 pole |
| Utilization category | | AC-1: Non-inductive or slightly inductive loads, resistance furnaces<br>NAC-3: Normal AC induction motors: starting, switch off during running<br>AC-4: Normal AC induction motors: starting, plugging, reversing, inching |
| | | **IE3** ✓ |
| Notes | | Also suitable for motors with efficiency class IE3.<br>IE3-ready devices are identified by the logo on their packaging. |
| Connection technique | | Screw terminals |
| Number of poles | | 3 pole |

## Rated operational current

| | | | |
|---|---|---|---|
| AC-3 | | | |
|   Notes | | | At maximum permissible ambient temperature (open.) |
|   380 V 400 V | $I_e$ | A | 7 |
| AC-1 | | | |
|   Conventional free air thermal current, 3 pole, 50 - 60 Hz | | | |
|     Open | | | |
|       at 40 °C | $I_{th} = I_e$ | A | 22 |
|       enclosed | $I_{th}$ | A | 18 |
|   Conventional free air thermal current, 1 pole | | | |
|     open | $I_{th}$ | A | 50 |
|     enclosed | $I_{th}$ | A | 45 |

## Max. rating for three-phase motors, 50 - 60 Hz

| | | | |
|---|---|---|---|
| AC-3 | | | |
|   220 V 230 V | P | kW | 2.2 |
|   380 V 400 V | P | kW | 3 |
|   660 V 690 V | P | kW | 3.5 |
| AC-4 | | | |
|   220 V 230 V | P | kW | 1 |
|   380 V 400 V | P | kW | 2.2 |
|   660 V 690 V | P | kW | 2.9 |

## Contacts

| | |
|---|---|
| N/O = Normally open | 1 N/O |
| Contact sequence |  |
| **Instructions** | Contacts to EN 50 012. |
| Can be combined with auxiliary contact | DILM32-XHI..<br>DILA-XHI(V).. |
| Actuating voltage | 230 V 50 Hz, 240 V 60 Hz |
| Voltage AC/DC | AC operation |
| Connection to SmartWire-DT | no |

# Technical data

## General

| | | | |
|---|---|---|---|
| Standards | | | IEC/EN 60947, VDE 0660, UL, CSA |
| Lifespan, mechanical | | | |
| AC operated | Operations | x 10$^6$ | 10 |
| Operating frequency, mechanical | | | |
| AC operated | Operations/h | | 9000 |
| Climatic proofing | | | Damp heat, constant, to IEC 60068-2-78<br>Damp heat, cyclic, to IEC 60068-2-30 |
| Ambient temperature | | | |
| Open | | °C | -25 - +60 |
| Enclosed | | °C | - 25 - 40 |
| Storage | | °C | - 40 - 80 |
| Mounting position | | |  |
| Mechanical shock resistance (IEC/EN 60068-2-27) | | | |
| Half-sinusoidal shock, 10 ms | | | |
| Main contacts | | | |
| N/O contact | | g | 10 |
| Auxiliary contacts | | | |
| N/O contact | | g | 7 |
| N/C contact | | g | 5 |
| Mechanical shock resistance (IEC/EN 60068-2-27) when tabletop-mounted | | | |
| Half-sinusoidal shock, 10 ms | | | |
| Main contacts | | | |
| N/O contact | | g | 5.7 |
| Auxiliary contacts | | | |
| N/O contact | | g | 3.4 |
| N/C contact | | g | 3.4 |
| Degree of Protection | | | IP20 |
| Protection against direct contact when actuated from front (EN 50274) | | | Finger and back-of-hand proof |
| Altitude | | m | Max. 2000 |
| Weight | | | |
| AC operated | | kg | 0.24 |
| Screw connector terminals | | | |
| Terminal capacity main cable | | | |
| Solid | | mm$^2$ | 1 x (0.75 - 4)<br>2 x (0.75 - 2.5) |
| Flexible with ferrule | | mm$^2$ | 1 x (0.75 - 2.5)<br>2 x (0.75 - 2,5) |
| Solid or stranded | | AWG | single 18 - 10, double 18 - 14 |
| Stripping length | | mm | 10 |
| Terminal screw | | | M3.5 |
| Tightening torque | | Nm | 1.2 |
| Tool | | | |
| Pozidriv screwdriver | | Size | 2 |
| Standard screwdriver | | mm | 0.8 x 5.5<br>1 x 6 |
| Terminal capacity control circuit cables | | | |
| Solid | | mm$^2$ | 1 x (0.75 - 4)<br>2 x (0.75 - 2.5) |
| Flexible with ferrule | | mm$^2$ | 1 x (0.75 - 2.5)<br>2 x (0.75 - 2.5) |
| Solid or stranded | | AWG | 18 - 14 |

| | | | |
|---|---|---|---|
| Stripping length | | mm | 10 |
| Terminal screw | | | M3.5 |
| Tightening torque | | Nm | 1.2 |
| Tool | | | |
| Pozidriv screwdriver | | Size | 2 |
| Standard screwdriver | | mm | 0.8 x 5.5<br>1 x 6 |

## Main conducting paths

| | | | |
|---|---|---|---|
| Rated impulse withstand voltage | $U_{imp}$ | V AC | 8000 |
| Overvoltage category/pollution degree | | | III/3 |
| Rated insulation voltage | $U_i$ | V AC | 690 |
| Rated operational voltage | $U_e$ | V AC | 690 |
| Safe isolation to EN 61140 | | | |
| between coil and contacts | | V AC | 400 |
| between the contacts | | V AC | 400 |
| Making capacity (p.f. to IEC/EN 60947) | | | |
| | Up to 690 V | A | 112 |
| Breaking capacity | | | |
| 220 V 230 V | | A | 70 |
| 380 V 400 V | | A | 70 |
| 500 V | | A | 50 |
| 660 V 690 V | | A | 40 |
| Short-circuit rating | | | |
| Short-circuit protection maximum fuse | | | |
| Type "2" coordination | | | |
| 400 V | gG/gL 500 V | A | 20 |
| 690 V | gG/gL 690 V | A | 16 |
| Type "1" coordination | | | |
| 400 V | gG/gL 500 V | A | 35 |
| 690 V | gG/gL 690 V | A | 20 |

## AC

| | | | |
|---|---|---|---|
| AC-1 | | | |
| Rated operational current | | | |
| Conventional free air thermal current, 3 pole, 50 - 60 Hz | | | |
| Open | | | |
| at 40 °C | $I_{th} = I_e$ | A | 22 |
| at 50 °C | $I_{th} = I_e$ | A | 21 |
| at 55 °C | $I_{th} = I_e$ | A | 21 |
| at 60 °C | $I_{th} = I_e$ | A | 20 |
| enclosed | $I_{th}$ | A | 18 |
| Conventional free air thermal current, 1 pole | | | |
| open | $I_{th}$ | A | 50 |
| enclosed | $I_{th}$ | A | 45 |
| AC-3 | | | |
| Rated operational current | | | |
| Open, 3-pole: 50 – 60 Hz | | | |
| Notes | | | At maximum permissible ambient temperature (open.) |
| 220 V 230 V | $I_e$ | A | 7 |
| 240 V | $I_e$ | A | 7 |
| 380 V 400 V | $I_e$ | A | 7 |
| 415 V | $I_e$ | A | 7 |
| 440V | $I_e$ | A | 7 |
| 500 V | $I_e$ | A | 5 |
| 660 V 690 V | $I_e$ | A | 4 |
| 380 V 400 V | $I_e$ | A | 7 |

| | | | |
|---|---|---|---|
| Motor rating | P | kWh | |
| 220 V 230 V | P | kW | 2.2 |
| 240V | P | kW | 2.2 |
| 380 V 400 V | P | kW | 3 |
| 415 V | P | kW | 4 |
| 440 V | P | kW | 4.5 |
| 500 V | P | kW | 3.5 |
| 660 V 690 V | P | kW | 3.5 |
| **AC-4** | | | |
| Open, 3-pole: 50 – 60 Hz | | | |
| 220 V 230 V | $I_e$ | A | 5 |
| 240 V | $I_e$ | A | 5 |
| 380 V 400 V | $I_e$ | A | 5 |
| 415 V | $I_e$ | A | 5 |
| 440 V | $I_e$ | A | 5 |
| 500 V | $I_e$ | A | 4.5 |
| 660 V 690 V | $I_e$ | A | 4 |
| Motor rating | P | kWh | |
| 220 V 230 V | P | kW | 1 |
| 240 V | P | kW | 1.5 |
| 380 V 400 V | P | kW | 2.2 |
| 415 V | P | kW | 2.3 |
| 440 V | P | kW | 2.4 |
| 500 V | P | kW | 2.5 |
| 660 V 690 V | P | kW | 2.9 |

## DC

| | | | |
|---|---|---|---|
| Rated operational current, open | | | |
| DC-1 | | | |
| 60 V | $I_e$ | A | 20 |
| 110 V | $I_e$ | A | 20 |
| 220 V | $I_e$ | A | 15 |

## Current heat loss

| | | | |
|---|---|---|---|
| 3 pole, at $I_{th}$ (60°) | | W | 2.4 |
| Current heat loss at $I_e$ to AC-3/400 V | | W | 0.3 |
| Impedance per pole | | mΩ | 2.5 |

## Magnet systems

| | | | |
|---|---|---|---|
| Voltage tolerance | | | |
| AC operated | Pick-up | x $U_c$ | 0.8 - 1.1 |
| Drop-out voltage AC operated | Drop-out | x $U_c$ | 0.3 - 0.6 |
| Power consumption of the coil in a cold state and 1.0 x $U_S$ | | | |
| 50 Hz | Pick-up | VA | 24 |
| 50 Hz | Sealing | VA | 3.4 |
| 50 Hz | Sealing | W | 1.4 |
| 60 Hz | Pick-up | VA | 30 |
| 60 Hz | Sealing | VA | 4.4 |
| 60 Hz | Sealing | W | 1.4 |
| Duty factor | | % DF | 100 |
| Changeover time at 100 % $U_S$ (recommended value) | | | |
| Main contacts | | | |
| AC operated | | | |
| Closing delay | | ms | 15 - 21 |
| Opening delay | | ms | 9 - 18 |
| Arcing time | | ms | 10 |

## Electromagnetic compatibility (EMC)

| | | | |
|---|---|---|---|
| Emitted interference | | | to EN 60947-1 |

| Interference immunity | | | to EN 60947-1 |
|---|---|---|---|

**Rating data for approved types**

| Switching capacity | | | |
|---|---|---|---|
| Maximum motor rating | | | |
| Three-phase | | | |
| 200 V 208 V | | HP | 1.5 |
| 230 V 240 V | | HP | 2 |
| 460 V 480 V | | HP | 3 |
| 575 V 600 V | | HP | 5 |
| Single-phase | | | |
| 115 V 120 V | | HP | 0.25 |
| 230 V 240 V | | HP | 1 |
| General use | | A | 20 |
| Auxiliary contacts | | | |
| Pilot Duty | | | |
| AC operated | | | A600 |
| DC operated | | | P300 |
| General Use | | | |
| AC | | V | 600 |
| AC | | A | 10 |
| DC | | V | 250 |
| DC | | A | 1 |
| Short Circuit Current Rating | | SCCR | |
| Basic Rating | | | |
| SCCR | | kA | 5 |
| max. Fuse | | A | 45 |
| max. CB | | A | 60 |
| 480 V High Fault | | | |
| SCCR (fuse) | | kA | 30/100 |
| max. Fuse | | A | 25 Class RK5/20 Class J |
| SCCR (CB) | | kA | 65 |
| max. CB | | A | 16 |
| 600 V High Fault | | | |
| SCCR (fuse) | | kA | 30/100 |
| max. Fuse | | A | 25 Class RK5/20 Class J |
| Special Purpose Ratings | | | |
| Electrical Discharge Lamps (Ballast) | | | |
| 480V 60Hz 3phase, 277V 60Hz 1phase | | A | 12 |
| 600V 60Hz 3phase, 347V 60Hz 1phase | | A | 12 |
| Incandescent Lamps (Tungsten) | | | |
| 480V 60Hz 3phase, 277V 60Hz 1phase | | A | 14 |
| 600V 60Hz 3phase, 347V 60Hz 1phase | | A | 14 |
| Resistance Air Heating | | | |
| 480V 60Hz 3phase, 277V 60Hz 1phase | | A | 12 |
| 600V 60Hz 3phase, 347V 60Hz 1phase | | A | 12 |
| Refrigeration Control (CSA only) | | | |
| LRA 480V 60Hz 3phase | | A | 60 |
| FLA 480V 60Hz 3phase | | A | 10 |
| LRA 600V 60Hz 3phase | | A | 60 |
| FLA 600V 60Hz 3phase | | A | 10 |
| Definite Purpose Ratings (100,000 cycles acc. to UL 1995) | | | |
| LRA 480V 60Hz 3phase | | A | 42 |

| | | | |
|---|---|---|---|
| FLA 480V 60Hz 3phase | | A | 7 |
| Elevator Control | | | |
| 200V 60Hz 3phase | | HP | 0.75 |
| 200V 60Hz 3phase | | A | 3.7 |
| 240V 60Hz 3phase | | HP | 1.5 |
| 240V 60Hz 3phase | | A | 6 |
| 480V 60Hz 3phase | | HP | 2 |
| 480V 60Hz 3phase | | A | 3.4 |
| 600V 60Hz 3phase | | HP | 3 |
| 600V 60Hz 3phase | | A | 3.9 |

## Design verification as per IEC/EN 61439

| | | | |
|---|---|---|---|
| Technical data for design verification | | | |
| Rated operational current for specified heat dissipation | $I_n$ | A | 7 |
| Heat dissipation per pole, current-dependent | $P_{vid}$ | W | 0.1 |
| Equipment heat dissipation, current-dependent | $P_{vid}$ | W | 0 |
| Static heat dissipation, non-current-dependent | $P_{vs}$ | W | 1.4 |
| Heat dissipation capacity | $P_{diss}$ | W | 0 |
| Operating ambient temperature min. | | °C | -25 |
| Operating ambient temperature max. | | °C | 60 |
| IEC/EN 61439 design verification | | | |
| 10.2 Strength of materials and parts | | | |
| 10.2.2 Corrosion resistance | | | Meets the product standard's requirements. |
| 10.2.3.1 Verification of thermal stability of enclosures | | | Meets the product standard's requirements. |
| 10.2.3.2 Verification of resistance of insulating materials to normal heat | | | Meets the product standard's requirements. |
| 10.2.3.3 Verification of resistance of insulating materials to abnormal heat and fire due to internal electric effects | | | Meets the product standard's requirements. |
| 10.2.4 Resistance to ultra-violet (UV) radiation | | | Meets the product standard's requirements. |
| 10.2.5 Lifting | | | Does not apply, since the entire switchgear needs to be evaluated. |
| 10.2.6 Mechanical impact | | | Does not apply, since the entire switchgear needs to be evaluated. |
| 10.2.7 Inscriptions | | | Meets the product standard's requirements. |
| 10.3 Degree of protection of ASSEMBLIES | | | Does not apply, since the entire switchgear needs to be evaluated. |
| 10.4 Clearances and creepage distances | | | Meets the product standard's requirements. |
| 10.5 Protection against electric shock | | | Does not apply, since the entire switchgear needs to be evaluated. |
| 10.6 Incorporation of switching devices and components | | | Does not apply, since the entire switchgear needs to be evaluated. |
| 10.7 Internal electrical circuits and connections | | | Is the panel builder's responsibility. |
| 10.8 Connections for external conductors | | | Is the panel builder's responsibility. |
| 10.9 Insulation properties | | | |
| 10.9.2 Power-frequency electric strength | | | Is the panel builder's responsibility. |
| 10.9.3 Impulse withstand voltage | | | Is the panel builder's responsibility. |
| 10.9.4 Testing of enclosures made of insulating material | | | Is the panel builder's responsibility. |
| 10.10 Temperature rise | | | The panel builder is responsible for the temperature rise calculation. Eaton will provide heat dissipation data for the devices. |
| 10.11 Short-circuit rating | | | Is the panel builder's responsibility. The specifications for the switchgear must be observed. |
| 10.12 Electromagnetic compatibility | | | Is the panel builder's responsibility. The specifications for the switchgear must be observed. |
| 10.13 Mechanical function | | | The device meets the requirements, provided the information in the instruction leaflet (IL) is observed. |

## Technical data ETIM 7.0

| | | | |
|---|---|---|---|
| Low-voltage industrial components (EG000017) / Power contactor, AC switching (EC000066) | | | |
| Electric engineering, automation, process control engineering / Low-voltage switch technology / Contactor (LV) / Power contactor, AC switching (ecl@ss10.0.1-27-37-10-03 [AAB718015]) | | | |
| Rated control supply voltage Us at AC 50HZ | | V | 230 - 230 |
| Rated control supply voltage Us at AC 60HZ | | V | 240 - 240 |
| Rated control supply voltage Us at DC | | V | 0 - 0 |
| Voltage type for actuating | | | AC |

| | | | |
|---|---|---|---|
| Rated operation current Ie at AC-1, 400 V | | A | 22 |
| Rated operation current Ie at AC-3, 400 V | | A | 7 |
| Rated operation power at AC-3, 400 V | | kW | 3 |
| Rated operation current Ie at AC-4, 400 V | | A | 5 |
| Rated operation power at AC-4, 400 V | | kW | 2.2 |
| Rated operation power NEMA | | kW | 2.2 |
| Modular version | | | No |
| Number of auxiliary contacts as normally open contact | | | 1 |
| Number of auxiliary contacts as normally closed contact | | | 0 |
| Type of electrical connection of main circuit | | | Screw connection |
| Number of normally closed contacts as main contact | | | 0 |
| Number of main contacts as normally open contact | | | 3 |

## Approvals

| | | |
|---|---|---|
| Product Standards | | IEC/EN 60947-4-1; UL 60947-4-1; CSA - C22.2 No. 60947-4-1-14; CE marking |
| UL File No. | | E29096 |
| UL Category Control No. | | NLDX |
| CSA File No. | | 012528 |
| CSA Class No. | | 2411-03, 3211-04 |
| North America Certification | | UL listed, CSA certified |
| Specially designed for North America | | No |
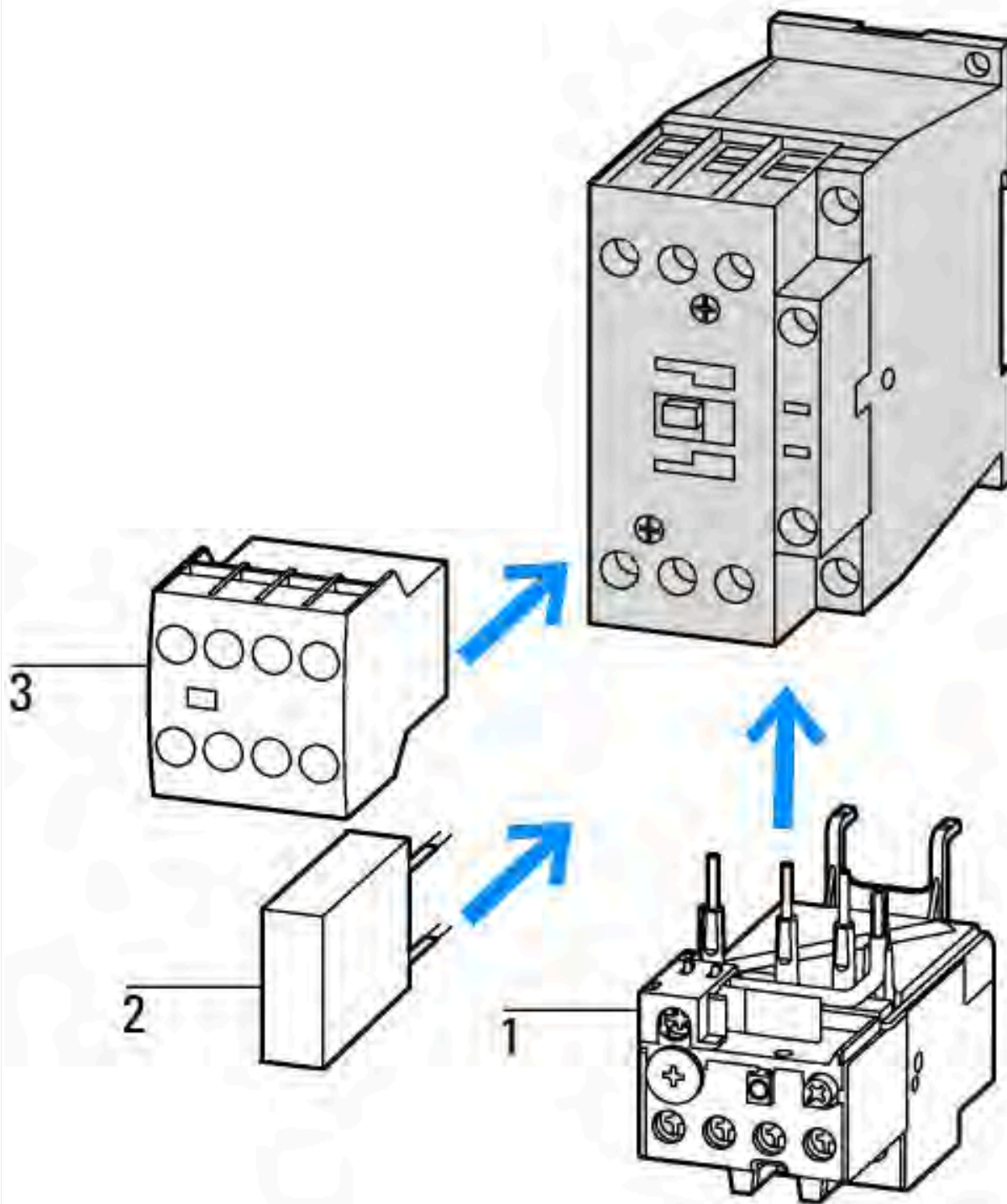
## Characteristics



1: Overload relay
2: Suppressor
3: Auxiliary contact modules

kW — Rated output of three-phase motors 50 - 60 Hz
A — Rated operational current $I_e$ 50 - 60 Hz

AC-3/400V

Axis (kW): 90 75 55 45 37 30 22 18.5 15 11 7.5 5.5 4 3

Axis (A): 170 150 115 95 80 65 50 40 32 25 18 12 9 7 5 4 3 2

Curve labels:
DILM170
DILM150
DILM115
DILM95
DILM80
DILM72
DILM65
DILM50
DILM40
DILM38
DILM32
DILM25
DILM17
DILM15
DILM12
DILM9, DILEM
DILM7
DILEM12
DILEM-G
DILEM

X-axis: 0.01  0.02  0.04  0.06  0.1  0.2  0.4  0.6  1  2  4  6  10

→ Component lifespan [millions of operations]

Squirrel-cage motor
Operating characteristics
Starting:from rest
Stopping:after attaining full running speed
Electrical characteristics
Make: up to 6 x rated motor current
Break: up to 1 x rated motor current
Utilization category
100 % AC-3
Typical applications
Compressors
Lifts
Mixers
Pumps
Escalators
Agitators
Fans
Conveyor belts
Centrifuges
Hinged flaps
Bucket-elevators
Air conditioning system
General drives in manufacturing and processing machines
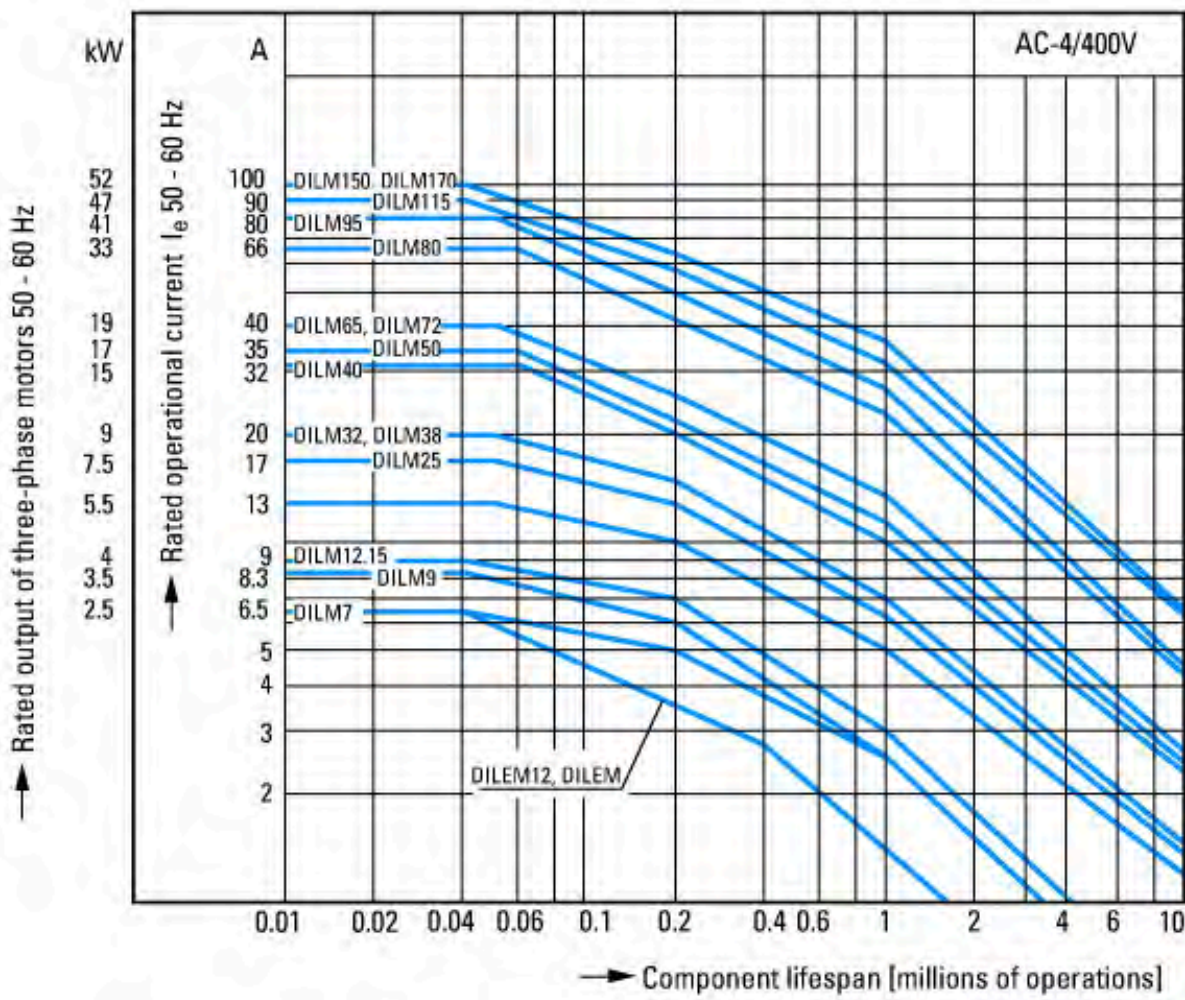
Extreme switching duty
Squirrel-cage motor
Operating characteristics
Inching, plugging, reversing
Electrical characteristics
Make: up to 6 x rated motor current
Break: up to 6 x rated motor current
Utilization category
100 % AC-4
Typical applications
Printing presses
Wire-drawing machines
Centrifuges
Special drives for manufacturing and processing machines
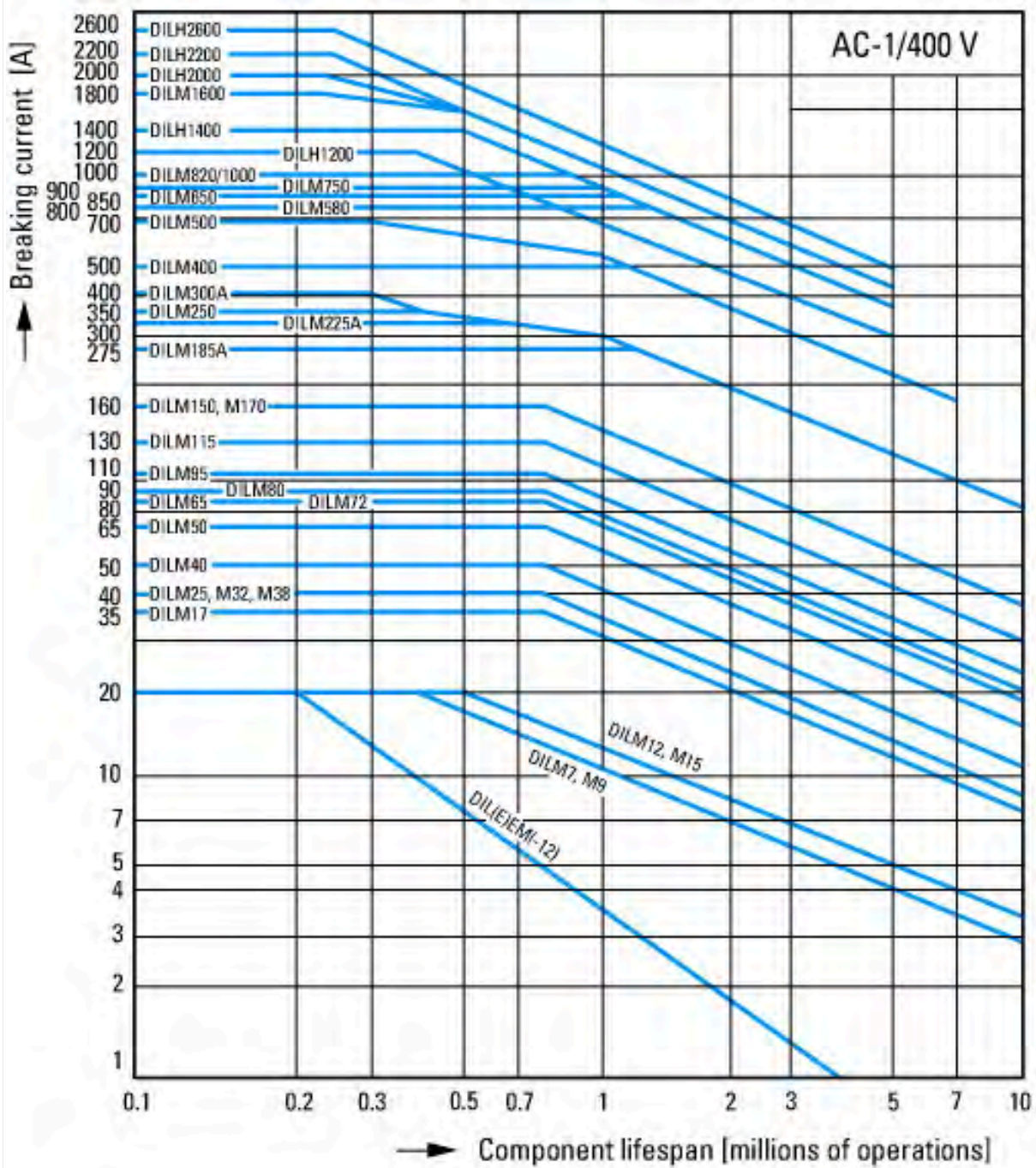
Switching conditions for non-motor consumers, 3 pole, 4 pole
Operating characteristics
Non inductive and slightly inductive loads
Electrical characteristics
Switch on: 1 x rated operational current
Switch off: 1 x rated operational current
Utilization category
100 % AC-1
Typical examples of application
Electric heat

# Dimensions
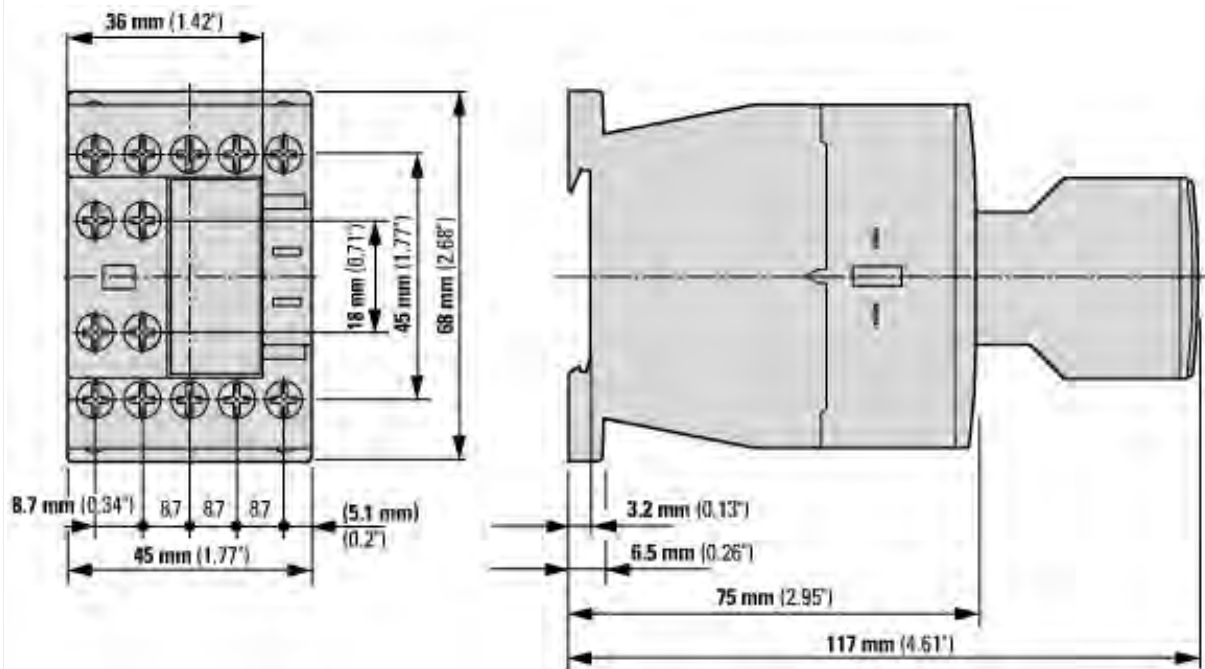


Contactor with auxiliary contact module DILM32-XHI.../DILA-XHI...
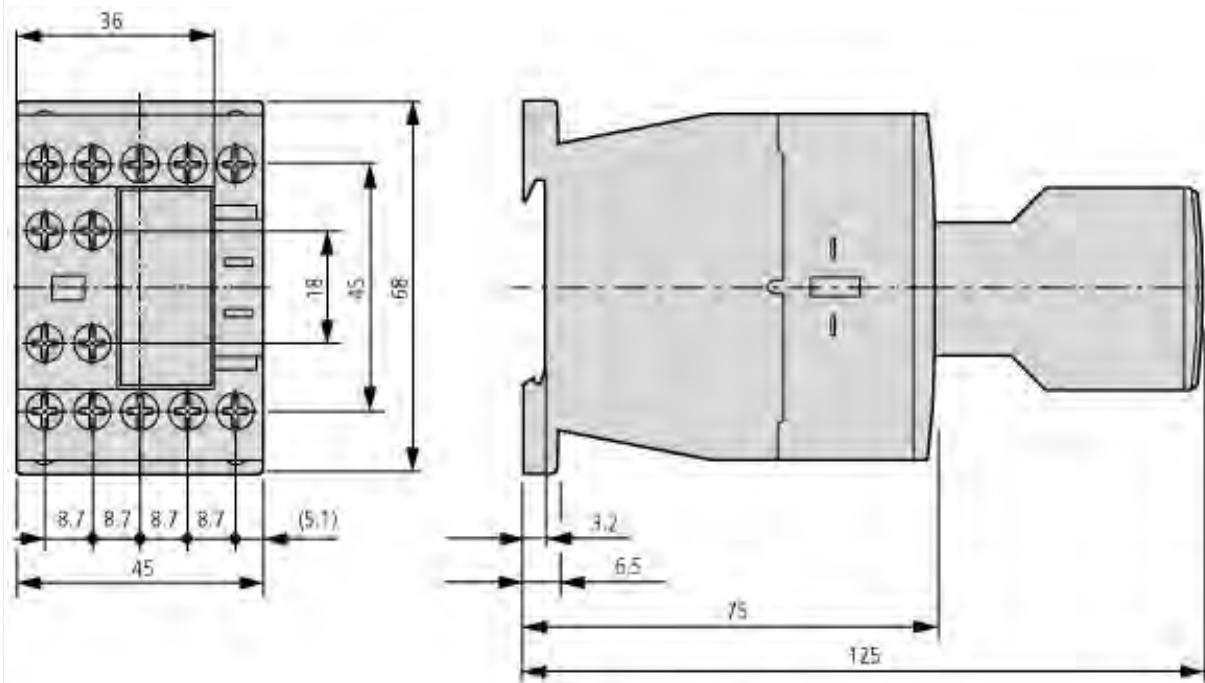


Contactor with auxiliary contact module DILA-XHIT…
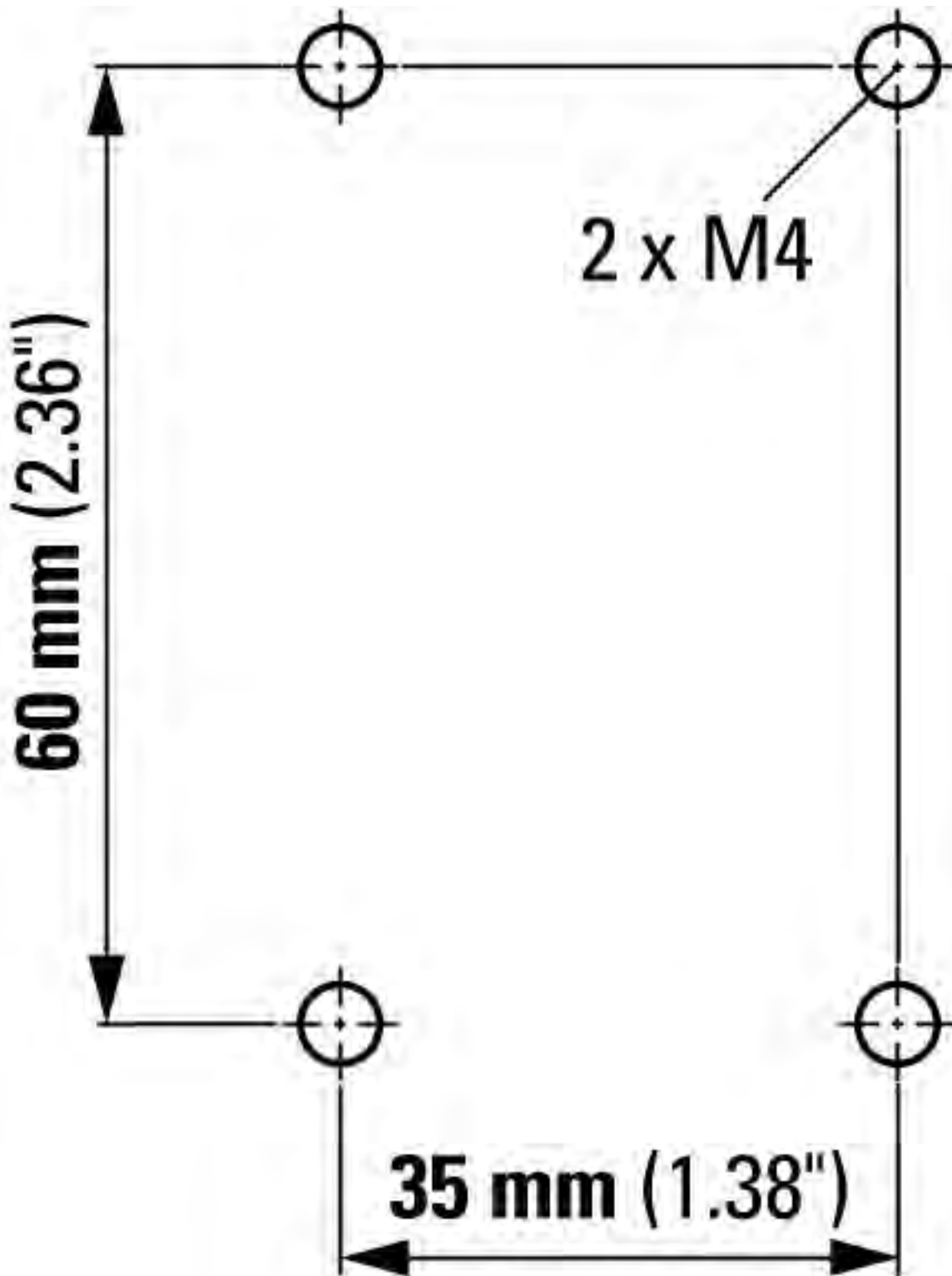
DILM7…DILM15
DILA…
Contactor with auxiliary contact module

## Additional product information (links)

**IL03407013Z (AWA2100-2126) Contactors**

| | |
|---|---|
| IL03407013Z (AWA2100-2126) Contactors | ftp://ftp.moeller.net/DOCUMENTATION/AWA_INSTRUCTIONS/IL03407013Z2020_05.pdf |
| Motor starters and "Special Purpose Ratings" for the North American market | http://www.eaton.eu/ecm/groups/public/@pub/@europe/@electrical/documents/content/pct_3258146.pdf |
| Switchgear of Power Factor Correction Systems | http://www.moeller.net/binary/ver_techpapers/ver934en.pdf |
| X-Start - Modern Switching Installations Efficiently Fitted and Wired Securely | http://www.moeller.net/binary/ver_techpapers/ver938en.pdf |
| Mirror Contacts for Highly-Reliable Information Relating to Safety-Related Control Functions | http://www.moeller.net/binary/ver_techpapers/ver944en.pdf |
| Effect of the Cabel Capacitance of Long Control Cables on the Actuation of Contactors | http://www.moeller.net/binary/ver_techpapers/ver949en.pdf |

| | |
|---|---|
| Switchgear for Luminaires | http://www.moeller.net/binary/ver_techpapers/ver955en.pdf |
| Standard Compliant and Functionally Safe Engineering Design with Mechanical Auxiliary Contacts | http://www.moeller.net/binary/ver_techpapers/ver956en.pdf |
| The Interaction of Contactors with PLCs | http://www.moeller.net/binary/ver_techpapers/ver957en.pdf |
| Busbar Component Adapters for modern Industrial control panels | http://www.moeller.net/binary/ver_techpapers/ver960en.pdf |

## Description

Arduino® Mega 2560 is an exemplary development board dedicated for building extensive applications as compared to other maker boards by Arduino. The board accommodates the ATmega2560 microcontroller, which operates at a frequency of 16 MHz. The board contains 54 digital input/output pins, 16 analog inputs, 4 UARTs (hardware serial ports), a USB connection, a power jack, an ICSP header, and a reset button.

## Target Areas

3D Printing, Robotics, Maker

## Features

- **ATmega2560 Processor**

  - Up to 16 MIPS Throughput at 16MHz
  - 256k bytes (of which 8k is used for the bootloader)
  - 4k bytes EEPROM
  - 8k bytes Internal SRAM
  - 32 × 8 General Purpose Working Registers
  - Real Time Counter with Separate Oscillator
  - Four 8-bit PWM Channels
  - Four Programmable Serial USART
  - Controller/Peripheral SPI Serial Interface

- **ATmega16U2**

  - Up to 16 MIPS Throughput at 16 MHz
  - 16k bytes ISP Flash Memory
  - 512 bytes EEPROM
  - 512 bytes SRAM
  - USART with SPI master only mode and hardware flow control (RTS/CTS)
  - Master/Slave SPI Serial Interface

- **Sleep Modes**

  - Idle
  - ADC Noise Reduction
  - Power-save
  - Power-down
  - Standby
  - Extended Standby

- **Power**

  - USB Connection
  - External AC/DC Adapter

- **I/O**

  - 54 Digital
  - 16 Analog
  - 15 PWM Output

# Contents

# 1 The Board

Arduino® Mega 2560 is a successor board of Arduino Mega, it is dedicated to applications and projects that require large number of input output pins and the use cases which need high processing power. The Arduino® Mega 2560 comes with a much larger set of IOs when we compare it with traditional Uno board considering the form factor of both the boards.

## 1.1 Application Examples

- **Robotics**: Featuring the high processing capacity, the Arduino Mega 2560 can handle the extensive robotic applications. It is compatible with the motor controller shield that enables it to control multiple motors at an instance, thus making it perfect of robotic applications. The large number of I/O pins can accommodate many robotic sensors as well.

- **3D Printing**: Algorithms play a significant role in implementation of 3D printers. Arduino Mega 2560 has the power to process these complex algorithms required for 3D printing. Additionally, the slight changes to the code is easily possible with the Arduino IDE and thus 3D printing programs can be customized according to user requirements.

- **Wi-Fi**: Integrating wireless functionality enhances the utility of the applications. Arduino Mega 2560 is compatible with WiFi shields hence allowing the wireless features for the applications in 3D printing and Robotics.

## 1.2 Accessories

## 1.3 Related Products

- Arduino® Uno Rev 3
- Arduino® Nano
- Arduino® DUE without headers

## 2 Ratings

### 2.1 Recommended Operating Conditions

| Symbol | Description | Min | Max |
|---|---|---|---|
| TOP | Operating temperature: | -40 °C | 85 °C |

### 2.2 Power Consumption

| Symbol | Description | Min | Typ | Max | Unit |
|---|---|---|---|---|---|
| PWRIN | Input supply from power jack | | TBC | | mW |
| USB VCC | Input supply from USB | | TBC | | mW |
| VIN | Input from VIN pad | | TBC | | mW |

## 3 Functional Overview

### 3.1 Block Diagram
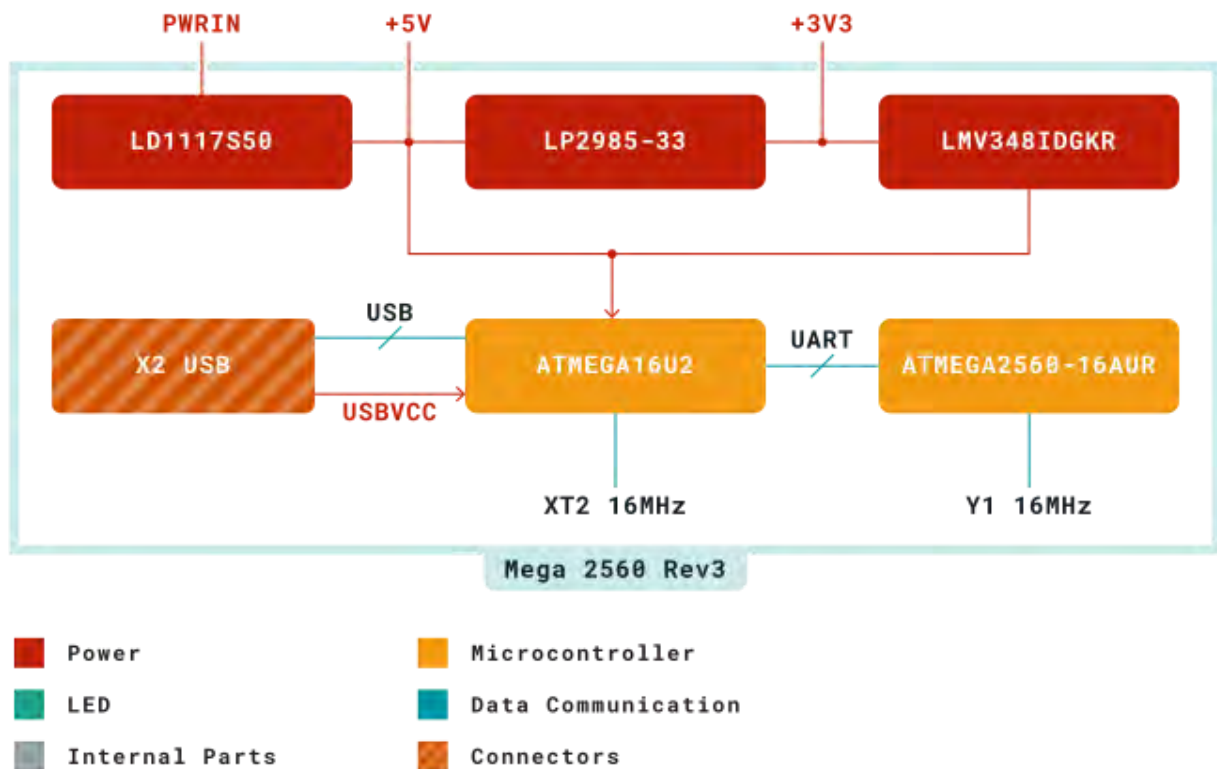


*Arduino MEGA Block Diagram*

## 3.2 Board Topology

**Front View**
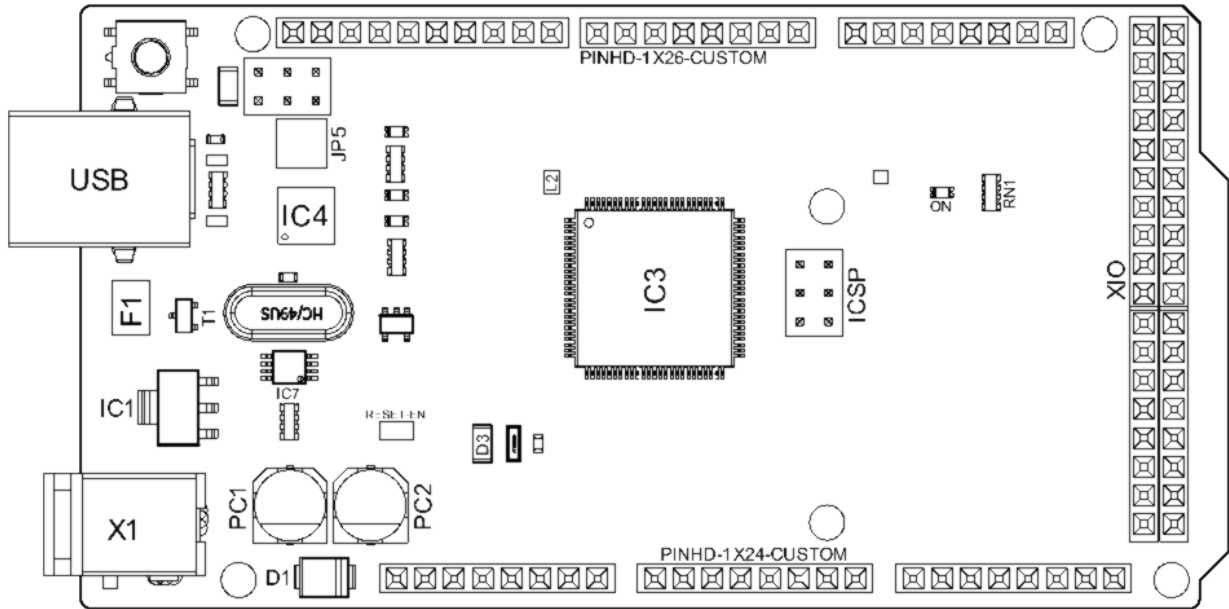


*Arduino MEGA Top View*

| Ref. | Description | Ref. | Description |
|------|-------------|------|-------------|
| USB | USB B Connector | F1 | Chip Capacitor |
| IC1 | 5V Linear Regulator | X1 | Power Jack Connector |
| JP5 | Plated Holes | IC4 | ATmega16U2 chip |
| PC1 | Electrolytic Alumninum Capacitor | PC2 | Electrolytic Alumninum Capacitor |
| D1 | General Purpose Rectifier | D3 | General Purpose Diode |
| L2 | Fixed Inductor | IC3 | ATmega2560 chip |
| ICSP | Connector Header | ON | Green LED |
| RN1 | Resistor Array | XIO | Connector |

### 3.3 Processor

Primary processor of Arduino Mega 2560 Rev3 board is ATmega2560 chip which operates at a frequency of 16 MHz. It accommodates a large number of input and output lines which gives the provision of interfacing many external devices. At the same time the operations and processing is not slowed due to its significantly larger RAM than the other processors. The board also features a USB serial processor ATmega16U2 which acts an interface between the USB input signals and the main processor. This increases the flexibility of interfacing and connecting peripherals to the Arduino Mega 2560 Rev 3 board.

### 3.4 Power Tree
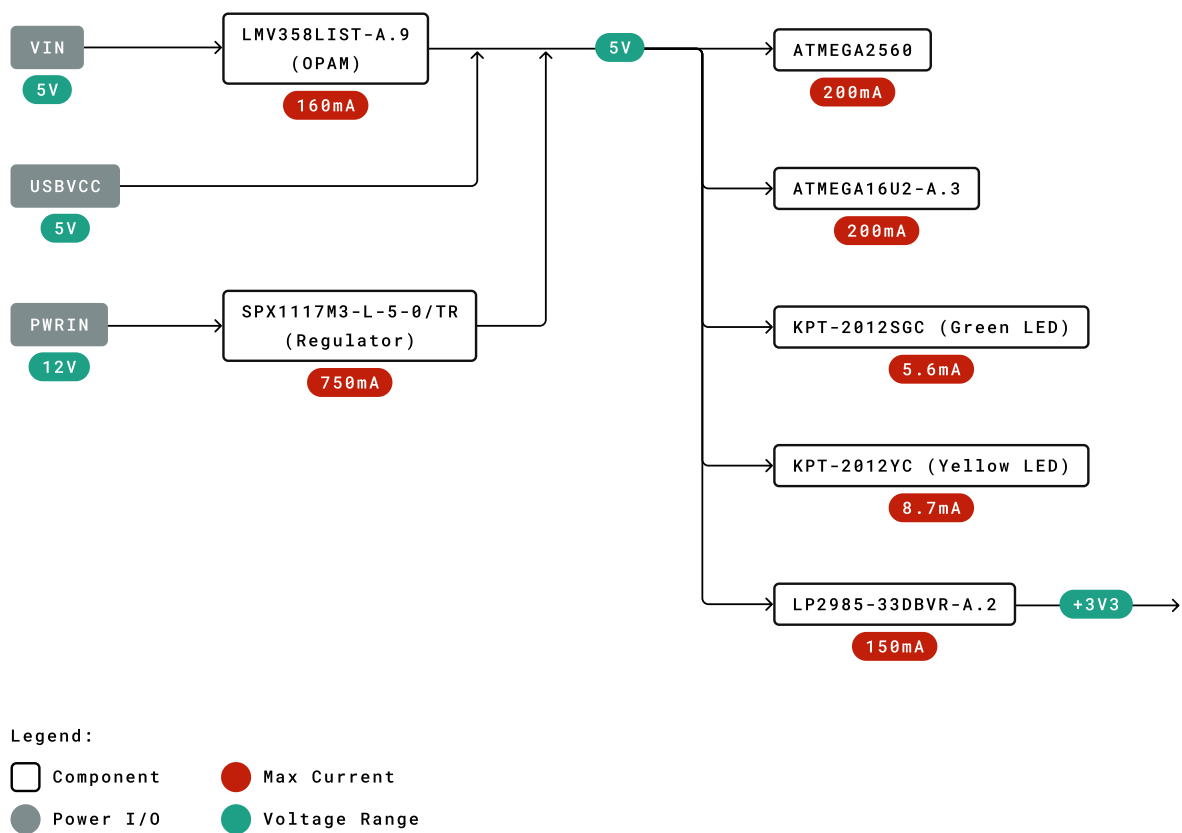


*Power Tree*

# 4 Board Operation

## 4.1 Getting Started - IDE

If you want to program your Arduino® MEGA 2560 while offline you need to install the Arduino® Desktop IDE **[1]** To connect the Arduino® MEGA 2560 to your computer, you'll need a Type-B USB cable. This also provides power to the board, as indicated by the LED.

## 4.2 Getting Started - Arduino Web Editor

All Arduino® boards, including this one, work out-of-the-box on the Arduino® Web Editor **[2]**, by just installing a simple plugin.

The Arduino® Web Editor is hosted online, therefore it will always be up-to-date with the latest features and support for all boards. Follow **[3]** to start coding on the browser and upload your sketches onto your board.

## 4.3 Sample Sketches

Sample sketches for the Arduino® MEGA 2560 can be found either in the "Examples" menu in the Arduino® IDE

## 4.4 Online Resources

Now that you have gone through the basics of what you can do with the board you can explore the endless possibilities it provides by checking exciting projects on ProjectHub **[5]**, the Arduino® Library Reference **[6]** and the online store **[7]** where you will be able to complement your board with sensors, actuators and more.

# 5 Connector Pinouts
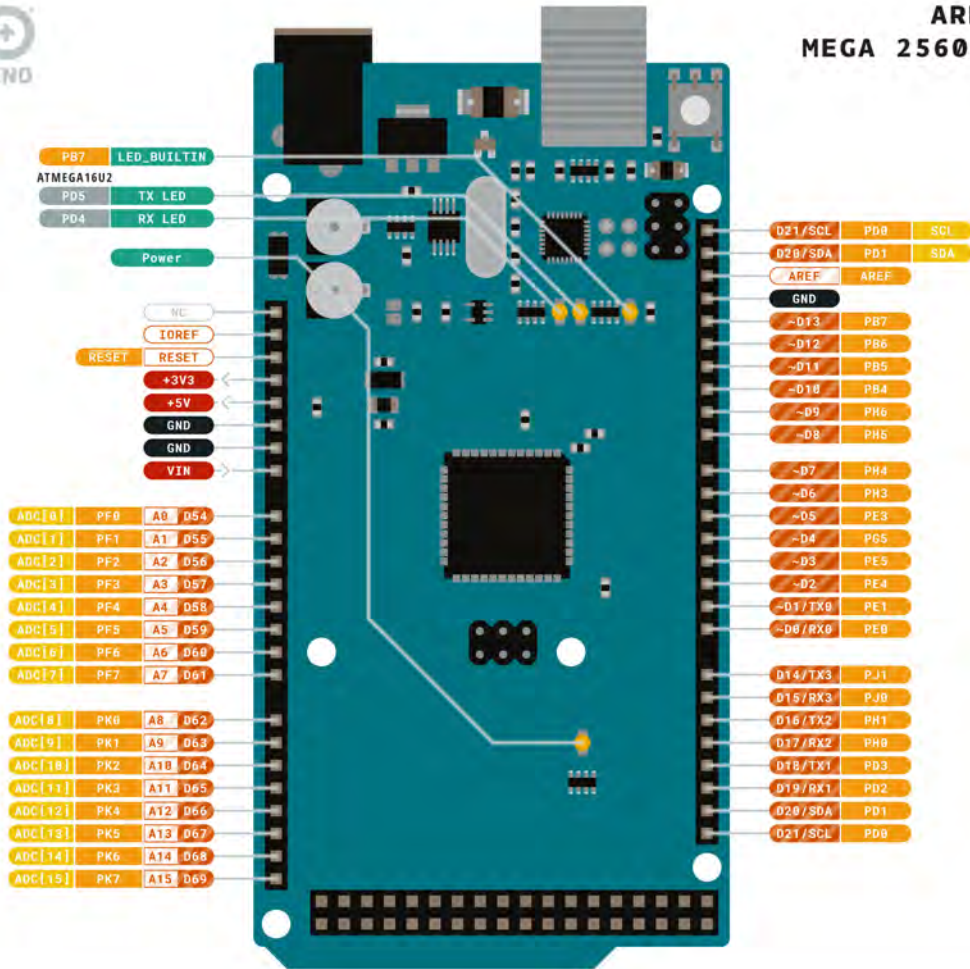
*Arduino Mega Pinout*

## 5.1 Analog

| Pin | Function | Type | Description |
|-----|----------|------|-------------|
| 1 | NC | NC | Not Connected |
| 2 | IOREF | IOREF | Reference for digital logic V - connected to 5V |
| 3 | Reset | Reset | Reset |
| 4 | +3V3 | Power | +3V3 Power Rail |
| 5 | +5V | Power | +5V Power Rail |
| 6 | GND | Power | Ground |
| 7 | GND | Power | Ground |
| 8 | VIN | Power | Voltage Input |
| 9 | A0 | Analog | Analog input 0 /GPIO |
| 10 | A1 | Analog | Analog input 1 /GPIO |
| 11 | A2 | Analog | Analog input 2 /GPIO |
| 12 | A3 | Analog | Analog input 3 /GPIO |
| 13 | A4 | Analog | Analog input 4 /GPIO |
| 14 | A5 | Analog | Analog input 5 /GPIO |
| 15 | A6 | Analog | Analog input 6 /GPIO |
| 16 | A7 | Analog | Analog input 7 /GPIO |
| 17 | A8 | Analog | Analog input 8 /GPIO |
| 18 | A9 | Analog | Analog input 9 /GPIO |
| 19 | A10 | Analog | Analog input 10 /GPIO |
| 20 | A11 | Analog | Analog input 11 /GPIO |
| 21 | A12 | Analog | Analog input 12 /GPIO |
| 22 | A13 | Analog | Analog input 13 /GPIO |
| 23 | A14 | Analog | Analog input 14 /GPIO |
| 24 | A15 | Analog | Analog input 15 /GPIO |

## 5.2 Digital

| Pin | Function | Type | Description |
|-----|----------|------|-------------|
| 1 | D21/SCL | Digital Input/I2C | Digital input 21/I2C Dataline |
| 2 | D20/SDA | Digital Input/I2C | Digital input 20/I2C Dataline |
| 3 | AREF | Digital | Analog Reference Voltage |
| 4 | GND | Power | Ground |
| 5 | D13 | Digital/GPIO | Digital input 13/GPIO |
| 6 | D12 | Digital/GPIO | Digital input 12/GPIO |
| 7 | D11 | Digital/GPIO | Digital input 11/GPIO |
| 8 | D10 | Digital/GPIO | Digital input 10/GPIO |
| 9 | D9 | Digital/GPIO | Digital input 9/GPIO |
| 10 | D8 | Digital/GPIO | Digital input 8/GPIO |
| 11 | D7 | Digital/GPIO | Digital input 7/GPIO |
| 12 | D6 | Digital/GPIO | Digital input 6/GPIO |
| 13 | D5 | Digital/GPIO | Digital input 5/GPIO |
| 14 | D4 | Digital/GPIO | Digital input 4/GPIO |

| Pin | Function | Type | Description |
|-----|----------|------|-------------|
| 15 | D3 | Digital/GPIO | Digital input 3/GPIO |
| 16 | D2 | Digital/GPIO | Digital input 2/GPIO |
| 17 | D1/TX0 | Digital/GPIO | Digital input 1 /GPIO |
| 18 | D0/Tx1 | Digital/GPIO | Digital input 0 /GPIO |
| 19 | D14 | Digital/GPIO | Digital input 14 /GPIO |
| 20 | D15 | Digital/GPIO | Digital input 15 /GPIO |
| 21 | D16 | Digital/GPIO | Digital input 16 /GPIO |
| 22 | D17 | Digital/GPIO | Digital input 17 /GPIO |
| 23 | D18 | Digital/GPIO | Digital input 18 /GPIO |
| 24 | D19 | Digital/GPIO | Digital input 19 /GPIO |
| 25 | D20 | Digital/GPIO | Digital input 20 /GPIO |
| 26 | D21 | Digital/GPIO | Digital input 21 /GPIO |
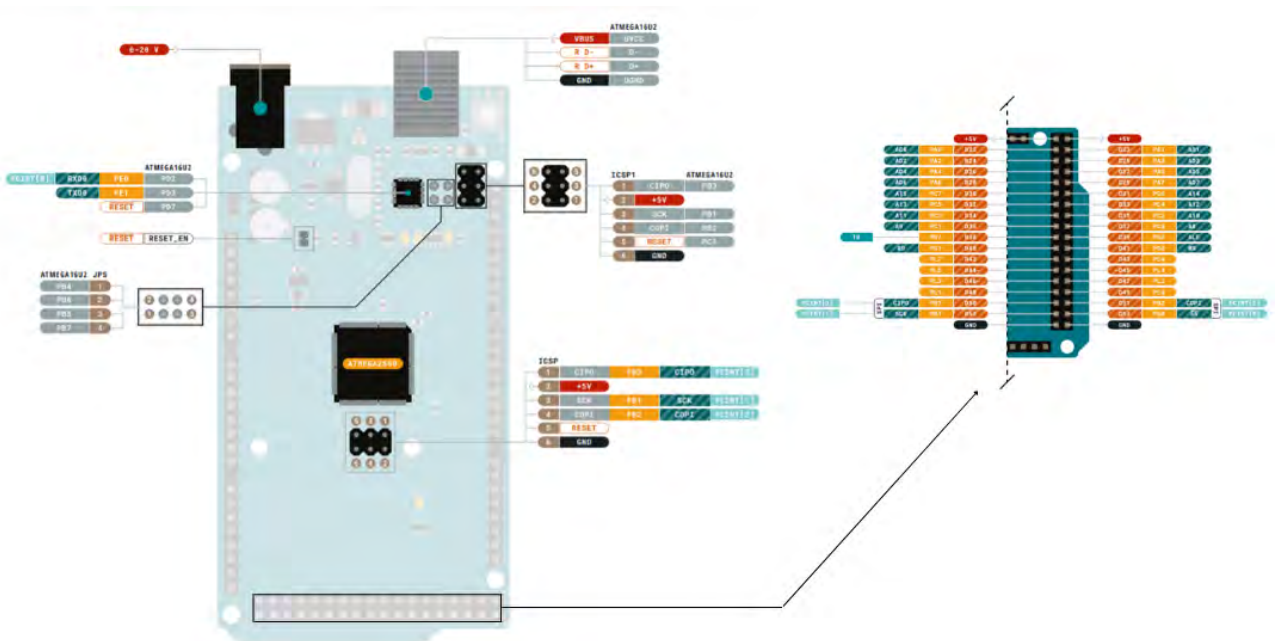


*Arduino Mega Pinout*

### 5.3 ATMEGA16U2 JP5

| Pin | Function | Type | Description |
|-----|----------|------|-------------|
| 1 | PB4 | Internal | Serial Wire Debug |
| 2 | PB6 | Internal | Serial Wire Debug |
| 3 | PB5 | Internal | Serial Wire Debug |
| 4 | PB7 | Internal | Serial Wire Debug |

### 5.4 ATMEGA16U2 ICSP1

| Pin | Function | Type | Description |
|-----|----------|------|-------------|
| 1 | CIPO | Internal | Controller In Peripheral Out |
| 2 | +5V | Internal | Power Supply of 5V |
| 3 | SCK | Internal | Serial Clock |
| 4 | COPI | Internal | Controller Out Peripheral In |
| 5 | RESET | Internal | Reset |
| 6 | GND | Internal | Ground |

### 5.5 Digital Pins D22 - D53 LHS

| Pin | Function | Type | Description |
|-----|----------|------|-------------|
| 1 | +5V | Power | Power Supply of 5V |
| 2 | D22 | Digital | Digital input 22/GPIO |
| 3 | D24 | Digital | Digital input 24/GPIO |
| 4 | D26 | Digital | Digital input 26/GPIO |
| 5 | D28 | Digital | Digital input 28/GPIO |
| 6 | D30 | Digital | Digital input 30/GPIO |
| 7 | D32 | Digital | Digital input 32/GPIO |
| 8 | D34 | Digital | Digital input 34/GPIO |
| 9 | D36 | Digital | Digital input 36/GPIO |
| 10 | D38 | Digital | Digital input 38/GPIO |
| 11 | D40 | Digital | Digital input 40/GPIO |
| 12 | D42 | Digital | Digital input 42/GPIO |
| 13 | D44 | Digital | Digital input 44/GPIO |
| 14 | D46 | Digital | Digital input 46/GPIO |
| 15 | D48 | Digital | Digital input 48/GPIO |
| 16 | D50 | Digital | Digital input 50/GPIO |
| 17 | D52 | Digital | Digital input 52/GPIO |
| 18 | GND | Power | Ground |

## 5.6 Digital Pins D22 - D53 RHS

| Pin | Function | Type | Description |
|---|---|---|---|
| 1 | +5V | Power | Power Supply of 5V |
| 2 | D23 | Digital | Digital input 23/GPIO |
| 3 | D25 | Digital | Digital input 25/GPIO |
| 4 | D27 | Digital | Digital input 27/GPIO |
| 5 | D29 | Digital | Digital input 29/GPIO |
| 6 | D31 | Digital | Digital input 31/GPIO |
| 7 | D33 | Digital | Digital input 33/GPIO |
| 8 | D35 | Digital | Digital input 35/GPIO |
| 9 | D37 | Digital | Digital input 37/GPIO |
| 10 | D39 | Digital | Digital input 39/GPIO |
| 11 | D41 | Digital | Digital input 41/GPIO |
| 12 | D43 | Digital | Digital input 43/GPIO |
| 13 | D45 | Digital | Digital input 45/GPIO |
| 14 | D47 | Digital | Digital input 47/GPIO |
| 15 | D49 | Digital | Digital input 49/GPIO |
| 16 | D51 | Digital | Digital input 51/GPIO |
| 17 | D53 | Digital | Digital input 53/GPIO |
| 18 | GND | Power | Ground |

# 6 Mechanical Information

## 6.1 Board Outline
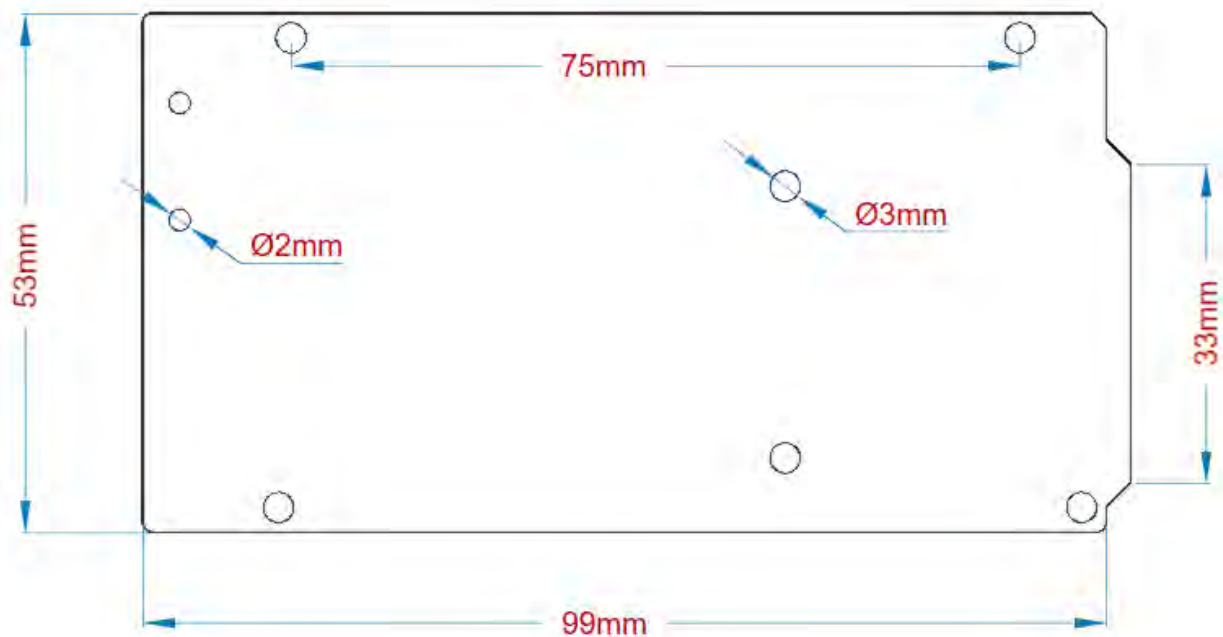
*Arduino Mega Outline*

## 6.2 Board Mount Holes
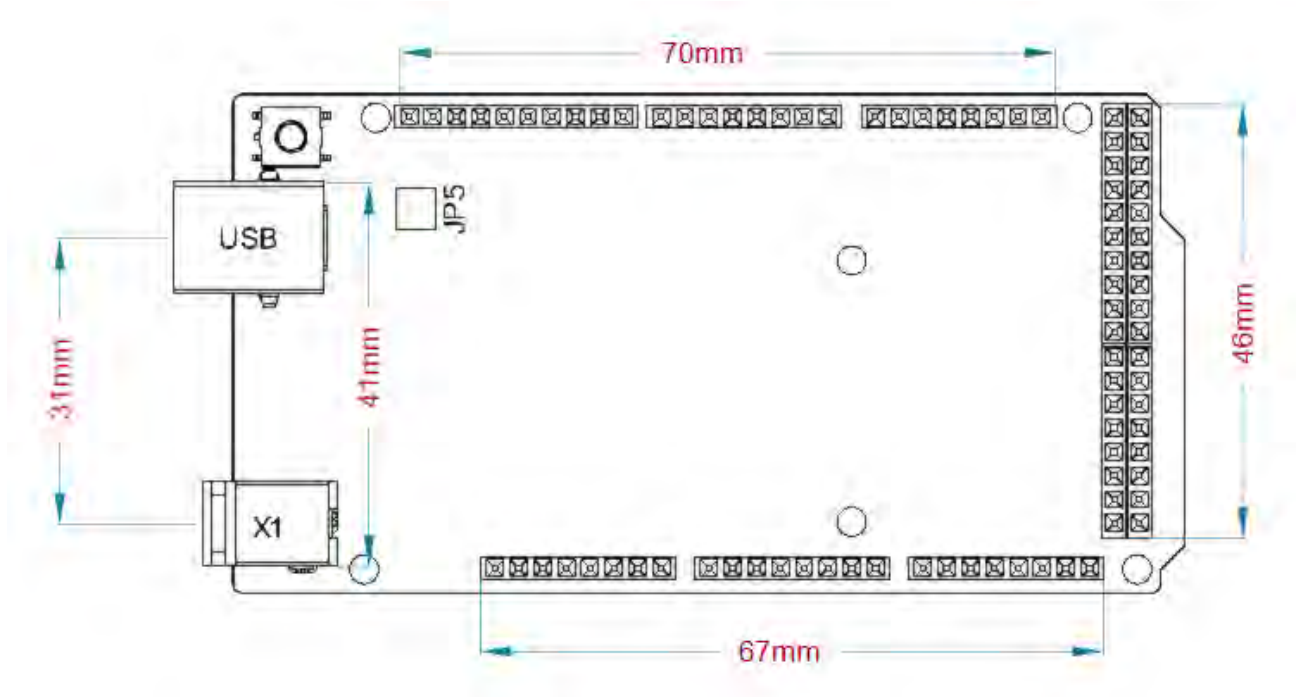


*Arduino Mega Mount Holes*

# Certifications

## 7 Declaration of Conformity CE DoC (EU)

We declare under our sole responsibility that the products above are in conformity with the essential requirements of the following EU Directives and therefore qualify for free movement within markets comprising the European Union (EU) and European Economic Area (EEA).

## 8 Declaration of Conformity to EU RoHS & REACH 211 01/19/2021

Arduino boards are in compliance with RoHS 2 Directive 2011/65/EU of the European Parliament and RoHS 3 Directive 2015/863/EU of the Council of 4 June 2015 on the restriction of the use of certain hazardous substances in electrical and electronic equipment.

| Substance | Maximum Limit (ppm) |
|---|---|
| Lead (Pb) | 1000 |
| Cadmium (Cd) | 100 |
| Mercury (Hg) | 1000 |
| Hexavalent Chromium (Cr6+) | 1000 |
| Poly Brominated Biphenyls (PBB) | 1000 |
| Poly Brominated Diphenyl ethers (PBDE) | 1000 |
| Bis(2-Ethylhexyl} phthalate (DEHP) | 1000 |
| Benzyl butyl phthalate (BBP) | 1000 |
| Dibutyl phthalate (DBP) | 1000 |
| Diisobutyl phthalate (DIBP) | 1000 |

Exemptions : No exemptions are claimed.

Arduino Boards are fully compliant with the related requirements of European Union Regulation (EC) 1907 /2006 concerning the Registration, Evaluation, Authorization and Restriction of Chemicals (REACH). We declare none of the SVHCs (https://echa.europa.eu/web/guest/candidate-list-table), the Candidate List of Substances of Very High Concern for authorization currently released by ECHA, is present in all products (and also package) in quantities totaling in a concentration equal or above 0.1%. To the best of our knowledge, we also declare that our products do not contain any of the substances listed on the "Authorization List" (Annex XIV of the REACH regulations) and Substances of Very High Concern (SVHC) in any significant amounts as specified by the Annex XVII of Candidate list published by ECHA (European Chemical Agency) 1907 /2006/EC.

# 9 Conflict Minerals Declaration

As a global supplier of electronic and electrical components, Arduino is aware of our obligations with regards to laws and regulations regarding Conflict Minerals, specifically the Dodd-Frank Wall Street Reform and Consumer Protection Act, Section 1502. Arduino does not directly source or process conflict minerals such as Tin, Tantalum, Tungsten, or Gold. Conflict minerals are contained in our products in the form of solder, or as a component in metal alloys. As part of our reasonable due diligence Arduino has contacted component suppliers within our supply chain to verify their continued compliance with the regulations. Based on the information received thus far we declare that our products contain Conflict Minerals sourced from conflict-free areas.

# 10 FCC Caution

Any Changes or modifications not expressly approved by the party responsible for compliance could void the user's authority to operate the equipment.

This device complies with part 15 of the FCC Rules. Operation is subject to the following two conditions:

(1) This device may not cause harmful interference

(2) this device must accept any interference received, including interference that may cause undesired operation.

**FCC RF Radiation Exposure Statement:**

1. This Transmitter must not be co-located or operating in conjunction with any other antenna or transmitter.

2. This equipment complies with RF radiation exposure limits set forth for an uncontrolled environment.

3. This equipment should be installed and operated with minimum distance 20cm between the radiator & your body.

English: User manuals for licence-exempt radio apparatus shall contain the following or equivalent notice in a conspicuous location in the user manual or alternatively on the device or both. This device complies with Industry Canada licence-exempt RSS standard(s). Operation is subject to the following two conditions:

(1) this device may not cause interference

(2) this device must accept any interference, including interference that may cause undesired operation of the device.

French: Le présent appareil est conforme aux CNR d'Industrie Canada applicables aux appareils radio exempts de licence. L'exploitation est autorisée aux deux conditions suivantes :

(1) l' appareil nedoit pas produire de brouillage

(2) l'utilisateur de l'appareil doit accepter tout brouillage radioélectrique subi, même si le brouillage est susceptible d'en compromettre le fonctionnement.

**IC SAR Warning:**

English This equipment should be installed and operated with minimum distance 20 cm between the radiator and your body.

French: Lors de l' installation et de l' exploitation de ce dispositif, la distance entre le radiateur et le corps est d 'au moins 20 cm.

**Important:** The operating temperature of the EUT can't exceed 85℃ and shouldn't be lower than -40℃.

Hereby, Arduino S.r.l. declares that this product is in compliance with essential requirements and other relevant provisions of Directive 201453/EU. This product is allowed to be used in all EU member states.

## 11 Company Information

| Company name | Arduino S.r.l. |
|---|---|
| Company Address | Arduino SRL, Via Andrea Appiani 25, 20900 Monza MB, Italy |

## 12 Reference Documentation

| Ref | Link |
|---|---|
| Arduino IDE (Desktop) | https://www.arduino.cc/en/Main/Software |
| Arduino IDE (Cloud) | https://create.arduino.cc/editor |
| Cloud IDE Getting Started | https://create.arduino.cc/projecthub/Arduino_Genuino/getting-started-with-arduino-web-editor-4b3e4a |
| Arduino Pro Website | https://www.arduino.cc/pro |
| Project Hub | https://create.arduino.cc/projecthub?by=part&part_id=11332&sort=trending |
| Library Reference | https://www.arduino.cc/reference/en/libraries/ |
| Online Store | https://store.arduino.cc/ |

## 13 Revision History

| Date | Revision | Changes |
|---|---|---|
| 29/09/2020 | 1 | First Release |

# velleman®

# VMA436

**8-CHANNEL RELAY MODULE**
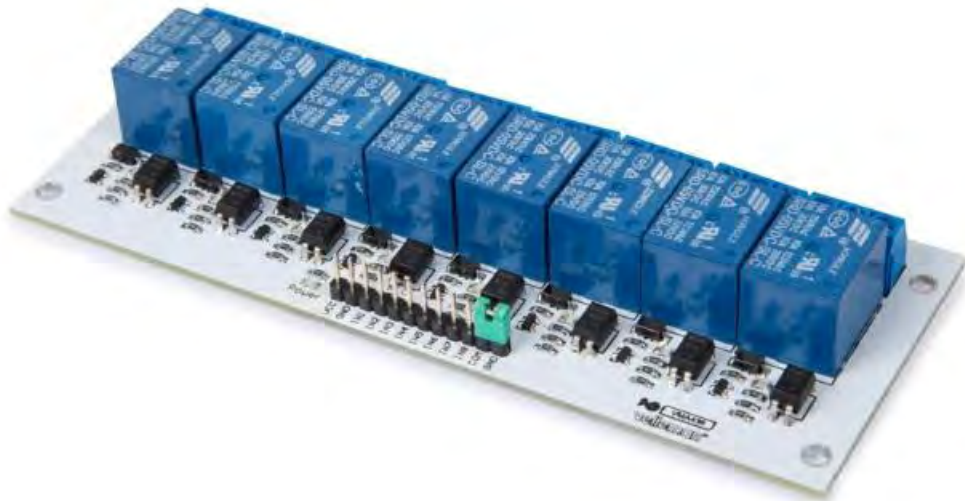


USER MANUAL

# USER MANUAL

## 1.    Introduction

**To all residents of the European Union**

**Important environmental information about this product**

This symbol on the device or the package indicates that disposal of the device after its lifecycle could harm the environment. Do not dispose of the unit (or batteries) as unsorted municipal waste; it should be taken to a specialized company for recycling. This device should be returned to your distributor or to a local recycling service. Respect the local environmental rules.

**If in doubt, contact your local waste disposal authorities.**

Thank you for choosing Velleman®! Please read the manual thoroughly before bringing this device into service. If the device was damaged in transit, do not install or use it and contact your dealer.

## 2.    Safety Instructions

| | |
|---|---|
| | • This device can be used by children aged from 8 years and above, and persons with reduced physical, sensory or mental capabilities or lack of experience and knowledge if they have been given supervision or instruction concerning the use of the device in a safe way and understand the hazards involved. Children shall not play with the device. Cleaning and user maintenance shall not be made by children without supervision. |

| | |
|---|---|
| | • Indoor use only. Keep away from rain, moisture, splashing and dripping liquids. |

## 3.    General Guidelines

| | |
|---|---|
| | • Refer to the Velleman® Service and Quality Warranty on the last pages of this manual. |
| | • Familiarise yourself with the functions of the device before actually using it. |
| | • All modifications of the device are forbidden for safety reasons. Damage caused by user modifications to the device is not covered by the warranty. |
| | • Only use the device for its intended purpose. Using the device in an unauthorised way will void the warranty. |
| | • Damage caused by disregard of certain guidelines in this manual is not covered by the warranty and the dealer will not accept responsibility for any ensuing defects or problems. |
| | • Nor Velleman nv nor its dealers can be held responsible for any damage (extraordinary, incidental or indirect) – of any nature (financial, physical…) arising from the possession, use or failure of this product. |
| | • Due to constant product improvements, the actual product appearance might differ from the shown images. |
| | • Product images are for illustrative purposes only. |
| | • Do not switch the device on immediately after it has been exposed to changes in temperature. Protect the device against damage by leaving it switched off until it has reached room temperature. |
| | • Keep this manual for future reference. |

## 4.    What is Arduino®

Arduino® is an open-source prototyping platform based in easy-to-use hardware and software. Arduino® boards are able to read inputs – light-on sensor, a finger on a button or a Twitter message – and turn it into an output – activating of a motor, turning on an LED, publishing something online. You can tell your board what to do by sending a set of instructions to the microcontroller on the board. To do so, you use the Arduino programming language (based on Wiring) and the Arduino® software IDE (based on Processing).

Surf to [www.arduino.cc](www.arduino.cc) and [www.arduino.org](www.arduino.org) for more information.

# 5.    Overview

**VMA436**

This 8-channel relay interface board can control various appliances and other equipment with high current. Directly controllable by any micro-controller.

control input current (in1 to in8): 5-25 mA
control input voltage: 5-12 VDC
relay output: 250 V~, 10 A / 30 VDC, 10 A (non-inductive)
relay coli vintage: 5 VDC
dimensions: 57 x 138 mm
operating voltage: 5 V

# 6.    Pin Layout

| | |
|---|---|
| VCC | power supply |
| GND | ground |
| IN1 | low-level signal triggering terminal 1 of relay module |
| IN2 | low-level signal triggering terminal 2 of relay module |
| IN3 | low-level signal triggering terminal 3 of relay module |
| IN4 | low-level signal triggering terminal 4 of relay module |
| IN5 | low-level signal triggering terminal 5 of relay module |
| IN6 | low-level signal triggering terminal 6 of relay module |
| IN7 | low-level signal triggering terminal 7 of relay module |
| IN8 | low-level signal triggering terminal 8 of relay module |
| COM | common ground for the relay, normally connected to GND by jumper |
| GND | ground |

# 7.    High vs. Low Level

(Inx = contact such as IN1, IN2, IN3…)

Triggered at high-level means a forward voltage exists between the signal-triggering terminal (INx) and negative supply voltage. It generally connects the positive supply voltage and the triggering terminal together. When the triggering terminal has a positive supply voltage or reaches triggering voltage, the relay will pull in.

Triggered at low-level means the voltage between the signal-triggering terminal (INx) and negative supply voltage is 0 V, or the voltage at the triggering terminal is lower than the positive supply voltage. If it lowers to a triggering voltage, the relay will pull in. It generally connects negative supply voltage and triggering terminal together.

The output:

Each sub modular of the relay has one NC (normally closed), one NO (normally open) and one COM (common). There are 8 NC, 8 NO and 8 COM of the channel relay in total. NC stands for the normally closed port contact and the state without power; NO stands for the normally open port contact and the state with power; COM means the common port. You can choose the NC port or NO port according to whether it will be powered or not.

# 8. Example

Connection.
IN4======pin 4
IN5======pin 5

```
//2 relays connected to
int IN4 = 4;
int IN5 = 5;

#define ON   0
#define OFF  1
void setup()
{
  relay_init();//initialize the relay
}

void loop() {

  relay_SetStatus(ON, OFF);//turn on RELAY_1
  delay(2000);//delay 2s
  relay_SetStatus(OFF, ON);//turn on RELAY_2
  delay(2000);//delay 2s
}
void relay_init(void)//initialize the relay
{
  //set all the relays OUTPUT
  pinMode(IN4, OUTPUT);
  pinMode(IN5, OUTPUT);

  relay_SetStatus(OFF,OFF);//turn off all the relay
}
//set the status of relays
void relay_SetStatus( unsigned char status_1,  unsigned char status_2)
{
  digitalWrite(IN4, status_1);
  digitalWrite(IN5, status_2);


}
```

# 9.    More Information

Please refer to the VMA436 product page on www.velleman.eu for more information.

**Use this device with original accessories only. Velleman nv cannot be held responsible in the event of damage or injury resulting from (incorrect) use of this device. For more info concerning this product and the latest version of this manual, please visit our website www.velleman.eu. The information in this manual is subject to change without prior notice.**

# Velleman® Service and Quality Warranty

Since its foundation in 1972, Velleman® acquired extensive experience in the electronics world and currently distributes its products in over 85 countries.

All our products fulfil strict quality requirements and legal stipulations in the EU. In order to ensure the quality, our products regularly go through an extra quality check, both by an internal quality department and by specialized external organisations. If, all precautionary measures notwithstanding, problems should occur, please make appeal to our warranty (see guarantee conditions).

## General Warranty Conditions Concerning Consumer Products (for EU):

• All consumer products are subject to a 24-month warranty on production flaws and defective material as from the original date of purchase.

• Velleman® can decide to replace an article with an equivalent article, or to refund the retail value totally or partially when the complaint is valid and a free repair or replacement of the article is impossible, or if the expenses are out of proportion.

You will be delivered a replacing article or a refund at the value of 100% of the purchase price in case of a flaw occurred in the first year after the date of purchase and delivery, or a replacing article at 50% of the purchase price or a refund at the value of 50% of the retail value in case of a flaw occurred in the second year after the date of purchase and delivery.

• **Not covered by warranty:**
- all direct or indirect damage caused after delivery to the article (e.g. by oxidation, shocks, falls, dust, dirt, humidity...), and by the article, as well as its contents (e.g. data loss), compensation for loss of profits;

- consumable goods, parts or accessories that are subject to an aging process during normal use, such as batteries (rechargeable, non-rechargeable, built-in or replaceable), lamps, rubber parts, drive belts... (unlimited list);

- flaws resulting from fire, water damage, lightning, accident, natural disaster, etc.…;

- flaws caused deliberately, negligently or resulting from improper handling, negligent maintenance, abusive use or use contrary to the manufacturer's instructions;

- damage caused by a commercial, professional or collective use of the article (the warranty validity will be reduced to six (6) months when the article is used professionally);

- damage resulting from an inappropriate packing and shipping of the article;

- all damage caused by modification, repair or alteration performed by a third party without written permission by Velleman®.

• Articles to be repaired must be delivered to your Velleman® dealer, solidly packed (preferably in the original packaging), and be completed with the original receipt of purchase and a clear flaw description.

• Hint: In order to save on cost and time, please reread the manual and check if the flaw is caused by obvious causes prior to presenting the article for repair. Note that returning a non-defective article can also involve handling costs.

• Repairs occurring after warranty expiration are subject to shipping costs.

• The above conditions are without prejudice to all commercial warranties.

**The above enumeration is subject to modification according to the article (see article's manual).**

# Hukseflux
## Thermal Sensors

# SR30-M2-D1
## Digital Class A (secondary standard) pyranometer with heating and tilt sensor

- *Heated for best data availability: RVH$^{TM}$ technology outperforms traditional pyranometer ventilation*
- *The first pyranometer compliant in its standard configuration with the IEC 61724-1:2017 requirements for Class A PV monitoring systems*
- *Low cost of ownership: remote diagnostics and supported by a worldwide calibration organisation*
- *Spectrally flat: WMO compliant, also suitable for Plane of Array, diffuse, and albedo measurement*

**compliant with IEC 61724-1:2017 Class A**

**RVH$^{TM}$ technology included**

**with heating**

**with tilt sensor**

**Figure 1** *SR30-M2-D1 spectrally flat Class A pyranometer with heating, internal ventilation and tilt sensor*

EU
USA
BRA
JPN
CHN
IND
SEA

**Figure 2** *SR30 users are supported by the worldwide Hukseflux calibration and service organisation*

## Introduction

Welcome to the next level in solar radiation monitoring! The all-digital heated SR30-M2-D1 offers the highest accuracy and highest data availability: using Recirculating Ventilation and Heating (RVH$^{TM}$) technology, SR30 outperforms pyranometers equipped with traditional ventilation systems. SR30 is the ideal instrument for use in PV system performance monitoring and meteorological networks. It measures the solar radiation received by a plane surface, in W/m$^2$, from a 180 º field of view angle. SR30 is an ISO 9060 spectrally flat Class A (previously "secondary standard") pyranometer. It is employed where the highest measurement accuracy is required. SR30-M2-D1 offers improved electronics over its predecessor SR30-D1.

SR30-M2-D1 offers several advantages over competing pyranometers:

## Spectrally flat as required for meteorology and PV monitoring

The new ISO 9060:2018 version defines pyranometer classes A, B and C. The standard also adds a new subclass, called "spectrally flat". The vast majority of users needs to use instruments of the spectrally flat subclass; only spectrally flat instruments measure with high accuracy, also when a cloud obscures the sun, or when the irradiance includes reflected radiation. These situations occur for example when you measure Global Horizontal irradiance (GHI) under partly or fully cloudy skies, when you measure Plane of Array (POA), albedo or net-radiation. Normal instruments, just of class A, B or C, and not spectrally flat, only measure accurately under clear sunny skies. Using "spectrally flat" instruments is essential because this ensures:

- you can measure accurately not only horizontally under clear-blue-sky but also general GHI, POA, albedo and net radiation
- you comply with WMO requirements
- you can use the normal standardised ISO and WMO calibration procedures
- you can also measure separately the diffuse component only (creating a diffusometer) with a shadow ring or shading ball, using the same instrument model
- you can perform uncertainty evaluations with negligible (zero) spectral errors

## Heated for high data availability, featuring RVH™ technology

High data availability is attained by heating of the outer dome using ventilation between the inner and outer dome. This space forms a closed circuit together with the instrument body; ventilated air is not in contact with ambient air. RVH™ - Recirculating Ventilation and Heating - technology, developed by Hukseflux, suppresses dew and frost deposition and is as effective as traditional ventilation systems, without the maintenance hassle and large footprint.

- low power consumption: SR30-M2-D1 requires less than 3 W, compared to 10 W for traditional ventilation systems
- low maintenance: SR30-M2-D1 does not require filter cleaning



**Figure 3** *Heated to counter frost and dew deposition: clear difference between a non-heated pyranometer (back) and SR30 with RVH™ technology (front)*

RVH™ uses SR30's built-in heater and ventilator. The dome of SR30 pyranometer is heated by ventilating the area between the inner and outer dome. RVH™ is much more efficient than traditional ventilation, where most of the heat is carried away with the ventilation air. Recirculating ventilation is as effective in suppressing dew and frost deposition at less than 3 W as traditional ventilation is at 10 W. RVH™ technology keeps domes and sensor in perfect thermal equilibrium, which also leads to a reduction of zero offsets.
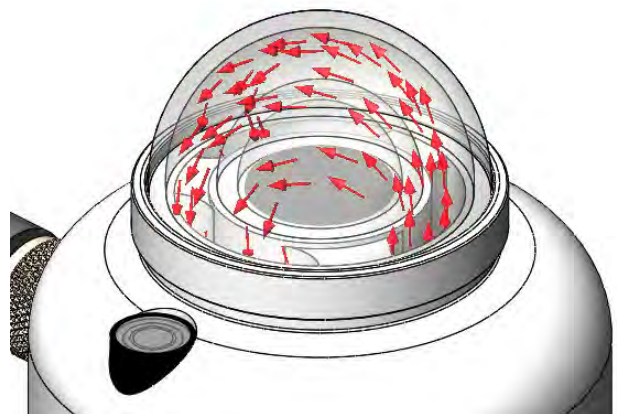


**Figure 4** *Heating, how it's done: recirculating ventilation and heating between the inner- and outer dome forming a closed circuit with the body is much more power efficient than traditional ventilation systems*

**Figure 5** *SR30-M2-D1 includes a digital tilt angle measurement, very practical for remote checks of instrument orientation. The image shows two SR30's in PV system monitoring, one measuring in Plane of Array (POA).*

## Tilt angle measurement included

SR30 includes a tilt sensor. This is very practical for remote checks of instrument condition or to monitor PV systems with solar trackers. The sensor measures with high accuracy, within 1 ˚, and is tested and temperature compensated between -30 and + 50 ˚C.

## Compliant with IEC 61724-1:2017, Class A and B

Only SR30 offers both, without the need for additional accessories. Most competing pyranometers do not even comply with Class B, which requires heating.

## Environmental impact

We analysed the environmental impact of SR30 by comparison to its closest competitors; externally ventilated pyranometers such as SR20 + VU01. SR30's impact is significantly lower due to:

- lower power consumption during use
- lower transport volume

Take a look at our analysis.

## Low cost of ownership

SR30-M2-D1 is an affordable spectrally flat Class A instrument and is designed for low cost of ownership, which is mainly determined by costs of installation, on-site inspections, servicing and

calibration:

- low demand on infrastructure: SR30's RVH$^{TM}$ requires less than 3 W power, compared to 10 W for traditional ventilation systems
- reduction of unnecessary on-site inspection by remote diagnostics
- designed for efficient servicing; easy local diagnostics.
- supported by an efficient calibration and maintenance organisation. Hukseflux offers local support in the main global economies: USA, EU, China, India, Japan and Brazil. Recalibration is recommended every 2 years, which is good practice in the industry.

## Remote sensor diagnostics

Besides solar radiation, SR30 outputs sensor diagnostics, including:

- tilt angle
- internal ventilator speed (RPM)
- internal humidity
- heater current

Remote diagnostics permits real-time status monitoring, reducing the need for (un)scheduled field inspections.

## Liabilities covered: test certificates

As required by ISO 9060 for Class A classification, each SR30 is supplied with test results:

- sensitivity
- directional response
- temperature response
- tilt angle measurement

## Diffuse radiation measurement

With its outstanding zero offset and spectrally flat specifications, SR30 is also the instrument of choice for high-accuracy diffuse radiation measurement.

## Operation in low power mode

Heater and ventilation may be remotely switched on and off; operation at < 0.1 W is possible by switching both the internal ventilator and heater off. Although zero offset will then increase slightly, overall performance will still comply with the Class A classification.

## Suggested use

- PV system performance monitoring
- scientific meteorological observations

## SR30 design

SR30 pyranometer employs a state-of-the-art thermopile sensor with black coated surface, two domes and an anodised aluminium body. It offers a digital output via Modbus RTU over 2-wire RS-485. The pyranometer dome is heated by ventilating the area between the inner and outer dome using RVH™ - Recirculating Ventilation and Heating - technology.
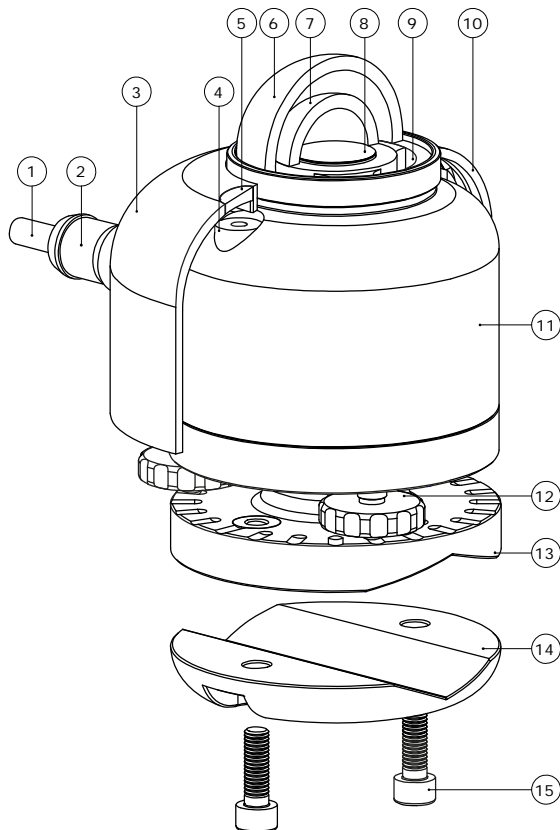


**Figure 6** *overview of SR30: (1) cable, (2) connector, (3) sun screen, (4) bubble level, (5) bubble level window, (6) outer dome, (7) inner dome, (8) thermal sensor with black coating, (9) internal ventilation vents, (10) quick release system of sun screen, (11) instrument body, (12) levelling feet, (13) optional spring-loaded levelling mount, (14) optional tube mount, (15) screws included with tube mount*

## Improved electronics

SR30-M2-D1 offers improved electronics design over its predecessor SR30-D1 and is delivered with new Hukseflux Sensor Manager software.

## New Hukseflux Sensor Manager software

For communication between a PC and SR30, new Sensor Manager software is included. It (version v2021 or higher) allows the user to plot and export data, and change the SR30-M2-D1 Modbus address and communication settings. Also, the digital outputs may be viewed for sensor diagnostics.

## SR30-M2-D1 specifications

| | |
|---|---|
| Measurand | hemispherical solar radiation |
| ISO classification | |
| ISO 9060:2018 | spectrally flat Class A pyranometer |
| ISO 9060:1990 | secondary standard pyranometer |
| WMO performance level | high quality pyranometer |
| IEC 61724-1 compliance | meets Class A and B PV monitoring system requirements |
| Calibration uncertainty | < 1.2 % (k = 2) |
| Measurand | sensor tilt angle |
| Tilt measurement uncertainty | ± 1 ° (0 to 90 ° tilt, -30 to + 50 °C) |
| Heating | included |
| Ventilation | included |
| Technology employed | Recirculating Ventilation and Heating (RVH™) |
| Standard operating mode | heated and ventilated |
| Power consumption | < 3 W at 12 VDC |
| Zero offset a | < 2 W/m$^2$ |
| Calibration traceability | to WRR |
| Calibration registers | accessible to users |
| Calibration certificate | included, content limited according to ISO/IEC 17025- 7.8.1.3. |
| Spectral range | 285 to 3000 x 10$^{-9}$ m |
| Rated operating temperature range | -40 to +80 ºC |
| Temperature response | < ± 0.4 % (-30 to +50 °C) |
| Temperature response test of individual instrument | report included |
| Directional response test of individual instrument | report included to 95 ° |
| Tilt sensor test of individual instrument | report included (0 to 90 ° tilt, -30 to + 50 °C) |
| Standard cable length | 5 m (see options) |
| Rated operating voltage range | 8 to 30 VDC |

## Optional operation in low power mode

| | |
|---|---|
| Operating condition | heater and ventilator [OFF] |
| Zero offset a | 5 W/m$^2$ (unventilated) |
| Power consumption | < 0.1 W at 12 VDC |

## Digital communication

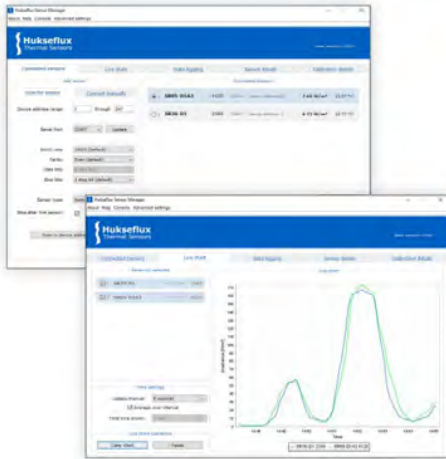| | |
|---|---|
| Digital output | - irradiance in W/m$^2$ |
| | - instrument body temperature in ºC |
| | - tilt angle in ° |
| | - internal humidity in % |
| | - ventilator speed in RPM |
| Communication protocol | Modbus |
| Transmission mode | RTU |
| Hardware interface | 2-wire (half duplex) RS-485 |

Figure 7 *improved Sensor Manager software, included with SR30 pyranometer, allows the user to change the Modbus address and communication settings*

## Options

- spring-loaded levelling; a practical mount for easy mounting, levelling and instrument exchange on flat surfaces
- tube levelling mount with set of bolts
- longer cable; 10 and 20 metres
- calibration certificate including name and contact information of the customer

## Levelling mounts

There are several mounting options available for SR30. They allow for simplified mounting, levelling and instrument exchange on a flat surface or a tube.



Figure 8 *optional spring-loaded levelling and tube mount for SR30*



Figure 9 *PMF01 pyranometer mounting fixture can be used for easy installation of a pyranometer, in this case SR30, in Plane of Array for PV system performance monitoring and meteorological applications*

## See also

- SRA30 albedometer consisting of two SR30's
- SR05, an economical solution often used for monitoring small scale PV systems
- PMF series mounting fixtures
- consult our pyranometer selection guide
- introduction of SR30 on our YouTube channel
- environmental impact analysis of SR30
- why ventilate and heat pyranometers
- view our complete range of solar sensors

## About Hukseflux

Hukseflux Thermal Sensors makes sensors and measuring systems. Our aim is to let our customers work with the best possible data. Many of our products are used in support of energy transition and efficient use of energy. We also provide services: calibration and material characterisation. Our main area of expertise is measurement of heat transfer and thermal quantities such as solar radiation, heat flux and thermal conductivity. Hukseflux is ISO 9001 certified. Hukseflux products and services are offered worldwide via our office in Delft, the Netherlands and local distributors.

Are you interested in this product?
E-mail us at: info@hukseflux.com

# Hukseflux
## Thermal Sensors

## SR30 digital spectrally flat Class A pyranometer with heating

Nowadays, the best pyranometers are made by Hukseflux Thermal Sensors. This overview of features and benefits of SR30-M2-D1 gives you some of the reasons why! Whatever your application is, Hukseflux offers the highest accuracy in every class at the most attractive price level.

### IEC

**Best compliance with standards**
- first pyranometer to comply with IEC 61724-1 Class A requirements
- heated domes, Recirculating Ventilation and Heating (RVH™) technology
- tilt measurement

### Best paperwork
- all ISO required reports with every individual sensor
- temperature response testing -30 to 50 ºC
- full directional response testing to 95°
- tilt sensor testing (0 to 90° tilt, -30 to + 50 °C)

### ISO

### Best accuracy and data availability
- spectrally flat
- suppresses dew and frost deposition
- lowest zero offsets
- no external ventilator required
- low power consumption

### Best diagnostics
- tilt angle
- humidity
- temperature
- ventilator speed (RPM)

### Best tilt sensor and levelling
- remote check using on-board tilt sensor
- window for visible bubble level
- with optional spring-loaded levelling mount
- easy mounting, levelling and instrument exchange

### Best worldwide support
- ISO/IEC 17025 calibration available
- efficient calibration support
- fast servicing organisation
- local stock of spare parts

# Hall Effect Linear Current Sensor with Overcurrent Fault Output for <100 V Isolation Applications

## Features and Benefits

- No external sense resistor required; single package solution
- Reduced Power Loss:
  - $0.6 \ m\Omega$ internal conductor resistance on EX package
  - $1.2 \ m\Omega$ internal conductor resistance on LC package
- Economical low- and high-side current sensing
- Output voltage proportional to AC or DC currents
- ±12.5 A and ±25 A full scale sensing ranges on LC package
- ±15.5 A and ±31 A full scale sensing ranges on EX package
- Overcurrent $\overline{FAULT}$ trips and latches at 100% of full-scale current
- Low-noise analog signal path
- 100 kHz bandwidth
- Small footprint, low-profile SOIC8 and QFN packages
- 3.0 to 5.5 V, single supply operation
- Integrated electrostatic shield for output stability
- Factory-trimmed for accuracy
- Extremely stable output offset voltage
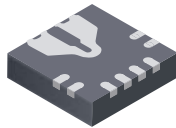- Zero magnetic hysteresis
- Ratiometric output from supply voltage

## Packages:
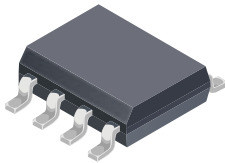
8-pin SOICN
with internally fused path
(LC package)
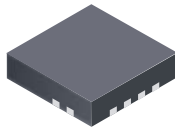
12-contact QFN
3 mm × 3 mm × 0.75 mm
(EX package)

Approximate Scale 1:1

## Description

The Allegro™ ACS711 provides economical and precise solutions for AC or DC current sensing in <100 V audio, communications systems, and white goods. The device package allows for easy implementation by the customer. Typical applications include circuit protection, current monitoring, and motor and inverter control.

The device consists of a linear Hall sensor circuit with a copper conduction path located near the surface of the die. Applied current flowing through this copper conduction path generates a magnetic field which is sensed by the integrated Hall IC and converted into a proportional voltage. Device accuracy is optimized through the close proximity of the magnetic signal to the Hall transducer.

The output of the device has a positive slope proportional to the current flow from IP+ to IP– (pins 1 and 2, to pins 3 and 4). The internal resistance of this conductive path is $0.6 \ m\Omega$ for the EX package, and $1.2 \ m\Omega$ for the LC package, providing a non-intrusive measurement interface that saves power in applications that require energy efficiency.

The ACS711 is optimized for low-side current sensing applications, although the terminals of the conductive path are electrically isolated from the sensor IC leads, providing sufficient internal creepage and clearance dimensions for a low AC or DC working voltage applications. The thickness

*Continued on the next page...*

## Typical Application
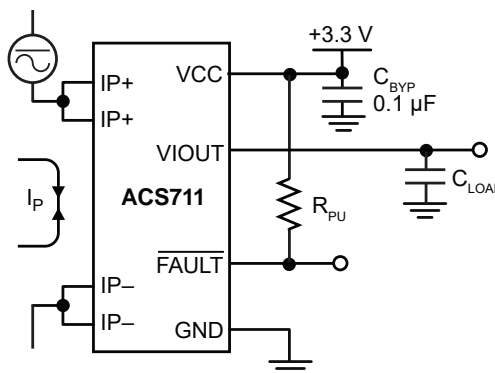


Application 1. The ACS711 outputs an analog signal, $V_{IOUT}$, that varies linearly with the bi-directional AC or DC primary current, $I_P$, within the range specified. The $\overline{FAULT}$ pin trips when $I_P$ reaches ±100% of its full-scale current.

## Description (continued)

of the copper conductor allows survival of the device at up to 5×
overcurrent conditions.

The ACS711 is provided in small, surface mount packages: SOIC8
and QFN12. The leadframe is plated with 100% matte tin, which
is compatible with standard lead (Pb) free printed circuit board

assembly processes. Internally, the device is Pb-free, except for
flip-chip high-temperature Pb-based solder balls, currently exempt
from RoHS. The device is fully calibrated prior to shipment from
the factory.

### Selection Guide

| Part Number | $T_A$ (°C) | Optimized Accuracy Range, $I_P$ (A) | Sensitivity[2], Sens (Typ) (mV/A) | Package | Packing[1] |
|---|---|---|---|---|---|
| ACS711ELCTR-12AB-T | –40 to 85 | ±12.5 | 110 | 8-pin SOICN | 3000 pieces/reel |
| ACS711KLCTR-12AB-T | –40 to 125 | | | | |
| ACS711ELCTR-25AB-T | –40 to 85 | ±25 | 55 | | |
| ACS711KLCTR-25AB-T | –40 to 125 | | | | |
| ACS711EEXLT-15AB-T[3] | –40 to 85 | ±15.5 | 90 | 12-contact QFN with fused current loop | 1500 pieces/reel |
| ACS711KEXLT-15AB-T[3] | –40 to 125 | | | | |
| ACS711EEXLT-31AB-T[3] | –40 to 85 | ±31 | 45 | | |
| ACS711KEXLT-31AB-T[3] | –40 to 125 | | | | |

[1]Contact Allegro for additional packing options.
[2]Sensitivity measured with $V_{CC}$ = 3.3 V.
[3]QFN package not qualified for automotive applications.

### Absolute Maximum Ratings

| Characteristic | Symbol | Notes | Rating | Units |
|---|---|---|---|---|
| Supply Voltage | $V_{CC}$ | | 7 | V |
| Reverse Supply Voltage | $V_{RCC}$ | | –0.1 | V |
| Output Voltage | $V_{IOUT}$ | | 7 | V |
| Reverse Output Voltage | $V_{RIOUT}$ | | –0.1 | V |
| Working Voltage for Basic Isolation | $V_{WORKING}$ | Voltage applied between pins 1-4 and 5-8 | 100 | VAC peak or VDC |
| $\overline{FAULT}$ Pin Voltage | $V_{FAULT}$ | | 7 | V |
| Overcurrent Transient Tolerance | $I_{POC}$ | 1 pulse, 100 ms | 100 | A |
| Nominal Operating Ambient Temperature | $T_A$ | Range E | –40 to 85 | ºC |
| | | Range K | –40 to 125 | ºC |
| Maximum Junction Temperature | $T_J$(max) | | 165 | ºC |
| Storage Temperature | $T_{stg}$ | | –65 to 170 | ºC |

Allegro MicroSystems, LLC
115 Northeast Cutoff
Worcester, Massachusetts 01615-0036 U.S.A.
1.508.853.5000; www.allegromicro.com

2

## Functional Block Diagram
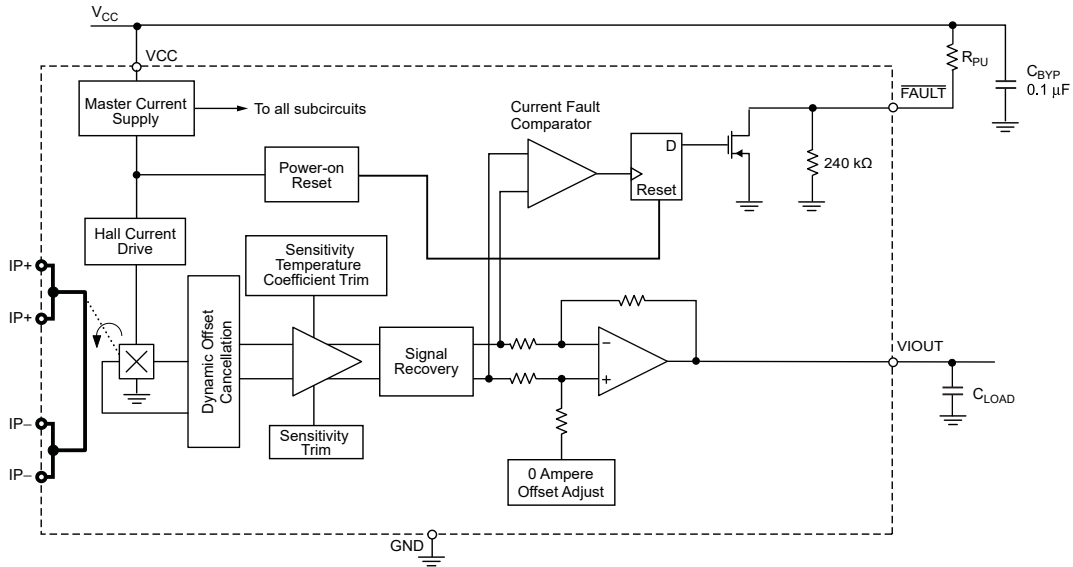


## Pin-out Diagrams
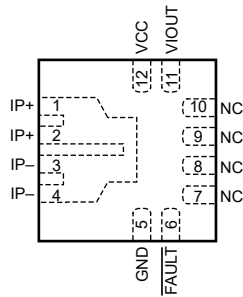


EX Package
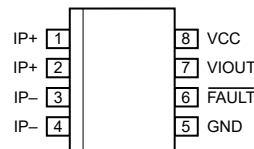
LC Package

## Terminal List Table

| Name | Number | | Description |
|------|--------|------|-------------|
| | **EX** | **LC** | |
| GND | 5 | 5 | Signal ground terminal |
| FAULT | 6 | 6 | Overcurrent fault; active low |
| IP– | 3 and 4 | 3 and 4 | Terminals for current being sensed; fused internally |
| IP+ | 1 and 2 | 1 and 2 | Terminals for current being sensed; fused internally |
| NC | 7, 8, 9, 10 | – | No connection |
| VCC | 12 | 8 | Device power supply terminal |
| VIOUT | 11 | 7 | Analog output signal |

**COMMON OPERATING CHARACTERISTICS** Valid across the full range of $T_A$ for the LC package and at $T_A$ = 25°C for the EX package, $V_{CC}$ = 3.3 V, unless otherwise specified

| Characteristic | Symbol | Test Conditions | Min. | Typ. | Max. | Units |
|---|---|---|---|---|---|---|
| **ELECTRICAL CHARACTERISTICS** | | | | | | |
| Supply Voltage[1] | $V_{CC}$ | | 3 | 3.3 | 5.5 | V |
| Supply Current | $I_{CC}$ | $V_{CC}$ = 3.3 V, output open | – | 4 | 5.5 | mA |
| Output Capacitance Load | $C_{LOAD}$ | VIOUT to GND | – | – | 1 | nF |
| Output Resistive Load | $R_{LOAD}$ | VIOUT to GND | 15 | – | – | kΩ |
| Primary Conductor Resistance | $R_{IP}$ | EX package | – | 0.6 | – | mΩ |
| | | LC package, $T_A$ = 25°C | – | 1.2 | – | mΩ |
| VIOUT Rise Time | $t_r$ | $I_P$ = $I_{PMAX}$, $T_A$ = 25°C, COUT = open | – | 3.5 | – | µs |
| Propagation Delay Time | $t_{PROP}$ | $I_P$ = $I_P$(max), $T_A$ = 25°C, COUT = open | – | 1.2 | – | µs |
| Response Time | $t_{RESPONSE}$ | $I_P$ = $I_P$(max), $T_A$ = 25°C, COUT = open | – | 4.6 | – | µs |
| Internal Bandwidth[2] | $BW_I$ | –3 dB, $T_A$ = 25°C | – | 100 | – | kHz |
| Nonlinearity | $E_{LIN}$ | Over full range of $I_P$ | – | ±1 | – | % |
| Symmetry | $E_{SYM}$ | Apply full scale $I_P$ | – | 100 | – | % |
| VIOUT Saturation Voltages | $V_{IOH}$ | | $V_{CC}$ – 0.3 | – | – | V |
| | $V_{IOL}$ | | – | – | 0.3 | V |
| Quiescent Output Voltage | $V_{IOUT(Q)}$ | $I_P$ = 0 A, $T_A$ = 25°C | – | $V_{CC}$ / 2 | – | V |
| Power-On Time | $t_{PO}$ | Output reaches 90% of steady-state level, $T_A$ = 25°C, 20 A present on primary conductor | – | 35 | – | µs |
| **$\overline{FAULT}$ Pin Characteristics** | | | | | | |
| $\overline{FAULT}$ Operating Point | $I_{FAULT}$ | | – | ± 1 x $I_P$ | – | A |
| $\overline{FAULT}$ Output Pullup Resistor | $R_{PU}$ | | 1 | – | – | kΩ |
| $\overline{FAULT}$ Output Voltage | $V_{OH}$ | | – | $V_{CC}$ – 0.3 | – | V |
| | $V_{OL}$ | $R_{PU}$ = 1 kΩ | – | 0.3 | – | V |
| $\overline{FAULT}$ Response Time | $t_{FAULT}$ | Measured from \| $I_P$ \| > \| $I_{FAULT}$ \| to $V_{FAULT}$ ≤ $V_{OL}$ | – | 1.3 | – | µs |
| $V_{CC}$ Off Voltage Level for Fault Reset[3] | $V_{CCFR}$ | | – | – | 200 | mV |
| $V_{CC}$ Off Duration for Fault Reset[3] | $t_{CCFR}$ | | 100 | – | – | µs |

[1]Devices are programmed for maximum accuracy at 3.3 V $V_{CC}$ levels. The device contains ratiometry circuits that accurately alter the 0 A Output Voltage and Sensitivity level of the device in proportion to the applied $V_{CC}$ level.  However, as a result of minor nonlinearities in the ratiometry circuit additional output error will result when $V_{CC}$ varies from the 3.3 V $V_{CC}$ level. Customers that plan to operate the device from a 5 V regulated supply should contact their local Allegro sales representative regarding expected device accuracy levels under these bias conditions.

[2]Calculated using the formula $BW_I$ = 0.35 / $t_r$.

[3]After the $\overline{FAULT}$ pin is latched low, the only way to reset it is through a power-off and power-on cycle on the VCC pin. For fault reset, $V_{CC}$ must stay below $V_{CCFR}$ for a period greater than $t_{CCFR}$ before settling to the normal operation voltage (3 to 5.5 V).

### x12AB PERFORMANCE CHARACTERISTICS for LC package and E Temperature Range[1]

$T_A$ = 25°C and $V_{CC}$ = 3.3 V, unless otherwise specified

| Characteristic | Symbol | Test Conditions | Min. | Typ. | Max. | Units |
|---|---|---|---|---|---|---|
| Optimized Accuracy Range | $I_P$ | | −12.5 | – | 12.5 | A |
| Sensitivity | Sens | Over full range of $I_P$ | – | 110 | – | mV/A |
| | | Full scale of $I_P$ applied for 5 ms, $T_A$ = –40°C to 25°C | – | 110 | – | mV/A |
| | | Full scale of $I_P$ applied for 5 ms, $T_A$ = 25°C to 85°C | – | 110 | – | mV/A |
| Noise[2] | $V_{NOISE}$ | $T_A$ = 25°C, no external low pass filter on VIOUT | – | 11 | – | mV |
| Electrical Offset Voltage | $V_{OE(TA)}$ | $I_P$ = 0 A, $T_A$ = 25°C | – | ±5 | – | mV |
| | $V_{OE(TOP)HT}$ | $I_P$ = 0 A, $T_A$ = 25°C to 85°C | – | ±40 | – | mV |
| | $V_{OE(TOP)LT}$ | $I_P$ = 0 A, $T_A$ = –40°C to 25°C | – | ±50 | – | mV |
| Total Output Error[3] | $E_{TOT}$ | $I_P$ = ±12.5 A, $T_A$ = –40°C to 85°C | – | ±5 | – | % |

[1]See Characteristic Performance Data for parameter distributions over temperature.

[2]±3 sigma noise voltage.

[3]Percentage of $I_P$, with $I_P$ = ±12.5 A.

### x12AB PERFORMANCE CHARACTERISTICS for LC package and K Temperature Range[1]

$T_A$ = 25°C and $V_{CC}$ = 3.3 V, unless otherwise specified

| Characteristic | Symbol | Test Conditions | Min. | Typ. | Max. | Units |
|---|---|---|---|---|---|---|
| Optimized Accuracy Range | $I_P$ | | −12.5 | – | 12.5 | A |
| Sensitivity | Sens | Over full range of $I_P$ | – | 110 | – | mV/A |
| | | Full scale of $I_P$ applied for 5 ms, $T_A$ = –40°C to 25°C | – | 110 | – | mV/A |
| | | Full scale of $I_P$ applied for 5 ms, $T_A$ = 25°C to 125°C | – | 110 | – | mV/A |
| Noise[2] | $V_{NOISE}$ | $T_A$ = 25°C, no external low pass filter on VIOUT | – | 11 | – | mV |
| Electrical Offset Voltage | $V_{OE(TA)}$ | $I_P$ = 0 A, $T_A$ = 25°C | – | ±5 | – | mV |
| | $V_{OE(TOP)HT}$ | $I_P$ = 0 A, $T_A$ = 25°C to 125°C | – | ±40 | – | mV |
| | $V_{OE(TOP)LT}$ | $I_P$ = 0 A, $T_A$ = –40°C to 25°C | – | ±50 | – | mV |
| Total Output Error[3] | $E_{TOT}$ | $I_P$ = ±12.5 A, $T_A$ = –40°C to 125°C | – | ±5 | – | % |

[1]See Characteristic Performance Data for parameter distributions over temperature.

[2]±3 sigma noise voltage.

[3]Percentage of $I_P$, with $I_P$ = ±12.5 A.

### x15AB PERFORMANCE CHARACTERISTICS[1]

$T_A$ = 25°C and $V_{CC}$ = 3.3 V, unless otherwise specified

| Characteristic | Symbol | Test Conditions | Min. | Typ. | Max. | Units |
|---|---|---|---|---|---|---|
| Optimized Accuracy Range | $I_P$ | | −15.5 | – | 15.5 | A |
| Sensitivity | Sens | Across full range of $I_P$ | – | 90 | – | mV/A |
| Noise[2] | $V_{NOISE}$ | No external low pass filter on VIOUT | – | 11 | – | mV |
| Electrical Offset Voltage | $V_{OE(TA)}$ | $I_P$ = 0 A | – | ±5 | – | mV |
| | $V_{OE(TOP)HT}$ | $I_P$ = 0 A, $T_A$ = 25°C to $T_A$(max) | – | ±40 | – | mV |
| | $V_{OE(TOP)LT}$ | $I_P$ = 0 A, $T_A$ = –40°C to 25°C | – | ±50 | – | mV |
| Total Output Error[3] | $E_{TOT}$ | $I_P$ = ±12.5 A, $T_A$ = –40°C to $T_A$(max) | – | ±5 | – | % |

[1]See Characteristic Performance Data for parameter distributions across the full temperature range.

[2]±3 sigma noise voltage.

[3]Percentage of $I_P$, with $I_P$ = ±15.5 A.

Allegro MicroSystems, LLC
115 Northeast Cutoff
Worcester, Massachusetts 01615-0036 U.S.A.
1.508.853.5000; www.allegromicro.com

5

## x25AB PERFORMANCE CHARACTERISTICS for for LC package and E Temperature Range[1]

$T_A$ = 25°C and $V_{CC}$ = 3.3 V, unless otherwise specified

| Characteristic | Symbol | Test Conditions | Min. | Typ. | Max. | Units |
|---|---|---|---|---|---|---|
| Optimized Accuracy Range | $I_P$ | | −25 | – | 25 | A |
| Sensitivity | Sens | Over full range of $I_P$ | – | 55 | – | mV/A |
| | | Full scale of $I_P$ applied for 5 ms, $T_A$ = –40°C to 25°C | – | 55 | – | mV/A |
| | | Full scale of $I_P$ applied for 5 ms, $T_A$ = 25°C to 85°C | – | 55 | – | mV/A |
| Noise[2] | $V_{NOISE}$ | $T_A$ = 25°C, no external low pass filter on VIOUT | – | 8 | – | mV |
| Electrical Offset Voltage | $V_{OE(TA)}$ | $I_P$ = 0 A, $T_A$ = 25°C | – | ±5 | – | mV |
| | $V_{OE(TOP)HT}$ | $I_P$ = 0 A, $T_A$ = 25°C to 85°C | – | ±30 | – | mV |
| | $V_{OE(TOP)LT}$ | $I_P$ = 0 A, $T_A$ = –40°C to 25°C | – | ±35 | – | mV |
| Total Output Error[3] | $E_{TOT}$ | $I_P$ =±25 A, $T_A$ = –40°C to 85°C | – | ±4 | – | % |

[1]See Characteristic Performance Data for parameter distributions over temperature.

[2]±3 sigma noise voltage.

[3]Percentage of $I_P$, with $I_P$ = ±25 A.

## x25AB PERFORMANCE CHARACTERISTICS for LC package and K Temperature Range[1]

$T_A$ = 25°C and $V_{CC}$ = 3.3 V, unless otherwise specified

| Characteristic | Symbol | Test Conditions | Min. | Typ. | Max. | Units |
|---|---|---|---|---|---|---|
| Optimized Accuracy Range | $I_P$ | | −25 | – | 25 | A |
| Sensitivity | Sens | Over full range of $I_P$ | – | 55 | – | mV/A |
| | | Full scale of $I_P$ applied for 5 ms, $T_A$ = –40°C to 25°C | – | 55 | – | mV/A |
| | | Full scale of $I_P$ applied for 5 ms, $T_A$ = 25°C to 125°C | – | 55 | – | mV/A |
| Noise[2] | $V_{NOISE}$ | $T_A$ = 25°C, no external low pass filter on VIOUT | – | 8 | – | mV |
| Electrical Offset Voltage | $V_{OE(TA)}$ | $I_P$ = 0 A, $T_A$ = 25°C | – | ±5 | – | mV |
| | $V_{OE(TOP)HT}$ | $I_P$ = 0 A, $T_A$ = 25°C to 125°C | – | ±30 | – | mV |
| | $V_{OE(TOP)LT}$ | $I_P$ = 0 A, $T_A$ = –40°C to 25°C | – | ±35 | – | mV |
| Total Output Error[3] | $E_{TOT}$ | $I_P$ =±25 A, $T_A$ = –40°C to 125°C | – | ±4 | – | % |

[1]See Characteristic Performance Data for parameter distributions over temperature.

[2]±3 sigma noise voltage.

[3]Percentage of $I_P$, with $I_P$ = ±25 A.

## x31AB PERFORMANCE CHARACTERISTICS[1]

$T_A$ = 25°C and $V_{CC}$ = 3.3 V, unless otherwise specified

| Characteristic | Symbol | Test Conditions | Min. | Typ. | Max. | Units |
|---|---|---|---|---|---|---|
| Optimized Accuracy Range | $I_P$ | | −31 | – | 31 | A |
| Sensitivity | Sens | Across full range of $I_P$ | – | 45 | – | mV/A |
| Noise[2] | $V_{NOISE}$ | No external low pass filter on VIOUT | – | 8 | – | mV |
| Electrical Offset Voltage | $V_{OE(TA)}$ | $I_P$ = 0 A | – | ±5 | – | mV |
| | $V_{OE(TOP)HT}$ | $I_P$ = 0 A, $T_A$ = 25°C to $T_A$(max) | – | ±30 | – | mV |
| | $V_{OE(TOP)LT}$ | $I_P$ = 0 A, $T_A$ = –40°C to 25°C | – | ±35 | – | mV |
| Total Output Error[3] | $E_{TOT}$ | $I_P$ =±25 A, $T_A$ = –40°C to $T_A$(max) | – | ±4 | – | % |

[1]See Characteristic Performance Data for parameter distributions across the full temperature range.

[2]±3 sigma noise voltage.

[3]Percentage of $I_P$, with $I_P$ = ±31 A.

**Thermal Characteristics**

| Characteristic | Symbol | Test Conditions[1] | Value | Units |
|---|---|---|---|---|
| Package Thermal Resistance, Junction to Lead | $R_{\theta JL}$ | LC package, mounted on Allegro ASEK 711 evaluation board | 5 | ºC/W |
| Package Thermal Resistance, Junction to Ambient[2] | $R_{\theta JA}$ | LC package, mounted on Allegro 85-0404 evaluation board, includes the power consumed by the board | 23 | ºC/W |
| | | EX package, mounted on Allegro 85-0528 evaluation board, includes the power consumed by the board | 24 | ºC/W |

[1]Additional thermal information available on the Allegro website
[2]The Allegro evaluation board has 1500 mm[2] of 2 oz. copper on each side, connected to pins 1 and 2, and to pins 3 and 4, with thermal vias connecting the layers. Performance values include the power consumed by the PCB. Further details on the board are available from the Frequently Asked Questions document on our website.

*Allegro*™
MicroSystems, LLC

Allegro MicroSystems, LLC
115 Northeast Cutoff
Worcester, Massachusetts 01615-0036 U.S.A.
1.508.853.5000; www.allegromicro.com
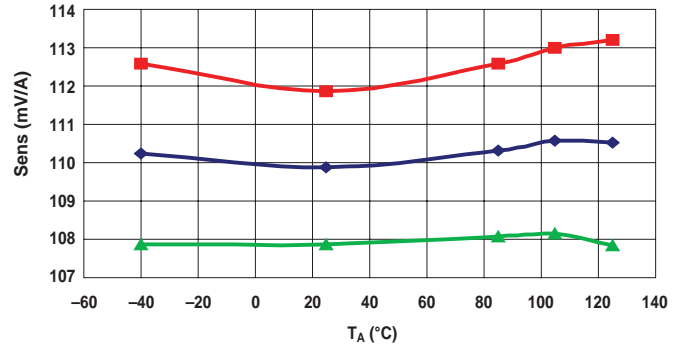
7

## Characteristic Performance Data
Data taken using the ACS711KLC-12A, $V_{CC}$ = 3.3 V
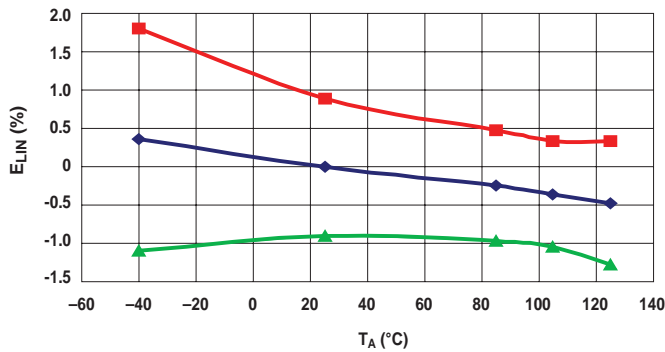
### Accuracy Data
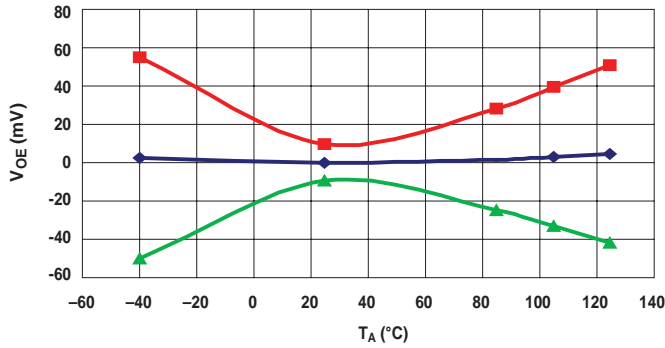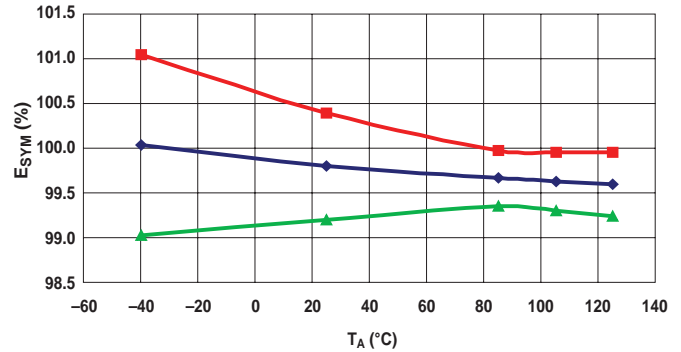
**Electrical Offset Voltage versus Ambient Temperature**

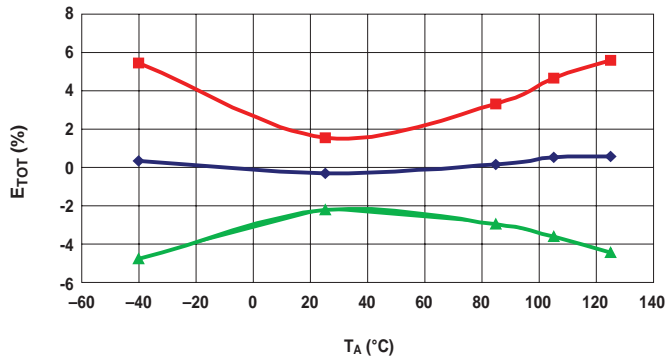**Sensitivity versus Ambient Temperature**

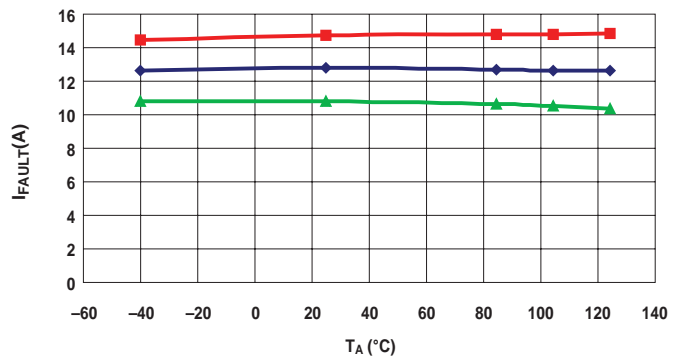**Nonlinearity versus Ambient Temperature**

**Symmetry versus Ambient Temperature**

**Total Output Error versus Ambient Temperature**

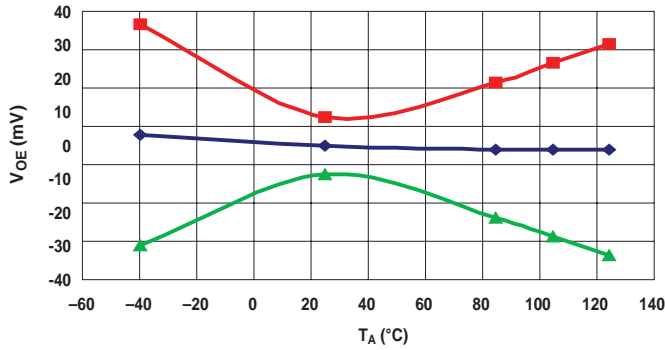**Fault Operating Point versus Ambient Temperature**
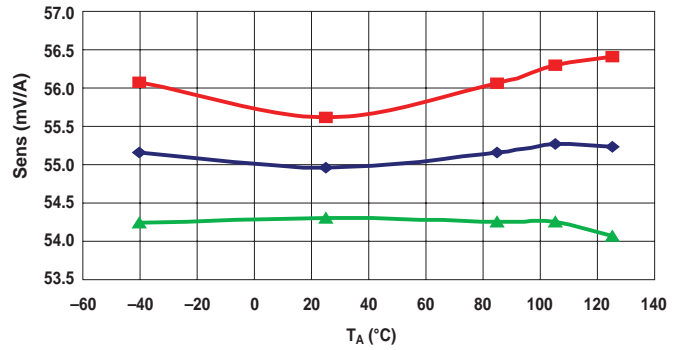
Typical Maximum Limit — Mean — Typical Minimum Limit

## Characteristic Performance Data
Data taken using the ACS711KLC-25A, $V_{CC}$ = 3.3 V
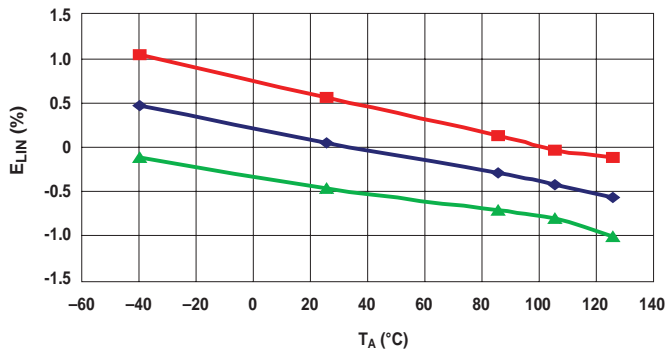
### Accuracy Data
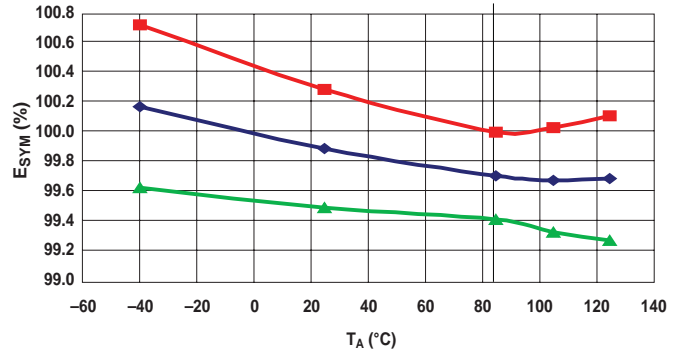
**Electrical Offset Voltage versus Ambient Temperature**

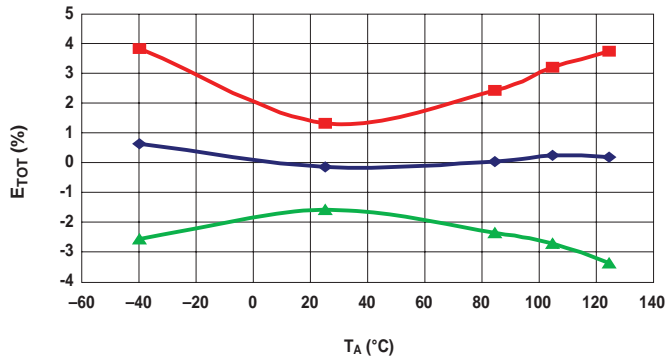**Sensitivity versus Ambient Temperature**

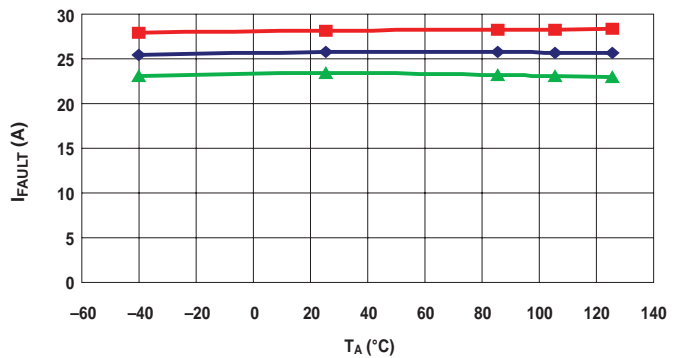**Nonlinearity versus Ambient Temperature**

**Symmetry versus Ambient Temperature**

**Total Output Error versus Ambient Temperature**

**Fault Operating Point versus Ambient Temperature**
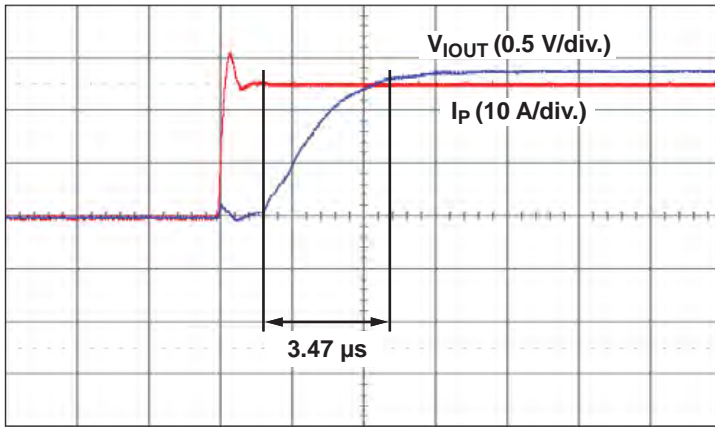
— ■ — Typical Maximum Limit    — ◆ — Mean    — ▲ — Typical Minimum Limit

## Characteristic Performance Data
Data taken using the ACS711KLC-25A

### Timing Data

**Rise Time**



V$_{IOUT}$ (0.5 V/div.)

I$_P$ (10 A/div.)

3.47 µs

t (2 µs/div.)

**Propagation Delay Time**



V$_{IOUT}$ (0.5 V/div.)

I$_P$ (10 A/div.)

1.24 µs

t (2 µs/div.)

**Response Time**



V$_{IOUT}$ (0.5 V/div.)

I$_P$ (10 A/div.)

4.62 µs

t (2 µs/div.)

**Fault Response**



I$_P$ (10 A/div.)

1.28 µs

Fault (2 V/div.)

t (2 µs/div.)

*Allegro* MicroSystems, LLC

Allegro MicroSystems, LLC
115 Northeast Cutoff
Worcester, Massachusetts 01615-0036 U.S.A.
1.508.853.5000; www.allegromicro.com

10
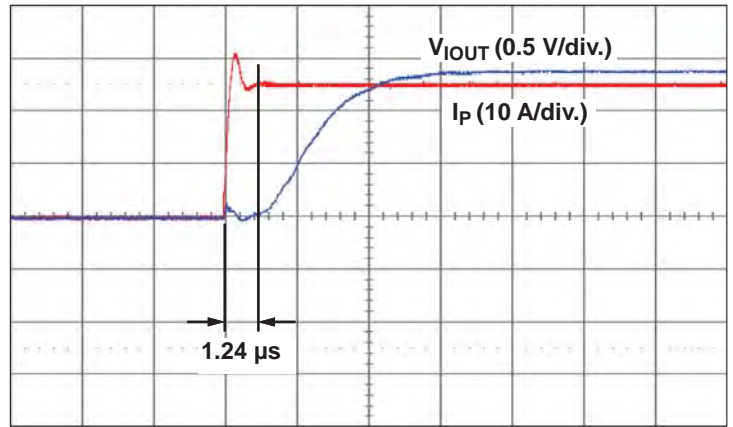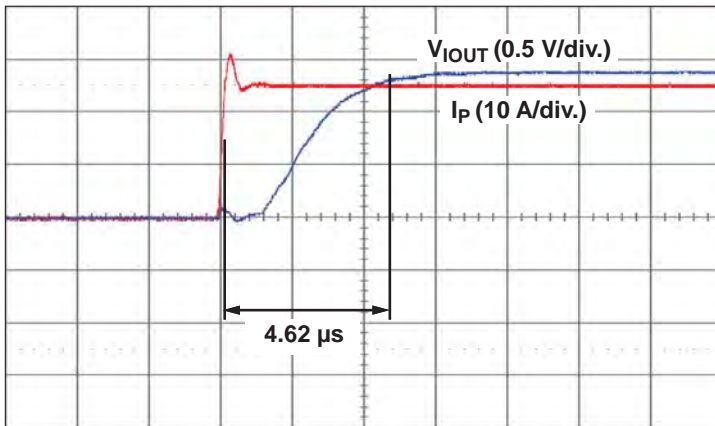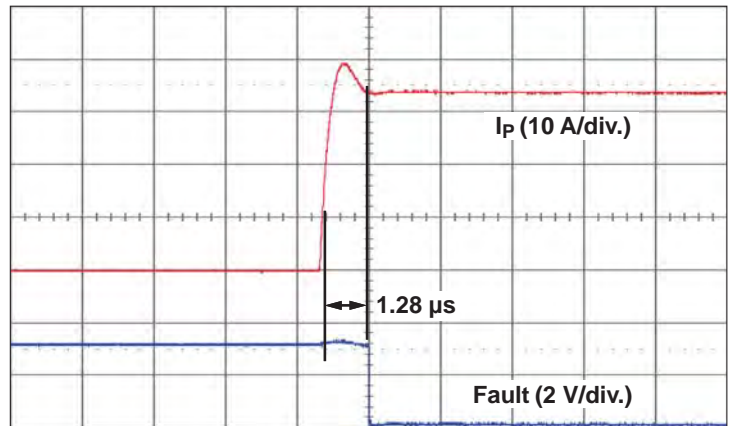
## Definitions of Accuracy Characteristics

**Sensitivity (Sens).** The change in sensor output in response to a 1A change through the primary conductor. The sensitivity is the product of the magnetic circuit sensitivity (G/A) and the linear IC amplifier gain (mV/G). The linear IC amplifier gain is programmed at the factory to optimize the sensitivity (mV/A) for the full-scale current of the device.

**Noise ($V_{NOISE}$).** The product of the linear IC amplifier gain (mV) and the noise floor for the Allegro Hall effect linear IC. The noise floor is derived from the thermal and shot noise observed in Hall elements. Dividing the noise (mV) by the sensitivity (mV/A) provides the smallest current that the device is able to resolve.

**Linearity ($E_{LIN}$).** The degree to which the voltage output from the sensor varies in direct proportion to the primary current through its full-scale amplitude. Nonlinearity in the output can be attributed to the saturation of the flux concentrator approaching the full-scale current. The following equation is used to derive the linearity:

$$100 \left\{ 1 - \left[ \frac{\Delta \text{ gain} \times \% \text{ sat } (V_{\text{IOUT\_full-scale amperes}} - V_{\text{IOUT(Q)}})}{2 (V_{\text{IOUT\_half-scale amperes}} - V_{\text{IOUT(Q)}})} \right] \right\}$$

where $V_{\text{IOUT\_full-scale amperes}}$ = the output voltage (V) when the sensed current approximates full-scale $\pm I_P$.

**Symmetry ($E_{SYM}$).** The degree to which the absolute voltage output from the sensor varies in proportion to either a positive or negative full-scale primary current. The following formula is used to derive symmetry:

$$100 \left( \frac{V_{\text{IOUT\_+ full-scale amperes}} - V_{\text{IOUT(Q)}}}{V_{\text{IOUT(Q)}} - V_{\text{IOUT\_-full-scale amperes}}} \right)$$

**Quiescent output voltage ($V_{IOUT(Q)}$).** The output of the sensor when the primary current is zero. For a unipolar supply voltage, it nominally remains at $V_{CC}/2$. Thus, $V_{CC}$ = 3.3 V translates into $V_{IOUT(Q)}$ = 1.65 V. Variation in $V_{IOUT(Q)}$ can be attributed to the resolution of the Allegro linear IC quiescent voltage trim and thermal drift.

**Electrical offset voltage ($V_{OE}$).** The deviation of the device output from its ideal quiescent value of $V_{CC}/2$ due to nonmagnetic causes. To convert this voltage to amperes, divide by the device sensitivity, Sens.

**Accuracy ($E_{TOT}$).** The accuracy represents the maximum deviation of the actual output from its ideal value. This is also known as the total ouput error. The accuracy is illustrated graphically in the output voltage versus current chart below.
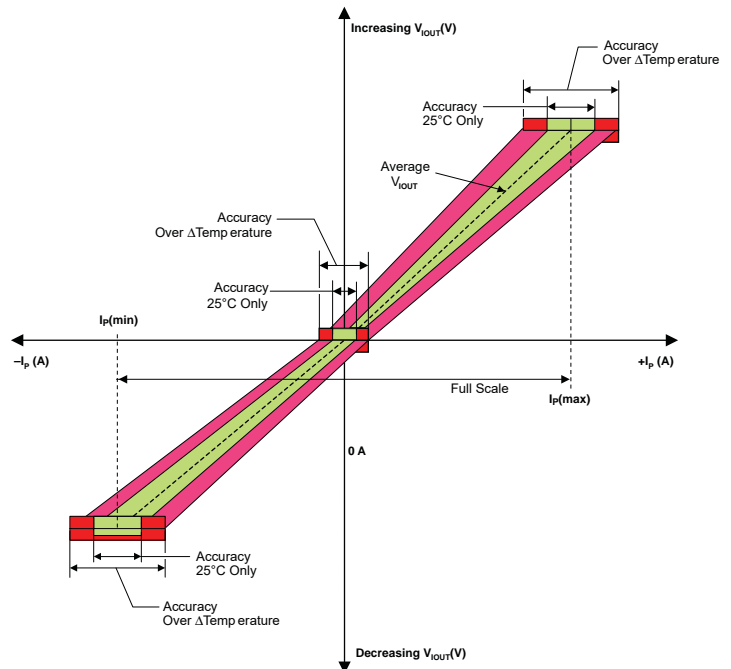
**Ratiometry.** The ratiometric feature means that its 0 A output, $V_{IOUT(Q)}$, (nominally equal to $V_{CC}/2$) and sensitivity, Sens, are proportional to its supply voltage, $V_{CC}$. The following formula is used to derive the ratiometric change in 0 A output voltage, $\Delta V_{IOUT(Q)RAT}$ (%):

$$100 \left( \frac{V_{\text{IOUT(Q)VCC}} / V_{\text{IOUT(Q)3.3V}}}{V_{CC} / 3.3 \text{ V}} \right)$$

The ratiometric change in sensitivity, $\Delta \text{Sens}_{RAT}$ (%), is defined as:

$$100 \left( \frac{\text{Sens}_{VCC} / \text{Sens}_{3.3V}}{V_{CC} / 3.3 \text{ V}} \right)$$

### Output Voltage versus Sensed Current
Accuracy at 0 A and at Full-Scale Current

Allegro MicroSystems, LLC
115 Northeast Cutoff
Worcester, Massachusetts 01615-0036 U.S.A.
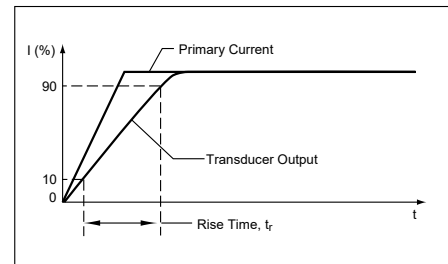1.508.853.5000; www.allegromicro.com

11

## Definitions of Dynamic Response Characteristics

**Power-On Time ($t_{PO}$).** When the supply is ramped to its operating voltage, the device requires a finite time to power its internal components before responding to an input magnetic field. Power-On Time, $t_{PO}$, is defined as the time it takes for the output voltage to settle within ±10% of its steady state value under an applied magnetic field, after the power supply has reached its minimum specified operating voltage, $V_{CC}$(min), as shown in the chart at right.
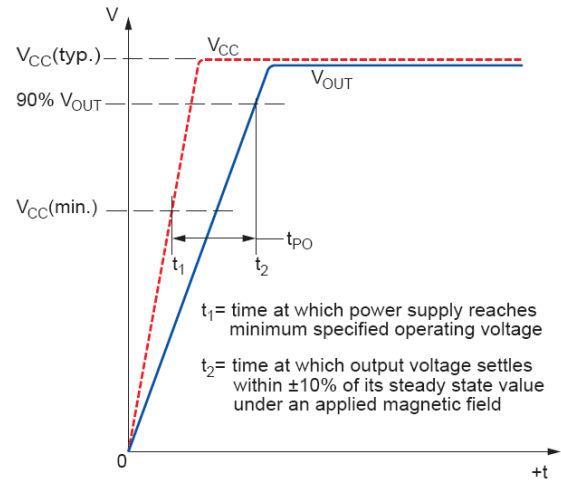


**Rise time ($t_r$).** The time interval between a) when the sensor reaches 10% of its full scale value, and b) when it reaches 90% of its full scale value. The rise time to a step response is used to derive the bandwidth of the current sensor, in which $f(-3\,\text{dB}) = 0.35 / t_r$. Both $t_r$ and $t_{RESPONSE}$ are detrimentally affected by eddy current losses observed in the conductive IC ground plane.



Allegro MicroSystems, LLC
115 Northeast Cutoff
Worcester, Massachusetts 01615-0036 U.S.A.
1.508.853.5000; www.allegromicro.com
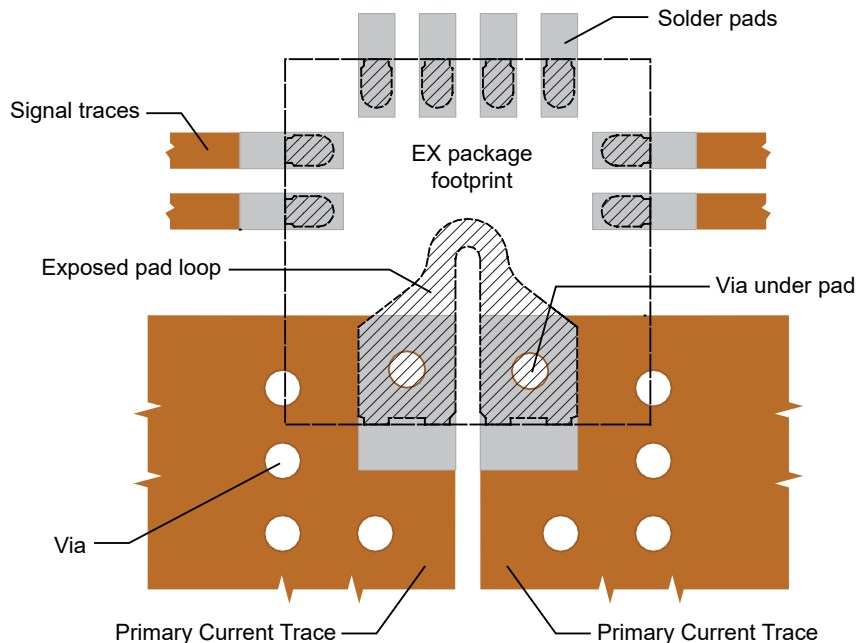
12

## Application Information

### Layout

To optimize thermal and electrical performance, the following features should be included in the printed circuit board:

• The primary leads should be connected to as much copper area as is available.

• The copper should be 2 oz. or heavier.

• Additional layers of the board should be used for conducting the primary current if possible, and
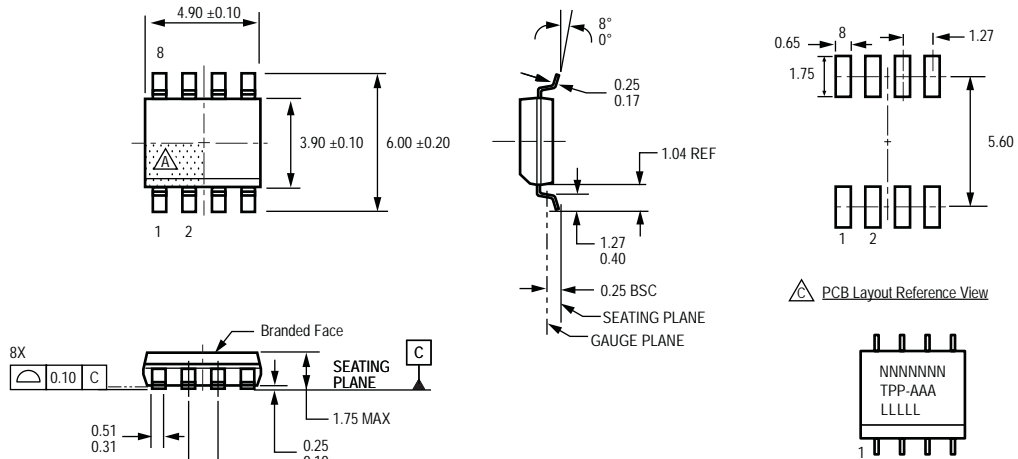
should be connected using the arrangement of vias shown below.

• The two solder pads at the ends of the exposed pad loop should be placed directly on the copper trace that conducts the primary current.

• When using vias under exposed pads, such as with the EX package, using plugged vias prevents wicking of the solder from the pad into the via during reflow. Whether or not to use plugged vias should be evaluated in the application.



Suggested Layout. EX package shown.

Allegro MicroSystems, LLC
115 Northeast Cutoff
Worcester, Massachusetts 01615-0036 U.S.A.
1.508.853.5000; www.allegromicro.com

13

**Package LC, 8-pin SOIC**



4.90 ±0.10

8

3.90 ±0.10     6.00 ±0.20

1     2

8°
0°

0.25
0.17

1.04 REF

1.27
0.40

0.25 BSC

SEATING PLANE
GAUGE PLANE

0.65     8     1.27

1.75

5.60

1     2

⚠C PCB Layout Reference View

8X

⌒ 0.10 C

Branded Face

C

SEATING
PLANE

1.75 MAX

0.51
0.31

0.25
0.10

1.27 BSC

NNNNNNN
TPP-AAA
LLLLL

1

⚠B Standard Branding Reference View

N = Device part number
T = Device temperature range
P = Package Designator
A = Amperage
L = Lot number
Belly Brand = Country of Origin

For Reference Only; not for tooling use (reference MS-012AA)
Dimensions in millimeters
Dimensions exclusive of mold flash, gate burrs, and dambar protrusions
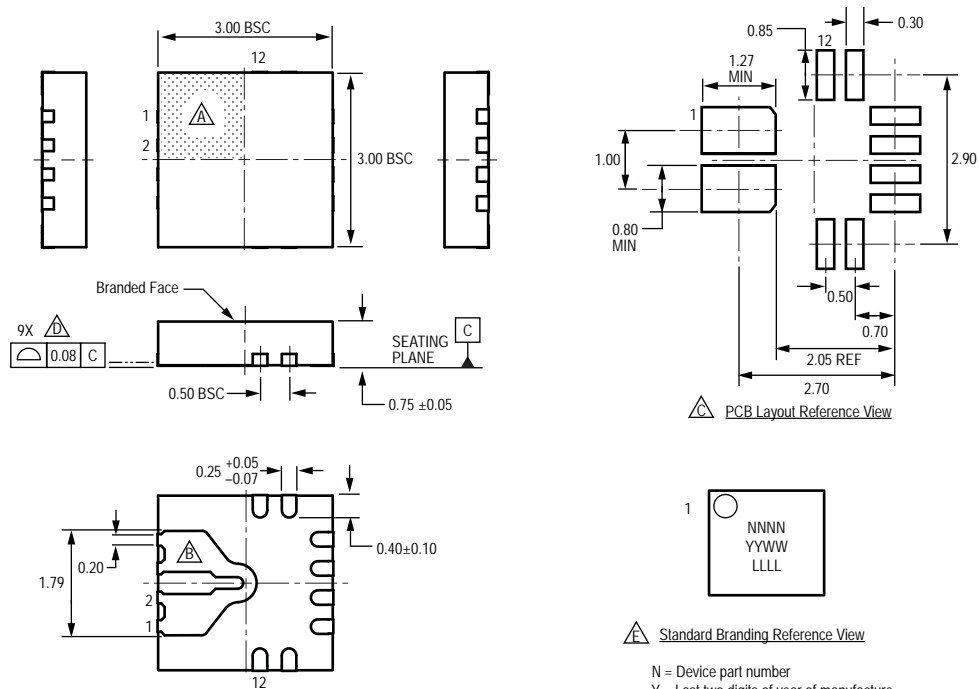Exact case and lead configuration at supplier discretion within limits shown

⚠A Terminal #1 mark area

⚠B Branding scale and appearance at supplier discretion

⚠C Reference land pattern layout (reference IPC7351

⚠D SOIC127P600X175-8M); all pads a minimum of 0.20 mm from all
adjacent pads; adjust as necessary to meet application process
requirements and PCB layout tolerances

Allegro MicroSystems, LLC
115 Northeast Cutoff
Worcester, Massachusetts 01615-0036 U.S.A.
1.508.853.5000; www.allegromicro.com

14

**Package EX, 12-Contact QFN**
**With Fused Sensed Current Loop**

3.00 BSC

12

1

2

3.00 BSC

0.85

12

0.30

1.27
MIN

1

1.00

2.90

0.80
MIN

0.50

0.70

2.05 REF

2.70

Branded Face

9X [D]

[⌒ 0.08 C]

SEATING
PLANE [C]

0.50 BSC

0.75 ±0.05

[C] PCB Layout Reference View

0.25 +0.05 −0.07

0.40±0.10

1.79

0.20

[B]

2

1

12

1

NNNN
YYWW
LLLL

[E] Standard Branding Reference View

N = Device part number
Y = Last two digits of year of manufacture
W = Week of manufacture
L = Lot number

For reference only, not for tooling use (reference JEDEC MO-220WEED except for fused current path)
Dimensions in millimeters
Exact case and lead configuration at supplier discretion within limits shown

[A] Terminal #1 mark area

[B] Fused sensed current path

[C] Reference land pattern layout (reference IPC7351 QFN50P300X300X80-17W4M);
All pads a minimum of 0.20 mm from all adjacent pads; adjust as necessary to meet application process requirements and PCB layout tolerances; when mounting on a multilayer PCB, thermal vias at the exposed thermal pad land can improve thermal dissipation (reference EIA/JEDEC Standard JESD51-5)

[D] Coplanarity includes exposed current path and terminals

[E] Branding scale and appearance at supplier discretion

Allegro MicroSystems, LLC
115 Northeast Cutoff
Worcester, Massachusetts 01615-0036 U.S.A.
1.508.853.5000; www.allegromicro.com

15

**Revision History**

| Revision | Revision Date | Description of Revision |
|----------|---------------|------------------------|
| Rev. 2 | July 18, 2013 | Update characteristics tables references |
| | | |

For the latest version of this document, visit our website:

**www.allegromicro.com**

Allegro MicroSystems, LLC
115 Northeast Cutoff
Worcester, Massachusetts 01615-0036 U.S.A.
1.508.853.5000; www.allegromicro.com

16